ISSN 8755-6839

SCIENCE OF **TSUNAMI HAZARDS**

Journal of Tsunami Society International

Volume 41 Number 3 2022

Binar Kurnia Prahani [*1], **Yusril Alfarizy** [1], **Madlazim** [1], **Eko Hariyono** [1],
Saiyidah Mahtari [2], **Firmanul Catur Wibowo** [3]

[1] *Universitas Negeri Surabaya, Surabaya 60231,* ***INDONESIA***
[2] *Universitas Lambung Mangkurat, Banjarmasin 70123,* ***INDONESIA***
[3] *Universitas Negeri Jakarta, Jakarta 13220,* ***INDONESIA***
Email: binarprahani@unesa.ac.id

Mazova R.Kh [1,2], **Baranova N.A** [3], **Alekseev D.A.** [1,4,5], **Lobkovsky L.I.** [1,4]
J. F. [6], **Oses G. A.** [6], **Jorge Van Den Bosch F.** [6], **Gustavo Oses A.** [6]

[1] *P.P. Shirshov Institute of Oceanology RAS, Moscow 917435* ***RUSSIA,***
e-mail address: llobkovsky@ocean.ru
[2] *R.E. Alekseev Nizhny Novgorod State Technical University, 24, Minin str., 603095 Nizhny Novgorod, Russia. e-mail address: raissamazova@yandex.ru*
[3] *uriga, 6/6 Nartova st., office 829, 603104 Nizhny Novgorod,* ***RUSSIA.***
e-mail address: Natalia.baranova@inbox.ru
[4] *Moscow Institute of Physics and Technology (MIPT), Moscow Region,* ***RUSSIA,***
[5] *Schmidt Institute of Physics of the Earth RAS, Moscow 917435* ***RUSSIA,***
alexeevgeo@gmail.com
[6] *Engineering Center Mitigation Natural Catastrophes Faculty of Engineering, University of Antofagasta, Antofagasta,* ***CHILE.***

WWW.TSUNAMISOCIETY.ORG

TSUNAMI SOCIETY INTERNATIONAL, 1325 South 33rd Avenue, Hollywood, Florida 33021, USA.

SCIENCE OF TSUNAMI HAZARDS is a CERTIFIED OPEN ACCESS Journal included in the prestigious international academic journal database DOAJ.
SCIENCE OF TSUNAMI HAZARDS is also preserved, archived and disseminated by the National Library, The Hague, NETHERLANDS, the Library of Congress, Washington D.C., USA, the Electronic Library of Los Alamos, National Laboratory, New Mexico, USA, the EBSCO Publishing databases and ELSEVIER Publishing in Amsterdam. The vast dissemination gives the journal additional global exposure and readership in 90% of the academic institutions worldwide, including nation-wide access to databases in more than 70 countries.

OBJECTIVE: Tsunami Society International publishes this interdisciplinary journal to increase and disseminate knowledge about tsunamis and their hazards.

DISCLAIMER: Although the articles in SCIENCE OF TSUNAMI HAZARDS have been technically reviewed by peers, Tsunami Society International is not responsible for the veracity of any statement, opinion or consequences.

Submit manuscripts of research papers, notes or letters to the Editor. If a research paper is accepted for publication the author(s) must submit a scan-ready manuscript, a Doc, TeX or a PDF file in the journal format. Issues of the journal are published electronically in PDF format. There is a minimal publication fee for authors who are members of Tsunami Society International for three years and slightly higher for non-members. Tsunami Society International members are notified by e-mail when a new issue is available. Permission to use figures, tables and brief excerpts from this journal in scientific and educational works is granted provided that the source is acknowledged.

Recent and all past journal issues are available at: http://www.TsunamiSociety.org CD-ROMs of past volumes may be purchased by contacting Tsunami Society International at postmaster@tsunamisociety.org Issues of the journal from 1982 thru 2005 are also available in PDF format at the U.S. Los Alamos National Laboratory Library http://epubs.lanl.gov/tsunami/

ISSN 8755-6839

SCIENCE OF **TSUNAMI HAZARDS**

Journal of Tsunami Society International

Volume 41 **Number 3** **2022**

ANALYZE THE MECHANISM OF TSUNAMI BASED ON THE SCOPUS DATABASE

Binar Kurnia Prahani*[1], Yusril Alfarizy[1], Madlazim[1], Eko Hariyono[1], Saiyidah Mahtari[2], Firmanul Catur Wibowo[3]

[1] Universitas Negeri Surabaya, Surabaya 60231, INDONESIA

[2] Universitas Lambung Mangkurat, Banjarmasin 70123, INDONESIA

[3] Universitas Negeri Jakarta, Jakarta 13220, INDONESIA

Email: binarprahani@unesa.ac.id

ABSTRACT

The primary objective research is to obtain information from the Scopus database from 1972 to 2021 related to tsunamis from a mechanical perspective. The preliminary data get from the Scopus database considering that the Scopus indexed documents have gone through a rigorous review process and have credibility in publishing research results. 119 documents (years 1972-2021) get from Scopus data-based obtained based on the keyword Tsunami Mechanism. The VOSViewer application visualizes the research results related to the tsunami mechanism. Of all the papers, there are 80 of 119 documents in the form of articles on Tsunami Mechanisms from 1972 to 2021. Then, the scientist who studied the most tsunamis was Pararas-Carayannis, G., with seven documents. The author is in the first position of all written documents published in International Journals indexed by Scopus. The cities most affected by the tsunami were Japan. The affiliate most associated with tsunamis is The University of Tokyo in Japan. Earth and Planetary Sciences is the subject area in the first position with 77 documents. The keyword that appears the most is "tsunami" in 59 documents. The journal "Pure and Applied Geophysics" was the primary source. The implication of this research is to provide empirical evidence that research related to tsunami is still an exciting topic at present and in the future.

Keywords: *Bibliometric, Mechanism, Tsunami, Top 100 cited, VOSViewer.*

1. INTRODUCTION

A tsunami is one of the most hazardous disasters for humankind as displacing an enormous volume of water through sea waves. Annually, there are $4 billion (US$) in assets, and 60,000 people globally are affected by tsunami disasters (Bernard & Titov, 2015). The tsunami disaster negatively impacted the area it traversed, such as human casualties and economic losses, which increased 100 times over the last twenty years compared to the previous two decades (UNISDR, 2018). When this phenomenon occurs, the resulting disaster marked fatalities due to the increasing number of people living in coastal areas. Therefore, in the last few decades, research related to tsunamis has been growing, aiming to overcome the problem of tsunami disasters in the future (Jain et al., 2021).

Repeated or even a single tsunami occurrence has affected several countries such as India, Japan, Thailand, Turkey, and Indonesia. In history, three significant tsunamis occurred around the world, namely the 2004 Indian tsunami (Satake, 2014), the 2011 Tohoku tsunami (Pararas-Carayannis, 2014), and the 2018 Palu tsunami (Madlazim et al., 2020). The three tsunamis occurred without local institutions' warning or false warning, resulting in fatalities and considerable economic losses. The three tsunamis happened without any prior notice, or the warnings announced were false warnings, resulting in loss of life and substantial economic damage. Therefore, scientists and researchers conduct pre-and post-tsunami analyses of various tsunami events to obtain clues and solutions for future tsunami events. Several algorithms, methods, simulations, and modeling describe a tsunami event's occurrence, prediction, or impact. Various journals focus on discussing developments related to tsunami events, for example, Marine Geology which has produced articles that are very useful for future studies (Kuriyama et al., 2020; Grilli et al., 2021; Prizomwala et al., 2022). Another example is the Science of Tsunami Hazard, which has published articles related to various tsunami events worldwide (Mazova et al., 2020; Zaytsev et al., 2021; Toulkeridis et al., 2022).

Bibliometric analysis is a discipline that studies literature and science in a particular field quantitatively (Blümel & Schniedermann, 2020). The analysis provides a broad view of a specific area to identify research gaps. The gaps identified can provide a way to conduct probabilistic research and present particular results. Recently, several articles carried out the bibliometric analysis in tsunami research, namely Anil et al. (2010), who used the Scopus database from 1997 to 2008, then Jain et al. (2021) using the Scopus database and the Web of Science (WoS), followed by a state-of-the-art-study from 2004 to 2021. One of the powerful tools used to conduct bibliometric analysis studies is to use VOSViewer. The advantage of this tool is it makes it easier to interpret the data visually. In addition, this analysis has the advantage of analyzing the many scientific publications written on a particular topic. In bibliometric studies, researchers can use citation analysis to examine the level of systematic metrics (Suprapto et al., 2021)

Research Objective

The research aims to analyze the mechanism of tsunami based on the Scopus database from 1972 to 2021. Specifically, to obtain information related to:

1. Document type, source type, and authors in mechanism of tsunami research based on the Scopus database.
2. Country and affiliation in mechanism of tsunami research based on the Scopus database.

3. Keywords, sources title, and subject area in mechanism of tsunami research based on the Scopus database.
4. Subject area, SJR, and Citescore in mechanism of tsunami research based on the Scopus database.
5. Visualization by VOSViewer in mechanism of tsunami research based on the Scopus database.
6. Literature review of the top-cited paper in the mechanism of tsunami research based on the Scopus database.
7. Analyze the process of tsunami mechanism.

2. METHODS

This research is a desk study (Amarasinghe & Chandanie, 2020; Amarasinghe et al., 2019; Atkinson et al., 2018; Miller, 2015) that uses bibliometric analysis (Azad & Parvin, 2022; Nguyen, 2022; Liu et al., 2022; Maisonobe, 2022; Tang et al., 2022) and literature review (Makinoshima et al., 2020; Harahap & Huan, 2014; Gnoni et al., 2022; Kumar et al., 2022; Mina et al., 2022; Yang et al., 2022) focusing in the mechanism of tsunami. The primary objective research is to obtain information from the Scopus database from 1972 to 2021 related to tsunamis from a mechanical perspective. The main data of this research is from the Scopus database, considering that the Scopus indexed documents have gone through a rigorous review process and have credibility in the publication of research results. Briefly, the flow of this research described in Figure 1.

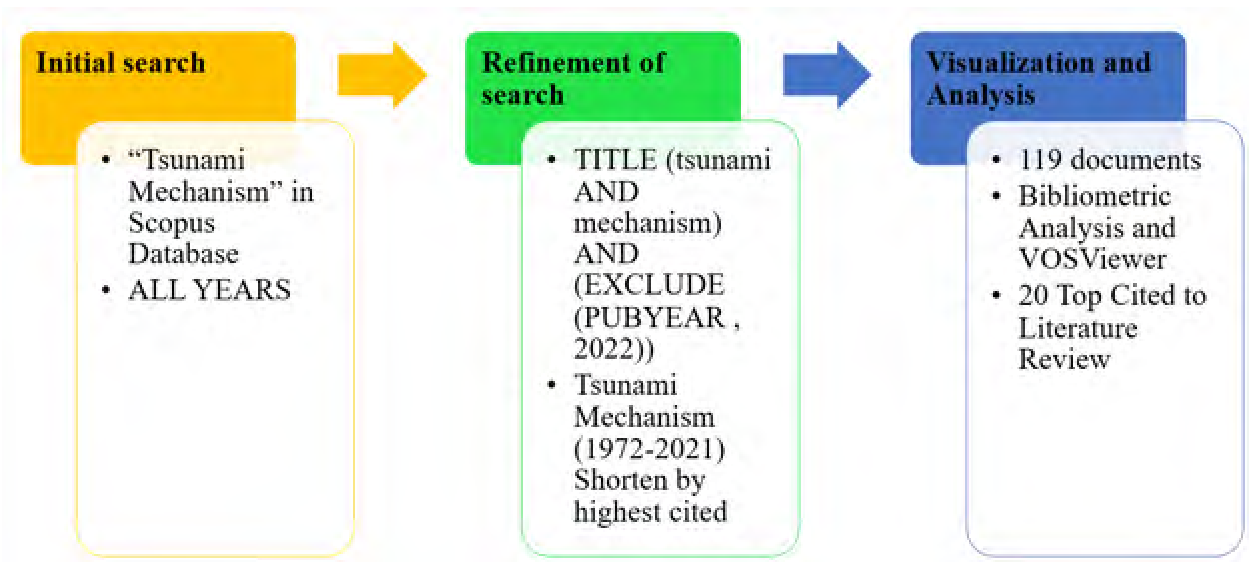

Figure 1. Flowchart research

Data from Scopus from 1972-2021 related to tsunamis from a mechanical perspective with the keyword "Mechanism Tsunami" was taken on March 01, 2022. For SJR data for each journal, it was taken from https://www.scimagojr.com/, and journal citescore data was taken from https://www.scopus.com/sources.uri

A total of 119 documents relevant to the mechanism of tsunami were visualized using VOSViewer. VOSViewer has proven to be effective for viewing profiles and research updates (Soegoto et al., 2022; Tamala et al., 2022; Nandiyanto, 2021; Chen et al., 2021; Sood et al., 2021).

3. RESULTS AND DISCUSSION

3A. Document Type, Source Type, and Authors

Table 1. Document type, source type, and authors in the mechanism of tsunami research

Document Type	Total	Source Type	Total
Article	80	Journal	89
Conference	26	Conference Proceeding	22
Book Chapter	5	Book	4
Review	4	Book Series	4
Erratum	3		
Note	1		
Authors			**Document**
Pararas-Carayannis, G.			7
Satake, K.			6
Løvholt, F., Tanaka, H., Udo, K.			4
Arikawa, T., Beppu, M., Harbitz, C.B., Ishikawa, N., Mano, A., Nistor, I., Nosov, M.A., Paris, R., Tatesawa, H., Tinti, S.			3
Armigliato, A., Chen, C., Esteban, M., Haugen, K.B., Iida, T., Imamura, F., Kanamori, H., Mazova, R.K., Mikami, T., Mota, D.F., Robertson, I., Sakellariou, D., Shibayama, T., Skachko, S.N., Takanashi, H., Tanioka, Y., Tappin, D.R., Tomita, T., Watts, P., Yalçiner, A.C., Yamamoto, Y.			2

Table 1 shows the top types of documents with 119 documents cited on tsunamis from 1972 to 2021. Of all the papers, there are 80 papers in the form of articles, 26 papers in conferences, five papers in book chapters, four papers indicating review, three papers included in the erratum, and one paper in the note. Then, in the "Authors" table, the scientist who studied the most tsunamis was

Pararas-Carayannis, G. with seven documents, followed by other researchers. The exciting thing isthat the documents discussing the most tsunamis are published in journals. It is in line with the "Authors" table, the author in the first position of all written documents published in International Journals indexed by Scopus.

3B. Country and Affiliation

Table 2. Country and Affiliation in the mechanism of tsunami research

Country	Doc.	Affiliation	Document
Japan	40	The University of Tokyo	11
United States	26	Tohoku University	9
Indonesia, United Kingdom	9	Tsunami Society International	6
China	8	Port and Airport Research Institute, Universitetet i Oslo, Norges Geotekniske Institutt, Alma Mater Studiorum Università di Bologna, Nizhny Novgorod State Technical University n.a. R.E. Alekseev	4
France, Russian Federation	7	Ministry of Education China, National Defense Academy of Japanö Middle East Technical University METU, Nanyang Technological University, CNRS Centre National de la Recherche Scientifique, Tokai University, Hohai University, Kyoto University, Kobe University, University of Hawai‘i at Mānoa, Hokkaido University, Russian Academy of Sciences, University of Ottawa, Institut Teknologi Bandung, P.P.Shirshov Institute of Oceanology, Russian Academy of Sciences, Laboratoire Magmas et Volcans, Clermont-Ferrand	3
Norwaz	6	National Marine Environmental Forecasting Center, Applied Fluids Engineering, Inc., Bousai Consultant Co. Ltd., Nagoya University, Hellenic Centre for Marine Research, Japan Agency for Marine-Earth Science and Technology, Yale University, University of Rhode Island, University of Canterbury, British Geological Survey, Waseda University, National Institute of Advanced Industrial Science and Technology, National Central University, Universitas Gadjah Mada, University of Moratuwa, Universidade de Lisboa, Earth Observatory of Singapore, Université Clermont Auvergne	2

Table 2 discusses the cities and affiliations most associated with tsunamis. The cities most affected by the tsunami were Japan, and then in second place were Indonesia and the United Kingdom. It is very relevant because Japan is a country that has a very high level of seismicity. Therefore many earthquakes occur in Japan, with the result that tsunamis occur. In addition, one of the most powerful tsunamis in Japan was the 2011 Tohoku tsunami. Many researchers have discussed the tsunami's impact, mechanism, and source (Veszteg et al., 2014; Strusińska-Correia, 2017; Goto et al., 2021). Furthermore, the affiliate most associated with tsunamis is The University of Tokyo in Japan which is the country most associated with tsunamis.

3C. Keywords, Sources Title, and Subject Area

Table 3. Keywords, sources title, and subject area in the mechanism of tsunami research

Keywords	Document	Subject Area	Document
Tsunami	59	Earth and Planetary Sciences	77
Tsunamis	56	Engineering	38
Earthquakes	28	Environmental Science	21
Coastal Engineering, Numerical Model	11	Physics and Astronomy	10
Earthquake	10	Social Sciences	6
Tsunami Generation	9	Energy	5
Bathymetry, Landslide, Pacific Ocean, Submarine Landslide	8	Mathematics, Multidisciplinary	4

Keywords are an essential part of a paper; with keywords, we can find out the words that most often appear and are discussed in a paper. Table 3 states that the keyword that appears the most is "tsunami" in 59 documents. Then the keywords "tsunamis" contained in 56 documents are followed by keywords associated with tsunamis such as Earthquakes, Tsunami Generation, Bathymetry, Landslide, Pacific Ocean, Submarine Landslide, etcetera. Furthermore, in Table 3, it can be seen that Earth and Planetary Sciences is the subject area in the first position with a total of 77 documents. It correlates with several journals discussing tsunamis with a subject area of Earth and Planetary Sciences, which can be confirmed on the https://www.scimagojr.com/ page.

3D. Subject Area, SJR, and Citescore

The journal "Pure and Applied Geophysics" was the primary source which published nine papers, followed by "Marine Geology," which published eight papers, and "Science of Tsunami Hazards" which published six papers. "Pure and Applied Geophysics" has a relatively high H-index value of 87 with an SJR of 0.72, while "Marine Geology" has a high H-index of 134 with an SJR of 1.24. Then in the third position, there is "Science of Tsunami Hazards," which has an H-index of 14 with an SJR of 0.24. The relationship between H-Index and SJR with the number of documents is related to citations from the journal. It is just that here, the H-Index and SJR cannot be used as the primary reference because the top 2 journals discuss tsunami-related issues and other topics such as earthquakes, fluid mechanics, and fluid geophysics. However, in the third position, namely "Science of Tsunami Hazards," this journal focuses on tsunamis, even though it has not a relatively high H-Index and SJR. Each volume published in this journal always discusses tsunamis.

Table 4. Subject area, SJR, and Citescore in the mechanism of tsunami research

Source Title	Doc.	SJR	H-index	Top Percentile	CiteScore
Pure and Applied Geophysics	9	0.72	87	64	3.5
Marine Geology	6	1.24	134	88	5.6
Science of Tsunami Hazards	6	0.24	14	58	2.4
Geophysical Research Letters	4	2.01	273	97	7.8
Natural Hazards	4	0.76	105	81	4.9
Physics of the Earth and Planetary Interiors	4	1.00	115	78	4.1
Journal of Coastal Research	3	0.25	90	26	0.8
Scientific Reports	3	1.24	213	93	7.1
China Ocean Engineering	2	0.40	25	50	1.8
Coastal Engineering Journal	2	0.99	40	73	3.9
Geotechnique	2	2.78	135	95	8.3
Journal of Asian Earth Sciences	2	1.32	125	90	6.0
Journal of Hydraulic Research	2	0.78	76	76	4.3
Natural Hazards and Earth System Sciences	2	1.12	99	87	5.8

Source Title	Doc.	SJR	H-index	Top Percentile	CiteScore
Proceedings of the International Offshore and Polar Engineering Conference	2	0.18	45	20	0.5

Proceedings of The Coastal Engineering Conference (7 documents) and Vestnik Moskovskogo Universita Ser 3 Fizika Astronomiya (2 documents) have been discontinued.

3F. Visualization by VOSViewer

There are 119 documents (years 1972-2021) from Scopus data-based obtained based on the keyword *Tsunami Mechanism*. The research results related to the tsunami mechanism are visualized using the VOSViewer application, which is presented in Figure 2.

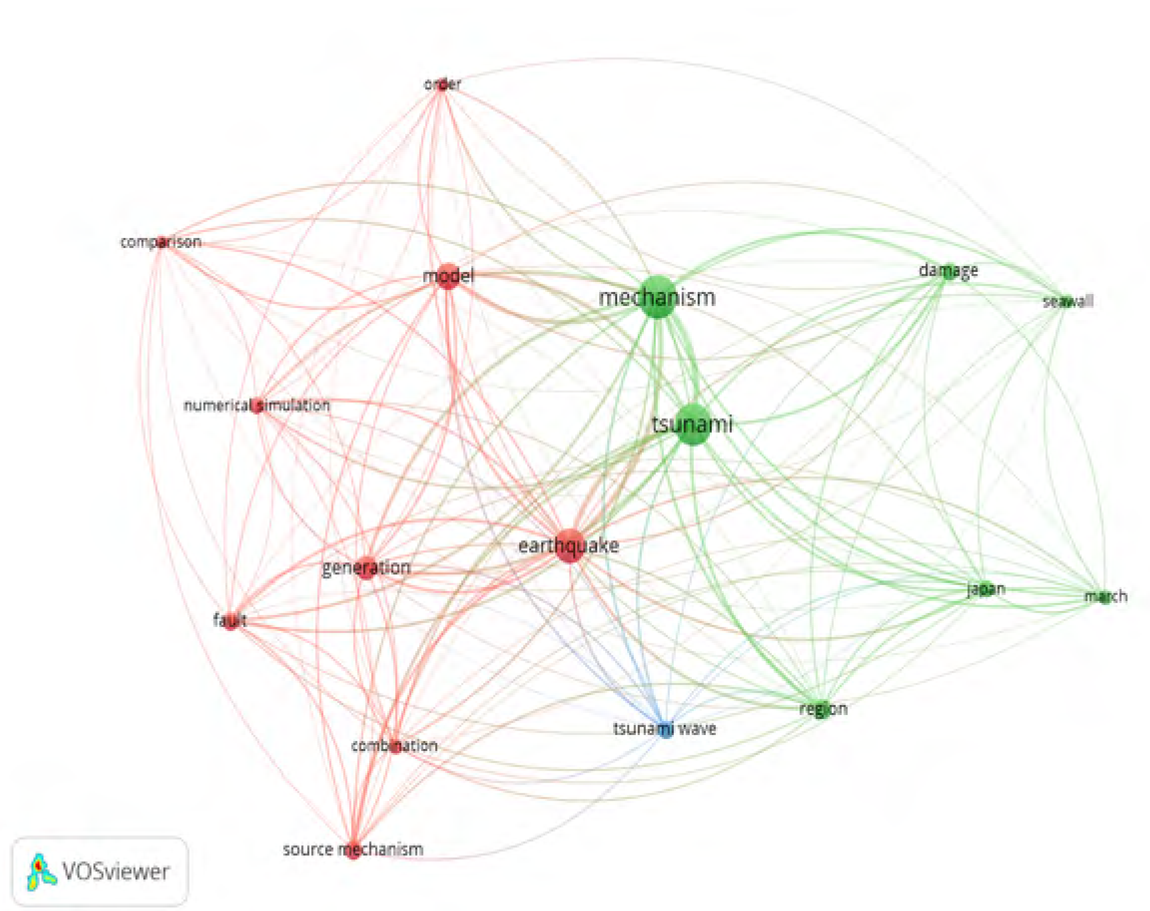

Figure 2. Networking visualizes of tsunami mechanism based on the Scopus database from 1972-2021 by VOSViewer

Observations on the map using VOSViewer obtained four different clusters consisting of 17 keywords, as shown in Figure 2. The first red cluster contains nine items such as earthquake, generation, combination, source mechanism, fault, numerical simulation, comparison, order, and model. The second green cluster contains six items: Tsunami, mechanism, damage, seawall, region, japan, and march. The blue cluster only consists of 1 item, namely the tsunami wave.

3G. Literature Review of Top Cited Paper

Table 5. Literature review of 20 top-cited in the mechanism of tsunami research

Name (Year)	Finding / Results
Kanamori, H. (1972)	With different periods, the 1946 Aleutian and 1896 Sanriku earthquakes produced similar seismic wave excitations. The weak zone is possible due to friction heating at the interface between the oceanic and continental lithosphere.
Tappin, D.R., Watts, P., McMurtry, G.M., Lafoy, Y., Matsumoto, T. (2001)	In the Sissano offshore area, it produces movement along a plane with limited lateral boundaries that mostly dip-slips to the north.
Wang, X., Liu, P.L.-F. (2006)	Using numerical results, the rupture velocity and slip duration from the rupture zone up to 1300 km are still relatively shorter when compared to the propagation and time scale.
Harbitz, C.B., Løvholt, F., Pedersen, G., Masson, D.G. (2006)	Bathymetry, slide permeability, the velocity of rock slide impact on water bodies, and rock slide frontal area are factors that determine rock slides and the resulting tsunami.
Satake, K. (1994)	A comparison of the distribution of tsunami heights shows that the estimated fault length is 250 km, slightly longer than the aftershock area. Around shallow faults, it is possible to have less stiffness than standard underthrust faults.
Abe, K. (1973)	The tectonic deformation of the submarine slump and large landslides generates a tsunami. The tsunami in the Nankaido earthquake of 1946 was caused by a source deformation greater than the seismic waves.

Name (Year)	Finding / Results
Papadopoulos, G.A., Gràcia, E., Urgeles, R., (...), Novikova, T., Papageorgiou, A. (2014)	The characterization of the seismic landslide tsunami source is very effective using numerical modeling as well as empirical discrimination criteria. Interdisciplinary research efforts on tsunamis are needed in terms of tsunami generation.
Paris, R., Switzer, A.D., Belousova, M., (...), Whelley, P.L., Ulvrova, M. (2014).	The abundance of potentially tsunamigenic volcanoes puts the region's rapidly developing beaches at risk. Strategies in dealing with future events using scientific investigations are very important.
Nomanbhoy, N., Satake, K. (1995).	The largest tsunami waves and the largest pressure changes were caused by the same event. The mechanism for tsunami generation is still poorly understood.
Yolsal, S., Taymaz, T., Yalçiner, A.C. (2007).	An important component in the tsunami wave simulation is a high-resolution bathymetric map based on a simulation study.
Haugen, K.B., Løvholt, F., Harbitz, C.B. (2005)	The small fraction of the surface elevation can be increased for small-time lags behind the avalanche, which is in accordance with the results of retrogressive avalanche analysis.
Kato, F., Suwa, Y., Watanabe, K., Hatogai, S. (2012)	There are eight factors that caused the failure of the coastal embankment in the Great East Japan Earthquake. These factors refer to the structure of the seawall, parapet, and armor.
Tinti, S., Armigliato, A., Manucci, A., (...), Yalçiner, A.C., Altinok, Y. (2006).	A very stable slump before the earthquake was demonstrated through a stability analysis using the concept of boundary balance.
Paris, R. (2015).	Difficulties in integrating and harmonizing sources in numerical models and probabilistic tsunami hazard maps are caused by the diversity of waves in terms of amplitude, period, shape, dispersion, etc.
Satake, K. (1985)	Slips and faults can be prevented by tsunami simulation for the topography. The fault is divided into two segments in the area of the aftershock and tsunami recording.
Satake, K., Tanioka, Y. (2003)	Not only splay faults or submarine slumps but a seismological fault model is also needed to reproduce the waveforms of far-field tsunamis.

Name (Year)	Finding / Results
Ma, S. (2012)	Shallow fault subsidence causes a significant inelastic uplift of the seabed. Shallow subduction zone deformation is affected by changes in pore pressure in the overriding wedge.
Wright, S.G., Rathje, E.M. (2003)	Changes in soil shear strength and slope stability over time are produced by excess pore water pressure due to earthquakes.
Witter, R.C., Kelsey, H.M., Hemphill-Haley, E. (2001)	The setting of washovers on the Oregon coast in the sand deposition mechanism is a potential cause of the storm-wave runup and long-distance tsunamis.
Huang, Z., Zhao, D. (2013)	The huge tsunami occurred because the Okhotsk plate was shot out toward the Japan Trench caused by most of the pressure being released in a short time and the plate interface became separated after the Mw 9.0 earthquake.

3H. Analyze the Mechanism of Tsunami

Tsunamis are waves caused by the impulsive movement of ocean disturbances between tides and swell waves in the gravitational spectrum of water waves (Haugen et al., 2005). When the seabed experiences vertical motion in the Earth's crust, the balance of the water surface is disturbed due to the sudden rise or fall of the seabed. A tsunami is a very large ocean wave triggered by an underwater earthquake, volcanic activity, or landslide as a large-scale disturbance (Yolsal, 2007). In addition, tsunamis can also be caused by collisions between extraterrestrial objects and the sea.

Earthquakes that occur below sea level occur due to the meeting of two Earth's plates colliding with each other. When the two plates collide, and there is an up and down fault pattern, it will cause a big wave. When the plate moves vertically, this will trigger the water above it to form waves in all directions, including towards the mainland, which will cause a tsunami. This is what happens for water to regain its balance on top of the colliding plates and change its position. The rupture dynamics of shallow subduction zone earthquakes and their tsunami genesis are influenced by dynamic pore pressure changes in the overriding wedge above the shallow subduction plate interface (Ma, 2012).

Tsunamis caused by submarine landslides are characterized by volume and shear mass dynamics, as well as water depth (Harbitz et al., 2006). Tsunamic submarine landslides and landslides that occur on land are caused by the same thing, namely due to the accumulation of sand, which has a critical angle and is getting thinner day by day, causing collapse. In geomorphology, this is called the "angle of repose". The critical angle of the seabed at the tip is the most vulnerable. If the slope of this critical angle is in the path of the earthquake and there is a small disturbing vibration, it is certain that landslides will occur frequently. Plate movements will cause underwater landslides that can trigger powerful waves. The effects of a tsunami caused by submarine sediment avalanches can be greater than those in subduction zones.

Volcanic activity is a triggering factor for tsunamis, especially from volcanoes located near or under the sea. Volcanic activity generally causes the lip of the volcano to rise or fall, which then triggers large waves similar to a tsunami under the sea. Tsunamis generated by volcanic eruptions are difficult to predict. Its characteristics are the existence of waves that have a short period and greater dispersion than the tsunami generated by an earthquake (Paris et al., 2014). Volcanic tsunamis are generated by underwater explosions, pyroclastic flows, volcanic-tectonic earthquakes, unstable slopes, shock waves, and collapsing calderas (Paris, 2015).

Tsunami waves are mechanical waves that have a propagation speed proportional to the density of the propagation medium. Tsunami waves are classified as transverse waves whose vibration direction is perpendicular to their propagation. In addition, tsunami waves also include longitudinal waves whose vibration direction is parallel to their propagation. An illustration of the tsunami

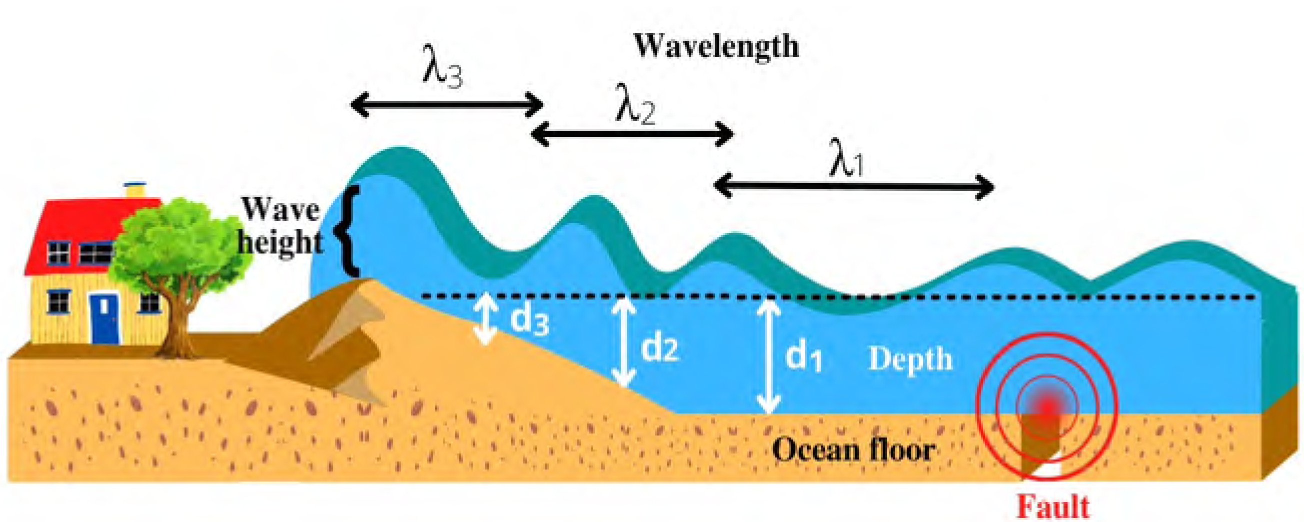

mechanism is shown in Figure 5.

(Source: authors)

Figure 5. Illustration of the tsunami mechanism

A tsunami will vibrate harmoniously when it is in an area where the sea surface is very deep with a large wavelength and speed. The energy of a tsunami wave is always constant so that when a wave enters a shallow area, its wavelength and speed will be smaller while its amplitude will be larger. This process can be formulated as follows:

$$v = \lambda \, . f$$

We know that $\omega = 2\pi f$ and $k = \dfrac{2\pi}{\lambda}$. So we can write :

$$v = \frac{\omega}{k}$$

Where : $\omega = \sqrt{gk\tanh\left(kd\right)}$

$$v = \frac{\sqrt{gk\tanh(kd)}}{\sqrt{k^2}}$$

$$v = \sqrt{\frac{g}{k}\tanh(kd)}$$

$$v = \sqrt{g\frac{\lambda}{2\pi}\tanh\left(2\pi\frac{d}{\lambda}\right)}$$

The hyperbolic tangent function has the following limits:

$$\tanh\left(2\pi\frac{d}{\lambda}\right) \approx \left(2\pi\frac{d}{\lambda}\right) \quad \text{for small } 2\pi\frac{d}{\lambda}$$

$$\tanh\left(2\pi\frac{d}{\lambda}\right) \approx 1 \quad \text{for large } 2\pi\frac{d}{\lambda}$$

So that the velocity value can be formulated as :

$$v \approx \sqrt{g\frac{\lambda}{2\pi}} \quad \text{for deep water}$$

$$v \approx \sqrt{gd} \quad \text{for shallow water}$$

Where v is the speed of the wave, g is the acceleration due to gravity, and d is the depth of the sea surface. This is what causes tsunami waves to have a very large height. The long wave or shallow water approach is applicable when the wavelength is longer than the water depth (Satake & Tanioka, 2003). The success of the tsunami propagation simulation and the accurate prediction of the arrival time of tsunamis occurring at different locations depending on the correct estimation of the fault plane mechanism (Wang & Liu, 2006). Tsunami data can be interpreted in terms of the volume V_T of water displaced at the tsunami source. This volume is equal to the volume of the seabed displaced if a shallow fault causes a base displacement, given by Kanamori. (1972), it can be written as :

$$V_T \approx \left(D_0 \sin\delta \sin\lambda\right) S$$

where D_0 is the dislocation, δ is the dip angle, λ is the slip angle, and S is the area of the fault plane. If the seismic moment M is equal to $\mu S D_0$, we can write :

$$V_T \approx S D_0 \sin\delta \sin\lambda$$

$$V_T \approx \frac{M}{\mu}\sin\delta\sin\lambda$$
$$M = \frac{\mu V_T}{\sin\delta\sin\lambda}$$

Linear shallow wave theory can explain the tsunami propagation process. The shallow water equation in a spherical coordinate system related to transient seafloor motion, given by Wang & Liu (2006), can be expressed as :

$$\frac{\partial h}{\partial t} + \frac{\partial \xi}{\partial t} + \frac{1}{R\cos\varphi}\left[\frac{\partial P}{\partial \psi} + \frac{\partial}{\partial \varphi}\left(\cos\varphi Q\right)\right] = 0$$

$$\frac{\partial \xi}{\partial t} + \frac{1}{Rcos\varphi}\left[\frac{\partial P}{\partial \psi} + \frac{\partial}{\partial \varphi}\left(\cos\varphi Q\right)\right] = -\frac{\partial h}{\partial t}$$

$$\frac{\partial P}{\partial t} + \frac{gh}{Rcos\varphi}\frac{\partial \zeta}{\partial \psi} - fQ = 0$$

$$\frac{\partial (hu)}{\partial t} + \frac{gh}{Rcos\varphi}\frac{\partial \zeta}{\partial \psi} - f(hv) = 0$$

$$\frac{\partial Q}{\partial t} + \frac{gh}{R}\frac{\partial \zeta}{\partial \varphi} + fP = 0$$

$$\frac{\partial (hv)}{\partial t} + \frac{gh}{R}\frac{\partial \zeta}{\partial \varphi} + f(hu) = 0$$

Where P and Q represent the volume flux ($P = hu$ and $Q = hv$, where u and v are the mean depth velocity in the latitude and longitude directions); h is the water depth; is the free surface elevation; (ψ, φ) indicate the longitude and latitude of the Earth; R is the radius of the Earth, and f represents the Coriolis force coefficient.

4. CONCLUSION

119 documents (years 1972-2021) from Scopus data-based were obtained based on the keyword Tsunami Mechanism. Of all the papers, there are 80 of 119 documents in the form of articles on Tsunami Mechanism from 1972 to 2021. Then, the scientist who studied the most tsunamis was Pararas-Carayannis, G., with seven documents. The author is in the first position of all written

documents published in International Journals indexed by Scopus. The cities most affected by the tsunami were Japan. Affiliate most associated with tsunamis is The University of Tokyo in Japan. Earth and Planetary Sciences is the subject area in the first position with 77 documents. The keyword that appears the most is "tsunami" in 59 documents. The journal "Pure and Applied Geophysics" was the primary source. The relationship between H-Index and SJR with the number of documents is related to citations from the journal. It is just that here, the H-Index and SJR cannot be used as the primary reference because the top 2 journals discuss tsunami-related issues and other topics such as earthquakes, fluid mechanics, and fluid geophysics. However, in the third position, namely "Science of Tsunami Hazards," this journal focuses on tsunamis, even though it has not a relatively high H-Index and SJR. Each volume published in this journal always discusses tsunamis. Observations on the map using VOSViewer obtained four different clusters consisting of 17 keywords. The first red cluster contains nine items such as earthquake, generation, combination, source mechanism, fault, numerical simulation, comparison, order, and model. The second green cluster contains six items: Tsunami, mechanism, damage, seawall, region, japan, and march. The blue cluster only consists of 1 item, namely the tsunami wave. Analysis of top-cited paper in mechanism of tsunami research based on the Scopus database (attachment). The implication of this research is to provide empirical evidence that research related to Tsunami is still an exciting topic at present and in the future. The limitation of this research is that it only uses the Scopus database. Further research needs to be supplemented with Google Scholar and Web of Science data access. In addition, further research following up on the findings of the VOSViewer and visualization, including current and future research trends, will be an exciting topic.

REFERENCES

Abe, K. (1973). Tsunami and mechanism of great earthquakes. *Physics of the Earth and Planetary Interiors,* 7(2), 143-153.

Amarasinghe, S.D.I.A., & Chandanie, H. (2020). Construction industries' LCA adaptability: A desk study based SWOT analysis. *Proceedings of the International Conference on Industrial Engineering and Operations Management*, March, pp. 110-121.

Amarasinghe, S.D.I.A., & Hadiwattage, C. (2019). Essential stakeholder contributions for establishing life cycle assessment (Lca) in the construction industry: A desk study. *World Construction Symposium*, pp. 320-329.

Anil, S., B. S., K., R. G., G., & Kumar, V. (2010). Scientometric mapping of tsunami publications: a citation based study. *Malaysian Journal of Library & Information Science*, *15*(1 SE-Articles), 23–40. https://ajba.um.edu.my/index.php/MJLIS/article/view/6720

Atkinson S., Bruen M., Turner J.N., Ball B., Bullock C., O'Sullivan J.J., Casserly C., King J.J., Cullagh A., Kelly-Quinn M. (2018). The value of a desk study for building a national river obstacle inventory. *River Research and Applications*, *34*(8), 1085-1094.

Azad, A.K., & Parvin, S. (2022). Bibliometric analysis of photovoltaic thermal (PV/T) system: From citation mapping to research agenda. *Energy Reports*, *8*, 2699-2711.

Bernard, E., & Titov, V. (2015). Evolution of tsunami warning systems and products. *Philosophical Transactions of the Royal Society A: Mathematical, Physical and Engineering Sciences*, *373*(2053), 20140371. https://doi.org/10.1098/rsta.2014.0371

Blümel, C., & Schniedermann, A. (2020). Studying review articles in scientometrics and beyond: a research agenda. *Scientometrics*, *124*(1), 711–728. https://doi.org/10.1007/s11192-020-03431-7

Chen, Y., Cheng, L., Lian, R., Song, Z., & Tian, J. (2021). COVID-19 Vaccine Research Focusses on Safety, Efficacy, Immunoinformatics, and Vaccine Production and Delivery: A Bibliometric Analysis Based on VOSviewer. *BioScience Trends*, *15*(2), 64-73.

Costa, P.J.M., Andrade, C., Cascalho, J., (...), Paris, R., Dawson, S. (2015). Onshore tsunami sediment transport mechanisms inferred from heavy mineral assemblages. *Holocene*, 25(5), 795-809.

Fukao, Y., Sandanbata, O., Sugioka, H., (...), Watada, S., Satake, K. (2018). Mechanism of the 2015 volcanic tsunami earthquake near torishima, Japan. *Science Advances*, 4(4), eaao0219.

Gnoni, M.G., Tornese, F., Guglielmi, A., Pellicci M., Campo, G., & De Merich, D. (2022). Near miss management systems in the industrial sector: A literature review. *Safety Science*, 150, 105704.

Goto, K., Ishizawa, T., Ebina, Y., Imamura, F., Sato, S., & Udo, K. (2021). Ten years after the 2011 Tohoku-oki earthquake and tsunami: Geological and environmental effects and implications for disaster policy changes. Earth-Science Reviews, 212, 103417. https://doi.org/https://doi.org/10.1016/j.earscirev.2020.103417

Grilli, S. T., Zhang, C., Kirby, J. T., Grilli, A. R., Tappin, D. R., Watt, S. F. L., Hunt, J. E., Novellino, A., Engwell, S., Nurshal, M. E. M., Abdurrachman, M., Cassidy, M., Madden-Nadeau, A. L., & Day, S. (2021). Modeling of the December 22 2018 Anak Krakatau volcano lateral collapse and tsunami based on recent field surveys: Comparison with observed tsunami impact. *Marine Geology*, *440*, 106566. https://doi.org/https://doi.org/10.1016/j.margeo.2021.106566

Gunawan, E., Meilano, I., Abidin, H.Z., Hanifa, N.R., Susilo. Investigation of the best coseismic fault model of the 2006 Java tsunami earthquake based on mechanisms of postseismic deformation. *Journal of Asian Earth Sciences*, 117, 64-72.

Hagala, R., Llinares, C., Mota, D.F. (2017). Cosmic Tsunamis in Modified Gravity: Disruption of Screening Mechanisms from Scalar Waves. *Physical Review Letters*, 118(10),101301.

Harahap, I.S.H., & Huan, V.N.P. (2014). Generation, propagation, run-up and impact of landslide triggered tsunami: A literature review. *Applied Mechanics and Materials*, 567, 724-729.

Harbitz, C.B., Løvholt, F., Pedersen, G., Masson, D.G. (2006). Mechanisms of tsunami generation by submarine landslides: A short review. *Norsk Geologisk Tidsskrift*, 86(3),255-264.

Haugen, K.B., Løvholt, F., Harbitz, C.B. (2005). Fundamental mechanisms for tsunami generation by submarine mass flows in idealised geometries. *Marine and Petroleum Geology*, 22(1-2 SPEC. ISS.), 209-217.

Huang, Z., Wu, T.-R., Chen, T.-Y., Sim, S.Y. (2013). A possible mechanism of destruction of coastal trees by tsunamis: Ahydrodynamic study on effects of coastal steep hills. *Journal of Hydro-Environment Research*, 7(2), 113-123.

Huang, Z., Zhao, D. (2013). Mechanism of the 2011 Tohoku-oki earthquake (Mw 9.0) and tsunami: Insight from seismic tomography. *Journal of Asian Earth Sciences*, 70-71, 160-168.

Imamura, F., Hashi, K. (2003). Re-examination of the source mechanism of the 1998 Papua New Guinea earthquake and tsunami. *Pure and Applied Geophysics*, 160(10-11), 2071-2086.

Jain, N., Virmani, D., & Abraham, A. (2021). Tsunami in the last 15 years: a bibliometric analysis with a detailed overview and future directions. *Natural Hazards*, *106*(1), 139–172. https://doi.org/10.1007/s11069-020-04454-2

Jayaratne, M.P.R., Premaratne, B., Adewale, A., (...), Esteban, M., Nistor, I. (2016). Failure mechanisms and local scour at coastal structures induced by Tsunami. *Coastal Engineering Journal*, 58(4),1640017.

Kaabouben, F., Brahim, A.I., Toto, E., (...), Soares, P., Luis, J.F. (2008). On the focal mechanism of the 26.05.1975 North Atlantic event contribution from tsunami modeling. *Journal of Seismology*, *12*(4), 575-583.

Kanamori, H. (1972). Mechanism of tsunami earthquakes. *Physics of the Earth and Planetary Interiors, 6*(5), 346-359.

Kato, F., Suwa, Y., Watanabe, K., Hatogai, S. (2012). Mechanisms of coastal dike failure induced by the Great East Japan Earthquake Tsunami. *Proceedings of the Coastal Engineering Conference 53 No.3 (2012).*

Kumar, A., Mangla, S.K., & Kumar, P. (2022). An integrated literature review on sustainable food supply chains: Exploring research themes and future directions. *Science of the Total Environment*, 821,153411.

Kuriyama, Y., Chida, Y., Uno, Y., & Honda, K. (2020). Numerical simulation of sedimentation and erosion caused by the 2011 Tohoku Tsunami in Oarai Port, Japan. *Marine Geology*, *427*, 106225. https://doi.org/https://doi.org/10.1016/j.margeo.2020.106225

Latcharote, P., Suppasri, A., Yamashita, A., (...), Kai, Y., Imamura, F. (2017). Possible failure mechanism of buildings overturned during the 2011 great east Japan tsunami in the town of Onagawa. *Frontiers in Built Environment*, 3,16.

Liu, W., Wang, Z., Li, R., & Wu, T. (2022). A bibliometric analysis of mountain ecosystem services, 2000–2019. *Environmental Science and Pollution Research*, *29*(11), 16633-16652.

Ma, K.-F., Kanamori, H., Satake, K. (1999). Mechanism of the 1975 Kalapana, Hawaii, earthquake inferred from tsunami data. *Journal of Geophysical Research: Solid Earth*, 104(B6), 1999JB900073, 13153-13167.

Ma, S. (2012). A self-consistent mechanism for slow dynamic deformation and large tsunami generation for earthquakes in the shallow subduction zone. *Geophysical Research Letters*, 39(11), L11310.

Madlazim, Prastowo, T., & Fahmi, M. N. (2020). Estimation of rupture directivity, cmt and earthquake tsunami parameters and their correlation with the main source of the first tsunami wave, September 28, 2018. *Science of Tsunami Hazards*, *39*(4), 228–242.

Maisonobe, M. (2022). The future of urban models in the Big Data and AI era: a bibliometric analysis (2000–2019). *AI and Society*, *37*(1), 177-194.

Makinoshima, F., Imamura, F., & Oishi, Y. (2020). Tsunami evacuation processes based on human behaviour in past earthquakes and tsunamis: A literature review. *Progress in Disaster Science*, 7,100113.

Mazova, R., Tyuntyayev, S., Giniyatullin, A., Orlov, Y., Orlov, E., & Mel'nikov, V. (2020). Numerical simulation of earthquakes and tsunamis in Mexico – Case Study: Earthquake and Tsunami of September 08 2018. *Science of Tsunami Hazards*, *39*(4), 210–227.

Miller, J. (2015). The Iron Bridge: Desk study and engineering assessment. *Proceedings of the ICE - Engineering History and Heritage*, *168*(4), 177-185.

Mina, D., Hadi, S., & Jalal, A. (2022). The incorporated environmental policies and regulations into bioenergy supply chain management: A literature review. *Science of the Total Environment*, 820,153202.

Nandiyanto, A.B.D., Al Husaeni, D.N., & Al Husaeni, D.F. (2021). A bibliometric analysis of chemical engineering research using vosviewer and its correlation with Covid-19 pandemic condition. *Journal of Engineering Science and Technology*, *16*(6), 4414-4422.

Nguyen, S.M. (2022). Visualization and bibliometric analysis on the research of financial wellbeing. *International Journal of Advanced and Applied Sciences*, *9*(3), 10-18.

Nomanbhoy, N., Satake, K. (1995). Generation mechanism of tsunamis from the 1883 Krakatau Eruption. *Geophysical Research Letters*, 22(4), 509-512.

Nosov, M.A., Skachko, S.N. (2001). Nonlinear tsunami generation mechanism. *Natural Hazards and Earth System Sciences*, 1(4), 251-253.

Papadopoulos, G.A., Gràcia, E., Urgeles, R., (...), Novikova, T., Papageorgiou, A. (2014). Historical and pre-historical tsunamis in the Mediterranean and its connected seas: Geological signatures, generation mechanisms and coastal impacts. *Marine Geology*, 354, 81-109.

Papazachos, B.C., Dimitriu, P.P. (1991). Tsunamis in and near Greece and their relation to the earthquake focal mechanisms. *Natural Hazard (s*, 4(2-3), 161-170.

Pararas-Carayannis, G. (2010). The earthquake and tsunami of February 27 2010 in Chile - evaluation of source mechanism and of near and far-field tsunami effects. *Science of Tsunami Hazards*, 29(2), 96-126.

Pararas-Carayannis, G. (2014). The Great Tohoku-Oki Earthquake and Tsunami of March 11, 2011 in Japan: A Critical Review and Evaluation of the Tsunami Source Mechanism. *Pure and Applied Geophysics*, 171(12), 3257-3278.

Pararas-Carayannis, G. (2014). The Great Tohoku-Oki Earthquake and Tsunami of March 11, 2011 in Japan: A Critical Review and Evaluation of the Tsunami Source Mechanism. *Pure and Applied Geophysics*, *171*(12), 3257–3278. https://doi.org/10.1007/s00024-013-0677-7

Paris, R. (2015). Source mechanisms of volcanic tsunamis. *Philosophical Transactions of the Royal Society A: Mathematical, Physical and Engineering Sciences*, 373(2053),20140380.

Paris, R., Switzer, A.D., Belousova, M., (...), Whelley, P.L., Ulvrova, M. (2014). Volcanic tsunami: A review of source mechanisms, past events and hazards in Southeast Asia (Indonesia, Philippines, Papua New Guinea). *Natural Hazards* 70(1), 447-470.

Pelayo, A.M., Wiens, D.A. (1990). The November 20,1960 Peru Tsunami Earthquake: Source mechanism of a slow event. *Geophysical Research Letters*, 17(6), 661-664.

Pelinovsky, E., Talipova, T., Kurkin, A., Kharif, C. (2001). Nonlinear mechanism of tsunami wave generation by atmospheric disturbances. *Natural Hazards and Earth System Sciences*, 1(4), 243-250.

Prizomwala, S. P., Vedpathak, C., Tandon, A., Das, A., Makwana, N., & Joshi, N. (2022). Geological footprints of the 1945 Makran tsunami from the west coast of India. *Marine Geology*, *446*, 106773. https://doi.org/https://doi.org/10.1016/j.margeo.2022.106773

Rahiman, T.I.H., Pettinga, J.R., Watts, P. (2007). The source mechanism and numerical modelling of the 1953 Suva tsunami, Fiji. *Marine Geology*, 237(1-2), 55-70.

Sakellariou, D., Rousakis, G., Nomikou, P., (...), Carey, S., Sigurdsson, H. (2012). Tsunami triggering mechanisms associated with the 17th cent. BC Minoan eruption of thera Volcano, Greece. *Proceedings of the International Offshore and Polar Engineering Conference*, 61-67.

Satake, K. (1985). The mechanism of the 1983 Japan Sea earthquake as inferred from long-period surface waves and tsunamis. *Physics of the Earth and Planetary Interiors*, 37(4), 249-260.

Satake, K. (1994). Mechanism of the 1992 Nicaragua Tsunami Earthquake. *Geophysical Research Letters*, 21(23), 2519-2522.

Satake, K. (2014). Advances in earthquake and tsunami sciences and disaster risk reduction since the 2004 Indian ocean tsunami. *Geoscience Letters*, *1*(1), 15. https://doi.org/10.1186/s40562-014-0015-7

Satake, K., Tanioka, Y. (2003). The July 1998 Papua New Guinea earthquake: Mechanism and quantification of unusual tsunami generation. *Pure and Applied Geophysics,* 160(10-11), 2087-2118.

Schambach, L., Grilli, S.T., Tappin, D.R. (2021). New High-Resolution Modeling of the 2018 Palu Tsunami, Based on Supershear Earthquake Mechanisms and Mapped Coastal Landslides, Supports a Dual Source. *Frontiers in Earth Science*, 8,598839.

Soegoto, H., Soegoto, E.S., Luckyardi, S., & Rafdhi, A.A. (2022). A Bibliometric Analysis of Management Bioenergy Research Using Vosviewer. *Indonesian Journal of Science and Technology*, *7*(1), 89-104.

Sood, S.K., Kumar, N., & Saini, M. (2021). Scientometric analysis of literature on distributed vehicular networks : VOSViewer visualization techniques. *Artificial Intelligence Review, 54*(8), 6309-6341.

Strusińska-Correia, A. (2017). Tsunami mitigation in Japan after the 2011 Tōhoku Tsunami. International Journal of Disaster Risk Reduction, 22, 397–411. https://doi.org/https://doi.org/10.1016/j.ijdrr.2017.02.001

Suprapto, N., Prahani, B. K., & Deta, U. A. (2021). Top 100 cited publications in physics education in the last thirty years: A bibliometric analysis. *Library Philosophy and Practice (e-Journal)*, *5928*, 1–13.

Tamala, J.K., Maramag, E.I., Simeon, K.A., & Ignacio, J.J. (2022). A bibliometric analysis of sustainable oil and gas production research using VOSviewer Application. *Cleaner Engineering and Technology*, *7*, 100437.

Tang, J., Vinayavekhin, S., Weeramongkolkul, M., Suksanon, C., Pattarapremcharoen, K., Thiwathittayanuphap, S., & Leelawat, N. (2022). Agent-Based Simulation and Modeling of COVID-19 Pandemic: A Bibliometric Analysis. *Journal of Disaster Research*, *17*(1), 93-102.

Tappin, D.R., Watts, P., McMurtry, G.M., Lafoy, Y., Matsumoto, T. (2001). The Sissano, Papua New Guinea tsunami of July 1998 - Offshore evidence on the source mechanism. *Marine Geology*, 175(1-4), 1-23.

Tinti, S., Armigliato, A., Manucci, A., (...), Yalçiner, A.C., Altinok, Y. (2006). The generating mechanisms of the August 17, 1999 İzmit bay (Turkey) tsunami: Regional (tectonic) and local (mass instabilities) causes. *Marine Geology,* 225(1-4), 311-330.

Tonini, R., Armigliato, A., Tinti, S. (2011). The September 29 2009 Samoa Islands Tsunami: Simulations based on the first focal mechanism solutions and implications on Tsunami early warning strategies. *Pure and Applied Geophysics*, 168(6-7), 1113-1123.

Toulkeridis, T., Martinez, N., Barrantes, G., Renteria, W., Barragan-Aroca, G., Simón-Baile, D., Palacios, I., Salaza, R., Salcedo-Hurtado, E. de J., & Pararas-Carayannis, G. (2022). Impact and response in central and south america due to the tsunami generated by the submarine eruption of hunga tonga-hunga ha'apai volcano. *Science of Tsunami Hazards*, *40*(1), 1–41.

United Nations Office for Disaster Risk Reduction (UNISDR). Tsunamis account for $280 billion in economic losses over last twenty years. UNISDR https://www.unisdr. org/archive/61619; 2018.

Veszteg, R. F., Funaki, Y., & Tanaka, A. (2014). The impact of the Tohoku earthquake and tsunami on social capital in Japan: Trust before and after the disaster. *International Political Science Review*, 36(2), 119–138. https://doi.org/10.1177/0192512113509501

von Huene, R., Miller, J.J., Klaeschen, D., Dartnell, P. (2016). A Possible Source Mechanism of the 1946 Unimak Alaska Far-Field Tsunami: Uplift of the Mid-Slope Terrace Above a Splay Fault Zone. *Pure and Applied Geophysics*, 173(12), pp. 4189-4201.

Wang, X., Liu, P.L.-F. (2006). An analysis of 2004 Sumatra earthquake fault plane mechanisms and Indian Ocean tsunami. *Journal of Hydraulic Research*, 44(2), 147-154.

Webster, J.M., George, N.P.J., Beaman, R.J., (...), Abbey, E.A., Daniell, J.J. (2016). Submarine landslides on the Great Barrier Reef shelf edge and upper slope: A mechanism for generating tsunamis on the north-east Australian coast?. *Marine Geology*, 371, 120-129.

Williams, D.M. (2010). Mechanisms of wave transport of megaclasts on elevated cliff-top platforms: Examples from western Ireland relevant to the storm-wave versus tsunami controversy. *Irish Journal of Earth Sciences*, 28, 13-23.

Witter, R.C., Kelsey, H.M., Hemphill-Haley, E. (2001). Pacific storms, El Niño and tsunamis: Competing mechanisms for sand deposition in a coastal marsh marsh, Euchre Creek, Oregon. *Journal of Coastal Research*, 17(3), 563-583.

Wright, S.G., Rathje, E.M. (2003). Triggering mechanisms of slope instability and their relationship to earthquakes and tsunamis. *Pure and Applied Geophysics,* 160(10-11), 1865-1877.

Yamamoto, Y., Takanashi, H., Hettiarachchi, S., Samarawickrama, S. (2006). Verification of the destruction mechanism of structures in Sri Lanka and Thailand due to the Indian Ocean tsunami. *Coastal Engineering Journal*, 48(2), 117-145.

Yang, H., Liu, L., Yang, W., Liu H., Ahmad W., Ahmad A., Aslam, F., & Joyklad, P. (2022). A comprehensive overview of geopolymer composites: A bibliometric analysis and literature review. *Case Studies in Construction Materials*, 16, e00830.

Yeh, H., Mason, H.B. 2014. Sediment response to tsunami loading: Mechanisms and estimates. *Geotechnique*, 64(2), 131-143.

Yolsal, S., Taymaz, T., Yalçiner, A.C. (2007). Understanding tsunamis, potential source regions and tsunami-prone mechanisms in the Eastern Mediterranean. *Geological Society Special Publication*, 291, 201-230.

Zaytsev, A., Pronin, P., Giniyatullin, A., Pelinovsky, E., & Zaytseva, M. (2021). Impact Analysis of The 2018 Tsunami on Sulawesi Island Using Satellite Imagery. *Science of Tsunami Hazards*, *40*(4), 218–227.

Zengaffinen, T., Løvholt, F., Pedersen, G.K., Muhari, A. (2020). Modelling 2018 Anak Krakatoa Flank Collapse and Tsunami: Effect of Landslide Failure Mechanism and Dynamics on Tsunami Generation. *Pure and Applied Geophysics*, 177(6), 2493-2516.

Attachment 1

Analysis of top-cited paper in mechanism of tsunami research based on the Scopus database

No	Name	Journal Identities	Title	Cited	SJR	H-index	Percentile	CiteScore
1	Kanamori, H. (1972)	1972 Physics of the Earth and Planetary Interiors 6(5), pp. 346-359	Mechanism of tsunami earthquakes	610	1.1 (Q1)	115	78th	4.1
2	Tappin, D.R., Watts, P., McMurtry, G.M., Lafoy, Y., Matsumoto, T.	2001 Marine Geology 175(1-4), pp. 1-23	The Sissano, Papua New Guinea tsunami of July 1998 - Offshore evidence on the source mechanism	285	1.24 (Q1)	134	88th	5.6
3	Wang, X., Liu, P.L.-F	2006 Journal of Hydraulic Research 44(2), pp. 147-154	An analysis of 2004 Sumatra earthquake fault plane mechanisms and Indian Ocean tsunami	186	0.67 (Q2)	76	76th	4.3
4	Harbitz, C.B., Løvholt, F., Pedersen, G., Masson, D.G.	2006 Norsk Geologisk Tidsskrift 86(3), pp. 255-264	Mechanisms of tsunami generation by submarine landslides: A short review	162	0.67 (Q2)	43	70th	3.2
5	Satake, K.	1994 Geophysical Research Letters 21(23), pp. 2519-2522	Mechanism of the 1992 Nicaragua Tsunami Earthquake	128	2.01 (Q1)	273	97th	7.8
6	Abe, K	1973 Physics of the Earth and Planetary Interiors 7(2), pp. 143-153	Tsunami and mechanism of great earthquakes	103	1.1 (Q1)	115	78th	4.1
7	Papadopoulos, G.A., Gràcia, E., Urgeles, R., (...), Novikova, T., Papageorgiou, A	2014 Marine Geology 354, pp. 81-109	Historical and pre-historical tsunamis in the Mediterranean and its connected seas: Geological signatures, generation mechanisms and coastal impacts	95	1.24 (Q1)	134	88th	5.6

No	Name	Journal Identities	Title	Cited	SJR	H-index	Percentile	CiteScore
8	Paris, R., Switzer, A.D., Belousova, M., (...), Whelley, P.L., Ulvrova, M.	2014 Natural Hazards 70(1), pp. 447-470	Volcanic tsunami: A review of source mechanisms, past events and hazards in Southeast Asia (Indonesia, Philippines, Papua New Guinea)	72	0.76 (Q1)	105	81st	4.9
9	Nomanbhoy, N., Satake, K.	1995 Geophysical Research Letters 22(4), pp. 509-512	Generation mechanism of tsunamis from the 1883 Krakatau Eruption	70	2.01 (Q1)	273	97th	7.8
10	Yolsal, S., Taymaz, T., Yalçiner, A.C.	2007 Geological Society Special Publication 291, pp. 201-230	Understanding tsunamis, potential source regions and tsunami-prone mechanisms in the Eastern Mediterranean	59	0.67 (Q1)	132	90th	5.4
11	Haugen, K.B., Løvholt, F., Harbitz, C.B.	2005 Marine and Petroleum Geology 22(1-2 SPEC. ISS.), pp. 209-217	Fundamental mechanisms for tsunami generation by submarine mass flows in idealized geometries	59	1.34 (Q1)	116	96th	6.7
12	Kato, F., Suwa, Y., Watanabe, K., Hatogai, S.	2012 Proceedings of the Coastal Engineering Conference 53 No.3 (2012)	Mechanisms of coastal dike failure induced by the Great East Japan Earthquake Tsunami	53	1.56 (Q1)	110	98th	8.3
13	Tinti, S., Armigliato, A., Manucci, A., (...), Yalçiner, A.C., Altinok, Y.	2006 Marine Geology 225(1-4), pp. 311-330	The generating mechanisms of the August 17, 1999 İzmit bay (Turkey) tsunami: Regional (tectonic) and local (mass instabilities) causes	50	1.24 (Q1)	134	88th	5.6
14	Paris, R.	2015 Philosophical Transactions of the Royal Society A: Mathematical, Physical and Engineering Sciences 373(2053),20140380	Source mechanisms of volcanic tsunamis	48	1.07 (Q1)	169	98th	6.9

No	Name	Journal Identities	Title	Cited	SJR	H-index	Percentile	CiteScore
15	Satake, K.	1985 Physics of the Earth and Planetary Interiors 37(4), pp. 249-260	The mechanism of the 1983 Japan Sea earthquake as inferred from long-period surface waves and tsunamis	48	1.1 (Q1)	115	78th	4.1
16	Satake, K., Tanioka, Y.	2003 Pure and Applied Geophysics 160(10-11), pp. 2087-2118	The July 1998 Papua New Guinea earthquake: Mechanism and quantification of unusual tsunami generation	47	0.72 (Q2)	87	64th	3.5
17	Ma, S	2012 Geophysical Research Letters 39(11),L11310	A self-consistent mechanism for slow dynamic deformation and large tsunami generation for earthquakes in the shallow subduction zone	46	2.01 (Q1)	273	97th	7.8
18	Wright, S.G., Rathje, E.M.	2003 Pure and Applied Geophysics 160(10-11), pp. 1865-1877	Triggering mechanisms of slope instability and their relationship to earthquakes and tsunamis	46	0.72 (Q2)	87	64th	3.5
19	Witter, R.C., Kelsey, H.M., Hemphill-Haley, E.	2001 Journal of Coastal Research 17(3), pp. 563-583	Pacific storms, El Niño and tsunamis: Competing mechanisms for sand deposition in a coastal marsh marsh, Euchre Creek, Oregon	42	0.25 (Q3)	90	26th	0.8
20	Huang, Z., Zhao, D.	2013 Journal of Asian Earth Sciences 70-71, pp. 160-168	Mechanism of the 2011 tohoku-oki earthquake (Mw 9.0) and tsunami: Insight from seismic tomography	41	1.32 (Q1)	125	90th	6.0
21	Ma, K.-F., Kanamori, H., Satake, K.	1999 Journal of Geophysical Research: Solid Earth 104(B6),1999JB900073, pp. 13153-13167	Mechanism of the 1975 Kalapana, Hawaii, earthquake inferred from tsunami data	40	1.98 (Q1)	232	91st	6.5

No	Name	Journal Identities	Title	Cited	SJR	H-index	Percentile	CiteScore
22	Papazachos, B.C., Dimitriu, P.P.	1991 Natural Hazards 4(2-3), pp. 161-170	Tsunamis in and near Greece and their relation to the earthquake focal mechanisms	36	0.76 (Q1)	105	81st	4.9
23	Pelayo, A.M., Wiens, D.A.	1990 Geophysical Research Letters 17(6), pp. 661-664	The November 20,1960 Peru Tsunami Earthquake: Source mechanism of a slow event	34	2.01 (Q1)	273	97th	7.8
24	Jayaratne, M.P.R., Premaratne, B., Adewale, A., (...), Esteban, M., Nistor, I.	2016 Coastal Engineering Journal 58(4),1640017	Failure mechanisms and local scour at coastal structures induced by Tsunami	31	0.99 (Q1)	40	73rd	3.9
25	Yeh, H., Mason, H.B.	2014 Geotechnique 64(2), pp. 131-143	Sediment response to tsunami loading: Mechanisms and estimates	30	2.78 (Q1)	135	95th	8.3
26	Rahiman, T.I.H., Pettinga, J.R., Watts, P.	2007 Marine Geology 237(1-2), pp. 55-70	The source mechanism and numerical modelling of the 1953 Suva tsunami, Fiji	30	1.24 (Q1)	134	88th	5.6
27	Yamamoto, Y., Takanashi, H., Hettiarachchi, S., Samarawickrama, S.	2006 Coastal Engineering Journal 48(2), pp. 117-145	Verification of the destruction mechanism of structures in Sri Lanka and Thailand due to the Indian Ocean tsunami	28	0.99 (Q1)	40	73rd	3.9
28	Gunawan, E., Meilano, I., Abidin, H.Z., Hanifa, N.R., Susilo	2016 Journal of Asian Earth Sciences 117, pp. 64-72	Investigation of the best coseismic fault model of the 2006 Java tsunami earthquake based on mechanisms of postseismic deformation	27	1.32 (Q1)	125	90th	6.0

No	Name	Journal Identities	Title	Cited	SJR	H-index	Percentile	CiteScore
29	Pararas-Carayannis, G.	2010 Science of Tsunami Hazards 29(2), pp. 96-126	The earthquake and tsunami of February 27 2010 in Chile - evaluation of source mechanism and of near and far-field tsunami effects	27	0.24 (Q3)	14	58th	2.4
30	Costa, P.J.M., Andrade, C., Cascalho, J., (...), Paris, R., Dawson, S	2015 Holocene 25(5), pp. 795-809	Onshore tsunami sediment transport mechanisms inferred from heavy mineral assemblages	23	1.01 (Q1)	117	96th	4.7
31	Pelinovsky, E., Talipova, T., Kurkin, A., Kharif, C.	2001 Natural Hazards and Earth System Sciences 1(4), pp. 243-250	Nonlinear mechanism of tsunami wave generation by atmospheric disturbances	21	1.12 (Q1)	99	87th	5.8
32	Webster, J.M., George, N.P.J., Beaman, R.J., (...), Abbey, E.A., Daniell, J.J.	2016 Marine Geology 371, pp. 120-129	Submarine landslides on the Great Barrier Reef shelf edge and upper slope: A mechanism for generating tsunamis on the north-east Australian coast?	19	1.24 (Q1)	134	88th	5.6
33	Pararas-Carayannis, G.	2014 Pure and Applied Geophysics 171(12), pp. 3257-3278	The Great Tohoku-Oki Earthquake and Tsunami of March 11, 2011 in Japan: A Critical Review and Evaluation of the Tsunami Source Mechanism	19	0.72 (Q2)	87	64th	3.5
34	Imamura, F., Hashi, K.	2003 Pure and Applied Geophysics 160(10-11), pp. 2071-2086	Re-examination of the source mechanism of the 1998 Papua New Guinea earthquake and tsunami	19	0.72 (Q2)	87	64th	3.5

No	Name	Journal Identities	Title	Cited	SJR	H-index	Percentile	CiteScore
35	Fukao, Y., Sandanbata, O., Sugioka, H., (...), Watada, S., Satake, K.	2018 Science Advances 4(4),eaao0219	Mechanism of the 2015 volcanic tsunami earthquake near torishima, Japan	17	5.93 (Q1)	146	97th	16.6
36	Kaabouben, F., Brahim, A.I., Toto, E., (...), Soares, P., Luis, J.F.	2008 Journal of Seismology 12(4), pp. 575-583	On the focal mechanism of the 26.05.1975 North Atlantic event contribution from tsunami modeling	17	0.52 (Q2)	55	56th	2.7
37	Hagala, R., Llinares, C., Mota, D.F.	2017 Physical Review Letters 118(10),101301	Cosmic Tsunamis in Modified Gravity: Disruption of Screening Mechanisms from Scalar Waves	15	3.69 (Q1)	673	95th	15.2
38	Nosov, M.A., Skachko, S.N.	2001 Natural Hazards and Earth System Sciences 1(4), pp. 251-253	Nonlinear tsunami generation mechanism	13	1.12 (Q1)	99	87th	5.8
39	Huang, Z., Wu, T.-R., Chen, T.-Y., Sim, S.Y.	2013 Journal of Hydro-Environment Research 7(2), pp. 113-123	A possible mechanism of destruction of coastal trees by tsunamis: Ahydrodynamic study on effects of coastal steep hills	12	0.68 (Q2)	38	80th	4.7
40	Williams, D.M.	2010 Irish Journal of Earth Sciences 28, pp. 13-23	Mechanisms of wave transport of megaclasts on elevated cliff-top platforms: Examples from western Ireland relevant to the storm-wave versus tsunami controversy	12	0.16 (Q4)	11	30th	0.9
41	Zengaffinen, T., Løvholt, F., Pedersen, G.K., Muhari, A.	2020 Pure and Applied Geophysics 177(6), pp. 2493-2516	Modelling 2018 Anak Krakatoa Flank Collapse and Tsunami: Effect of Landslide Failure Mechanism and Dynamics on Tsunami Generation	10	0.72 (Q2)	87	64th	3.5

No	Name	Journal Identities	Title	Cited	SJR	H-index	Percentile	CiteScore
42	Sakellariou, D., Rousakis, G., Nomikou, P., (...), Carey, S., Sigurdsson, H.	2012 Proceedings of the International Offshore and Polar Engineering Conference pp. 61-67	Tsunami triggering mechanisms associated with the 17th cent. BC Minoan eruption of thera Volcano, Greece	10	0.18	45	20th	0.5
43	Tonini, R., Armigliato, A., Tinti, S.	2011 Pure and Applied Geophysics 168(6-7), pp. 1113-1123	The September 29 2009 Samoa Islands Tsunami: Simulations based on the first focal mechanism solutions and implications on Tsunami early warning strategies	10	0.72 (Q2)	87	64th	3.5
44	Haugen, K.B., Løvholt, F., Harbitz, C.B.	2005 Marine and Petroleum Geology 22(1):209-217	Fundamental mechanisms for tsunami generation by submarine mass flows in idealised geometries (Book Chapter)	10	1.34 (Q1)	116	96th	6.7
45	Schambach, L., Grilli, S.T., Tappin, D.R.	2021 Frontiers in Earth Science 8,598839	New High-Resolution Modeling of the 2018 Palu Tsunami, Based on Supershear Earthquake Mechanisms and Mapped Coastal Landslides, Supports a Dual Source	9	1.1 (Q1)	30	74th	3.3
46	Latcharote, P., Suppasri, A., Yamashita, A., (...), Kai, Y., Imamura, F.	2017 Frontiers in Built Environment 3,16	Possible failure mechanism of buildings overturned during the 2011 great east Japan tsunami in the town of Onagawa	9	0.51 (Q2)	18	77th	2.6
47	von Huene, R., Miller, J.J., Klaeschen, D., Dartnell, P.	2016 Pure and Applied Geophysics 173(12), pp. 4189-4201	A Possible Source Mechanism of the 1946 Unimak Alaska Far-Field Tsunami: Uplift of the Mid-Slope Terrace Above a Splay Fault Zone	9	0.72 (Q2)	87	64th	3.5

ISSN 8755-6839

SCIENCE OF TSUNAMI HAZARDS

Journal of Tsunami Society International

Volume 41 Number 3 2022

NUMERICAL SIMULATION OF THE CATASTROPHIC EARTHQUAKE AND TSUNAMI IN CHILE ON 9 MAY 1877

Mazova R.Kh [1,2], Baranova N.A [3], Alekseev D.A.[1,4,5], Lobkovsky L.I.[1,4] J. F.[6], Oses G. A.[6] , Jorge Van Den Bosch F.[6] , Gustavo Oses A.[6]

[1]*P.P. Shirshov Institute of Oceanology RAS, Moscow 917435 Russia, e-mail address: llobkovsky@ocean.ru*
[2]*R.E. Alekseev Nizhny Novgorod State Technical University, 24, Minin str., 603095 Nizhny Novgorod, Russia. e-mail address: raissamazova@yandex.ru*
[3]*uriga, 6/6 Nartova st., office 829, 603104 Nizhny Novgorod, Russia. e-mail address: Natalia.baranova@inbox.ru*
[4]*Moscow Institute of Physics and Technology (MIPT), Moscow Region, Russia*
[5]*Schmidt Institute of Physics of the Earth RAS, Moscow 917435 Russia, alexeevgeo@gmail.com*
[6]*Engineering Center Mitigation Natural Catastrophes Faculty of Engineering, University of Antofagasta, Antofagasta, Chile. e-mail address: Jorge.VanDenBosch@uantof.cl Gustavo.oses@uantof.cl*

ABSTRACT

In this paper, on the basis of the available historical data and geodynamic studies, numerical simulation of the historical catastrophic earthquake and tsunami of May 9, 1877 is carried out by making use the so called “keyboard” geodynamical model providing the computational formalism for seismic cycles and crustal block motion analysis. 23 scenarios of the kinematic movement of the keyboard blocks were implemented, when the earthquake source was fragmented from larger to smaller segments. Using the proposed methodology, for each scenario, the generation of a tsunami source is simulated and the computation of wave fields up to the 5-meter isobath is carried out. Analysis of the entire set of simulated earthquake scenarios makes it possible to choose a tsunamigenic earthquake scenario with the most adequate characteristics of tsunami waves in the coastal zone. The results obtained are compared with both historical data and those obtained for this event by other authors using various numerical models. Large-magnitude earthquakes in northern Chile and

southern Peru occur every 108 years on average. It should be noted that over 143 years since the catastrophic earthquake of May 9, 1877, any similar events were completely absent. In 2007, a 7.7 Mw earthquake occurred near Tocopilla, and in 2014 a catastrophic *M* = 8.1 earthquake hits Pisagua. It is believed that only part of the energy accumulated over 143 years has been released during those events, while most of it is yet to be released. Thus, we can conclude that a serious tsunami hazard exists for all coastal cities of southern Peru and northern Chile.

Key words: *earthquake source, tsunami source, numerical simulation of tsunami.*

1. INTRODUCTION

At approximately 8:30 pm on Wednesday, May 9, 1877, a strong *M* = 8.7 earthquake struck near Patache (González-Corrasco et al., 2020), with shakes being strongly felt in La Paz, Bolivia, about 550 km away from the epicenter area. It also caused pronounced tremors in Santiago de Chile, at a distance of 1400 km from the source (Vidal Gormáz, 1884), and resulted in extensive rupturing from the north of Pisagua to Mejillones region, (González-Corrasco et al., 2020), see Fig.1 where the blue ellipse shows the size of the rupture zone during the 1877 earthquake. Historical notice describing this great earthquake and tsunami, was written by Francisco Vidal Gormáz in November 1877, and published later in 1884 from which we have extracted important data.

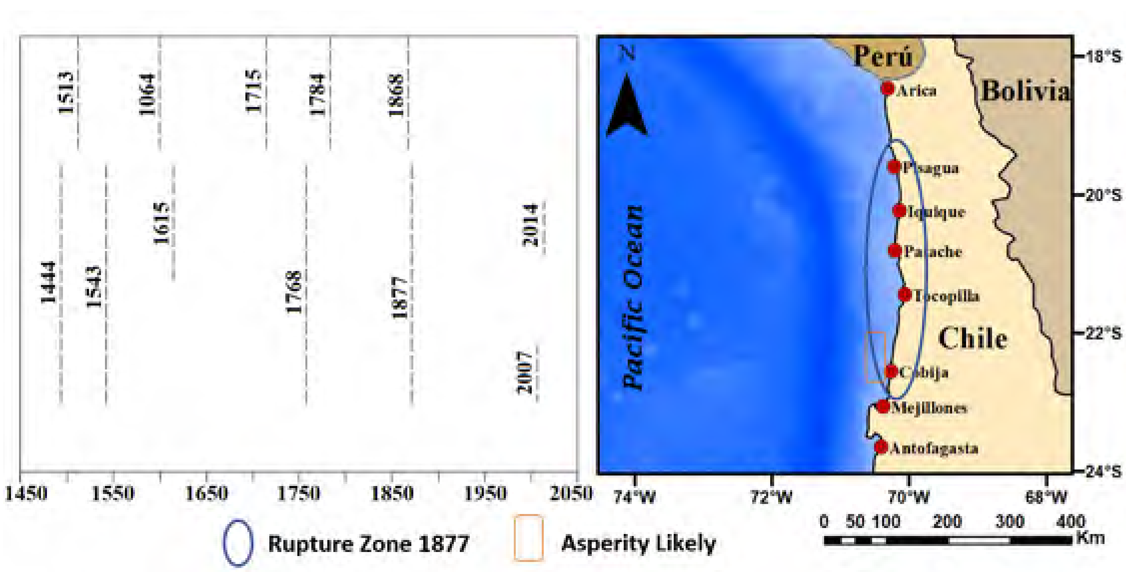

Fig. 1. Great earthquake and tsunami sequence in the northern Chile and southern Peru. taken from (Vargas et al., 2005) and modified in the right panel to include the names and locations of the historical and current cities. The ellipse corresponds to the rupture zone.

The coastal areas of northern Chile and southern Peru are the ones of the most active in the world in terms of seismicity, with frequent occurrence of large-magnitude earthquakes, both in the present and in the recent past due to the proximity of the subduction interface between Nazca and South American tectonic plates, extending from Colombia to the Taitao Peninsula in the extreme south of Chile (CIGIDEN, 2017). In this region, the historical and paleo-historical evidence indicates a series of great earthquakes accompanied by transoceanic tsunamis that show the potential for the similar events in the near future. This series begins in 1444 (this year it was based on a study of drilling of the seabed in the bay of Mejillones (Vargas et al., 2005)), followed by historical large-magnitude earthquakes in 1543, 1615, 1768, and 1877 (Fig. 1; Vargas et al., 2005), with average time interval between great earthquakes being 108 years.

The direct observation shows the absence of a large-magnitude earthquake after 1877 (Fig. 1) during the 143 years following the event. In 2007, a $M = 7.7$ earthquake occurred near Tocopilla, and in 2014 there was another one $M = 8.1$ shock near Pisagua and Iquique, however it is believed that those events led to partial release of the accumulated energy, while most of the stress remains to be released in the future (Chlieh et al., 2011; González-Corrasco et al. to 2020). The seismic rupture in southern Peru and northern Chile is believed to likely cause in the nearest future an earthquake with magnitude of up to 8.9 (see, e.g. (Mazova & Ramirez, 1999)). Thus, we can conclude that a serious tsunami hazard exists for all coastal cities in southern Peru and northern Chile. The nature of the generated tsunami waves, for each of catastrophic events of the Chilean coast, their distribution and behavior in the coastal zone, have been analyzed in sufficient detail in the literature (see, e.g., Pararas-Carayannis 2010; Okal et al., 2006; Kulikov, 2005; Vargas et al., 2005; Mazova and Ramirez 1999; Ramirez et al. 1997; Mazova and Soloviev1994).

Therefore, it is likely that in the near future this series will be continued with much stronger earthquake, accompanied by a devastating tsunami. Obviously, simulating such an event employing the modernized computational methods will allow for the development of an adequate response to protect the communities at risk, both in northern Chile and probably in the rest of the Pacific Ring of Fire. At the same time, knowledge of the history of this event is of great importance when choosing seismic modeling scenarios that are closest to historical data, so that the modeling results could reliably simulate the possible aftermath.

From the analysis of the tsunami wave arrival times at three nearby locations, available from the historical records, it can be seen that the first wave arrived at Cobija 7 minutes after the earthquake, at Mejillones 20 minutes after the shock and at Antofagasta 15 minutes post earthquake. At Iquique, the wave came about half an hour later, since the historical evidence indicates that immediately after the quake, the firefighters were scooping water from the sea to extinguish the fires caused by the earthquake in the coastal area of the city before tsunami (Vidal Gormáz, 1884). There is no specific arrival time available for Arica, which suggests that it took the wave about half an hour to reach this location. From the above it can be concluded that the maximum seafloor displacement, triggering the tsunami, most likely occurred between the northernmost Mejillones and Cobija, consequently it can be assumed that there was an important asperity, in the Fig. 1 the red rectangle corresponds to size of the asperity likely probable, estimated from the arrival times of the first tsunami waves recorded in history at Cobija 7 min, Mejillones 20 min and Antofagasta 15 (Vidal Gormáz, 1884).

Similarly, during the Antofagasta M = 8.1 earthquake in July 1995, by making use of the first tsunami wave arrival times at three tide gauges it was possible to determine the tsunami's source location, 100 km south of the epicenter, near Caleta Blanco place (Ramírez et al., 1997). In a later study, the Nazca plate dislocation contour map was compiled (Mendoza, 1997), showing the maximum displacement (2 meters in magnitude) in this particular area, while in the epicentral region the dislocation is smaller, around 1 m (Fig. 2). There, in the maximum dislocation area, the coseismic acceleration must have been higher than the one recorded in the city of Antofagasta (275 см / с^2, UCN 1995), where despite the proximity to the epicenter (22 km) there were only minor damages. No doubt, if the city of Antofagasta had been located 80 km further south, the earthquake would likely devastate it.

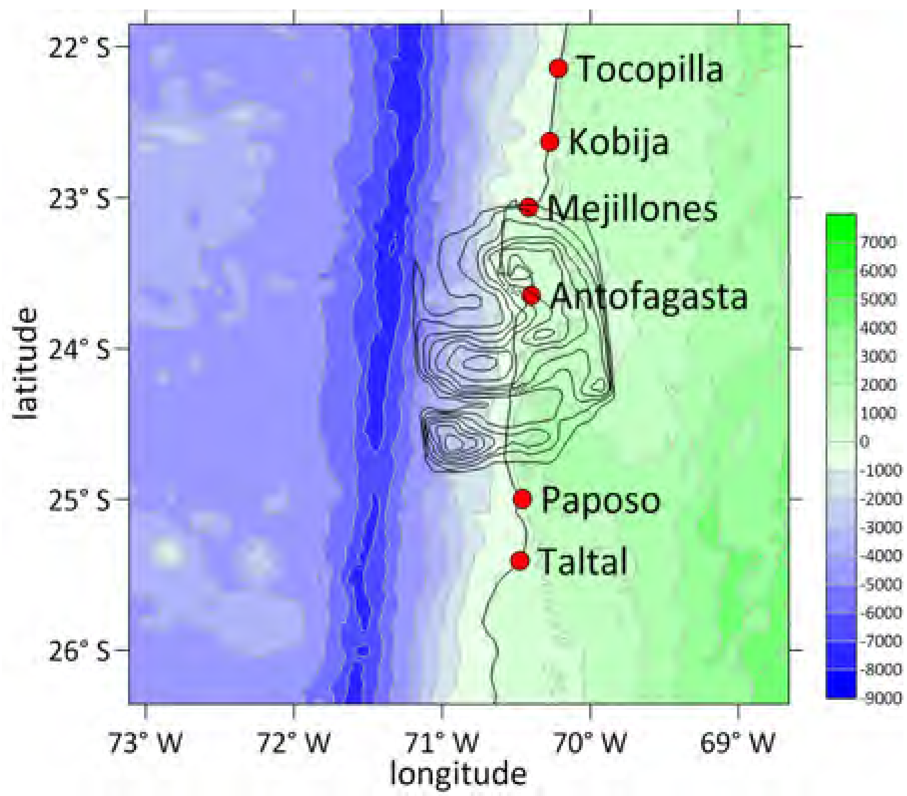

Fig. 2. Large-magnitude block displacement seen from Nazca plate surface contour map created for 1995 Antofagasta earthquake (for more details, see (Mendoza, 1997)).

According to the model presented in (Kanamori & Stewart, 1978; Lay & Kanamori, 1981), such regions with the highest energy release are called asperities. Transoceanic tsunami caused by 1877 earthquake was recorded at multiple locations around globe, with heights of about 1.5 m in New Zealand, 3 m with severe damage in Hawaii and Makai Island, 4 m with severe damage at Marquesas Islands. In Acapulco, Mexico, the flood reached the central square (Vidal Gormáz, 1884). The highest flood levels causing severe damage and numerous human fatalities were observed in northern Chile and southern Peru (north to south): 19 m in Arica, 9 m in Iquique (estimated from historical data in (Titichoca and Guiñez, 1992)), 11.9 m in Cobija, 11.5 m in Mejillones, 6 m in Antofagasta. In Chañaral city located 300 km south of Antofagasta, tsunami had caused severe damage, but the data on flood levels weren't available, as the town has changed its location several times. Starting from 26º south latitude southwards, the flood levels began to decrease. Another interesting evidence says that a 27-meter-high seafloor rise occurred in the Pisagua port area, accompanied by a 2-meter wave run up (Vidal Gormáz, 1884), which is also an important constraint for justification of the geodynamical model employed for tsunami simulation.

2. DESCRIPTION OF EARTHQUAKE NEAR NORTH-WESTERN CHILEAN COAST ON 9 MAY1877

On May 9, 1877, at 21:16 local time, an earthquake and subsequent tsunami were recorded in the area of the city of Iquique. The epicenter of the earthquake was in the Pacific Ocean near the city of Iquique. The greatest intensity was noted between the cities of Arica, Iquique and Antofagasta, and Tocopilla, Gatiko and Cobija were also severely affected. All these cities were destroyed. Earthquake victims were recorded in the area from Pisco to Antofagasta. In Iquique, Gatiko and Cobija, five minutes after the earthquake, tsunami waves arrived with a slow rise in sea level, the wave height eventually ranged from 10 to 15 meters. The second wave was more powerful - its height was from 20 to 23 meters, and it came 15 minutes after the main shock, and this wave destroyed the buildings that remained standing after the earthquake.

In Mejillones, an earthquake of exceptional strength lasted 7 minutes, and the second wave was reported to be 23 meters high. In Iquique, 20 minutes before the earthquake, a faint rolling rumble was heard, accompanied by slow vibrations of the earth, which soon turned into terrible tremors that lasted about 4 minutes. The first wave came 20-30 minutes after the earthquake and was not high. But the second wave was much more intense.

In Antofagasta, the tremors were very strong, the houses swayed like ships during a storm. During the earthquake, the ocean was completely calm, but 10 minutes after the earthquake it overflowed the coast - the tsunami devastated the coastal part of the city. The height of the flood, according to some estimates, was 6 m, according to others - 2.5 m above mean ocean level or 2 m above tide level.

A terrible rumble accompanied an earthquake in San Pedro. In Caleta-Pabellon de Pica, an earthquake with increasing strength lasted 5 minutes and about 25 minutes after the earthquake, the ocean hit the shore. In Chanabaya, the retreat of water was noticed immediately after the earthquake, out of 400 houses, allegedly, only two survived. In 20 minutes after the beginning of the tremors, the tide came. There were three waves at intervals of 8-10 minutes. The second wave was the largest and rose to a height of up to 10 m.

In Tocopilla, the ocean rose 15 min (according to other sources, 30 min) after the earthquake. The height of the rise is estimated at 24 m. Tocopilla was destroyed. In Caldera, the earthquake was of moderate intensity and lasted for about 3 minutes. At about 21 hours the ocean began to recede from the coast, and at about 21:30 the first high tide came. The highest heights are 2 m above the mean ocean level. It was stronger in Copiapo. In Coquimbo, the earthquake lasted 4-5 minutes. Valparaiso has a long but weak earthquake. In Punta Lobos, immediately after the earthquake, the ocean moved away from the coast and after 10 minutes it returned in the form of a tidal wave 6 m high. After 30 minutes, a second wave surged in, washing everything off to a height of 10 m.

Table 1. Impact of Tsunami on Coastal Cities (Soloviev and Go, 1975)

Observation point	**Time between earth-quake and the beginning of noticeable level of oscillations (hours)**	**Maximum wave height (м)**	**Manifestations and the sequence of the tsunami**
Arica	0.7	8-9	The lower part of the city was washed away
Pisagua	2.5	5	The train station and other buildings were destroyed
Iquique	0.3	6	The lower quarter of the city, the customs, were washed away; brought ashore, sunk or damaged ships and boats; killed 30 people
Chanabaya	0.1	10	The city is completely flooded; victims; ships were killed
Caleta Pabellon de Pica	0.4	10	The lower part of the city is destroyed; sunk 5 ships and 27 homes damaged
Punta-Lobos	0.1	10	2 ships sunk and 14 damaged
Huanillos	0.25	9-18	20 houses were washed away; 4 ships sunk and 13 damaged; victims
Tocopilla	0.1	24?	Houses were destroyed and washed away
Cobija	0.1	9	¾ cities were flooded 14 people were killed.
Mejillones	0.5	21	2/3 of the city destroyed; 33 people were killed
Antofagasta	0.1	6	Homes w3as destroyed
Chanyaral	0.9	4-5	City partially flooded
Caldera	0.7	2	-
Carrizal-Bajo	2	1.5	The ships suffered
Coquimbo	2	2	-
Valpariso	2.5	1.1	-
Costitucion	1.5	3	-
Tome	3.5	0.7	-

The complexity of the numerical simulation of this earthquake is associated with a significant discrepancy between field data in some of the considered settlements, given in different sources. Below are data on wave heights from several sources (Soloviev and Go, 1975; Diaz, 1992; Araneda et.al, 2003; Okada, 1992; Barrientos and Ward, 2009; Gusiakov, 2021; Tsunamis in Peru-Chile (noaa.gov); NGDC/WDS Global Historical Tsunami Database (https://www.ngdc.noaa.gov/hazard/ tsu_db.html) (see. Table 2).

Table 2. Refined data on the heights of the tsunami wave run-up during the 1877 earthquake (Soloviev and Go, 1975; Diaz, 1992; Okada, 1992; Barrientos and Ward, 2009).

№	Point	Runup height (m) (Soloviev and Go, 1975	Runup height (m) (Okada, 1992, Barrientos and Ward, 2009)
1	Arica	9	20
2	Pisagua	5	-
3	Iquique	6	9
4	Chanabaya	10	-
5	Caleta Pabellon de Pica	10	-
6	Punta-Lobos	10	-
7	Huanillos	14	-
8	Tocopilla	24	-
9	Cobija	9	12
10	Mejillones	21	12
11	Antofagasta	6	7

1. STATEMENT OF THE PROBLEM

It is well known that the nature of a tsunami depends on the dynamics of displacements in the zone of the earthquake source. Localization of earthquake source for 1877 event, taken from documental data (Gebco Digital Atlas), is presented in Fig.3. (a). In most cases, wave generation computations use seismic data to determine source displacement. Then the static problem of recalculating the displacements of the bottom to the ocean surface is solved. Depending on the speed of movement of the blocks in the seismic source, various scenarios for the formation of a tsunami source on the water surface can be realized. This 1877 event of earthquake and tsunami was studied in many works (see, e.g. Silgado, 1985),). In work (Barrientos and Ward, 2009), the tide gauge data of the 1877 tsunami and the recent tsunami data from strong earthquakes were compared, and numerical simulations were performed.

The parameters of the seismic source were consistent with the works (Abe, 1972; Diaz, 1992), where, based on the characteristics of the run-up and the time of arrival of waves at the coast, the maximum rupture length was estimated at 500 km and the corresponding displacement of 10 m for the 1877 event. In work (Riquelme et al., 2012), where the study of the 1877 event was also carried out, it was noted that the parameters of the fault and the slip distribution of this earthquake are not well studied, because only a few tide gauges recorded this event at a great distance

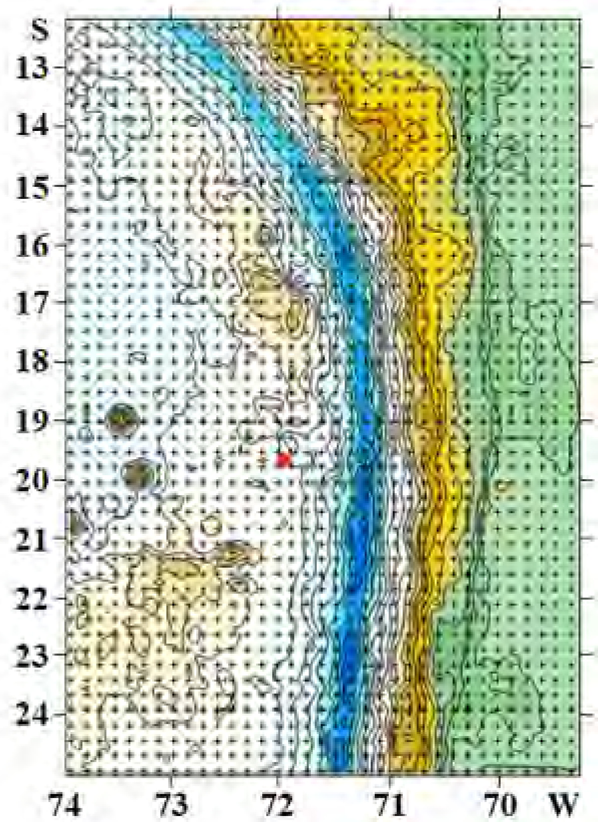

Fig. 3. Bathymetric (a) and geographical (b) maps of the northwestern part of the Chilean coast. The red dot indicates the epicenter of the 1877 earthquake. (Gebco Digital Atlas)

Therefore, to numerically simulate the generation and propagation of tsunamis, they used several rupture scenarios using the NEOWAVE software package. The recent work (Ruiz and Madariaga, 2018), had demonstrated that "subduction earthquakes present a large diversity that it is not incorporated in the traditional interpretation of Chilean seismicity".

In Fig. 4, the seismotectonic map of the northern Chile and southern Peru subduction zone is presented. In this figure, "dark red dots correspond to the subduction area. The information was processed by the GFZ with a change in the localization of about 300 epicenters in this area. The information was used as an earthquake subduction domain to simulate the process. The area in the green rectangle corresponds to the start area of the simulation. The red line corresponds to the total data set. Table 3 and Fig.5 show the data on the land deformation for the tsunami of 1877 and fault parameters (SHOA, 1997), which were used by us for the initial assessment of the seismic source (see also (Ruiz et al., 2015)).

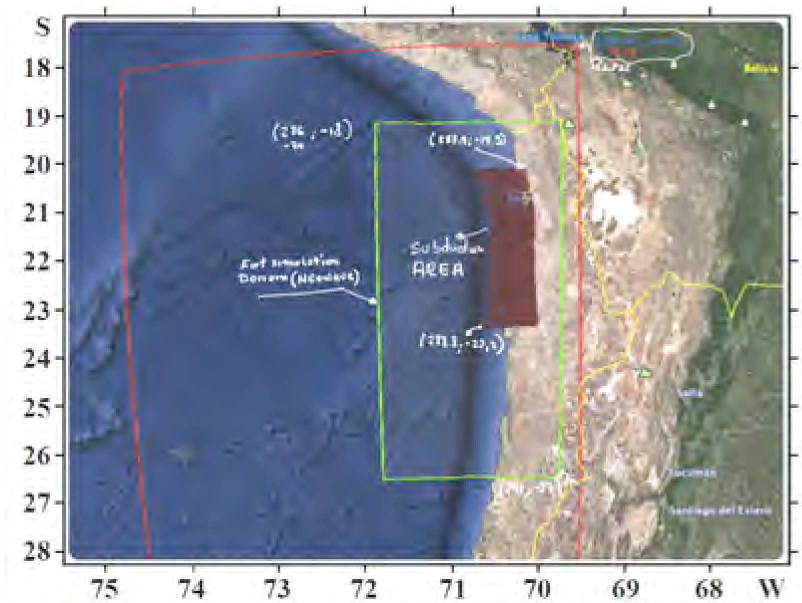

Fig. 4.. Map with marked subduction zone and computed area by Gabriel Álvarez A. (2019) "Centro Ingeniería Mitigación Catástrofes Naturales Facultad de ingeniería. Univ. Antofagasta. Chile.

Table 3: Land deformation generated by earthquake 1877.

SOUTH END	Dislocation	Long	Width	Rhumb	DIP	DEPTH	Angle of Displacement
23° S 71° W	12 m.	490 Km.	150 Km.	359°	19°	10 Km.	90°

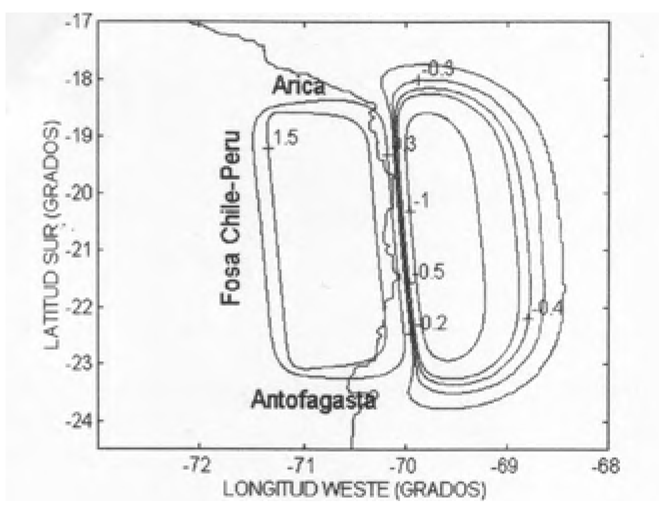

Fig. 5. Slab surface displacement generated by 1877 earthquake. Contour-line lables show dislocation in meters (SHOA, 1997).

The left panel in Fig. 6. shows the tsunami and paleotsunami database relative to the coastal zone. The localization of the source of the 1877 earthquake is marked in red. On the right panel, a part of the computation area used to computation the earthquake of 1877 by ("Centro Ingeniería Mitigación Catástrofes Naturales Facultad de ingeniería. Univ. Antofagasta. Chile."), as well as a section of the coastal zone with the marked localization of the seismic source are presented.

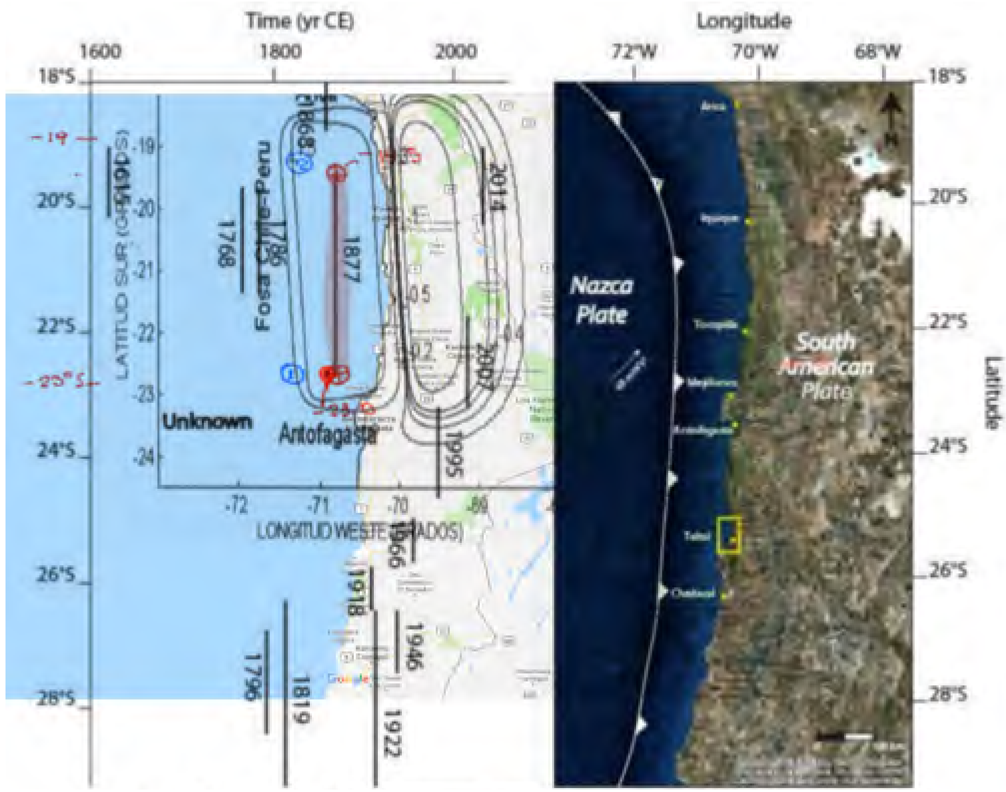

a) b)

Fig. 6. a) Tsunami database for the earthquake coastal zone (for more details, see (DATA, 2021); b) as well as a section of the coastal zone with a marked localization of the seismic source (Barrientos and Ward, 2009; Comte and Pardo, 1991).

4. NUMERICAL SIMULATIONS OF THE 1877 TSUNAMI IN NORTHERN CHILE

Using the key-block model by Lobkovsky (Lobkovsky & Baranov, 1984) and the available geophysical and seismological data, the displacements of blocks in the earthquake source were preliminary estimated for the concrete scenarios. These estimates were used to obtain the tsunami source under using nonlinear shallow water equations (see, e.g., Voltzinger et.al, 1989; Pelinovsky, 1996; Lobkovsky et.al, 2006; Lobkovsky et.al, 2017; Mazova et.al, 2018) we obtain the formation of a tsunami source on the water surface above the earthquake source. Since the movement of the blocks occurs alternately at different speeds and has a different displacement, the formation of the tsunami source and wave propagation from it is a continuous process from the moment the first block begins to move in the earthquake source.

The very formation of the tsunami source and the further propagation of waves in the near part of the coastal water area is a complex process determined by both the given scenario of block movement and the geometry of the coastal zone (see Fig. 3.). Wave propagation into the open ocean obviously has a simpler picture. The computation of this tsunami was carried out by various groups of scientists, according to different programs (see above), including the program (Okada, 1992). But such computations, on the information of Chilean group of co-authors did not give results close to real data. Using the data on the isoseims of the 1877 earthquake, the regions where the highest tsunami intensity was noted, the wave heights on the coast, taking into account the phase of the wave approach to the coast (Soloviev and Go, 1975), and the data on the heights at the same points given in (Diaz, 1992; Okada, 1992; Barrientos and Ward, 2009; Gusiakov, 2021; NGDC/WDS, 2021), a map of the computational area was compiled with points along the coast and the localization of the seismic source of the 1877 earthquake (Fig.7).

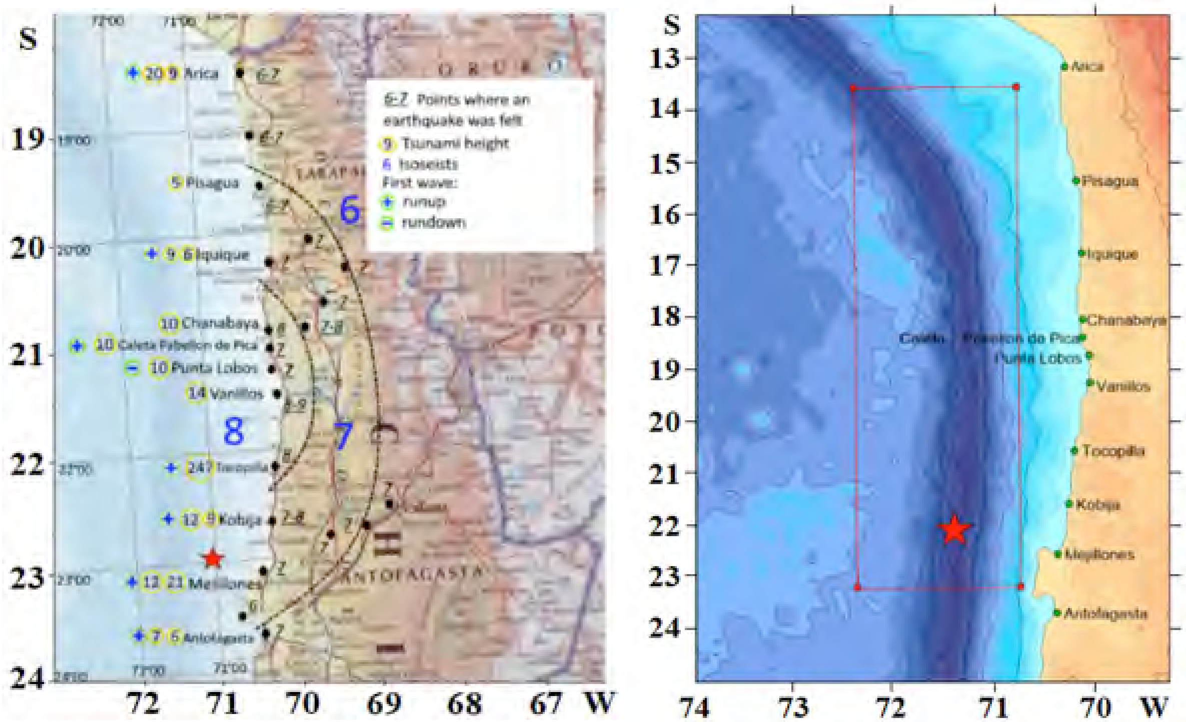

a) b)

Fig. 7. a) Computational domain based on the data proposed in (Soloviev and Go, 1975; Diaz, 1992; Okada, 1992; Barrientos and Ward, 2009): large blue numbers identify the areas where the tsunami was most intense; small numbers - data on tsunami heights at a particular point based on data from works (Soloviev and Go, 1975; Diaz, 1992; Okada, 1992; Barrientos and Ward, 2009); signs (+) and (-) near the numbers on the left determine the nature of the approach of the first wave to the shore: (+) wave run-up to the shore, (-) wave rollback from the shore; dotted black lines - isoseismic; b) The initial contour of the earthquake source of 1877 (according to the initial data 530 x 150 km); The red asterisk is the epicenter of the earthquake.

It should be noted that the data on wave heights at coastal points (numbers in yellow circles) shown on this map in a number of points, differ significantly from each other, although they represent real data taken from works (Soloviev and Go, 1975; Diaz, 1992; Okada, 1992; Barrientos and Ward, 2009; Gusiakov, 2021; NGDC/WDS, 2021) which we had to determine when calculating. The same data are presented further in the Tables comparing the obtained computation results with field data.

In the course of the study, 23 Scenarios of various kinematic movements of the keyboard blocks were considered, into which the earthquake source was fragmentally split divided. The fragmentation of the earthquake source into sub-faults was determined both by documentary data on descriptions of earthquakes and tsunamis at specific points on the coast (Soloviev and Go, 1975; Diaz, 1992; Barrientos and Ward, 2009). Multi-block sources of a virtual earthquake with the given characteristics of the process were considered: 4-block, 8-block, 12-block, 13-block and 14-block, and the parameters of a possible tsunami were estimated at 11 points of the coast, for which there is documentary evidence in various literature. In this work, 4 computations with the closest data to the documentary ones are presented. Estimates of the tsunami arrival times at various locations along the coast for the events of 1877, given in (Soloviev and Go, 1975; Diaz, 1992), made it possible to determine the maximum rupture lengths in the source of more than 500 km. Based on the data of the works (Soloviev and Go, 1975; Diaz, 1992; Okada, 1992; Barrientos and Ward, 2009), which provide different data about earthquake magnitude, computations were carried out for $M = 8.5$ and $M = 8.8$.

Using the ratio of the earthquake magnitude and the characteristics of the rupture in the earthquake source (Diaz, 1992), using the formulas of (Wells and Coppersmith, 1994) and (Iida, 1963) we obtained the following estimates for the length and width of the rupture in the earthquake source.

$$\lg L = 0.59\, M\mathrm{w} - 2.44 \pm 0.16, \ (L \text{ in km})$$

$$\lg W = 0.32\, M\mathrm{w} - 1.01 \pm 0.15, \ (W \text{ in km}) \qquad (1)$$

where L is the length of the rupture in the source, W is the width of the rupture plane:

For a magnitude $M = 8.5$ from formulas (1) we obtain:

$$L = 543 \text{ km} \quad W = 72 \text{ km} \qquad (2)$$

For a magnitude $M = 8.8$ from formulas (1) it is obtained:

$$L = 817 \text{ km} \quad \mathrm{W}=90 \text{ km} \qquad (3)$$

Thus, the estimate of the length L of the rupture in the source, the width of the rupture plane W gives values close to those in (Soloviev and Go, 1975; Diaz, 1992; Okada, 1992), (see Fig. 7b).

5. MATHEMATICAL FORMULATION OF THE PROBLEM

A system of nonlinear shallow water equations is used to describe the simulation of tsunami generation and propagation (Voltzinger et.al, 1989, Lobkovsky et.al, 2006; Lobkovsky et.al, 2017). The depth of the basin depends on both spatial coordinates and time, which allows account for the seabed displacement the during an earthquake. The equation of continuity describes the relationship between the displacement of the bottom and the water surface. In numerical simulation, a bathymetric map of the Pacific Ocean with a one-minute of isobath section was used, which includes the area of 4.000 - 47.6167 S, 65.9500 - 87.4667 W. Bathymetry contains 2618 × 1292 points. The simulation was performed with time step in 1 s. At a depth of 5 m, the condition of total reflection (vertical wall) is set, which makes it possible to fix the maximum and minimum values of the wave level displacement at this depth. The difference scheme from the book (Marchuk et al., 1983), which approximates shallow water equations (Voltzinger et.al, 1989) was taken as a basis. The scheme is based on spaced-apart template, which, in combination with the central-difference approximation of the spatial derivatives, simplifies the numerical implementation of the boundary conditions.

6. PRELIMINARY ANALYSIS OF THE DYNAMICS OF THE EARTHQUAKE SOURCE

For the numerical simulation of this earthquake process, the keyboard-block model was used (Lobkovsky and Baranov, 1984; Lobkovsky et al., 2017; 2021), which makes it possible to fragment the earthquake source into a number of keyboard blocks with further kinematic block motion. The displacement of each block in the earthquake source occurs by a different amount for a different time. When numerically simulating an earthquake and generating tsunami waves, the keyboard model of an earthquake source allows one to obtain a complex distribution of maximum wave heights on the coast, for a given dynamics of block movement in the earthquake source. The coordinates of the earthquake epicenter for given computation are taken from SHOA, 1997 (see Table 1).

6A - Scenario 1. Seismic source of 8 blocks

Initially, the authors considered scenarios with a rough fragmentation of the seismic source area into large blocks from 4 to 8. In this work, the first is the Scenario for an 8-block source from the general series of computations, designated here as Scenario 1.

Fig. 8 shows an 8-block source formed from available data, taking into account the distribution of the maximum tsunami wave heights along the coast, the phase of the first wave approach, and the number of waves approaching a given point (Soloviev and Go, 1975; Diaz, 1992; Gusiakov, 2021). Taking into account the available data, those movements in the source of the earthquake were selected that would be able to adequately simulate the processes on the coast. So in Chanabaya, Punta Lobos, Huanilios, the change in ocean level began with low tide. And in the points of Tocopilla, Cobija, Mejillones, the tsunami began with a rise in the water level. All these changes in levels were given in Table 4. The (+) sign corresponds to the upward displacement of the block in the seismic source; sign (-) corresponds to a downward shift (which corresponds to the wave run-up and rundown from the coast).

Table 4. Sequence of movement of blocks for Scenario 1.

Move ment	Block Lumber	1	2	3	4	5	6	7	8
1	Height (m)	-4	5	4	-4	3	4	-3	4
	Start time of movement (s)	30	0	70	50	110	90	165	130
	Final time of movement (s)	50	30	90	70	130	110	180	165

In this scenario, the trend of the blocks is a sequential movement from south to north. The first movements of keyboard blocks with the maximum amplitude are in the earthquake epicenter area.

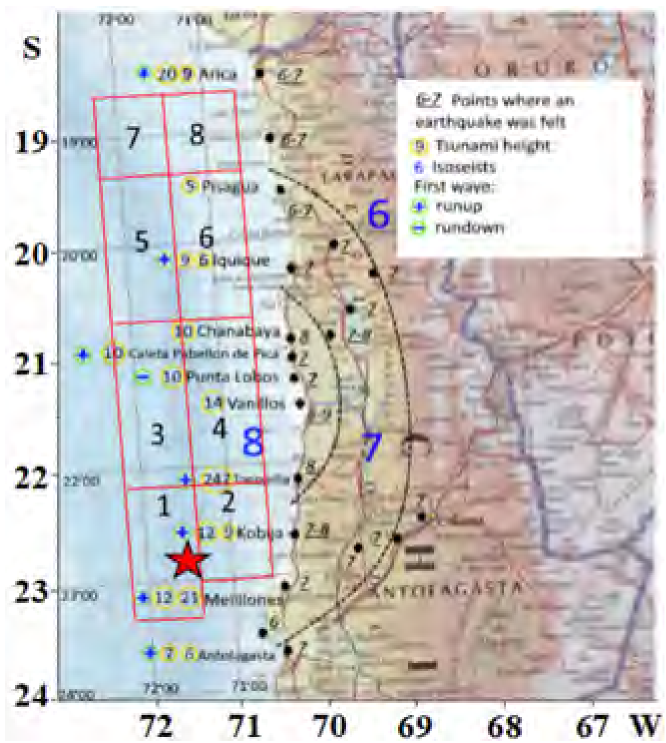

Fig. 8. Keyboard-block source of the Chilean earthquake of 1877 (Scenario 1). 8-block earthquake source, according to updated data (543 x 72 km). The red star indicates the earthquake epicenter.

Moreover, blocks numbered 1, 4 and 7 are moving down. The rest of the blocks move up sequentially (see Table 4). The first panel in the Fig.9 shows time moment during the generation of the tsunami source. In panel 2, the first wave front reaches the Chilean coast near Tocopilla and Cobija. Panels 3-5 show sequentially propagating wave fronts. Panel 6 shows the maximum wave height distribution over the water area when this scenario is

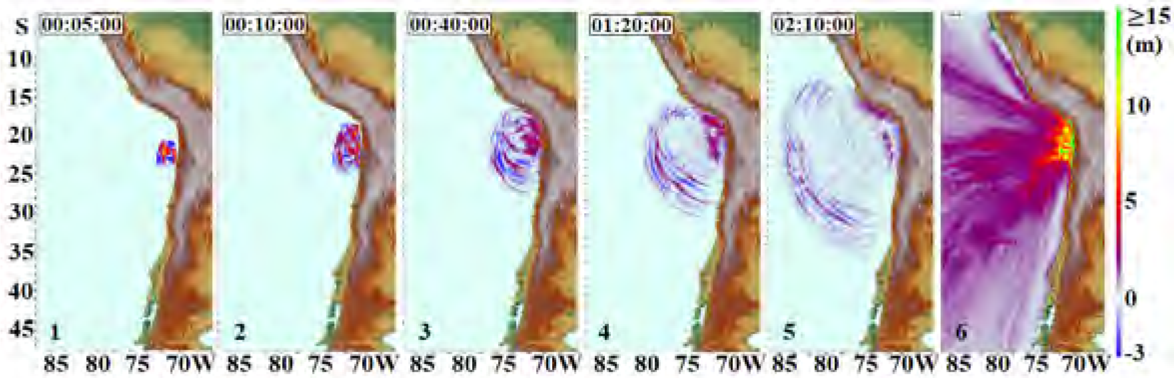

Fig. 9. Propagation of tsunami waves under scenario 1 (numbers 1–5) and distribution of maximum wave heights (6).

implemented. Wave heights on the coast are recorded at the 5-meter isobath. According to the results of this scenario, it can be seen that the average wave heights on the entire coast of the considered zone are not less than 15 meters, which is confirmed by the following histogram of the maximum wave height distribution along the coast (Fig. 10). It is clearly seen that the maximum wave heights on the coast reach 38 m, which is significantly different from the documentary data. Panels 1, 2 show a picture of the tsunami source generation. In panel 3, the first wave front reaches the coast of Chile between Antofagasta and Arica. Panels 3-7 show sequentially propagating wave fronts. Panel 8 shows the distribution of the maximum wave heights over the water area.

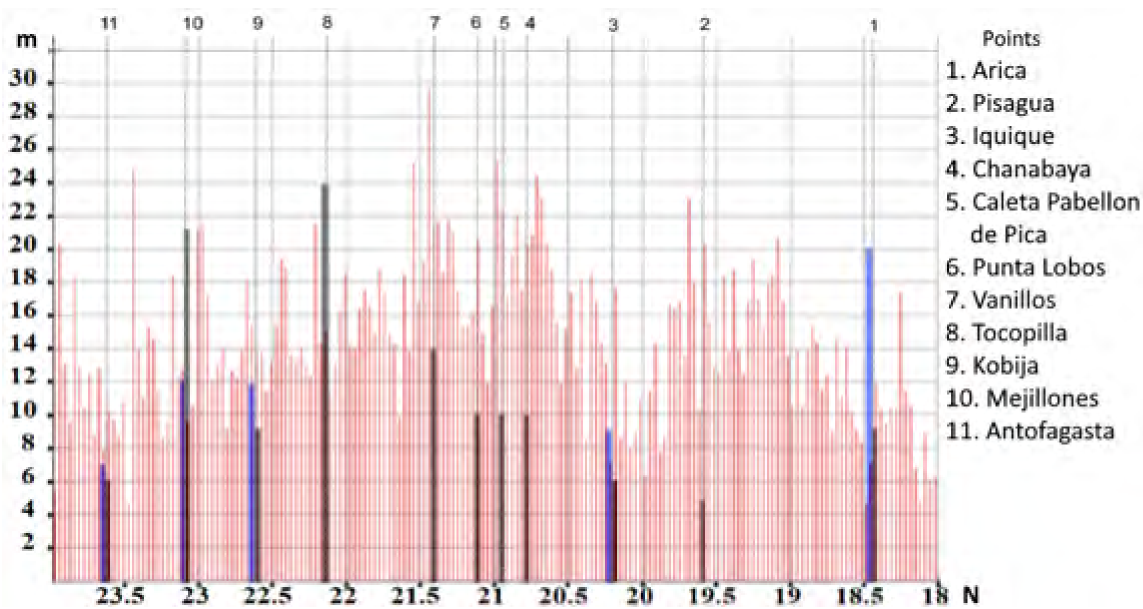

Fig. 10. Histogram of the distribution of the maximum heights of tsunami waves along the considered section of the coast for a 8-block source: red color – computed histogram; gray - data according to the catalogue by S. L. Soloviev and Ch.H.Go; blue - data from works (Diaz, 1992; Barrientos and Ward, 2009; Comte and Pardo, 1991). (Scenario 1).

Wave heights on the coast are recorded at the 5-meter isobath. According to the results of this scenario, it can be seen that the average wave heights on the entire coast of the considered zone are not less than 15 meters, which is confirmed by the following histogram of the distribution of the maximum wave heights along the coast (Fig. 10). It is clearly seen that the maximum wave heights on the coast reach 28m, which is significantly different from the documentary data. Based on the histogram for a visual comparison with documentary data, the following Table 5 can be constructed:

Table 5. Real and computed, according to Scenario 1, data on wave heights

Earthquake data											
No.	**1**	**2**	**3**	**4**	**5**	**6**	**7**	**8**	**9**	**10**	**11**
Point / Data	Arica	Pisa-gua	Iqui-que	Chana-baya	Caleta Pabellon de Pica	Punta Lobos	Vani-llos	Toco-pilla	Co-bija	Mejil-lones	Anto-fagasta
Real data,m	9 (20)	5	6 (9)	10	10	10	14	24	9 (12)	21 (12)	6(7)
Scenario 1,m	7	20	7	19	22	20	22	15	14	12	10

As seen from the Table 5, at most points, the wave heights significantly exceeded the field data. Especially in the central cities (Chanabaya, Caleta Pabellon de Pica, Punta Lobos). It should be noted that in the column (Real data) for some items there are two numbers that are significantly different from each other. This is due, as noted above, with different documentary data presented in the works (Soloviev and Go, 1975; Diaz, 1992; Okada, 1992; Barrientos and Ward, 2009; Gusiakov, 2021).

6B Scenario 2: 12 - block earthquake source

Additional analysis of Scenario 1 made it possible to conduct a more accurate comparison of all available field data with the computed ones. Based on the results, in which the wave heights significantly exceeded the field data (excluding Mejillones and Tocopilla), the movement of the blocks was corrected. As a result, the subduction zone was segmented into a larger number of blocks, while leaving the source contour unchanged. So, in Fig. 11a you can see a newly formed source, consisting of 12 key-blocks, and the amplitudes of block movements have been also changed. In addition, the amplitudes of block movements were changed.

Since, in Chanabaya, Punta Lobos, Huanilios, the change in ocean level began with low tide, it was decided that blocks 6 and 8 closest to them were shifted down. It is analogical, since in the points of Tocopilla, Cobija, Mejillones the tsunami began with a rise in the water level, the movement of blocks 2 and 4 began with their moving up. Table 6 of block movements for Scenario 2 can be presented as follows

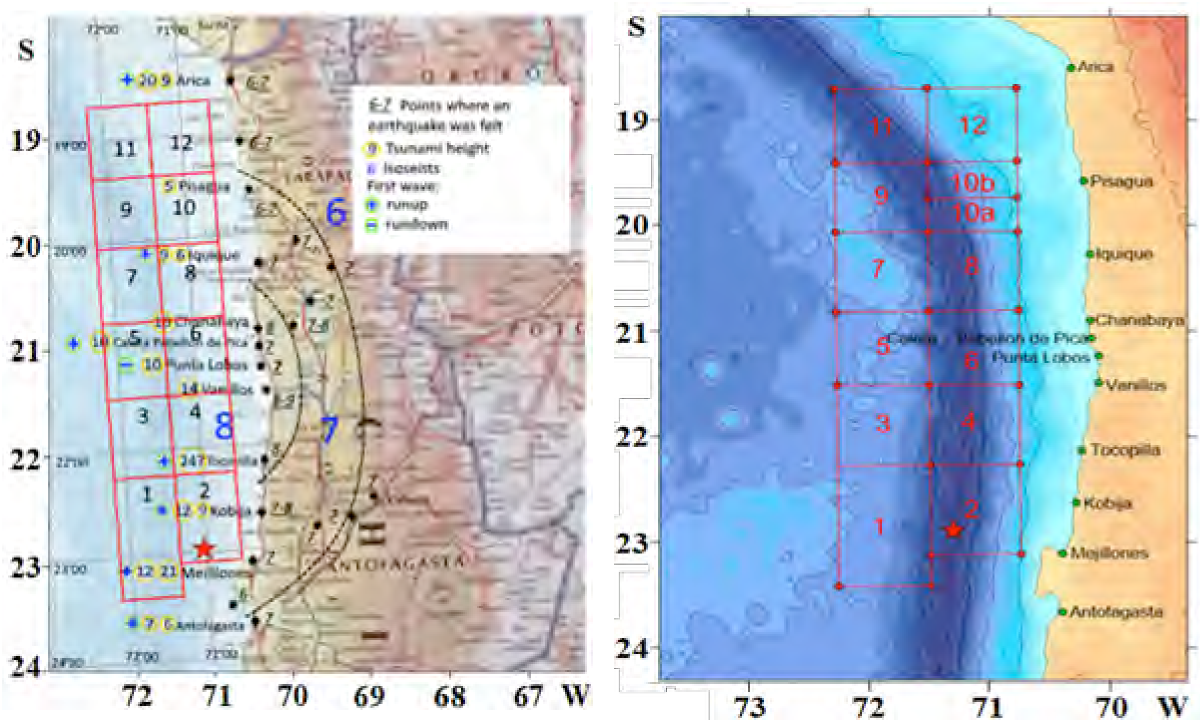

a) b)

Fig. 11. The source of the earthquake of 1877: a) 12 blocks (Scenario 2); b) 13 blocks (Scenario 3).

Table 6. Block movements for Scenario 2

Move-ment	Block number	1	2	3	4	5	6	7	8	9	10	11	12
1	Height (m)	-3.5	3.5	10	8	2	-4	1.8	-1.8	1.5	-1	-3	5
	Start time of movement (s)	135	120	90	60	30	0	45	15	105	75	165	150
	Final time of movement (s)	150	135	105	75	45	15	60	30	120	90	180	165

On panels 1 and 2, it can be seen a complex wave front at the initial time moment. Then, the wave front takes on the usual circular shape. The wave reached the central part of the coast under consideration in 7-10 minutes (Chanabaya, Punta Lobos, Tocopilla, Cobija), in 15-20 minutes to the cities of Antofagasta, Mejiliones. Based on the computation results, the histogram of the distribution of the maximum wave heights is shown below (Fig. 13). As compared with computations on Scenario 1, in the area of the settlement of Iquique, the wave heights decreased. However, in the area of central settlements, they increased markedly, and began to exceed the field data significantly. Thus, the considered kinematics of movement of the keyboard blocks in the earthquake source and the displacement values of the blocks require further correction.

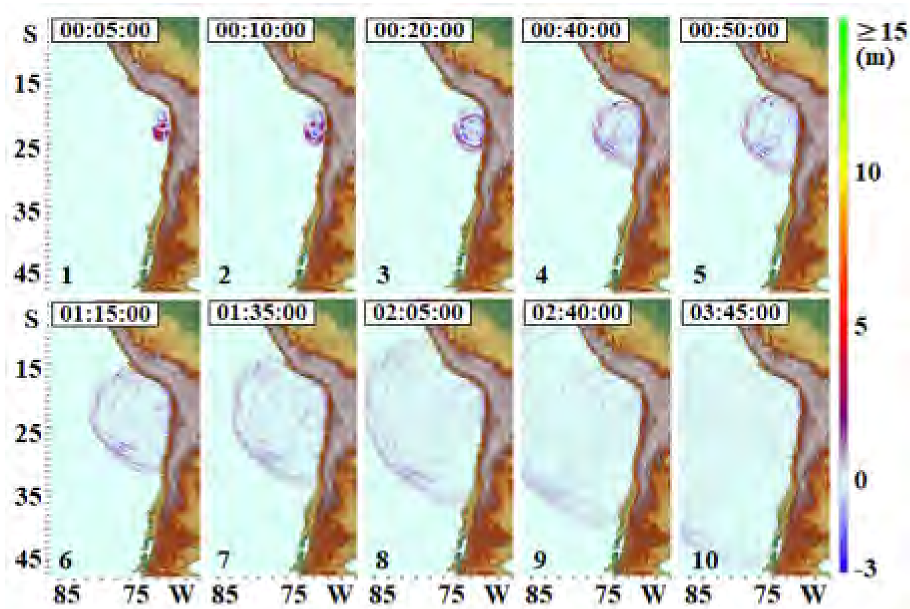

Fig. 12. Generation of the tsunami source and propagation of wave fronts for 10 times moments (Scenario 2).

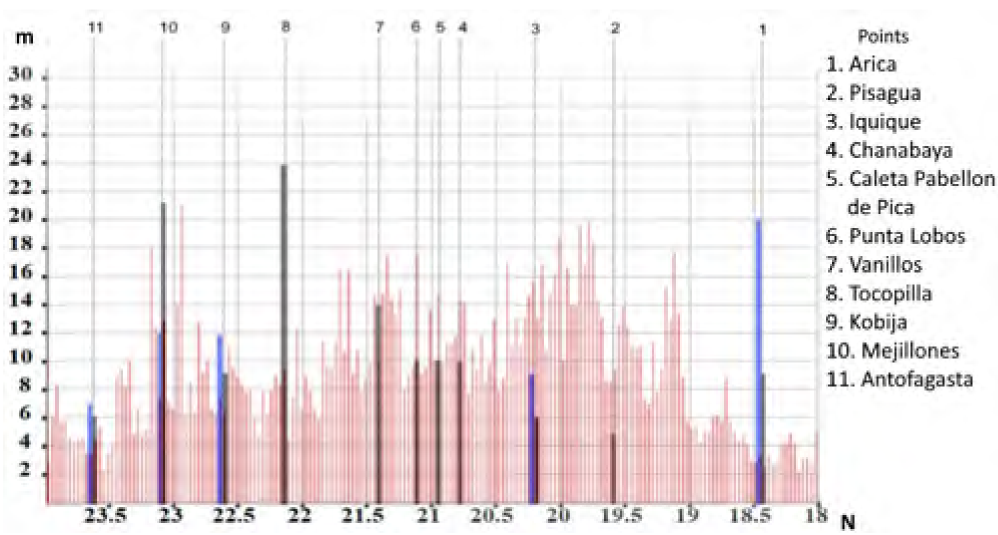

Fig. 13. Histogram of the distribution of the maximum heights of tsunami waves along the considered section of the coast for a 12-block source: red color – computed histogram; gray - data according to the catalog by S. L. Soloviev and Ch.N. Go; blue - data from works (Diaz, 1992; Barrientos and Ward, 2009; Comte and Pardo, 1991). (Scenario 2)

6C - Scenario 3: 13-block source

Based on the last two scenarios and taking into account the distribution of wave heights in the area of Iquique and Pisagua, the nearby block (block 10) was segmented to more small ones. Such segmentation of block 10 allows the movement of the seabed in the source to be corrected.

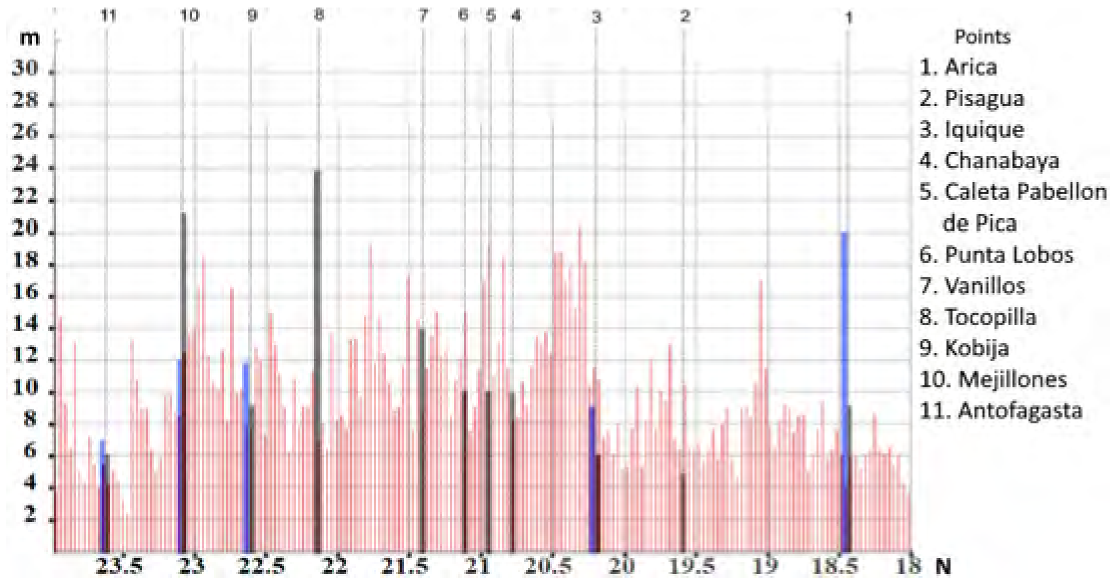

Fig. 14. Histogram of the distribution of the maximum heights of tsunami waves along the considered coastal area for a 13-block source: red color - calculated histogram; gray - data according to the catalogue by S. L. Soloviev and Ch.N Go; blue - data from works (Diaz, 1992; Barrientos and Ward, 2009; Comte and Pardo, 1991). (Scenario 3).

This helps to more accurately determine the wave height distribution in the settlements: Pisagua and Iquique. Thus formed 13-block earthquake source is shown in Fig. 11b. Based on the results of this computation, below is a histogram of the distribution of the maximum wave heights (Fig.14). The histograms of Scenarios 2 and 3 are similar, but there are a number of differences. In the area of Arica, an increase in the maximum wave heights is noticeable, which is associated with an increase in the vertical shift of movement of block 2. It can be seen that at the points of Punta Lobos, Calet-Pabellon de Pica, the wave heights approached the documentary data, but at the points, Pisagua and Iquique the values of the wave heights diverged significantly. Successive analysis of the computed results for Scenario 3 indicates a positive trend in the approach of waves to field data. However, at the points of Tocopilla, Cobija and Mejillones, significant differences in the results of computations and documentary data are visible. The histograms of Scenarios 2 and 3 are close to each other (see Fig. 13 and Fig. 14), however, there are a number of differences in the computations. In the area of Arika, an increase in the maximum wave heights is noticeable, which, apparently, is associated with an incorrect value of the displacement of block 2.

Since, as can be seen from the analysis of Scenarios 2,3, we have not yet achieved close coincidence with documentary data in a number of points. The goal of the next scenario is to achieve an approximation to the documentary data of waves at the points of Iquique and Pisagua, Tocopilla, Vanilios and Cobija, where the documentary data are much higher than the computed ones.

7. NUMERICAL SIMULATION WITH A CHANGED LOCALIZATION OF THE EARTHQUAKE SOURCE

Twelve computations were carried out with the available data on the localization of the source and epicenter of the earthquake. However, an additional analysis of the available data on the realization of this earthquake leads to the conclusion about the possible incorrect information on the localization of the epicenter of the earthquake on May 9, 1877. Taking into account such possibility the epicenter of this earthquake, under present numerical simulation, it was assumed to be shifted by about 21 ° latitude (Fig. 15). And the coordinates of the epicenter of the earthquake for further computations are proposed to be (21 S, 71.3 W). Changing the localization of the earthquake epicenter, a more complex seismic source was formed, comprising 14 blocks. Having analyzed the dynamics and direction of tsunami waves approaching the coast from the moment the earthquake began, the times of approach and the height of approaching waves on the coast, the direction of movement of blocks in the model seismic source was changed, corresponding to the direction of the rupture displacement in the earthquake source.

Thus, it was determined that the movement of blocks when modeling the dynamics of rupture in the source of the earthquake of 1877 should be directed from the earthquake epicenter (see Fig. 15) to the north-west and south-west alternately, taking into account the time of wave arrival to a specific point on the coast.

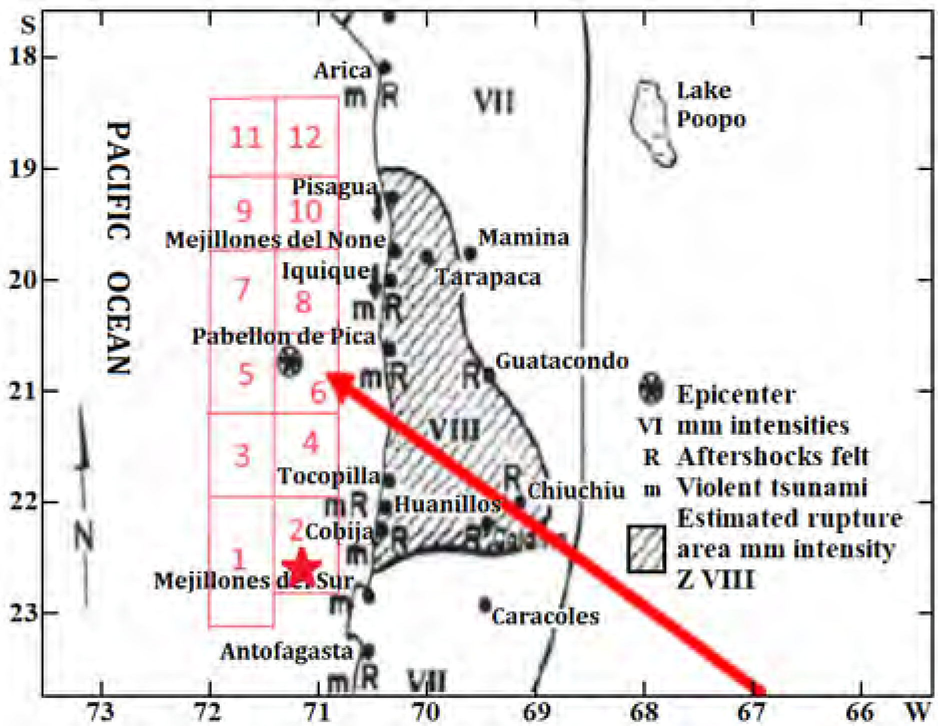

Fig. 15. Corrected epicenter of the 1877 earthquake Chile (block 6 (21 S, 71.3 W). (Kausel and Campos, 1992). Initial epicenter (block 2, red asterisk, 21.1 S, 71.3 W).

8. 14 - BLOCK SEISMIC SOURCE. SHIFTED EARTHQUAKE EPICENTER- (SCENARIO 4)

In Fig. 16 below, one can see a complex keyboard block source of the earthquake under consideration with an earthquake epicenter in the area of Caleta Pabellon de Pica. The block 4 being segmented into two sub-blocks allows the movement of the seabed in the source to be corrected. This allows one to more accurately select the distribution of waves in the settlements: Vanilios, Tocopilla and Cobija and others. In this scenario, blocks 4a and 4b will move sequentially and rise higher than in the previous ones. The location of blocks 4a and 4b has been adjusted to reflect the bottom topography near these points. When considering the area of settlements Chanabaya, Iquique, Pisagua, the analysis becomes more complex. An additional, third, offset of some blocks is introduced. With the new localization of the earthquake epicenter and the dynamics of the earthquake source, 11 additional scenarios of computations were carried out. Here, as more closer to some documentary data, scenario 4 (scenario 23) is given, where an additional, third offset is introduced for blocks 1, 4a, 7, 11 (see Table 7).

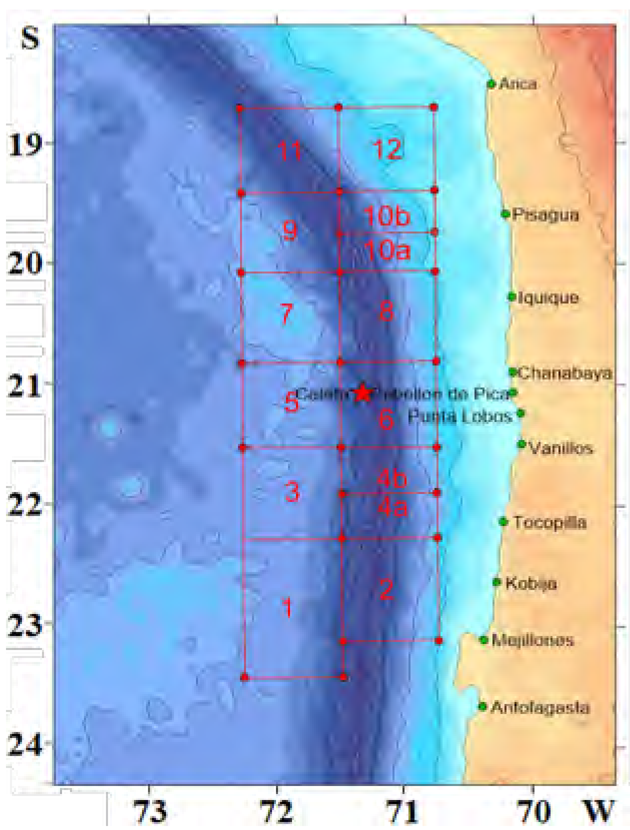

Fig. 16. Source of the earthquake of 1877: 14 blocks (Scenario 4)

Table 7. Sequence of movement of blocks for Scenario 4

Move ment	Block Lumber	1	2	3	4^a	4b	5	6	7	8	9	10^a	10b	11	12
1	Height (m)	-3,5	2	5,5	3,5	3	0	-3	1	-1	1	1,5	-3	2	4
	Start time of movement (s)	90	75	60	30	30		15	0	0	45	45	45	120	105
	Final time of movement (s)	105	90	75	45	45		30	15	15	60	60	60	135	120
2	Height (m)	3			1,5									1,5	
	Start time of movement (s)	165			150									135	
	Final time of movement (s)	180			165									150	

Figure 17 shows a histogram of the distribution of the maximum tsunami wave heights along the considered coastal area for a 14-block seismic source for Scenario 4.

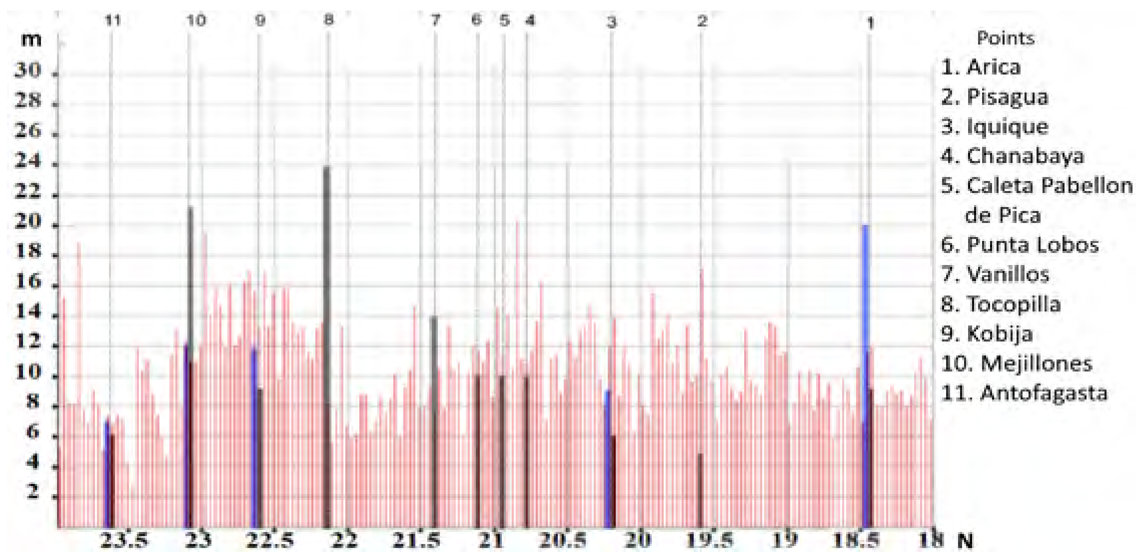

Fig. 17. Histogram of the distribution of the maximum heights of tsunami waves along the considered coastal area for a 14-block source: red color - calculated histogram; gray - data from the catalogue by S. L. Soloviev and Ch.N. Go; blue - data from works (Diaz, 1992; Barrientos, and Ward, 2009; Comte and Pardo, 1991). (Scenario 4).

Figure 18 shows the picture of the propagation of tsunami waves for 9 times moments and the distribution of the maximum wave heights over the computed water area. Panel 1 shows the generated tsunami source, and panels 2-9 show sequentially propagating wave fronts over the computed water area. Panel 10 shows the maximum wave heights distribution over the water area. Table 8 shows the computation data for the selected scenarios.

It can be seen that with an increase in the segmentation of the blocks from which the earthquake source was made into smaller ones (Scenarios: 1 → 2 → 3 → 4), the computation data noticeably approached the documentary data. When changing the localization of the earthquake epicenter and the appropriate selection of the kinematic movement of the keyboard blocks, the values of the wave heights most consistent with data were obtained (scenario 4).

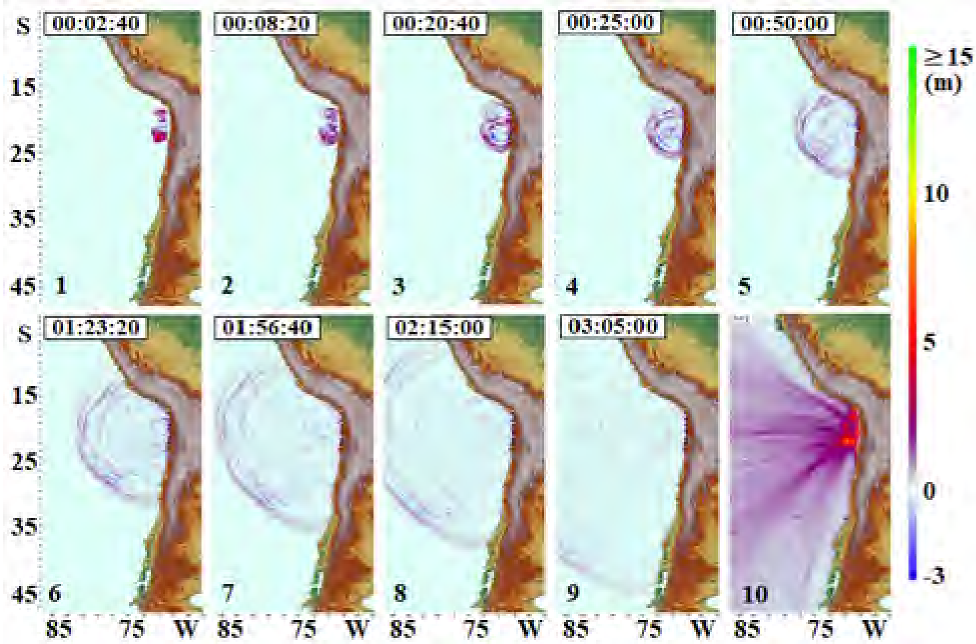

Fig. 18. Tsunami wave propagation under scenario 4 (numbers 1–9) and distribution of maximum wave heights in the computation water area (10)

Table 8. Results of numerical modeling of the seismic source and computations of the heights of tsunami waves with a changed localization of the epicenter of the 1877 earthquake

Points	Arica	Pisagua	Iquique	Chana-baya	Caleta Pabellon de Pica	Punta Lobos	Vanillos	Tocopilla	Kobija	Mejillones	Antofagasta
Real data, m	9 (20)	5	6 (9)	10	10	10	14	24	9 (12)	21 (12)	6 (7)
Scenario 1	7	20	7	19	22	20	22	15	14	12	10
Scenario 2	3	9	15,5	14	14,5	17,5	10	9	6	8	4
Scenario 3	8	6	7	8	11	18	19	14	15	14	5
Scenario 4	7	12	13	8	8	12	11	11	12	10	12

The most adequate, seems to be the scenario 4 (scenario 23 from a series of computations). The computation was carried out on a 5-meter isobath, which allowed us to reduce the computation time for each scenario and choose the best one according to the given wave heights on a particular isobath. At the same time, the wave height on the shore will be different, namely, slightly higher, since when recalculating from isobath to shore for the considered points of this coast, the recalculation coefficients evaluated are in the range from 1.07 to 1.8. (see, for example, (Pelinovsky & Mazova, 1992).

Thus, the performed analysis leads to positive results in the simulation of tsunami waves showed that the keyboard-block model of the subduction zone, even in a simplified kinematic formulation, most adequately describes the possible mechanism of the seismic process. You can see that the histogram has "outliers" in a number of points, which, in general, correspond to ambiguous documentary data on the event in question.

CONCLUSIONS

The article deals with a historical event: an earthquake and tsunami on May 9, 1877 with a source located off the northwestern coast of Chile. Within the framework of the keyboard-block model of the earthquake source, the article considers 4 series of calculations with different segmentation of the earthquake source. In total, 23 scenarios were considered, of which 4 calculations are presented in the article with the characteristics of the wave fields closest to each option along the Chilean coast. The transition from series to series is associated with increased segmentation, i.e. by changing the size of the blocks in the earthquake source, it made it possible to obtain closer values for the distribution of maximum wave heights along the coastal area of the central part of Chile. The choice of the dynamics of the seismic source was complicated by significantly different historical data, both on the recorded wave heights on the coast after the of tsunami waves propagation, and inaccurate data on the localization of the earthquake epicenter. The results of calculating the maximum wave heights for 4 various source segmentations show that the keyboard-block source model used in our work to model the generation and propagation of a tsunami wave for the Chilean coast seems to be the most suitable for the 1877 tsunami. The use of a simplified geodynamic model of the Lobkowski seismic source made it possible to obtain the most adequate model solution in terms of less discrepancy between model and historical data for a number of coastal areas.

ACKNOWLEDGEMENTS

This study was supported by the Russian Science Foundation, Project No. 20-17-00140.

REFERENCES

Abe, K., (1972). Tsunami and mechanism of great earthquakes. *Physics of the Earth and Planetary Interior*, *7,* 143-153.

Araneda, M., Avendaño, M.S., Díaz, Gerardo del Río, (2003). Cambios físicos detectados después del sismo de 1995, Antofagasta, Chile. Revista Geofísica Nº59. Instituto Panamericano de Geografia e Historia IPGH. https://www.revistasipgh.org/index.php/regeofi/article/view/565

Barrientos, S., Ward, S.N. (2009). The 1868 (Southern Peru) and 1877 (Northern Chile) tsunamis recorded at Fort Point, California. *XII Congreso Geológico Chileno Santiago*, 22-26 Noviembre, 2009.

Chlieh, M., Perfettini, H., Tavera, H., Avouac, J. P., Remy, D., Nocquet, J. M., Bonvalot, S. (2011). Interseismic coupling and seismic potential along the Central Andes subduction zone,. *Journal of Geophysical Research: Solid Earth,* 116, Vol. B12

CIGIDEN (2017) “Elaboración de un escenario sísmico en Iquique” pp.17-23 Santiago, Chile.

Comte, D., & Pardo, M. (1991). Reappraisal of Great Historical Earthquakes in the Northern Chile and Southern Peru Seismic Gaps, *Natural Hazards, 4,*23-44.

DATA (2021) Materials of "Centro Ingeniería Mitigación Catástrofes Naturales Facultad de ingeniería (University of Antofagasta, Chile).

Diaz, J. (1992). Estudio de Fuentes de Tsunamis y de Terremotos: Aplicación en el Norte de Chile y Sur de Perú. Tesis para optar el título profesional de Oceanógrafo. Escuela de Ciencias del Mar, Facultad de Recursos naturales, Universidad Católica de Valparaíso

Electronic bathymetry Gebco Digital Atlas [Electronic resource]. - Access mode: http://www.gebco.net

González-Carrasco, J.F., González, G., Aranguiz, R., Melgar, D., Zamora, N., Shrivastava, M.N., Das, R., Catalan, P.A., Cienfuegos, R. (2020). A hybrid deterministic and stochastic approach for tsunami hazard assessment in Iquique, Chile. *Natural Hazards, 100,* 231–254.

Gusiakov, V.K. (2021), Global Tsunami Database, 2100 BC to Present, (2021). Novosibirsk Tsunami Laboratory, Institute of Computational Mathematics and Mathematical Geophysics, 4. Siberian Division of the Russian Academy of Sciences, Available at: https://tsun.sscc.ru/nh/ tsunami.php, Accessed 19.06.2021.

Iida K. (1963) A relation of earthquake energy to tsunami energy and the estimation of the vertical displacement in a tsunami source.- J.Earth Sci, Nagoya Univ., v.11, N.1, p.49-67.

Kanamori, H., & Stewart, G.S. (1978). Seismological aspects of the Guatemala Earthquake of February 4, 1976. *Journal of Geophysical Research: Solid Earth* *83*(B7), 3427-3434.

Kausel, E. & Campos, J., (1992). The *M* = 8 tensional earthquake of 9 December 1950 of northern Chile and its relation to the seismic potential of the region. *Physics of the Earth and Planetapy Interior*, *72*, 220—235.

Kulikov, E.A., Rabinovich, A.B., & Thomson, R.E. (2005). Estimation of tsunami risk for the coasts of Peru and Northern Chile. *Natural Hazards*, *35*(2), 185-209; https://doi.org/10.1007/ s11069-004-4809-3

Lay, T., & Kanamori, H. (1981). An asperity model of large earthquake sequences. Earthquake prediction: An international review. Washington, D.C.: AGU. 1981. P. 579–592.

Lobkovsky, L. I., & Baranov, B.V. (1984). Keyboard model of strong earthquakes in island arcs and active continental margins. *Doklady of the Academy of Sciences of the USSR. 275*, 843-847 (in Russian).

Lobkovsky, L.I., Mazova, R.Kh., Kataeva, L.Yu., Baranov B.V. (2006). Generation and propagation of catastrophic tsunamis in the Sea of Okhotsk. Possible scenarios. *Doklady RAS*. . *410*, 528-531.

Lobkovsky L.I., .Baranov G. B., Mazova R., Baranova N., 2017. Modeling Features of Both the Rupture Process and the Local Tsunami Wave Field from the 2011 Tohoku Earthquake // Pure Appl. Geophys. (2017). V.174, p. 3919-3938, doi:10.1007/s00024-017-1539-5 (March 2017) pp.1-20.

Marchuk, A.G., Chubarov, L.B., Shokin, Yu.I. (1983). *Numerical modeling of tsunami waves*. (Nauka Press, Moscow, USSR, in Russian).

Mazova, R.Kh., & Ramirez, J.F. (1999). Tsunami waves with an initial negative wave on the Chilean coast. *Natural Hazards 20*, 83-92.

Mazova R.Kh., Tyuntyayev S., Giniyatullin A. EtAl., 2020. Numerical Simulation of Earthquakes and Tsunami in Mexico. Case Study: Earthquake and Tsunami of 8 September 2018//STH, V.39, N 4, p.210-227 (2020).

Mendoza, C., (1997). (USGS) "Basic Seismology for Geotechnics, Construction and Risks", course. Faculty of Engineering. University of Antofagasta. 6-7 Nov 1997. (private communication).

Okada, Y. (1992). Internal deformation due to shear and tensile faults in a half-space. *Bulletin of Seismological Society of America 82*, 1018-1040.

Okal, E.A., Borrero, J.C., Synolakis, C.E. (2006). Evaluation of tsunami risk from regional earthquakes at Pisco, Peru. *Bulletin of Seismological Society of America 96*, 1634–1648. https://doi.org/10.1785/ 0120050158

Pararas-Carayannis, G. (2010). The earthquake and tsunami of 27 February 2010 in Chile - Evaluation of source mechanism and of near- and far-field tsunami effects. *Science of Tsunami Hazards 29*, 96-126.

Pelinovsky, E. (1996). Hydrodynamics of tsunami waves. (IAP of the Russian Academy of Sciences, Nizhny Novgorod, RUSSIA).

Ramirez, J. Titichoca, H. Lander, J. & Whiteside, L. (1997). The minor destructive tsunami occurring near Antofagsta, northen Chile, July 30 1995. *Science of Tsunami Hazards*, *15*(1), 3-22.

Riquelme, S., Schwarze H., Fuentes M., & Campos J. (2020). Nearfield effects of earthquake rupture velocity into tsunami runup heights, *Journal of Geophysical Research*. *125*(6), e2019JB018946.

Ruiz, S, & Madariaga, R. (2018). Historical and recent large megathrust earthquakes in Chile. *Tectonophysics 733*, 37-56, https:doi.org/10.1016/j.tecto.2018.01.015.

Ruiz, J.A., Fuentes, M, Riquelme, S., Campos. J., Cisternas. A. (2015). Numerical simulation of tsunami runup in northern Chile based on non-uniform k22 slip distributions. *Natural Hazards 79*, 1177–1198.

Silgado, E. (1985), Destructive Earthquakes of South America 1530–1894, Earthquake Mitigation Program in the Andean Region, Vol. 10, CERESIS, Lima, Peru, 328 pp.

Soloviev, S.L., and Go, Ch. N. (1975), Catalogue of Tsunamis on the Eastern Shore of the Pacific Ocean, Nauka, Moscow, 310 pp. [in Russian; English Translation: Canadian Transl. Fish. Aquatic Sci., No. 5077, Ottawa, 1984, 439 pp.].

Titichoca, H. & Guiñez, D. (1992). Recontitución paleogeográfica de las curvas de inundación producidas por tsunami en el norte de Chile Iquique-Arica en los años 1868-1877. II Congreso de Ciencias de la Tierra. Instituto Geográfico Militar Santiago Chile.

Vargas, G., Ortlieb, L., Chapron, E., Valdés, J., Marquardt C. (2005). "Paleoseismic inferences from high resolution marine sedimentary record in northern Chile (23°S)". *Tectonophysics 399* (1-4), 381-398.

Vidal Gormáz, F., "Datos sobre el terremoto del 9 de mayo de 1877" (1884) pp 193-221 Observatorio Astronómico. Imprenta Nacional. Santiago. Chile.

Wells, D.L., & Coppersmith, K.J. (1994) New empirical relationships among magnitude, rupture length, rupture width, rupture area, and surface displacement Bulletin of Seismical Society of America. *4,* 974-1002.

Voltzinger, N.E., Klevanny, K.A., & Pelinovsky, E.N. (1989). *Long-wave dynamics of the coastal zone,* (Gidrometeoizdat Press, Leningrad, USSR) (in Russian).

Tsunamis in Peru-Chile (noaa.gov).

NGDC/WDS Global Historical Tsunami Database (https://www.ngdc.noaa.gov/hazard/tsu_db.html).

Gebco Digital Atlas

SHOA, 1997

ISSN 8755-6839

SCIENCE OF **TSUNAMI HAZARDS**

Journal of Tsunami Society International

Volume 41 Number 3 2022

RESEARCH PROFILE OF CLIMATE CHANGE AND TSUNAMI MITIGATION: EFFORTS TO REALIZE SDGS 11 AND 13

Eko Hariyono[1], Madlazim[1], Nurita Apridiana Lestari[1], Iqbal Ainur Rizki[1]

Universitas Negeri Surabaya, Surabaya, **INDONESIA**
Email: ekohariyono@unesa.ac.id

ABSTRACT

Both tsunamis and climate change have a significant impact in many aspects. Therefore, it is necessary to conduct research through scientific publications on the most effective mitigation efforts to reduce these impacts. This study's objectives are to analyze the research profile of climate change and tsunami mitigation using bibliometric analysis. A total of 1750 climate change mitigation documents and 139 tsunami mitigation documents were analyzed. The study results show that the publication of climate change mitigation has increased rapidly in the last decade exponentially, while the publication of tsunami mitigation tends to stagnate. Furthermore, research trends in climate change mitigation, namely emission control, environmental policy, and carbon sequestration, are the most researched mitigation efforts. Meanwhile, the leading causes of climate change are greenhouse gases and carbon dioxide. On the other hand, the trend of tsunami mitigation research is more towards disaster management and mitigation, the causes of tsunamis by earthquakes, and coastal area mitigation objects. The research profile on climate change mitigation follows the 13th goal of the SDGs, namely climate action, while tsunami mitigation follows the 11th goal of the SDGs.

***Keywords**: Climate Change, Tsunami, Mitigation*

1. INTRODUCTION

The United Nations has initiated the Sustainable Development Goals (SDGs), a global commitment that includes 17 goals. The development commitment focuses on human development and pays attention to aspects of urban development, society, and the environment (Parnell, 2016). This is stated in the 11th goal (Sustainable Cities and Communities), which mainly focuses on building inclusive, safe, durable, and sustainable cities and settlements. In addition, the 13th goal (Climate Action) also focuses on tackling climate change by taking swift action to deal with climate change and its impacts. There are many ways to realize these two goals, one of which is through efforts to mitigate and reduce the risks of tsunamis and climate change. Therefore, a tsunami mitigation system with a particular focus on community awareness and preparedness to respond is very relevant to the 11th goal of SDGs (Kumar & Manneela, 2021). Meanwhile, climate change mitigation is the primary goal of the 13 SDGs, namely combating climate change (Doni et al., 2020).

A tsunami is a large wave with a speed of up to 900 km/h caused by disturbances on the seabed, such as earthquakes (Guler et al., 2018; Kumaat et al., 2018; Satake et al., 2020). Tsunamis may have significant repercussions on crucial infrastructure, direct and indirect societal losses, necessary supply lines, criminality, increased unemployment, and mental health concerns if preparation is not handled effectively (Himaz, 2022). In general, one of the reasons the tsunami was so devastating was that the tsunami warning system was still inadequate at the time, unable to issue advisories or warnings to communities, particularly in rural areas (Suprapto et al., 2022). One of the most famous tsunami phenomena is the tsunami in the Indian Ocean on December 26, 2004, which hit off the west coast of Sumatra (Aceh), causing the deaths of up to 150,000 people (Satyarno, 2013).

Climate change refers to long-term temperature and weather changes that can seriously affect the planet (Fu & Waltman, 2022). For example, extreme weather events such as heavy rains and heat waves are caused by climate change, and floods are becoming more common due to global warming (Taylor et al., 2014). In addition, environmental factors such as rising temperatures and greenhouse gas levels impact plant growth and wildlife, posing a growing threat to plant resources, biodiversity, and global food security (Chakraborty & Newton, 2011). Thus, the issue of climate change is critical and urgent today because it has a massive and global impact.

Based on the impacts caused by both tsunamis and climate change, it is necessary to conduct research through scientific publications on the most effective mitigation efforts to reduce these impacts. Scientific publications provide essential insight into how the scientific community responds to climate change and tsunamis because they reflect the priorities set by governments that support climate change and tsunami research as well as the study areas that scientists choose to focus on (Fu & Waltman, 2022). However, the rapidly increasing number of climate change and tsunami publications makes it difficult for this field researchers to keep an up-to-date overview of the literature (Rodrigues et al., 2014). Bibliometrics is a powerful method for quantitatively analyzing the development of scientific literature in a research field, and it has been widely used in many global studies (Kokol et al., 2021; Oliveira, 2019; Suprapto et al., 2022).

Therefore, this study will conduct a bibliometric analysis to determine the research profile on climate change mitigation and tsunamis. This research also discusses the wedges or relationships between climate change and tsunamis. The contribution of this research will provide information to researchers and policymakers on climate change and tsunamis regarding appropriate mitigation efforts to realize SDGs 11 and 13. The specific objectives of this study are as follows:

1. Analyzing the number of publications by year on climate change mitigation and tsunamis.
2. Analyzing the most productive countries and affiliations of climate change and tsunami mitigation publications.
3. Analyzing researcher profiles and source titles of climate change and tsunami mitigation publications.
4. Identifying the keywords occurrence and its visualizations mapping of climate change and tsunami mitigation publications.
5. Analyzing the intersection or linkage between the impacts of climate change on tsunamis.
6. Analyzing the relationship between climate change and tsunami mitigation with efforts to realize SDGs 11 and 13.

2. METHOD

This study used bibliometrics to provide a precise method to evaluate the contribution of a paper to the advancement of knowledge (Chen & Ho, 2015; Moyle et al., 2021; Nurhasan et al., 2022), especially in climate change and tsunami mitigation. The steps of conducting bibliometric research include: finding keywords, initial search results, refinement of the search, compiling initial data statistics, and data analysis (see Figure 1).

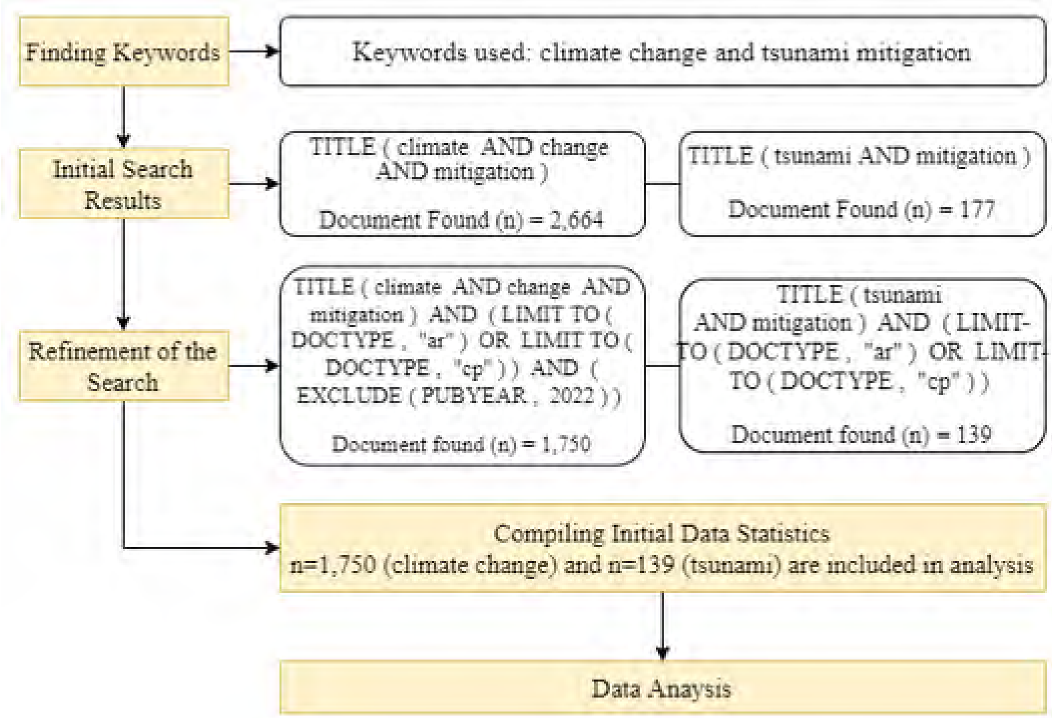

Figure 1. Research process and metadata collection

2.1 Finding Keywords

The keywords used are in accordance with the research objectives, namely "climate change mitigation" and "tsunami mitigation". The search year is also limited to 2021, as in 2022, the number of publications will still continue. The metadata used for data mining is the

Scopus database (www.scopus.com) because it has the world's largest academic database, with citations that provide abstracts from various scientific and research literature that have been examined, making it useful for visualizing, tracking, and evaluating publications.

2.2 Initial Search Results

Data mining will be carried out on June 16, 2022. Preliminary search results can find 2,664 documents for climate change mitigation and 177 for tsunami mitigation. However, this raw data still needs to be filtrated later.

2.3 Refinement of the Search

The findings are then specifically filtered for documents in journals and conference proceedings because these documents contain primary research results that are more credible and up-to-date than books, book chapters, and editorials because they are peer-reviewed by experts. After screening and filtering, 1,750 documents were found for climate change mitigation and 139 for tsunami mitigation.

2.4 Compiling Initial Data Statistics

The final document is then extracted in .csv format and inserted in VOS viewer and Microsoft Excel applications to visualize the data into graphs, tables, and maps. These applications were chosen because they are open source, produce simple visualizations, and can operate on large databases (van Eck & Waltman, 2010).

2.5 Data Analysis

The climate change and tsunami mitigation publications were analysed descriptively to determine the type of publication, distribution of articles/papers by year, publication source, author, institution, country, and keywords. Based on the results of mapping or visualization with VOS viewer, analysis can also be performed by looking at node size and link strength. Finally, the analysis was carried out based on a literature review to determine the intersection and linkage between climate change and tsunamis.

3. RESULTS AND DISCUSSION

3.1 Publications by Year

The publication trend of climate change and tsunami mitigation by year can be seen in Figure 2. The orange graph shows the trend of climate change mitigation publications has increased very rapidly in the last decade exponentially with equations $y = 0.3662x^2 – 1462.7x + 1E+06$. For example, if in 2011 there were 80 documents, then in 2021 there were 219 documents, so there was an increase of up to 273.75%. One of the triggers was that on November 28, 2011 in Durban, South Africa, there was a conference that discussed reaching a new agreement for reducing greenhouse gas emissions and other pollutants to combat climate change (Roberts, 2016). The problem of climate change is currently still in a critical phase, so many researchers are to find the most appropriate mitigation efforts.

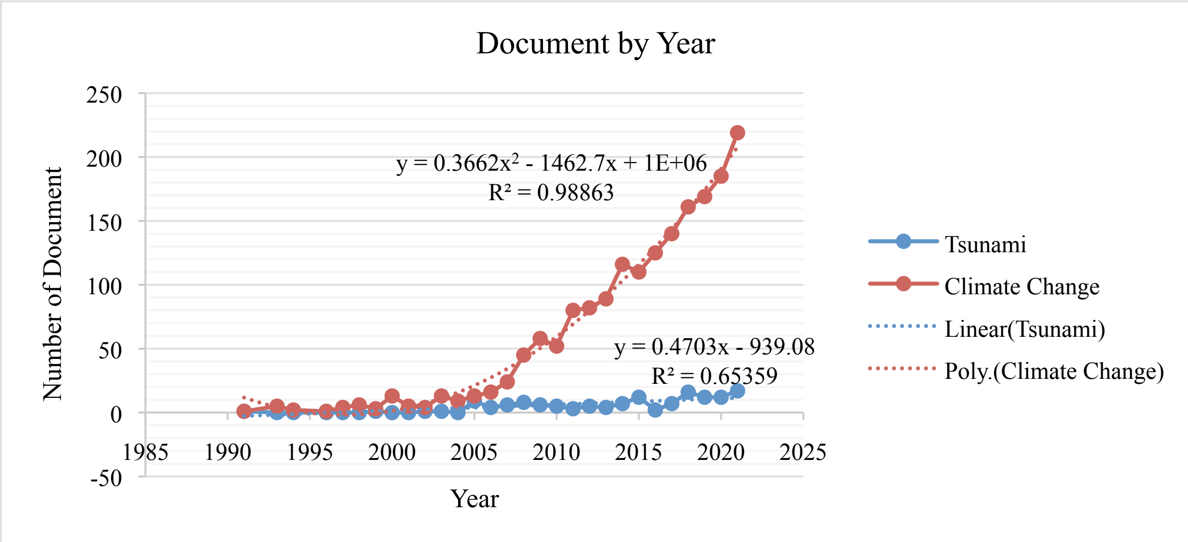

Figure 2. Distribution of climate change and tsunami mitigation publications by year

Contrary to climate change, tsunami mitigation publications tend to stagnate, and there is no significant increase. However, if it looks at the pattern, the number of publications will increase after a significant tsunami occurs. For example, in 2004 there were no publications on this at all, then in 2005, it increased rapidly to 9 documents. The cause was after the massive tsunami in Aceh, Indonesia, which caused the death of up to 150,000 people.

3.2 Countries and Affiliations

A list of the top 10 countries in the publication climate change and tsunami mitigation can be seen in Table 1. The United States is the richest country in climate change mitigation, with 424 publications. Followed by the United Kingdom with (n=217) publications, Germany (n=191), Australia (n=115), and China (n=105). Meanwhile, Japan led the highest number of publications in tsunami mitigation with 47. Followed by Indonesia (n=39), United States (n=25), United Kingdom (n=6), and China, India, New Zealand, and Sri Lanka 5 each. The majority of countries that dominate tsunami publications have coastlines prone to tsunami hazards, such as Japan, Indonesia, and Chile (Esteban et al., 2013; Mulia & Satake, 2020).

Table 1. Top 10 countries with the most climate change and tsunami mitigation publications

Climate Change		**Tsunami**	
Country	**Amount**	**Country**	**Amount**
United States	424	Japan	47
United Kingdom	217	Indonesia	39
Germany	191	United States	25
Australia	115	United Kingdom	6
China	105	China	5
Netherlands	103	India	5
India	95	New Zealand	5
Canada	93	Sri Lanka	5
France	78	Germany	4
Italy	76	Chile	3

A list of the top 10 affiliates with the most climate change and tsunami mitigation publications can be found in Table 2. In climate change mitigation, the International Institute for Applied Systems Analysis, Laxenburg, became the most productive affiliate with a total of 40 publications. It was followed by *Potsdam Institut fur Klimafolgenforschung* (n=38), Wageningen University & Research (n=33), PBL (*Planbureau voor de Leefomgeving*) Netherlands Environmental Assessment Agency and the University of California, Berkeley 23 each. Meanwhile, Saitama University led the highest number of publications of 12 documents in tsunami mitigation. Then Tohoku University (n=9), The University of Tokyo (n=6), *Institut Teknologi Bandung* and *Universitas Syiah Kuala* 5 documents each. This is in line with the most significant number of countries, where the most domiciled affiliates come from Japan and Indonesia.

Table 2. Top 10 affiliates with the most climate change and tsunami mitigation publications

Climate Change		**Tsunami**	
Affiliation	**Amount**	**Affiliation**	**Amount**
International Institute for Applied Systems Analysis, Laxenburg	40	Saitama University	12
Potsdam Institut fur Klimafolgenforschung	38	Tohoku University	9
Wageningen University & Research	33	The University of Tokyo	6
PBL Netherlands Environmental Assessment Agency	23	*Institut Teknologi Bandung*	5
University of California, Berkeley	23	*Universitas Syiah Kuala*	5
Universiteit Utrecht	22	*Universiti Sains Malaysia*	4
The Australian National University	22	University of Miyazaki	4
National Institute for Environmental Studies of Japan	22	National Oceanic and Atmospheric Administration	4
Helsingin Yliopisto	21	*Universitas Negeri Surabaya*	4
Lawrence Berkeley National Laboratory	20	The University of Auckland	3

3.3 Researcher Profile and Subject Area

The list of the top 10 researchers with the most climate change and tsunami mitigation publications can be seen in Table 3. On the topic of climate change mitigation, van Vuuren became the most prolific researcher with 12 documents. One of his articles with the most citations (121 times) titled "Exploring SSP land-use dynamics using the IMAGE model: Regional and gridded scenarios of land-use change and land-based climate change mitigation" which describes regional and gridded scenarios up to the year 2100 were generated using five iterations of the Shared Socio-economic Pathways (SSP) within the framework of the IMAGE 3.0 integrated assessment model. This collection of SSP land-use scenarios provides a thorough quantification of interrelated trends in the land system, both socioeconomically and biophysically (Doelman et al., 2018). The other researchers with the highest number of documents are Fujimori and Smith (11 each), Creutzig, Hasegawa, and Popp (10 each).

Table 3. Top 10 researchers with the most climate change and tsunami mitigation publications

Climate Change		Tsunami	
Researcher	**Amount**	**Researcher**	**Amount**
van Vuuren, D.P.	12	Tanaka, N.	11
Fujimori, S.	11	Imamura, F.	4
Smith, P.	11	Koshimura, S.	4
Creutzig, F.	10	Muhari, A.	4
Hasegawa, T.	10	Nandasena, N.A.K.	4
Popp, A.	10	Bernard, E.N.	4
Kurz, W.A.	9	Comfort, L.K.	4
Bauer, N.	7	Dengler, L.	3
Daioglou, V.	7	Hariyono, E.	3
Edenhofer, O.	7	Igarashi, Y.	3

Meanwhile, Tanaka became the most productive researcher on the topic of tsunami mitigation with 11 documents. One of his articles with the most citations (102 times) was titled "Vegetation bioshields for tsunami mitigation: A review of effectiveness, limitations, construction, and sustainable management" which conducted a review of vegetation bioshields for tsunami mitigation. This paper highlighted that proper planning and management of vegetation are required to maintain the tsunami buffering function of coastal forests (Tanaka, 2009). Other researchers with 4 documents are Imamura, Koshimura, Muhari, Nandasena, Bernard, and Comfort.

A list of the top 10 subject areas with the most climate change and tsunami mitigation publications can be found in Table 4.

Table 4. Top 10 source titles with the most climate change and tsunami mitigation publications

Climate Change		Tsunami	
Source Title	**Amount**	**Source Title**	**Amount**
Climatic Change	59	Natural Hazards	8
Mitigation And Adaptation Strategies For Global Change	49	IOP Conference Series Earth And Environmental Science	6
Energy Policy	46	AIP Conference Proceedings	5
Journal of Cleaner Production	38	International Journal of Disaster Risk Reduction	5
Climate Policy	37	Journal Of Physics Conference Series	5
Environmental Research Letters	36	Ocean Engineering	5
IOP Conference Series Earth And Environmental Science	36	Journal Of Earthquake And Tsunami	4
Sustainability Switzerland	35	Proceedings Of The International Offshore And Polar Engineering Conference	4
Global Environmental Change	23	Pure And Applied Geophysics	4
Environmental Science And Policy	18	Science of Tsunami Hazards	3

On the topic of climate change mitigation, "Climatic Change" is the source with the most publications, namely 59 documents. This source has Scopus CiteScore 7.4 as of 2021 and the 84th percentile for Atmospheric Science and 81st percentile for Global and Planetary Change. One of the articles with the most citations (4437 times) on the Climatic Change source is titled "The representative concentration pathways: An overview". This paper summarizes the method of creation and critical features of the Representative Concentration Pathways (RCPs), a group of four new pathways created for the climate modeling community as the foundation for both long-term and short-term modeling experiments. Some of the other sources with the highest number of documents are Mitigation And Adaptation Strategies For Global Change (n=49), Energy Policy (n=46), Journal of Cleaner Production (n=38), and Climate Policy (n=37).

Meanwhile, on the tsunami mitigation topic, "Natural Hazards" became the most published source with eight documents. One of his articles with the most citations (774 times) was titled "People at risk of flooding: Why some residents take precautionary action while others do not", the results of this study showed that the explanatory power of the socio-psychological model, with important implications for public risk communication efforts. It is crucial to convey not only the risk of flooding and its potential consequences, but also the possibility, effectiveness, and cost of taking private precautions in order to encourage residents in flood-prone areas to contribute to damage prevention (Grothmann & Reusswig, 2006). Other sources with the highest number of documents afterwards are IOP Conference Series Earth And Environmental Science (n=6), AIP Conference Proceedings, International Journal of Disaster Risk Reduction, Journal of Physics Conference Series, and Ocean Engineering (5 each).

3.4 Keyword Trends

A list of the top 10 keywords in climate change and tsunami mitigation research can be seen in Table 5.

Table 5. Top 10 keywords with the most climate change and tsunami mitigation publications

Climate Change		**Tsunami**	
Keyword	**Occurence**	**Keyword**	**Occurence**
Climate Change	1406	Tsunamis	73
Climate Change Mitigation	541	Tsunami	60
Mitigation	500	Disasters	34
Greenhouse Gases	263	Earthquakes	21
Greenhouse Gas	261	Mitigation	16
Emission Control	259	Disaster Management	15
Carbon Dioxide	233	Tsunami Disaster	15
Environmental Policy	224	Disaster Mitigation	14
Carbon	174	Coastal Zones	12
Carbon Sequestration	166	Hazards	12

It can be seen that the most keywords occurring in climate change mitigation research are climate change (n=1406), climate change mitigation (n=541), mitigation (n=500), greenhouse gases (n=263), greenhouse gas (n=261), emission control (n=259), carbon dioxide (n=233), environmental policy (n=224), carbon (n=174), and carbon sequestration (n=166).

Based on the list, it can be seen that emission control, environmental policy, and carbon sequestration are the most researched mitigation efforts. Meanwhile, the main causes of climate change are greenhouse gases and carbon dioxide. Consistent with Huang et al. (2020); B. Wang et al. (2014); Z. Wang et al. (2018) found that some of the most popular keywords in climate change research are climate change, mitigation, carbon sequestration, and carbon dioxide.

On the topic of tsunami mitigation, the most widely used keywords are Tsunamis (n=73), Tsunami (n=60), Disasters (n=34), Earthquakes (n=21), Mitigation (n=16), Disaster Management (n=15), Tsunami Disaster (n=15), Disaster Mitigation (n=14), Coastal Zones (n=12), and Hazards (n=12). Based on the list, it can be seen that research trends 1) mitigation efforts are more towards disaster management and mitigation; 2) the cause of the tsunami from the earthquake; 3) the object of mitigation is the coastal area. These findings are in line with research by (Chiu & Ho, 2007; Suprapto et al., 2022), who also found that earthquake, disaster mitigation, and tsunami disaster are the top keyword trends in research on tsunamis.

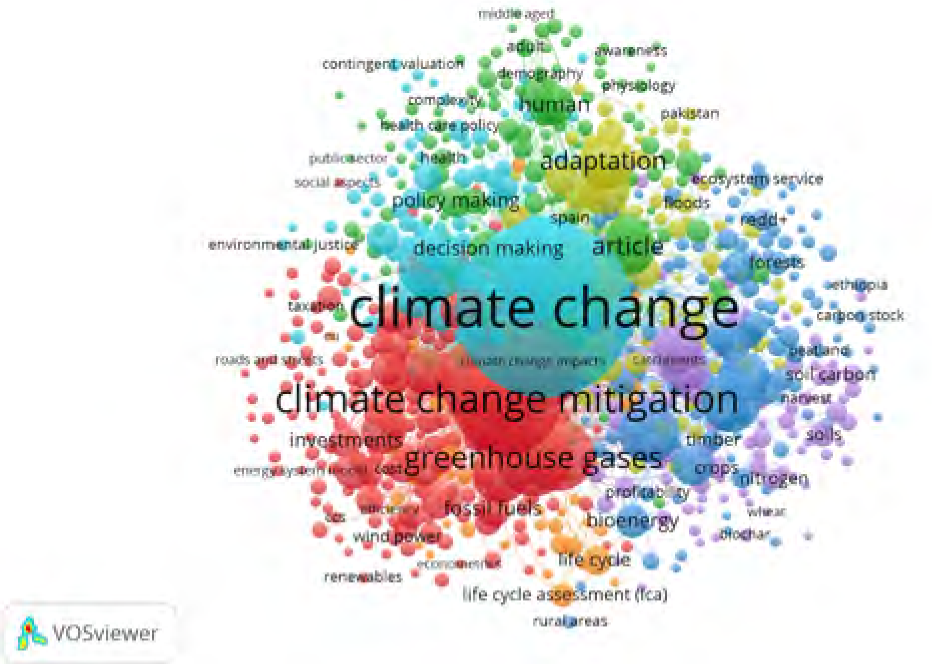

Figure 3. Visualization of Keyword Mapping in Climate Change Mitigation

Figure 3 shows seven clusters in the visualization of keyword mapping for climate change mitigation. In cluster 1 with red nodes (n=217) about aspects of climate change mitigation aspects, such as emission control, energy efficiency, carbon capture, climate models. Cluster 2 with green nodes (n=142) about the role of humans and government, such as human, environmental protection, policy making, decision making, and conservation of natural resources. Cluster 3 with blue nodes (n=126) about objects and locations, such as forest ecosystem, India, Nigeria, wetland, ecosystem, and peatland. Cluster 4 with yellow nodes (n=115) on climate change adaptation, such as adaptation, adaptive management, resilience, disaster management, and risk assessment. Cluster 5 with violet nodes (n=99) about the effect of climate change on the agricultural sector, such as agriculture, food security, land use, food supply, and agricultural emissions. While other clusters have fewer occurrences.

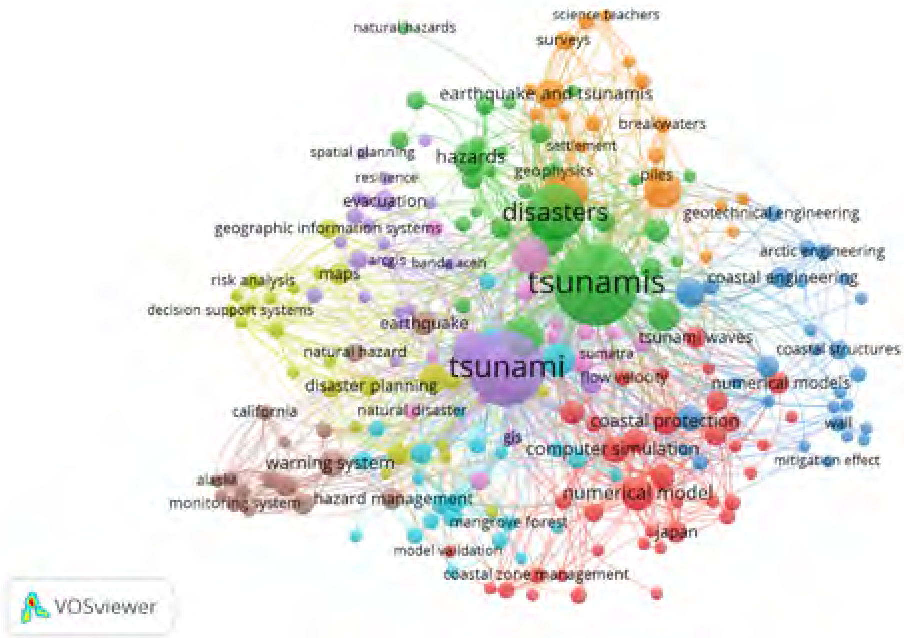

Figure 4. Visualization of Keyword Mapping in Tsunami Mitigation

Figure 4 shows there are nine clusters (n=221) in the visualization of keyword mapping for tsunami mitigation. In cluster 1 with red nodes (n=38) about coastal areas, such as coastal protection, coastal forest, coastal zone management, and coastal mitigation. Cluster 2 with green nodes (n=31) about evacuation, such as evacuation planning, evacuation route, evacuation modeling, and disaster prevention. Cluster 3 with blue nodes (n=28) on engineering aspects, such as arctic engineering, barrier (equipment), coastal engineering, impact force, and underwater foundations. Cluster 4 with yellow nodes (n=24) about aspects of informatics, such as geographic information, complex networks, information systems, and artificial intelligence. Cluster 5 with violet nodes (n=24) about tsunami-prone countries/areas, such as Banda Aceh, Java, Chile, and Indonesia. In comparison, other clusters have a smaller number of items.

3.5 Impacts of climate change on tsunamis

The most significant impact of climate change is the rise in global temperature or global warming. The average temperature of the Earth's climate system is rising over a lengthy period of time due to global warming. Rising sea levels, altered precipitation patterns, and the subtropical expansion of deserts are all ongoing or projected implications. Global sea level will increase by up to 60 cm by the end of the 21st century as a result of ocean warming and glacier melting, according to the Fourth Assessment Report of the Intergovernmental Panel on Climate Change (IPCC, 2007). Several types of research also revealed the possibility of a future sea-level rise of up to 2 m by 2100 (e.g., Grinsted et al., 2010; Martin & Stefan, 2009).

Independent of earthquake-triggered tsunamis, global warming, a long-term event, is expected to result in an accelerated increase in sea-level rise (Meehl et al., 2005; Nicholls & Cazenave, 2010). This may lead to a higher risk of inundating low-lying coastal areas (Galbraith et al., 2002). Consequently, damages due to coastal floods are expected to increase significantly during the 21st century and beyond as the sea level rises, making socio-economic damages in coastal regions more prevalent.

Yavuz et al. (2020) have done simulations using NAMI-DANCE software and showed that social risk level decreases due to sea-level rise and sea level rise+earthquake triggered tsunamis for Fethiye City Center due to a decrease in PGR from 2080 to 2100. However, relative to 2020, social risks due to sea level rise+earthquake triggered tsunamis at Fethiye and Cairo increased almost 90 and 900 fold, respectively. In conclusion, sea-level rise effects influence both sites' economic and social risks. However, this influence does not show the same trend at both sites. The topography of the region, proximity to the earthquake zones, economic growth rates, and population levels are other factors that need to be considered in this analysis.

Shao et al. (2019) study of the influence of climate change on the tsunami-like solitary wave inundation over fringing reefs, the shock-capturing Boussinesq wave model FUNWAVE-TVD was utilized. The numerical experiments clearly showed that as the water depth over the reef flat increased, there was a significant increase in the horizontal inundation distance over the back-reef beach. As the sea level rises, the impact of a tsunami will be worse over the back-reef beach, particularly in areas that are closer to the original shoreline in the inundation zone. Additional protective measures or adaptations might be required to lessen the tsunami damage that will be greatly increased by future sea-level rise for the low-lying zones of the reef-lined coasts. Sea-level rise has a more significant impact than the detrimental effects of the reef's surface roughness degradation on inundation distance and tsunami damage. The findings presented here give coastal managers a rough idea of how tsunami hazards change over fringing reefs in response to sea-level rise and coral bleaching caused by climate change. In order to mitigate the increased future tsunami hazards that many tropical and sub-tropical shorelines will face, efforts in response to climate change, especially sea-level rise, will be necessary. This is because climate change will significantly impact the protective capability of fringing reefs against tsunami hazards in the future.

3.6 Climate change and tsunami mitigation: efforts to realize SDGs 11 and 13

The research profile on climate change mitigation is in accordance with the 13th goal of the SDGs, namely climate action, while tsunami mitigation is in accordance with the 11th goal of the SDGs because it can provide information to the government, librarians, and subsequent researchers to make the best efforts in mitigating climate change and tsunamis. The government, as a policymaker, can design environmental policies, especially those related to climate change, that are efficient in accordance with the recommendations and research trends that have been carried out. Meanwhile, the government can also pay attention to coastal areas prone to tsunami hazards by making mitigation efforts to reduce the impacts caused, as well as creating resilient, resilient, and sustainable coastal communities. The mapped research profile can also provide information for librarians to provide reputable journal documents to the fullest. Researchers can then explore novelty ideas for developing climate change and tsunami mitigation (according to Figure 3 and Figure 4).

CONCLUSIONS

This study mapped the research profile of climate change and tsunami mitigation as an effort to realize SDGs 11 and 13. The profiles mapped are: (1) The trend of climate change mitigation publications has increased rapidly in the last decade, while tsunami mitigation publications tend to stagnate. (2) The most productive countries and institutions in climate change mitigation are the United States and the International Institute for Applied Systems Analysis Laxenburg, while in the publication of tsunami mitigation are Japan and Saitama

University. (3) The researchers and source titles that have produced the most successful climate change mitigation publications are van Vuuren and Climatic Change, while in tsunami mitigation are Tanaka and Natural Hazards. (4) Research trends in climate change mitigation, namely emission control, environmental policy, and carbon sequestration, are the most researched mitigation efforts. Meanwhile, the leading causes of climate change are greenhouse gases and carbon dioxide. On the other hand, the trend of tsunami mitigation research is more towards disaster management and mitigation, the causes of tsunamis by earthquakes, and coastal area mitigation objects. (5) Climate change will increase global temperatures so that it can trigger sea level rise, as the number of water increases and the impacts caused to coastal areas become significant. (6) The research profile on climate change mitigation follows the 13th goal of the SDGs, namely climate action, while tsunami mitigation follows the 11th goal of the SDGs because it can provide information to the government, librarians, and subsequent researchers to make the best efforts in mitigating climate change and tsunami.

REFERENCES

Chakraborty, S., & Newton, A. C. (2011). Climate change, plant diseases and food security: an overview. *Plant Pathology*, *60*(1), 2–14. https://doi.org/https://doi.org/10.1111/j.1365-3059.2010.02411.x

Chen, H., & Ho, Y.-S. (2015). Highly cited articles in biomass research: A bibliometric analysis. *Renewable and Sustainable Energy Reviews*, *49*, 12–20. https://doi.org/https://doi.org/10.1016/j.rser.2015.04.060

Chiu, W. T., & Ho, Y. S. (2007). Bibliometric analysis of tsunami research. *Scientometrics*, *73*(1), 3–17. https://doi.org/10.1007/s11192-005-1523-1

Doelman, J. C., Stehfest, E., Tabeau, A., van Meijl, H., Lassaletta, L., Gernaat, D. E. H. J., Hermans, K., Harmsen, M., Daioglou, V., Biemans, H., van der Sluis, S., & van Vuuren, D. P. (2018). Exploring SSP land-use dynamics using the IMAGE model: Regional and gridded scenarios of land-use change and land-based climate change mitigation. *Global Environmental Change*, *48*, 119–135. https://doi.org/https://doi.org/10.1016/j.gloenvcha.2017.11.014

Doni, F., Gasperini, A., & Soares, J. T. (2020). What is the SDG 13? In *SDG13 – Climate Action: Combating Climate Change and its Impacts* (pp. 21–30). Emerald Publishing Limited. https://doi.org/10.1108/978-1-78756-915-720201006

Esteban, M., Tsimopoulou, V., Mikami, T., Yun, N. Y., Suppasri, A., & Shibayama, T. (2013). Recent tsunamis events and preparedness: Development of tsunami awareness in Indonesia, Chile and Japan. *International Journal of Disaster Risk Reduction*, *5*, 84–97. https://doi.org/https://doi.org/10.1016/j.ijdrr.2013.07.002

Fu, H.-Z., & Waltman, L. (2022). A large-scale bibliometric analysis of global climate change research between 2001 and 2018. *Climatic Change*, *170*(3), 36. https://doi.org/10.1007/s10584-022-03324-z

Galbraith, H., Jones, R., Park, R., Clough, J., Herrod-Julius, S., Harrington, B., & Page, G. (2002). Global Climate Change and Sea Level Rise: Potential Losses of Intertidal Habitat for Shorebirds. *Waterbirds*, *25*(2), 173–183. https://doi.org/10.1675/1524-4695(2002)025[0173:GCCASL]2.0.CO;2

Grinsted, A., Moore, J. C., & Jevrejeva, S. (2010). Reconstructing sea level from paleo and projected temperatures 200 to 2100 ad. *Climate Dynamics*, *34*(4), 461–472. https://doi.org/10.1007/s00382-008-0507-2

Grothmann, T., & Reusswig, F. (2006). People at Risk of Flooding: Why Some Residents Take Precautionary Action While Others Do Not. *Natural Hazards*, *38*(1), 101–120. https://doi.org/10.1007/s11069-005-8604-6

Guler, H. G., Baykal, C., Arikawa, T., & Yalciner, A. C. (2018). Numerical assessment of tsunami attack on a rubble mound breakwater using OpenFOAM®. *Applied Ocean Research*, *72*, 76–91. https://doi.org/https://doi.org/10.1016/j.apor.2018.01.00

Himaz, R. (2022). Business recovery in Aceh and North Sumatra following the Indian Ocean Tsunami. *International Journal of Disaster Risk Reduction*, *73*, 102868. https://doi.org/https://doi.org/10.1016/j.ijdrr.2022.102868

Huang, L., Chen, K., & Zhou, M. (2020). Climate change and carbon sink: a bibliometric analysis. *Environmental Science and Pollution Research*, *27*(8), 8740–8758. https://doi.org/10.1007/s11356-019-07489-6

IPCC. (2007). *Climate Change 2007: The Physical Science Basis: Contribution of Working Group I to the Fourth Assessment Report of the Intergovernmental Panel on Climate Change*. Cambridge University Press.

Kokol, P., Blažun Vošner, H., & Završnik, J. (2021). Application of bibliometrics in medicine: a historical bibliometrics analysis. *Health Information & Libraries Journal*, *38*(2), 125–138. https://doi.org/https://doi.org/10.1111/hir.12295

Kumaat, J. C., Kandoli, S. T. B., & Laeloma, F. (2018). Spatial Modeling of Tsunami Impact in Manado City using Geographic Information System. *IOP Conference Series: Materials Science and Engineering*, *306*(1). https://doi.org/10.1088/1757-899X/306/1/012069

Kumar, T. S., & Manneela, S. (2021). A Review of the Progress, Challenges and Future Trends in Tsunami Early Warning Systems. *Journal of the Geological Society of India*, *97*(12), 1533–1544. https://doi.org/10.1007/s12594-021-1910-0

Martin, V., & Stefan, R. (2009). Global sea level linked to global temperature. *Proceedings of the National Academy of Sciences*, *106*(51), 21527–21532. https://doi.org/10.1073/pnas.0907765106

Meehl, G. A., Washington, W. M., Collins, W. D., Arblaster, J. M., Aixue, H., Buja, L. E., Strand, W. G., & Haiyan, T. (2005). How Much More Global Warming and Sea Level Rise? *Science*, *307*(5716), 1769–1772. https://doi.org/10.1126/science.1106663

Moyle, B., Moyle, C., Ruhanen, L., Weaver, D., & Hadinejad, A. (2021). Are we really progressing sustainable tourism research? A bibliometric analysis. *Journal of Sustainable Tourism*, *29*(1), 106–122. https://doi.org/10.1080/09669582.2020.1817048

Mulia, I. E., & Satake, K. (2020). Developments of Tsunami Observing Systems in Japan . In *Frontiers in Earth Science* (Vol. 8). https://www.frontiersin.org/article/10.3389/feart.2020.00145

Nicholls, R. J., & Cazenave, A. (2010). Sea-Level Rise and Its Impact on Coastal Zones. *Science*, *328*(5985), 1517–1520. https://doi.org/10.1126/science.1185782

Nurhasan, N., Prahani, B. K., Suprapto, N., Setiawan, B., Deta, U. A., & Al Ardha, M. A. (2022). Sports Research Trends in the Last 10 Years: Information to Librarians, Researchers, and Policy Makers. *TEM Journal*, *11*(1), 289–296. https://doi.org/10.18421/TEM111-36

Oliveira, O. J. de. (2019). *Bibliometric Method for Mapping the State-of-the-Art and Identifying Research Gaps and Trends in Literature: An Essential Instrument to Support the Development of Scientific Projects* (F. F. da Silva (ed.); p. Ch. 3). IntechOpen. https://doi.org/10.5772/intechopen.85856

Parnell, S. (2016). Defining a Global Urban Development Agenda. *World Development*, *78*, 529–540. https://doi.org/https://doi.org/10.1016/j.worlddev.2015.10.028

Roberts, D. (2016). A global roadmap for climate change action: From COP17 in Durban to COP21 in Paris . In *South African Journal of Science* (Vol. 112, pp. 1–3). scieloza .

Rodrigues, S. P., van Eck, N. J., Waltman, L., & Jansen, F. W. (2014). Mapping patient safety: a large-scale literature review using bibliometric visualisation techniques. *BMJ Open*, *4*(3), e004468. https://doi.org/10.1136/bmjopen-2013-004468

Satake, K., Heidarzadeh, M., Quiroz, M., & Cienfuegos, R. (2020). History and features of trans-oceanic tsunamis and implications for paleo-tsunami studies. *Earth-Science Reviews*, *202*, 103112. https://doi.org/https://doi.org/10.1016/j.earscirev.2020.103112

Satyarno, I. (2013). *Assessment of the 2004/2011 Earthquakes and Tsunamis in Indonesia and Japan: Lesson Learnt and Way Forward BT - Progress of Geo-Disaster Mitigation Technology in Asia* (F. Wang, M. Miyajima, T. Li, W. Shan, & T. F. Fathani (eds.); pp. 277–292). Springer Berlin Heidelberg. https://doi.org/10.1007/978-3-642-29107-4_14

Shao, K., Liu, W., Gao, Y., & Ning, Y. (2019). The influence of climate change on tsunami-like solitary wave inundation over fringing reefs. *Journal of Integrative Environmental Sciences*, *16*(1), 71–88. https://doi.org/10.1080/1943815X.2019.1614071

Suprapto, N., Yanti, V. K., & Hariyono, E. (2022). Global Research on Tsunami Education and Tsunami Mitigation: A Bibliometric Analysis. *Science of Tsunami Hazards*, *41*(2), 130–146.

Tanaka, N. (2009). Vegetation bioshields for tsunami mitigation: review of effectiveness, limitations, construction, and sustainable management. *Landscape and Ecological Engineering*, *5*(1), 71–79. https://doi.org/10.1007/s11355-008-0058-z

Taylor, A., de Bruin, W. B., & Dessai, S. (2014). Climate Change Beliefs and Perceptions of Weather-Related Changes in the United Kingdom. *Risk Analysis*, *34*(11), 1995–2004. https://doi.org/https://doi.org/10.1111/risa.12234

van Eck, N. J., & Waltman, L. (2010). Software survey: VOSviewer, a computer program for bibliometric mapping. *Scientometrics*, *84*(2), 523–538. https://doi.org/10.1007/s11192-009-0146-3

Wang, B., Pan, S.-Y., Ke, R.-Y., Wang, K., & Wei, Y.-M. (2014). An overview of climate change vulnerability: a bibliometric analysis based on Web of Science database. *Natural Hazards*, *74*(3), 1649–1666. https://doi.org/10.1007/s11069-014-1260-y

Wang, Z., Zhao, Y., & Wang, B. (2018). A bibliometric analysis of climate change adaptation based on massive research literature data. *Journal of Cleaner Production*, *199*, 1072–1082. https://doi.org/https://doi.org/10.1016/j.jclepro.2018.06.183

Yavuz, C., Kentel, E., & Aral, M. M. (2020). Climate Change Risk Evaluation of Tsunami Hazards in the Eastern Mediterranean Sea. In *Water* (Vol. 12, Issue 10). https://doi.org/10.3390/w12102881

ISSN 8755-6839

SCIENCE OF **TSUNAMI HAZARDS**

Journal of Tsunami Society International

Volume 41 **Number 3** **2022**

POSSIBLE TSUNAMIS IN THE ARCTIC

Mazova R. Kh., Kurkin A.A., Vinokurov M.S.

Nizhny Novgorod State Technical University n.a. R.E. Alekseev. Russia.
e-mail: ***raissamazova@yandex.ru***

ABSTRACT

The Arctic is the least studied region in terms of problems associated with earthquake and tsunami phenomena. Usually, the tsunami hazard in the Arctic is considered insignificant. This is primarily due to the low seismic activity of the region. In connection with the economic development of the shelf, the problem of tsunami hazard on the Arctic coast becomes to be actual and requires detailed studies of the probable events of tsunami wave generation. This present study considers the potential problem of the tsunami hazard in the Arctic region, and provides estimates of possible tsunami wave heights on the shelves of the Arctic coasts of the Baffin Sea, the Laptev Sea and the Beaufort Sea. On the basis of the keyboard model of the subduction zone, a number of scenarios of the possible occurrence of earthquakes with source in the area of localization of historical source of the earthquake in 1933, (M=7.7, 1964, M=6.7, 1920, M=6.4) were considered.

Key words: *Arctic Ocean, Arctic shelf, earthquake key-board model, tsunami, numerical simulation.*

1. INTRODUCTION

Presently, one of the main priorities is the Arctic Ocean region. Moreover, its geopolitical role and mainly its economic role is increasing globally. The Arctic region has a unique strategic hydrocarbon resource potential. Long-term interests of a large number of nations of the world are associated with the Arctic region. The territories of the Arctic include the northern part of the Earth, which includes five subarctic states. These are: Russia, Canada, the United States of America, Norway and Denmark. In general, today the northern regions are acquiring new significance in connection with the development of world economic ties. Questions of development of Arctic oil and gas resources are relevant due to the strategic importance of hydrocarbons [1-6].

It is well known that most earthquake epicenters are confined to tectonically active faults. In accordance with the classical picture of the division of the lithosphere into plates, the boundary between the North American and Eurasian plates runs along the mid-ocean ridge, stretching from Iceland through the Norwegian-Greenland basin and the Gakkel ridge in the Eurasian basin, and then abuts against the continental shelf of the Laptev Sea. In the Arctic region, modern tectonic processes in the Earth's crust are poorly understood, since stresses and strains in fault zones change rapidly as a result of tectonic movements [5,6,9-11]. For example, the seismicity of the shelf in the water area of the Laptev Sea is well known, but there is little data on the manifestation of past and present-day bottom crustal movements. Nothing much is known about crustal deformations and the possibly weak seismicity on the shelf of the East Siberian Sea. Due to insufficient information on the seismicity of the Arctic region, earthquakes and the possibility of tsunami generation are one of the main causes of man-made accidents in the development of the shelf. This is especially connected with the prospect of the extraction of hydrocarbon resources on the shelf, which are also vulnerable to potential landslides.

In connection with the intensive development of the natural resources of the Arctic, the analysis of the possible occurrence of tsunami waves on the shelves of the Arctic region is one of the priorities for the development of science. Since such natural phenomena as tsunamis have not been adequately studied in the Arctic region, the only possibility for assessing the tsunami hazard on the coasts of this region is by numerical modeling of a possible tsunami occurrences in areas with high tectonic activity, such as in the Lappet Sea [4-6,8,12]. A number of studies completed thus far indicate that tsunami waves in the Arctic can reach as much as 4-5 meters in height. On the Russian side of the shelf, wave heights have been small - up to 1 meter - but with an increase in wave activity, a trend is observed, indicating that these heights can be significantly higher [3,4,6,8]. Studies on the tsunami hazard on the coast of Canada [8,9,11], examined two zones of potential hazard on the Arctic coast: the Baffin Sea and the mouth of the Mackenzie River in the Beaufort Sea [10, 12]. Destructive waves at these two zones can also be generated by local effects such as landslides and icebergs but also by meteorites [5,6,7].

Estimates of potential tsunami wave generation by earthquakes and landslides on the Arctic shelves will result in better planning for the extraction of hydrocarbon resources on the shelf, as well as for the most relevant organization of marine activities. As presented in [9], the first instrumental information about earthquakes in the Arctic was obtained in the beginning of the 20th century and was based mainly on data from remote seismic stations. Basically, only events with magnitude M>5.5 were recorded in the Arctic. Figure 1 [3,8] shows the epicenters of the strongest earthquakes in the Arctic Ocean basin and in adjacent territories. It is clearly seen from this map that the strongest earthquakes in coastal areas, and the more likely to generate tsunamis, can occur in the Baffin, the Greenland, the Laptev, and the Beaufort Seas. These earthquakes in these seas had magnitudes of M>6. As a rule, smaller magnitude earthquakes with sources located far from the coasts, cannot generate tsunamis that can cause significant damage to the coastal infrastructures.

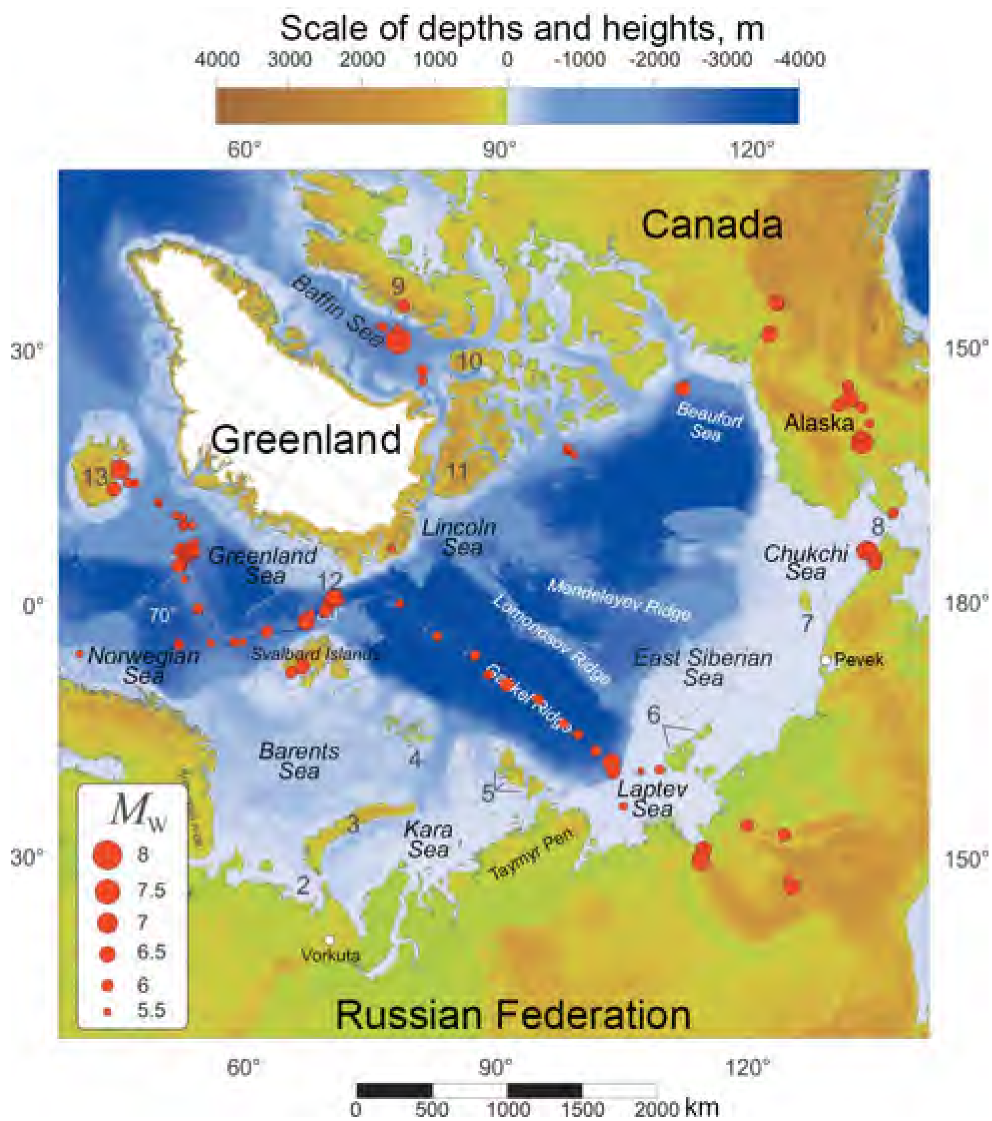

Fig.1. Epicenters of the strongest earthquakes in the Arctic Ocean basin and nearest areas (to the north from latitude 65°N) with magnitude Mw ≥ 5.5 for the period of instrumental seismological observations 1918-2011. [3,8]

2. PROBLEM STATEMENT

The present study considers areas of the Arctic waters where historical earthquakes with a magnitude of $M > 5.5$ were recorded, in some cases accompanied by tsunami waves. Earthquakes were considered in the Baffin Sea on November 20, 1933, $M = 7.7$, in the Laptev Sea on May 30, 1923, $M = 6.7$, on May 30, 23, $M = 6.0$, on April 7, 1969, $M = 5.5$, and in the Beaufort Sea on November 16, 1920, M=6.4 [8-12].

In contrast to the numerical simulation of these events considered in [8], in the proposed work, the dynamics of a seismic source is considered within the framework of a block-keyboard model of a seismic source [13]. The computational area used for modeling in the Baffin Sea is [-79.62^0 - 60.23^0 (E), 79.67^0 - 64.57^0 (N)]. In the water area of the Laptev Sea, the area [-79.62^0 -60.23^0 (E), 79.67^0 - 64.57^0 (N)] was used; for the Beaufort Sea, the area [121.29^0 -140.23^0(E), 69.92^0 -79.50^0(N)] was considered.

The simulation was carried out on a grid with a space step of 1 min and a time step of 1 s. Since, as noted above, there is little data on the manifestation of modern bottom movements in the Arctic region, the modeling was carried out on the basis of a keyboard- block- model of an earthquake, which allows us to consider different implementation of the dynamics of the earth's crust in the area of a seismic source for a given earthquake magnitude (see., e.g., [16, 18,19]). For this purpose, 2- and 3-block seismic sources were formed for the Baffin Sea, a 4-block seismic source for the Laptev Sea, and a two-block seismic source was considered for tsunami modeling in the Beaufort Sea.

The length and width of the rupture in the earthquake source was determined using the Lamb formulas for earthquake magnitudes for these events [15], and the maximum displacement of the wave surface above the earthquake source was determined using the Iida formula [16], (see.1a,b)

$$\lg L = 0.5M - 2{,}44 \pm 0{,}16 \qquad (1a)$$

$$\lg W = 0.32M - 1.01 \pm 0.15$$
$$\lg H = 0.8M - 5{,}6 \qquad (1b)$$

3. NUMERICAL SIMULATION OF TSUNAMI WAVES FROM THE 20 NOVEMBER 1933 BAFFIN SEA EARTHQUAKE

Numerical simulation was carried out within the framework of nonlinear shallow water equations (see., e.g., [17-20]). For numerical simulation of the processes of generation and propagation of waves in a two-dimensional formulation, the Sielecki scheme [21] was chosen. Two scenarios of generation of a tsunami source by a seismic source were considered in the work: Scenario 1 - two-block model; Scenario 2 - three-block model. Approximate dimensions of the outbreak were: 130 km x 30 km. The localization of the earthquake source is shown in fig. 2 and 3. Red dots and numbers mark the location of virtual tide gauges. Red squares highlight the area of localization of the focus.

Scenario 1.

Figure 2 shows the localization of a two-block earthquake source for this scenario. The epicenter of the earthquake is located in the first block, oriented towards the coast of Greenland. Table 1 shows the kinematics of blocks in the earthquake source. The movement of blocks starts from block 1, down by 4m, after 20 seconds the second block starts moving up by 7. m.

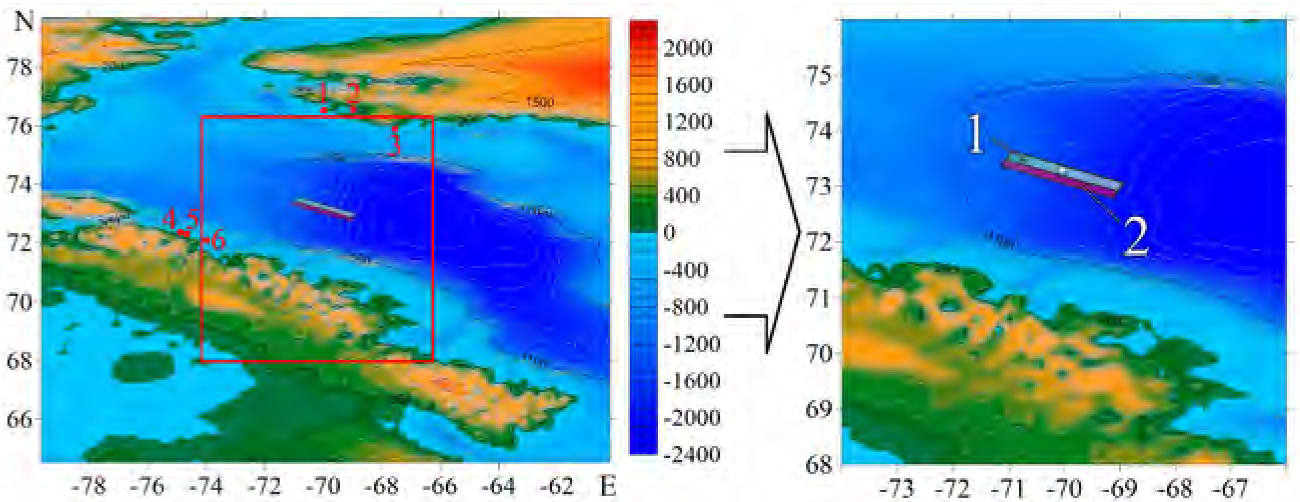

Fig. 2. Earthquake source location in the Baffin Sea (Scenario 1)

Table 1. Kinematics of block motion in the earthquake source (Scenario 1)

Scenario 1		
Block movement	**Block 1**	**Block 2**
Height (m)	**6**	**-4**
Start time of movement (s)	**0**	**0**
Final time of movement (s)	**60**	**20**

Fig.15 shows the picture of wave front propagation in the Beaufort Sea for 6 time moments. in Fig.15 (1)(2) it can be seen wave front position in the initial time moments. In Fig.15 (3) it is seen the approaching the wave front to Banks Island and the approach of the wave to the mouth

Scenario 2.

In this scenario, a three-block source was considered, with the same dimensions and the same magnitude of the earthquake. The epicenter of the earthquake is located in the first block. Figure 3 shows the localization of the earthquake source for Scenario 2 in the calculated water area.

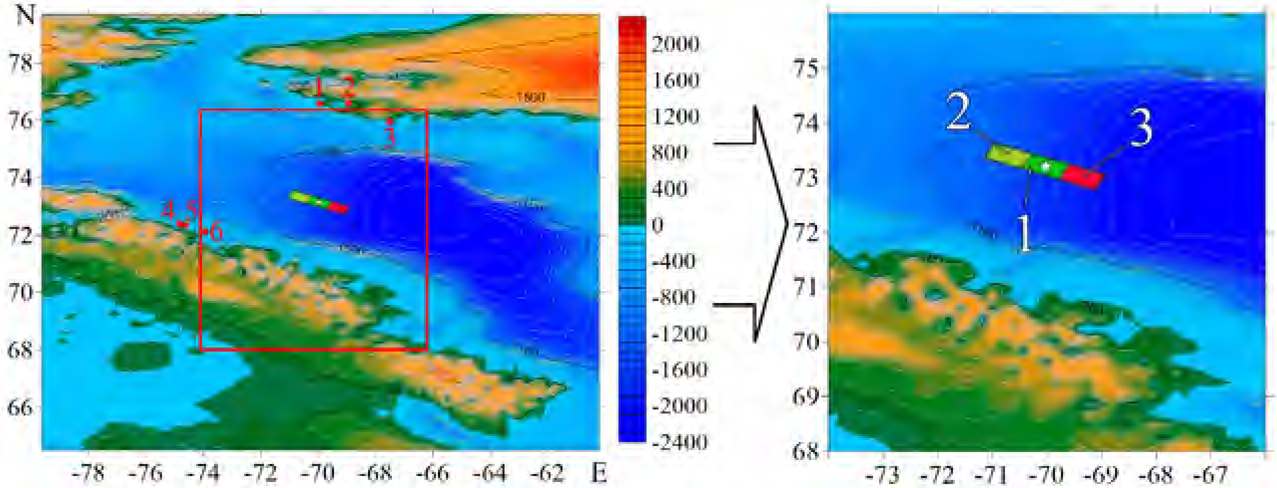

Fig. 3. Earthquake source location in the Baffin Sea (Scenario 2)

The kinematics of the movement of the blocks is presented in Table 2. The beginnings of the movement of each block were implemented at different times.

Table 2. Kinematics of blocks motion in the earthquake source (Scenario 2)

Scenario 2			
Block movement	**Block 1**	**Block 2**	**Block 3**
Height (m)	**6**	**-4**	**4**
Start time of movement (s)	**0**	**20**	**50**
Final time of movement (s)	**30**	**50**	**105**

For Scenario 1, Fig. 4 shows the generation of the tsunami source for 1 minute when the key-blocks move in the earthquake source (see Table 1), and the further propagation of tsunami waves over the water area.

For scenario 2, Fig. 5 shows the generation of the tsunami source for 105 sec when the keyblocks move in the earthquake source (see Table 2). It is clearly seen that the tsunami source is formed as the blocks move in the earthquake source. Figure 6 shows the propagation of wave fronts for two moments of time. The computation results show that in almost an hour the wave front reaches the coast of Greenland and then propagates along it. Figure 7 shows the distribution of maximum wave heights over the computed water area for both scenarios. It is clearly seen that for the first scenario, large wave heights off the coast of Nunavut. Near Round Island, wave heights are about 10 meters. Off the coast of Greenland, near the village of Pituffik, the wave heights are about 0.3m. However, when approaching Melville Bay, the heights of the waves grew sharply. Waves do not exceed 1 meter off Wolstenholme Island. On Bylot Island, in some areas, the wave height reached 3 meters, the average heights on the coast were much lower.

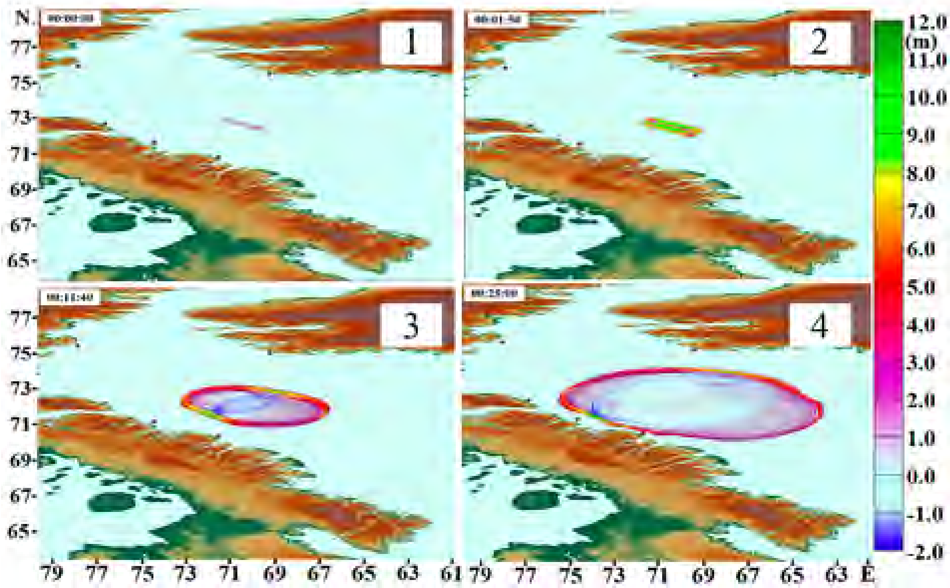

Fig. 4. Time moments of tsunami wave generation and propagation in the Baffin Sea: generation of the tsunami source and 3 moments of wave propagation time across the water area (Scenario 1)

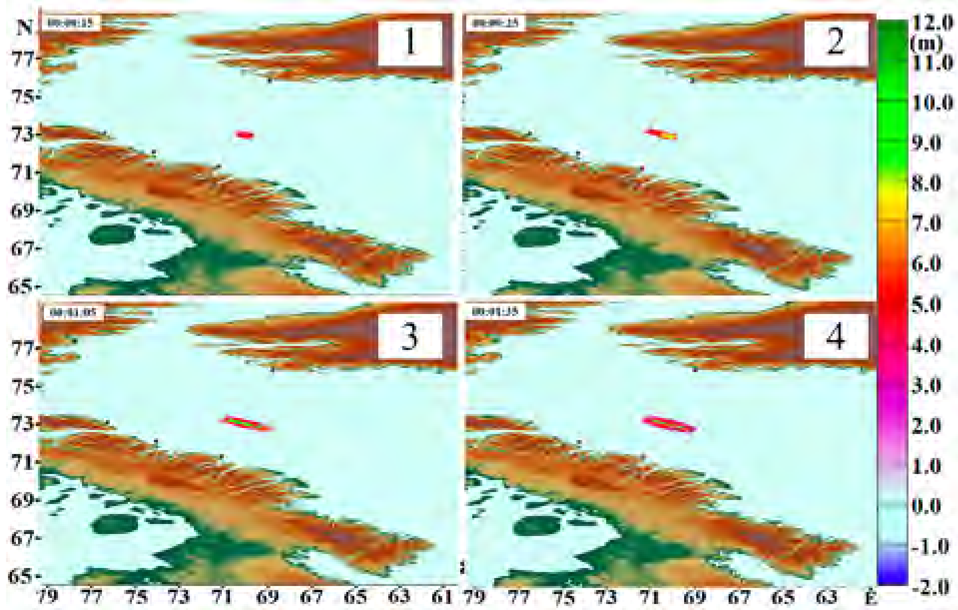

Fig. 5. Tsunami wave generation in the Baffin Sea (Scenario 2)

For the second scenario, wave heights off the coast of Nunavut, near Round Island, are significantly lower, but exceed 5 meters.

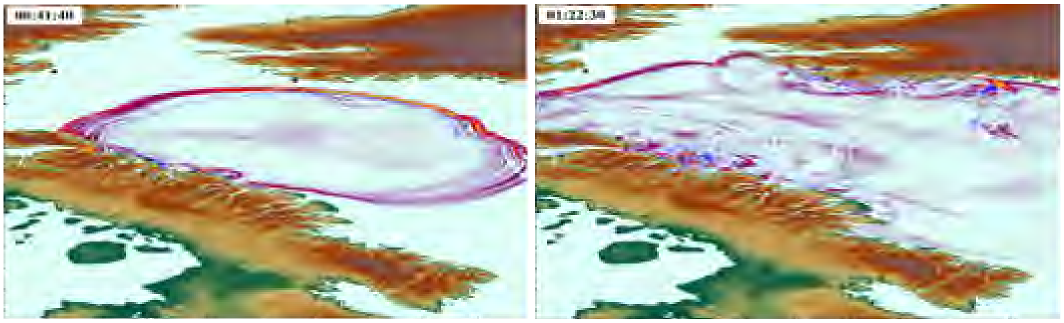

Fig. 6. Two time moments of the wave propagation in the Baffin Sea (Scenario 2).

Off the coast of Greenland, near the village of Pituffik, wave heights are about 0.5m. Near Melville Bay, waves reach heights of up to 5m. The average wave height on the coast is in the range of 2-3m. Unlike the first scenario, there is no sharp increase in wave height near the Round and Nova Zembolla islands, the waves do not exceed 5 meters.

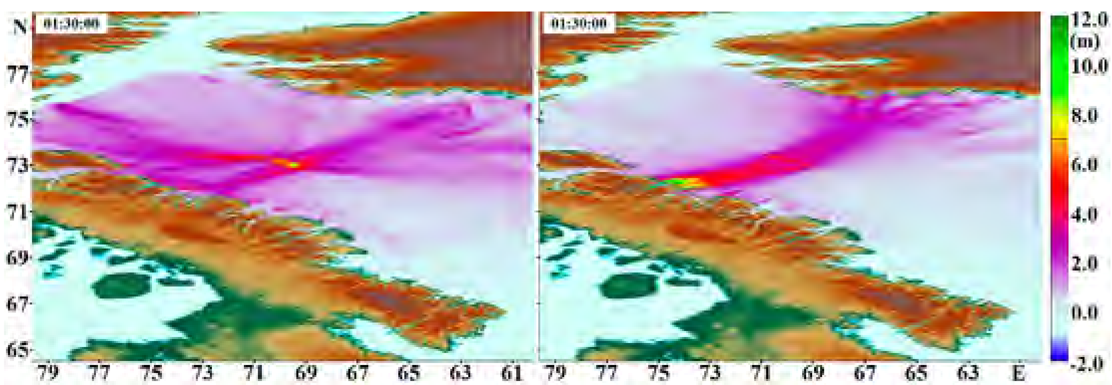

Fig. 7. Distribution of maximum wave heights in the computation area of the Baffin Sea for: a) two-block source (Scenario 1); c) three-block source (Scenario 2)

On Bylot Island, the height also fluctuates around 5m. This is clearly seen in the histograms shown in Fig. 8 and Fig. 9, and the average wave height was about 2 meters. The height of the waves on the coast of Greenland fluctuates on average at around 2 meters. A small surge in wave height is seen near Melville Bay, similar to Scenario 1, but in this case only up to four meters. On the histograms for Scenario 1 (Fig. 8a), one can see that on Bylot Island, the wave height reaches three meters in some parts of the coast, closer to Round Island. The average wave height is 1.5 meters. The wave height on the coast of Greenland is much higher, which is clearly seen in Fig. 8b. A sharp rise in height is seen near Melville Bay, with waves reaching over 8 meters in height. The average wave height off the coast of Greenland does not exceed four meters.

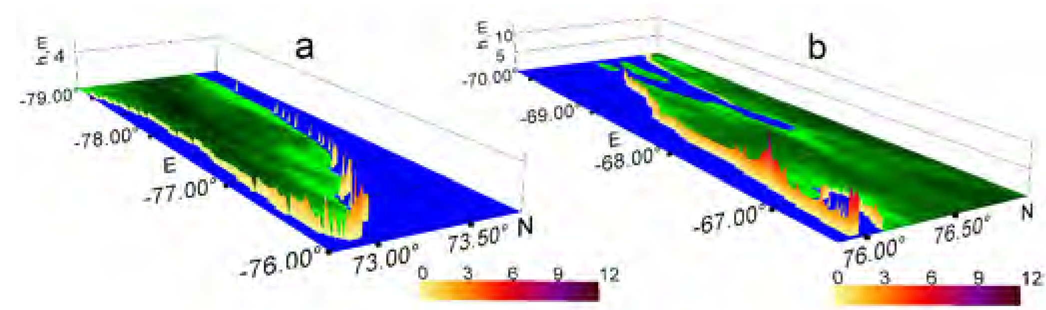

Fig. 8 3D histograms of the distribution of maximum wave heights on: a) Baylot Island; b) Greenland coast (Scenario 1)

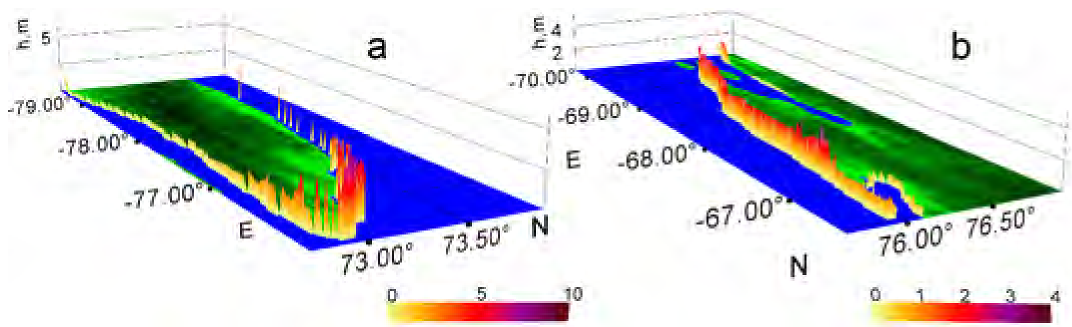

Fig. 9 3D histograms of the maximum wave height distribution on: a) Baylot Island; b) Greenland coast (Scenario 2).

Figure 9. shows histograms for Scenario 2. It is well seen that wave heights along overall coast are essentially lower as compared with scenario 1. The data from 6 virtual tide gauges (Fig.2, Fig.3) in different parts of the Baffin Sea for both scenarios are presented in Table.3.

Table 3. Data on maximum wave displacement at 5 m isobath (according to tide gauge data) for Scenario 1 and Scenario 2

Point	**Maximum height**	
	Scenario 1	**Scenario 2**
(1) Wolstenholme Island, Greenland	**0,53**	**0,81**
(2) Pituffik, Greenland	**0,30**	**0,26**
(3) Melville Bay, Greenland	**2,14**	**1,08**
(4) Nova Zembla Island, Canada	**5,27**	**2,43**
(5) Round Island, Canada	**7,76**	**2,15**
(6) Davis Strait, Canada	**5,88**	**3,83**

It is clearly seen that with different implementation of the movement of key-blocks in the seismic source for the same earthquake magnitude, the possible implementation of wave heights on the coast can be significantly different. This indicates the need to take into account additional factors, such as geostructures, detailed bathymetry, and coseismic displacements.

4. NUMERICAL SIMULATION OF TSUNAMI WAVE GENERATION AND PROPAGATION IN THE LAPTEV SEA - Tsunami source formation for the Laptev Sea.

A generalized source was formed in the Laptev Sea, which included three earthquakes: 1923, 1964 and 1969. The source was divided into 4 blocks, their movements and sizes were corrected for earthquakes of the corresponding magnitude. A generalized source was formed in the Laptev Sea, which included three earthquakes: 1923, 1964 and 1969. The source was divided into 4 blocks, their movements and sizes were corrected for earthquakes of the corresponding magnitude.

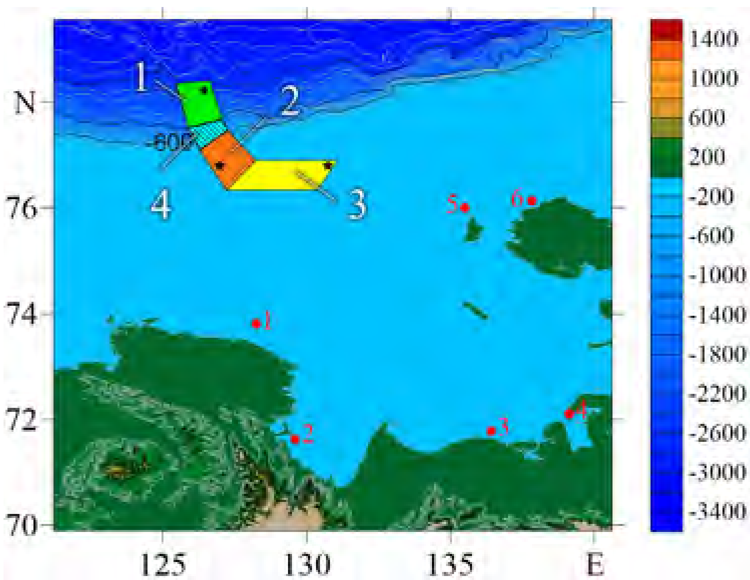

Fig. 10. Computation water area and earthquake source of the scenario in the Laptev Sea. Location of blocks (1,2,3,4) and virtual tide gauges in the scenario (red figures): 1 – coastal area of the Lena Reserve; 2 - Tiksi; 3 - Nizhneyansk; 4 - Yukagir; 5 - 6 near Belkovsky and Kotelny islands, respectively.

Figure 10 shows the location of the blocks in the calculated water area. The first one corresponds to the earthquake of 08/25/1964 with M=6.7, the localization of the second block corresponds to the earthquake of 05/30/1923 with M=6.0, the third block is located to the east of the second block and approximately corresponds to the earthquake of 04/07/1969 with M=5.5. The last, fourth block is formed between the first and fourth blocks, as an area of a possible earthquake. The shapes of the blocks are somewhat distorted due to the modeling in the Cartesian coordinate system.

Table 4 shows the kinematics of block motion in the source, based on a number of data from [6–9]. The first block moves up for 30 seconds to a height of 2m. The second block starts its downward movement 15 seconds after the start of the movement of the first block and moves for 15 seconds, the displacement is -1.5 m, and the third and fourth begin their movement after 10 and 20 seconds, respectively, and move for 15 and 10 seconds, with a positive displacement of 1, 8m and -1m.

Table. 4. Kinematics of blocks in the seismic source.

Scenario for a generalized seismic source				
Block movement	**Block 1 25.08.1964 M=6.7**	**Block 2 30.05.1923 M=6.0**	**Block 3 07.04.1969 M=5.5**	**Block 4**
Height (m)	**2,6**	**-1,5**	**2**	**-1,0**
Start time of movement (s)	**0**	**15**	**10**	**20**
Final time of movement (s)	**30**	**30**	**35**	**40**

4A. Numerical simulation results in the Laptev Sea

Figure 11 shows the results of numerical simulation of the generation of a model tsunami source during an earthquake in the Laptev Sea. At the moment of time 10 (Fig. 11.1) seconds, the tsunami center begins to form during the movement of the first block. The beginning of the formation of the tsunami source above block 2 can be seen in Fig. 11(2). By the 20th second, all blocks began to move, which is clearly seen from the formation of the tsunami source in Fig. 11(3). The completion of the generation of the tsunami source during the considered seismic process can be seen in Fig. 11(4).

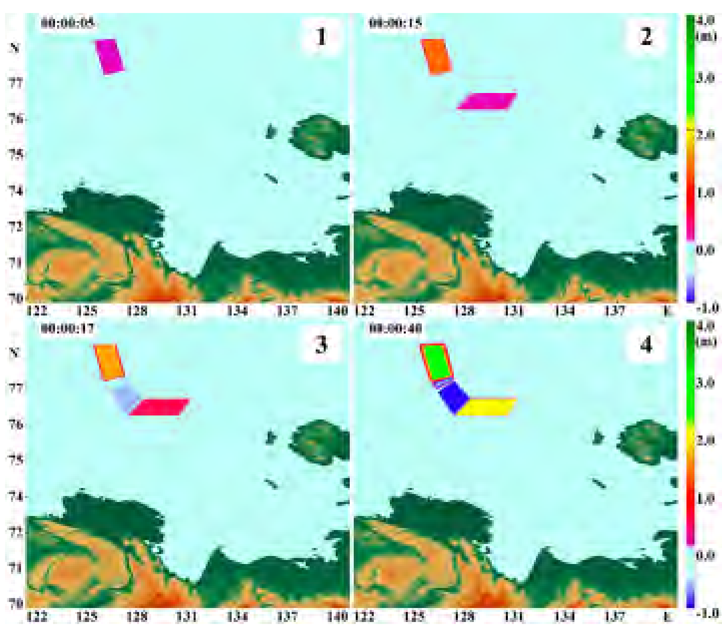

Fig. 11 Generation of the tsunami source by a four-block seismic source in the Laptev Sea.

Figure 12 (1-4) shows the formation of a wave front approaching Kotelny Island. In Fig.12(5). It is clearly seen that the wave front reaches the coast of Kotelny Island, the wave height at a given time (4 hours, 30 minutes) does not exceed one meter. In Fig. 12.6, the waves continue their propagation towards the continent.

Figure 13 shows 3D histograms: Figure 13a is a histogram of Kotelny Island from the southern side of the island. The maximum height on the histogram is just over two meters. The average height on the south side is about two meters. On the eastern side, the average wave height does not exceed one meter. Figure 13b shows the histogram of the Lensky Reserve, the maximum wave height does not exceed 1.3 meters. The average wave height is about 0.7 meters. The height of the waves to the east coast decreases. The maximum wave height reaches half a meter near the settlement of Nizhneyansk, in this area the highest wave height was recorded. On average, the wave height east of the Lensky Reserve did not exceed 0.3 meters.

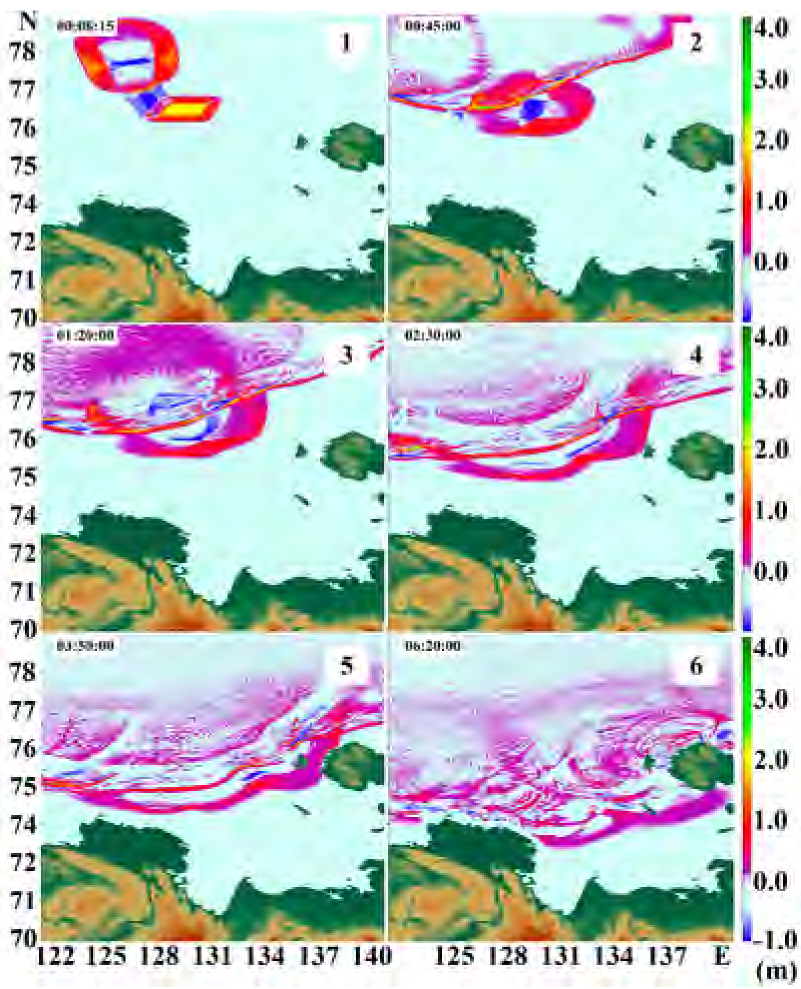

Fig. 12 Propagation of the wave fronts from the tsunami source in the Laptev Sea for 6 times moments.

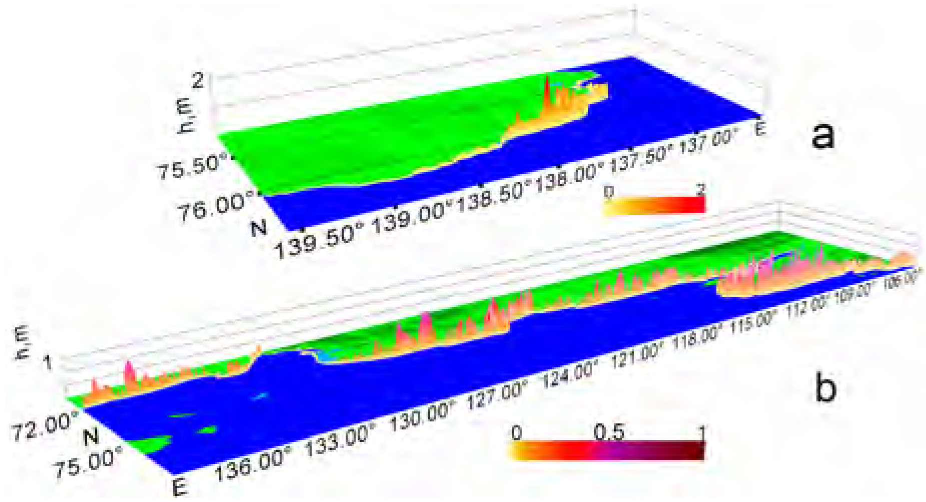

Fig.13. 3D histogram of the maximum wave height distribution : (a) along the coast of Kotel Island; (b) along the entire coast of the computation water area. Kotelny.

The data from 6 tide gauges (see Fig.10) are presented in Table 5.

Table 5. Data on maximum and minimum heights of wave displacement on the 5-meter isobath (according to tide gauge data) in the Laptev Sea

Point	Max. height, m	Min. height, m	Time, s
(1) Belkovsky Island, Russia	0.53	-0.68	2:42:05
(2) Kotelny Island, Russia	1.29	-2.13	3:49:35
(3) Nizhneyansk, Russia	0.29	-0.36	9:34:10
(4) Lensky Reserve, Russia	0.39	-0.71	4:04:10
(5) Tiksi, Russia	0.09	-0.08	10:19:35
(6) Yukagir, Russia	0.26	-0.36	10:08:45

It is clearly seen that at given magnitudes of earthquakes, the maximum wave heights near the continental and island coasts of the Laptev Sea do not exceed 1.3 m. The average wave height on the 5-meter isobath is about half a meter.

5. NUMERICAL SIMULATION OF TSUNAMI GENERATION AND PROPAGATION IN THE BEAUFORT SEA

The historical event that occurred on November 16, 1920 with a magnitude M=6.4 to the west of about. Banks is considered. Earthquake epicenter coordinates: -131.67 W (E), 72.638 N (N). To simulate the generation of tsunami waves in the calculated water area of the Beaufort Sea, by a seismic source (Fig. 14), the localization of the earthquake source was chosen in such a way that the epicenter is located in the first block, the second block is located closer to the coast of the island. Banks. The red numbers indicate the localization of virtual tide gauges. The red square marks the localization area of the earthquake source.

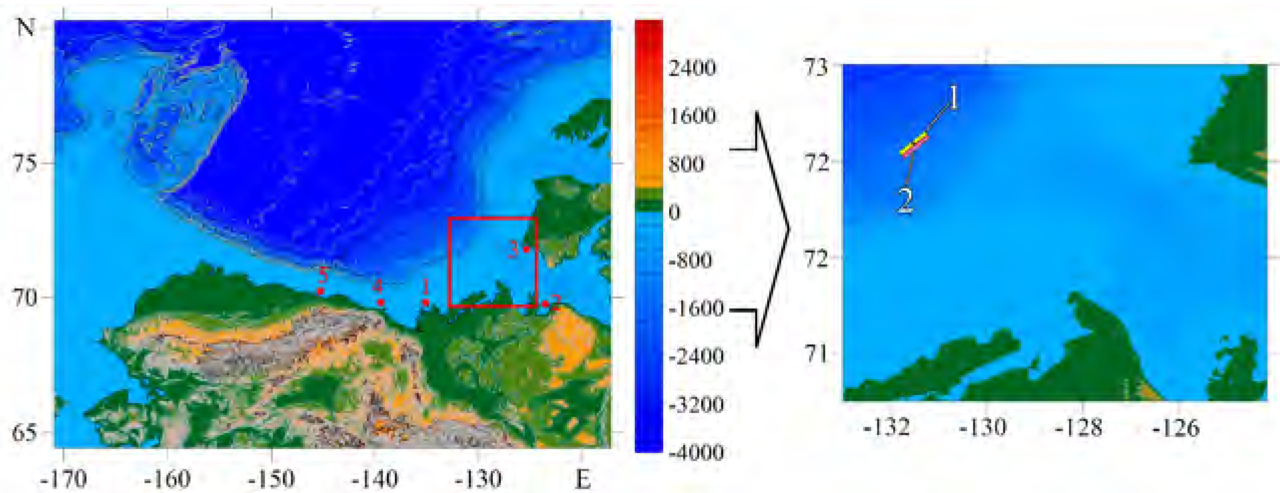

Fig. 14. Earthquake source location in the Beaufort Sea

Table 6 shows the magnitude of the displacement of the first and second blocks, as well as the times during which these displacements occurred. The size of the source, calculated according to the Wells formulas, was approximately 32x15 km. The displacement of the water surface above the earthquake source, found by the Iida formula, was about 3m. Block 1 starts moving up 3m in 30 seconds, after 10 seconds block 2 starts moving down 2.5m in 20 seconds. Thus, the generation of the tsunami source ends 30 sec after the blocks start moving in the earthquake source.

Table 6. Kinematics of blocks in the seismic source in the Beaufort Sea

Scenario for a generalized seismic source		
Block movement	**Block 1**	**Block 2**
Height (m)	**3**	**-2,5**
Start time of movement (s)	**0**	**10**
Final time of movement (s)	**30**	**30**

Fig.15 shows the picture of wave front propagation in the Beaufort Sea for 6 time moments/ in Fig.15 (1)(2) it can be seen wave front position in the initial time moments. In Fig.15 (3) it is seen the approaching the wave front to Banks Island and the approach of the wave to the mouth

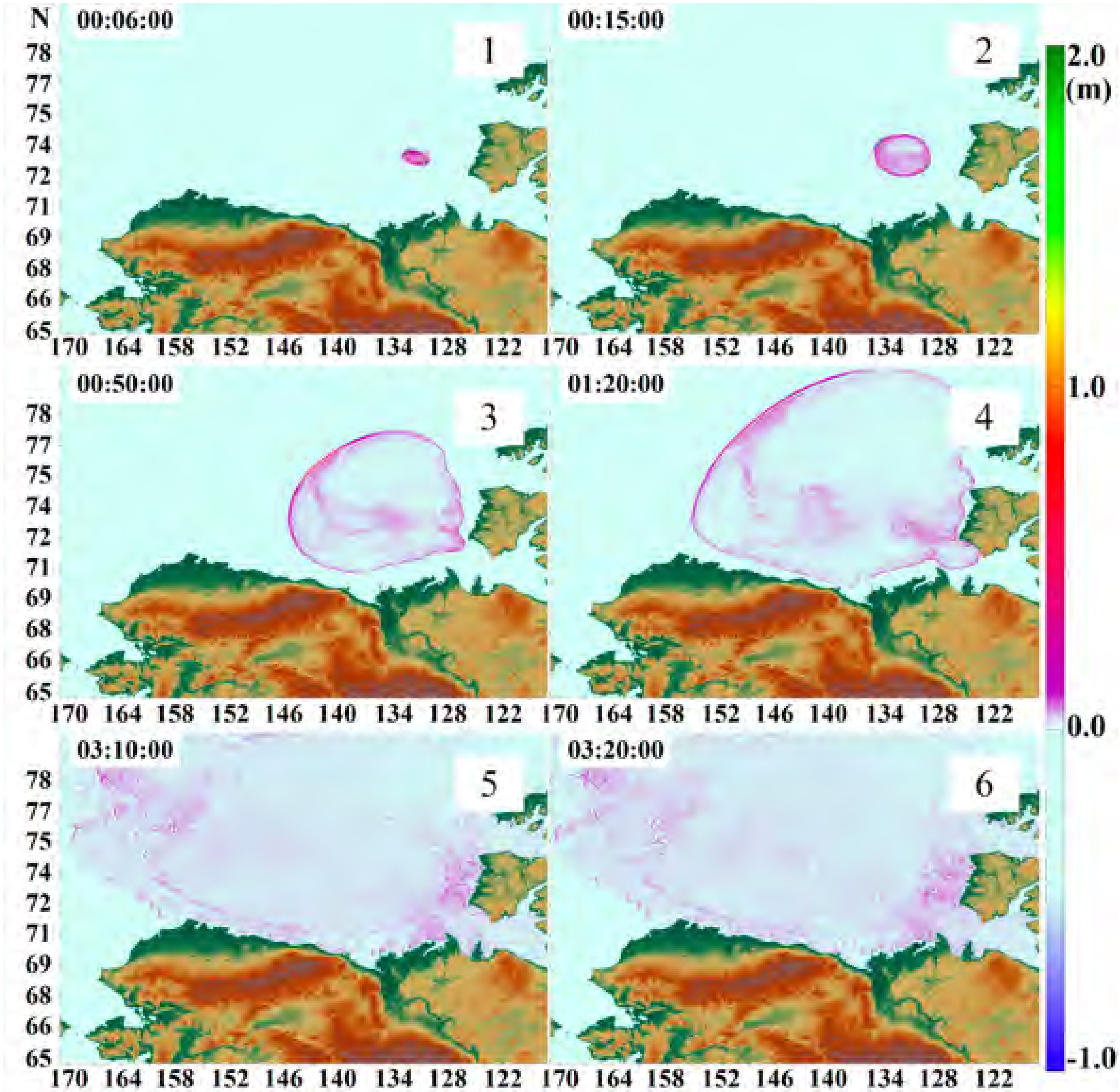

Fig. 15. Tsunami wave propagation in the Beaufort Sea for the scenario considered.

between the island and the continent. At the time point of 1 hour and 20 minutes (Fig. 15 (4)) the waves reach the Banks Islands and approach the coast of Canada. On fig. 15(5) and (6) it can be seen that the wave fronts reach the nearest parts of the coast. Thus, 3 hours and 30 minutes passed from the moment of wave generation to its approach to land. The distribution of maximum wave heights over the calculated water area is shown in Fig.16. After the movement of blocks in the earthquake source and the end of the generation of the tsunami source, the wave height rapidly decreases, and it is clearly seen that the approaching waves to the Banks Islands do not exceed 1.5 meters. According to fig. 16 and 17 you can see that the highest waves are possible on the western part of the Banks Islands.

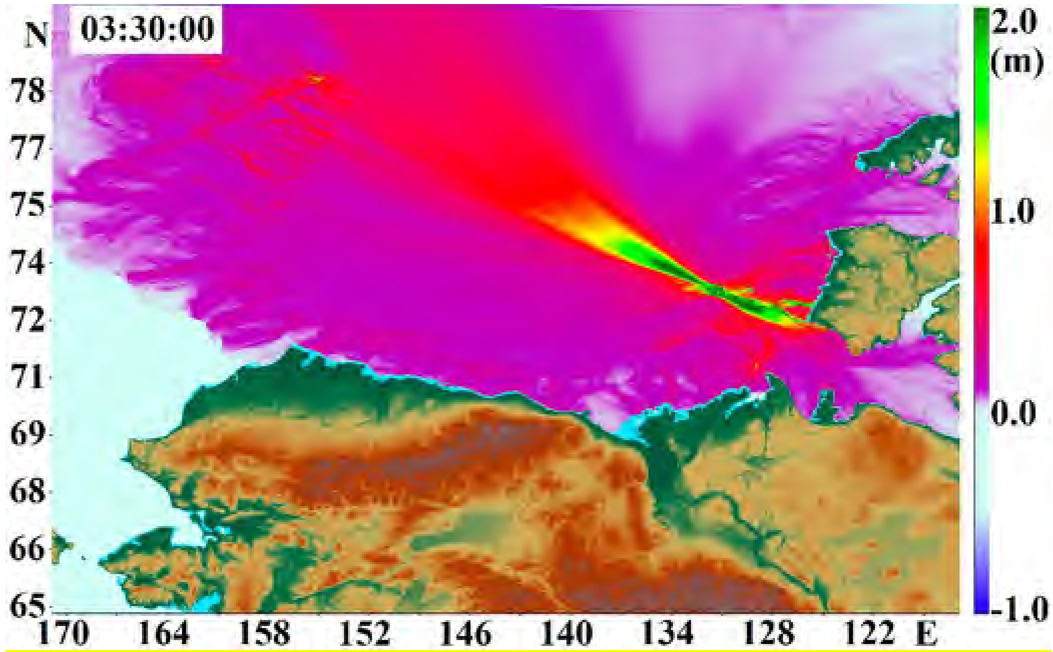

Fig. 16. Maximum wave heights in the Beaufort Sea water area in the studied scenario.

Waves of the order of one meter can be seen next to Sachs Harbour. Waves approaching the settlement of Tuktoyaktuk do not exceed 0.5 meters, and along numerous reserves in the southern direction, wave heights occasionally approach 0.5 meters, reaching an average of 0.3 meters. On the histogram in Fig. 17, it is clearly seen that the maximum wave heights are slightly more than 1 meter. The average wave height is about half a meter on the entire western coast of the island. Rare peaks of wave heights can be explained by bays and places of river mouths.

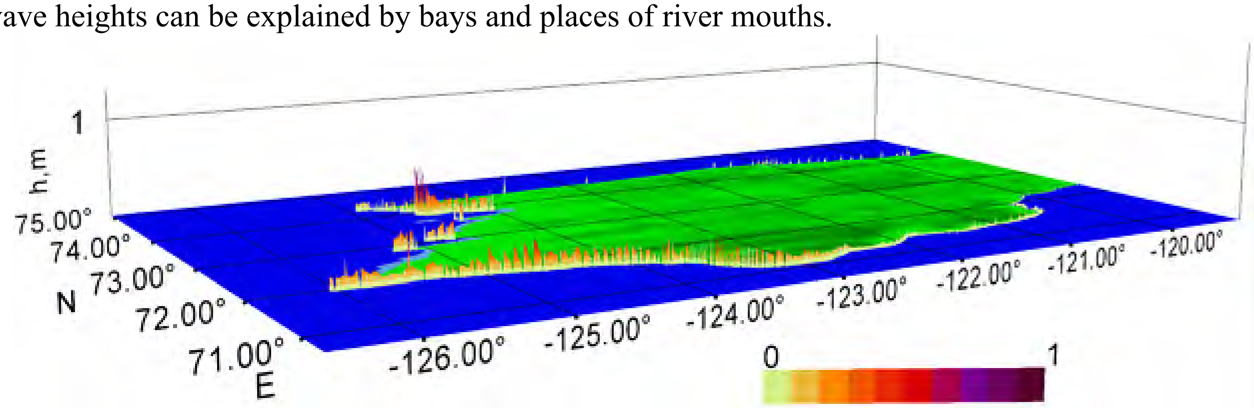

Fig. 17. 3D histogram of wave heights on Banks Island.

It should be noted that mainly on the coast, wave heights are minimal and do not exceed 10-15 centimeters. For a more detailed analysis of wave heights along the coast of the water area under consideration, data from virtual tide gauges (Table 7) were analyzed, which were placed near points along the coast of Canada. The wave with the largest amplitude came to the tide gauge located on the coast of Sachs Harbor.

Table 7. Data on maximum heights of wave displacement on the 5-meter isobath (according to tide gauge data) in the Beaufort Sea

Point	Max. height,m	Time, s
(1) Kendall Island Bird, Canada	**0,14**	**0:16:40**
(2) Paulatuk, Canada	**0,06**	**0:49:10**
(3) Sachs Harbour, Canada	**2,14**	**0:11:40**
(4) Ivvavik National Park, Canada	**0,90**	**0:25:25**
(5) Prudhoe Bay, USA	**0,15**	**0:40:25**

The wave started from a negative phase and went 0.6 meters relative to the water surface, after that the wave height rose to one meter and repeated about three times. The waves near the village of Paulatuk began with low tide, after which the height of the water surface rose by five centimeters. Ivvavik has a similar situation. The data captures the initial low tide, after which a uniform fluctuation of the water surface for two hours. In general, considering all tide gauge records one can conclude that all waves begin with a low tide and a sharp jump in wave heights of several tens of centimeters.

CONCLUSIONS

In this work, numerical simulation of possible tsunamis generated by seismic sources in the regions of historical earthquakes in the waters of the Arctic has been carried out. The strongest recorded earthquake in the Arctic Ocean basin was considered: in the Baffin Sea (1933) with a magnitude M = 7.7. 2 scenarios for each event were carried out within the framework of the keyboard model of the earthquake source, simulating different dynamics in the earthquake source. The results of numerical simulation were obtained in the work, in which the average height on the coast of Greenland lies in the range of 2-4m, and the maximum height of tsunami waves on the coast of the near zone of the source reaches 10-12m. In the Laptev Sea, 3 earthquakes with magnitudes 6.7 (1964), magnitude 6 (1923) and magnitude 5.5 (1969) were considered. A generalized earthquake source was built, which includes these 3 earthquakes with close localization. Estimates were made of the maximum wave heights for the mainland coast of Russia, where the population and infrastructure are most dense. The obtained wave characteristics were compared with the few available data of numerical simulations of these events by other authors. A comparison was made with the work of E.A. Kulikov et al., 2016, in which a certain difference was obtained, which, in our opinion, is associated with a more complex earthquake source model used in this work. In the Beaufort Sea, a simulation of the 1920 earthquake with a magnitude of 5.5 was carried out, an assessment of the wave fields was carried out according to this water area, and results were also obtained on the maximum wave heights along part of the coast of Canada. It was found that the wave heights do not exceed 1.5m, which is in good agreement with the works of other authors. In contrast to the currently available, very limited number of works on the Arctic region, the work carried out a detailed tsunami zoning of the coasts of the three considered water areas within the Arctic basin.

ACKNOWLEDGEMENTS

The authors acknowledge the funding of this study provided by grant of President of the Russian Federation for the state support of Leading Scientific Schools of the Russian Federation (Grant No. NSH-70.2022.1.5.).

REFERENCES

1. ANSS ComCat. Composite Earthquake Catalog, Northern California Earthquake Data Center. 2014 // http://www.quake.geo.berkeley.edu/cnss/.

2. NGDC/WDS Global Historical Tsunami Database. doi:10.7289/V5PN93H7 // https://www.ngdc.noaa.gov/ hazard/tsu_db.shtml.

4. Avetisov, G.P., 2004. Seismicity of the Arctic continental margin of Russia, Geol. T. 5: Arctic and Far Eastern seas. Book. 1: Arctic Seas / Ed. I. S. Gramberg, V. L. Ivanov, Yu. E. Pogrebitsky. SPb.: Publishing house of VSEGEI, 2004. S. 31-42.

5. Avetisov G. P., 1996. Seismically active zones of the Arctic. St. Petersburg: VNIIOkeanologiya, 1996. 186 p.

6. Mazur I.I., Ivanov O.P., 2004. Dangerous natural processes. Introductory course // M.: Economics, 2004. 702 p. ISBN 5-282-02406-3.

7. Kozelkov, A.S., Kurkin, A.A., Pelinovskii, E.N., Kurulin, V.V., 2015. Modeling the cosmogenic tsunami within the framework of the navier-stokes equations with sources of different types Fluid Dynamics, 2015, 50(2), pp. 306–313

8. E. A. Kulikov, A. I. Ivashchenko, I. P. Medvedev, O. I. Yakovenko, S. A. Kovachev, 2016. // Arctic: Ecology and Economics, No. 3 (23), 2016. P. 38 -49.

9. Phase et al., Kanao, S. Tsuboi, Rhett Butler, K. Anderson., 2016. Greenland Ice Sheet Dynamics and Glacial Earthquake Activities // BURRINO.19-T-12, 2013

10. Masaki Kanao, S. Tsuboi, Rhett Butler, K. Anderson, 2011. Greenland Ice Sheet Dynamics and Glacial Earthquake Activities // ROMBUNNO.15-T-15, 2011

11. Leonard L., Roger G., Mazotti S., 2014. Tsunami hazard assessment of Canada, Nat. Hazards. 2014. Vol. 70, No. 1. P. 237-274. DOI:10.1007/s11069-013-0809-5

12. The system of the Laptev Sea and the adjacent seas of the Arctic. 2009: the current state and history of development / Managing editors: X. Kassens, A.P. Lisitsyn, J. Tide, E.I. Polyakova, L.A. Timokhov, I.E. Frolov. - M.: Publishing House of Moscow. un-ta, 2009. 608 p.

13. Lobkovsky L.I., Baranov B.V. Keyboard, 1984. Model of strong earthquakes in island arcs and active continental margins // Doklady AN SSSR. T. 275. No. 4. S. 843-847. 1984.

14. Mazova R. Kh., Kurkin A. A, Giniyatullin A. R, Tyuntyayev C. M.. 2021. Earthquake of 30 October the Aegean Sea: Numerical Simulation of the Generation and Propagation of Tsunami Waves//(2021), V.40,N.3,pp.78-95

15. Wells D. L., Coppersmith K. J., 1994. New empirical relationships among magnitude, rupture length, rupture width, rupture area, and surface displacement // Bull. Seism. Soc. Am. 1994 Vol. 84. P. 974-1002.

16. Pelinovsky E.N., 1992. Nonlinear dynamics of tsunami waves. Gorky: Ed. IAP USSR Academy of Sciences. 1982. 226 p.

17. Voltsinger N.E., Klevanny K.A., Pelinovsky E.N., 1989. Long-wave dynamics of the coastal zone, Leningrad: Gidrometeoilzdat, 1989, 272 p.

18. Lobkovsky L.I., Baranov B.V., Mazova R.Kh., Kataeva L.Yu., 2006.Implications of the seismic source dynamics for the characteristics of a possible tsunami in a model problem of the seismic gap in the Central Kurile region // Russ. J. Earth Sci. 2006. V. 8. P. ES5002 (1–23). doi: 10.2205/2006ES000209 http://dx.doi.org/10.2205/2006ES000209

19. Lobkovsky, L.I. Garagash, B. Baranov, R. Mazova, N. Baranova, 2017. Modeling Features of Both the Rup ture Process and the Local Tsunami Wave Field from the 2011 Tohoku Earthquake // Pure Appl. Geophys. (2017). V.174, p. 3919-3938, doi:10.1007/s00024-017-1539-5 (March 2017) pp. 1-20.

20. Mazova R.Kh., Moiseenko T., Kurkin A.A., Jorge Van Den Bosch F., Gustavo Oses A., 2021 Numerical Simulation of a Catastrophic Earthquake and Strong Tsunami ofappril 1, 2014 near the Northwestern Part of the Chilian Coast// STH . (2021), , V.40, N.2, pp.83-100.

21. Sielecki, A., and M. Wurtele, 1970. The numerical integration of the nonlinear shallow water equations with sloping boundaries, J.Comput. Phys., 6, 219, 1970 doi: 10.1016/0021-9991(70)90022-7.

ISSN 8755-6839

SCIENCE OF **TSUNAMI HAZARDS**

Journal of Tsunami Society International

Volume 41 Number 3 2022

RESEARCH TRENDS ON LIQUEFACTION IN 2011-2021: A REVIEW AND BIBLIOMETRIC ANALYSIS

Nadi Suprapto[1,*], Della Shinta Bestiantono[1], Chih-Hsiung Ku[2], Akhmad Zamroni[3], and Eko Hariyono[1]

[1]*Universitas Negeri Surabaya, Surabaya, **INDONESIA***
[2]*National Dong Hwa University, Hualien, **TAIWAN***
[3]*Institut Teknologi Nasional Yogyakarta, **INDONESIA***
[*]Email: nadisuprapto@unesa.ac.id

ABSTRACT

Since the 2018 Palu earthquake in Central Sulawesi of Indonesia, many researchers worldwide have been concerned about the ground liquefaction phenomenon associated with seismic events. The present study analyzes research trends related to liquefaction through bibliometric methods and examines the contributions of Indonesian authors to the Scopus metadata. In performing this analysis 3,489 documents were identified, 95 of which were from Indonesia. The findings indicated that the number of scientific publications related to ground liquefaction had increased significantly, and that most of these studies were published in the United States. At the same time, the University of Canterbury in New Zealand has been a leading contributor. The most prolific author in this subject was G. Owen. Visualization of liquefaction research trends results in the following five clusters: (1) Reliability and accuracy of the occurrence of liquefaction; (2) Liquefaction consistency; (3) Map and city where such liquefaction occurred; (4) Ground deformation resulting from liquefaction; (5) The country(s) that experienced such liquefaction. The present study helps identify global trends and developments related to ground liquefaction by providing in addition a map for further studies.

Keywords: *Liquefaction, Review, Bibliometric Analysis*

1. INTRODUCTION

Collision and movement of tectonic plates along subduction zones often result in major and great earthquakes and generate destructive tsunamis. Destructive tsunamis also are generated by landslides, volcanic eruptions, volcanic flank collapses, atmospheric disturbances and falling meteorites. Traveling at high speed when such tsunami waves reach coastal areas, their heights can increase significantly, and even reach heights of up to 30 meters (Pararas-Carayannis, 2003; 2019; 2020; UNDRR, 2019). Often, other earthquake-related effects, such as landslides and ground liquefaction, can cause more damage and human casualties far greater than that of tsunami (Setyabudi, 2013; Sonmez & Gokceoglu, 2005).

Earthquake-caused ground liquefaction results in a decrease in soil strength due to increase in pore water pressure and in adequate pressure of the soil layer due to dynamic repetitive loading (Anda et al., 2021; Lee et al., 2003). In the soil layer, dynamic periodic stresses are generated by seismic wave propagation of crustal motions. According to Seed et al. (1975) and Liou (1976), liquefaction is a process by which water saturated granular soil changes from a solid-state and behaves like a liquid due to the increase in pore water pressure, and its value becomes equal to the total pressure by dynamic loading. Liquefaction can occur when loose saturated with water sediment near the surface loses strength due to a strong earthquake (Yogatama, 2012; Youd & Perkins, 1978).

The phenomenon of ground liquefaction has attracted the attention of experts, especially in the field of engineering geology, after the dramatic events that occurred from the 1964 Alaska earthquakes and the 2011 Japan. In Niigata, Japan, ground liquefaction from the latter earthquake caused the sand to boil, loss of soil bearing capacity, subsidence, and downward slope movement. These occurrences along a vast area, caused many buildings to loose their foundation support and to collapse. Similar ground liquefaction and landslides occurred in Valdez, Seward, and Anchorage during the 1964 earthquake in Alaska (Seed, 1968).

Some other known earthquake events that caused ground liquefaction was the 1971 Van Norman Earthquake in southern California which resulted in the collapse of the Fernando Dam, the 2004 Aceh and Nias Earthquakes in Indonesia, the 2006 Yogyakarta earthquake in Indonesia, and the 2011 Christchurch earthquake in New Zealand (Cubrinovski et al., 2011; Mase, 2013; Tonkin & Taylor International Ltd., 2013; Van Ballegooy et al., 2014).

A 2018 earthquake in Palu Central Sulawesi, Indonesia, also triggered ground liquefaction. This earthquake's magnitude was 7.5 SR, its focal depth was 11 km and epicenter 26 km from the city (Anda et al., 2021; Cilia et al., 2021; Ho et al., 2021; Zhao, 2021) and was caused by seismic stress horizontal fault structure deformation along Parcolo Fault north of Donggala, which also generated a tsunami that struck the city of Palu Bay. The deformation of the fault’s structure caused liquefaction in the Petobo and Baraloa Region (Hidayat et al., 2021; Kusumawardani et al., 2021). The ground liquefaction at these two areas was the latest and biggest disaster in Indonesia and caused the destruction of hundreds of buildings. The combined impact of the tsunami, of the earthquake-induced effects and of ground liquefaction in this area, amounted to losses in which in Palu amounted to about IDR 18.48 trillion (Wijanarko, 2019).

The extent of the ground liquefaction effect was enormous. Damage in Baraloa and Petobo extended over an area of about 158 hectares, while the area most impacted was about 34.5 hectares with a circumference of 2.5 km (Yulianur et al., 2020). In general, the land in both areas is residential. The extent of destruction was mostly due to geological and hydrological conditions of this area which are very responsive to effects of ground liquefaction (Soekamto et al. 1973).

In general, according to the opinion of some experts and the history of liquefaction, there are three conditions which contribute to its occurrence.

1. Saturated non-cohesive soil
2. Shallow groundwater level
3. Shallow earthquake (minimum 5.0 SR)

Technically, liquefaction occurs in soils that are saturated with water. This water is located between the cracks in the soil and forms the pore water pressure. During a powerful seismic impact, the pore water pressure rises suddenly, sometimes exceeding the frictional strength of the soil. As a result, the land loses its load-carrying capacity.

Phenomena related to liquefaction are of flow and cyclic mobility. It is crucial to consider both when assessing the potential risk of liquefaction. Flow liquefaction is the event that causes the undercurrent. It occurs when the calculated static shear stresses reach equilibrium at a mass much greater than the shear stress in the liquefied soil. In other words, the deformation that occurs results from static shear stress. A river liquefaction event has two characteristics: flow velocity and huge base material displacements (as in the case of the,2018 Palu earthquake in Central Sulawesi).

In contrast to flow liquefaction, cyclic mobility is another phenomenon that can cause enormous permanent strain due to earthquake impacts. (Yulianur et al., 2020). In cyclic mobility, the condition of the static shear stress is less than the shear stress in liquid soil. In this phenomenon, repeated loads and static shear stresses cause the deformation. In this case, the deformation is lateral (horizontal spread). The phenomenon is cracked soil, the water seems to carry sand, and the wells are filled with sand as if there had been sandblasting.

This study presents further discussion utilizing a bibliometric analysis because of the importance of further research related to liquefaction. “Performing a bibliometric analysis conveniently assesses article contributions toward advancing knowledge” (Suprapto et al., 2021a). The number of documents, documents source, languages source, country and institutional distribution, top authors, top citations, and top keywords are usually used to analyze research trends (Prahani et al., 2022; Zakhiyah et al., 2021). Therefore, the present study analyzes research trends related to liquefaction disasters through bibliometric analysis, and examines the contribution of Indonesian researchers to the Scopus database. Finally, the study focuses on research trends related to liquefaction disasters and presents the following six questions:

a) To what extent was the publication output of the liquefaction profile for 2011-2021?
b) To what extent was the distribution of liquefaction publications across countries and institutes globally?
c) Who were the top authors involved in liquefaction research globally?
d) How effective were the publication patterns of liquefaction?
e) How did the visualization results affect the trend in liquefaction research?
f) What were Indonesian authors' research extent and contributions to the understanding of liquefaction?

2. RESEARCH METHOD

In answering these research questions, the present study uses bibliometric analysis methodology recommended in published articles (Nurhasan et al., 2022; Suprapto et al., 2022; Suprapto et al., 2021a). Data on liquefaction is taken from the Scopus metadata. After entering keywords in the metadata search, “TITLE ("liquefaction") AND TITLE-ABS-KEY (earthquake OR tsunami)” a total of 3,489 documents related to liquefaction appeared. With the final search, 2,029 document results appeared with the keywords “TITLE ("liquefaction") AND TITLE-ABS-KEY(earthquake OR tsunami), AND (LIMIT-TO (PUBYEAR, 2021) OR LIMIT-TO (PUBYEAR, 2020) OR LIMIT-TO (PUBYEAR, 2019) OR LIMIT-TO (PUBYEAR, 2018) OR LIMIT-TO (PUBYEAR, 2017) OR LIMIT-TO (PUBYEAR, 2016) OR LIMIT-TO (PUBYEAR, 2015) OR LIMIT-TO (PUBYEAR, 2014) OR LIMIT-TO (PUBYEAR, 2013) OR LIMIT-TO (PUBYEAR, 2012) OR LIMIT-TO (PUBYEAR, 2011))”.

Metadata search results are saved in .csv and .ris formats for further analysis (Prahani et al., 2022; Suprapto et al., 2021b; Zakhiyah et al., 2021). Subsequently the authors used the software *VOSviewer* and Microsoft Excel to display data in tables, graphs, and maps. In addition, the study uses *VOSViewer* to identify trends in liquefaction studies (Suprapto et al., 2021c; Van Eck & Waltman, 2020). Besides that, publication profiles, distribution of publications across countries and laboratories, top authors studying liquefaction and containment of liquefaction worldwide, publication patterns, visualization results, and contributions in Indonesia which include authors involved in liquefaction research.

3. FINDINGS

3.1 Publication Output Profile

As previously mentioned, 3,489 documents related to liquefaction were found in the Scopus database, as shown in Figure 1 below, from 2011 to 2021. However, the documents have fluctuating data with an apparently increasing trend. From 2011 until 2014, there were more than 100 documents per year, but in 2016, there was a decrease by 27 documents from the previous year - the highest data was 327 documents in 2019. The number of papers and documents has decreased twice, in 2016 and 2020 as shown this Figure 1. However research trends have increased significantly over the last ten years and if this trend continues, it is expected to significantly increase the number of articles from the next following years.

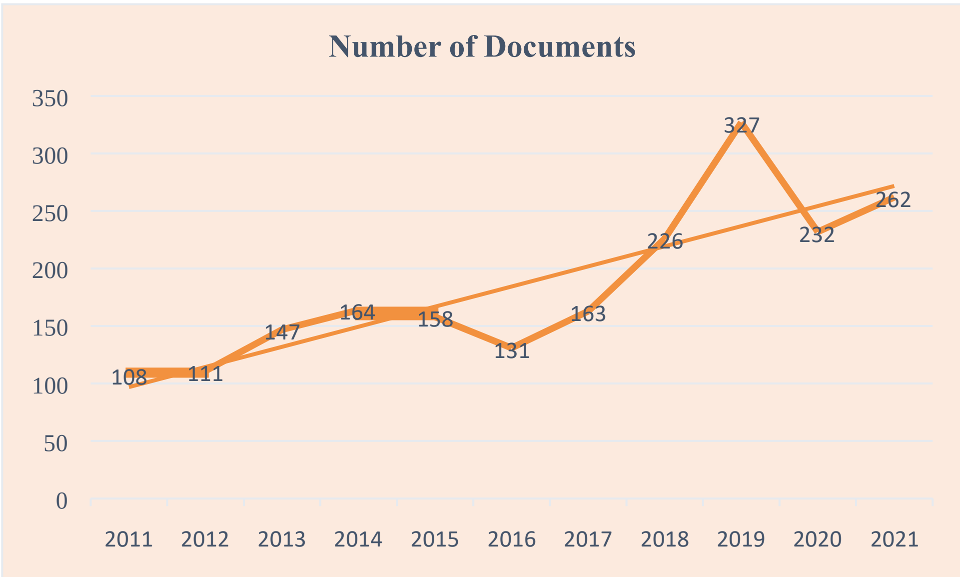

Figure 1. Number of documents on liquefaction (2011-2021)

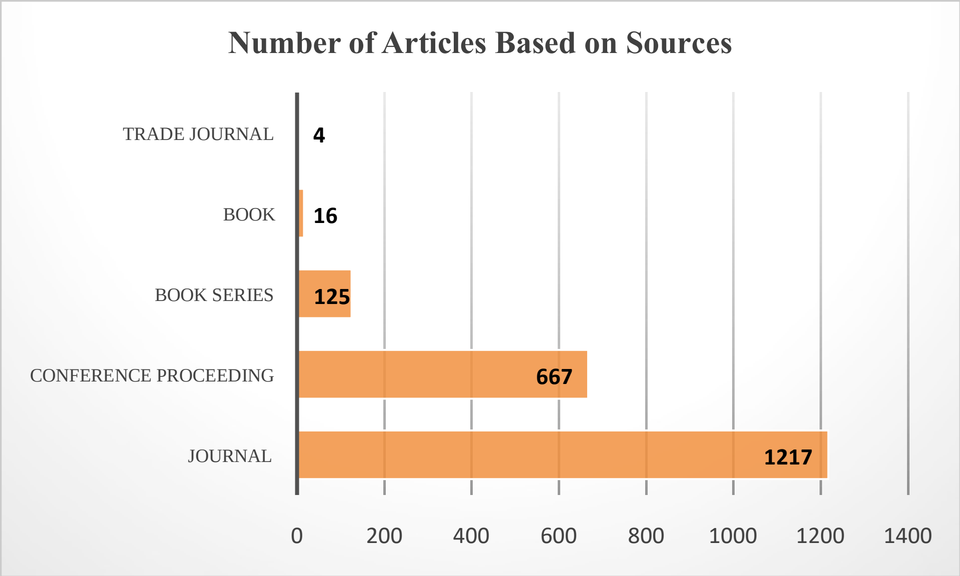

Figure 2. Documents' source types

As illustrated in Figure 2, there are five sources of documents relating to liquefaction. These include journals, conference proceedings, book series, books, and trade journals. Also, Figure 2 indicates that journals are more prominent in the number of documents amounting to 1,217 publications. Subsequently, conference proceedings contained up to 667 documents and a book series 125 documents. Books and trade journals were the fewer sources of documents.

Furthermore, there are 11 document types relating to liquefaction. These are articles, conference papers, book chapters, reviews, notes; data papers, erratums, editorials, letters, retractions, and conference reviews. As shown in Figure 3, the type of documents was a majority of 1,180 articles, followed by 758 conference papers and 41 book chapters.

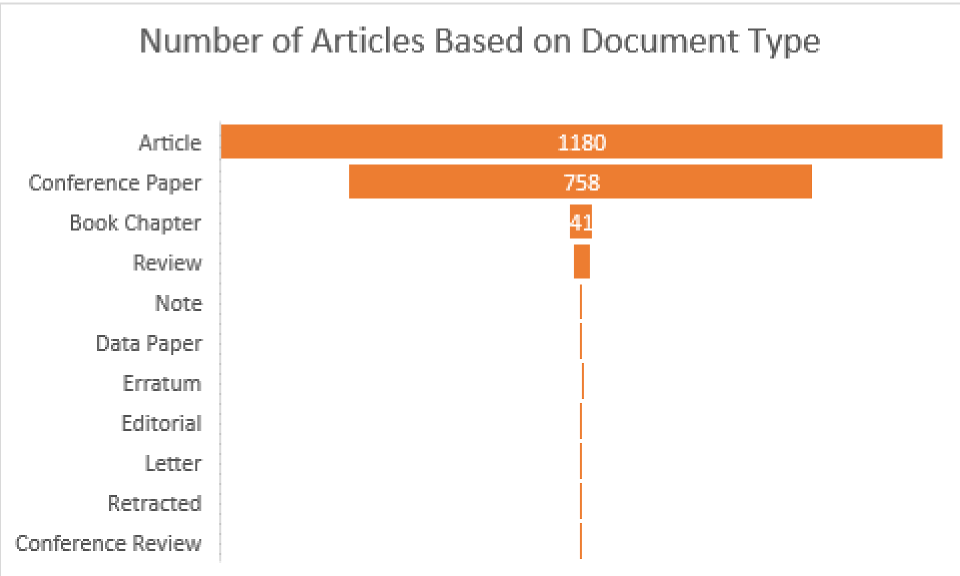

Figure 3. Types of documents

As illustrated in Figure 4 below, of the 3,489 documents, 878 documents were written in English. Other documents were 126 documents in Chinese, 10 in Turkish, 7 in Japanese, 5 in Spanish, 3 in German, 2 in Korean, and 1 in French.

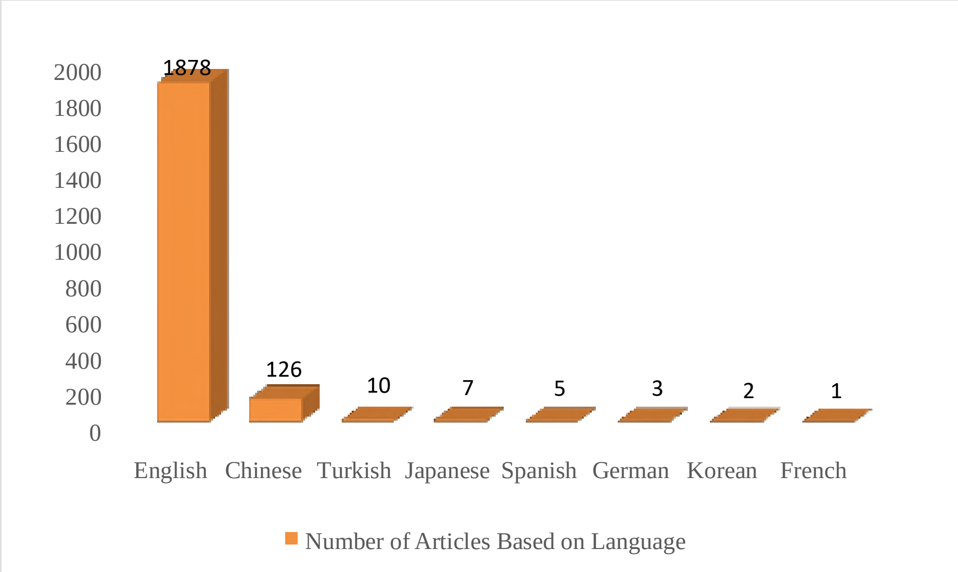

Figure 4. Language used

Furthermore, Figure 5 shows several keywords that were used in searches for the topic of liquefaction. Accordingly, the term "Liquefaction" was used in the search of 1,308 documents and "Soil Liquefaction" of 1,233 documents. The term "Earthquakes" was used in the search of 1056 documents, "Soils" with 691 documents, "Geotechnical Engineering" with 378 documents, "Liquefaction Potentials" with 337 documents, "Soil Mechanics" with 322 documents, "Earthquake Engineering" with 320 documents, "Sand" with 272 documents, and the last "Earthquake" with 236 documents.

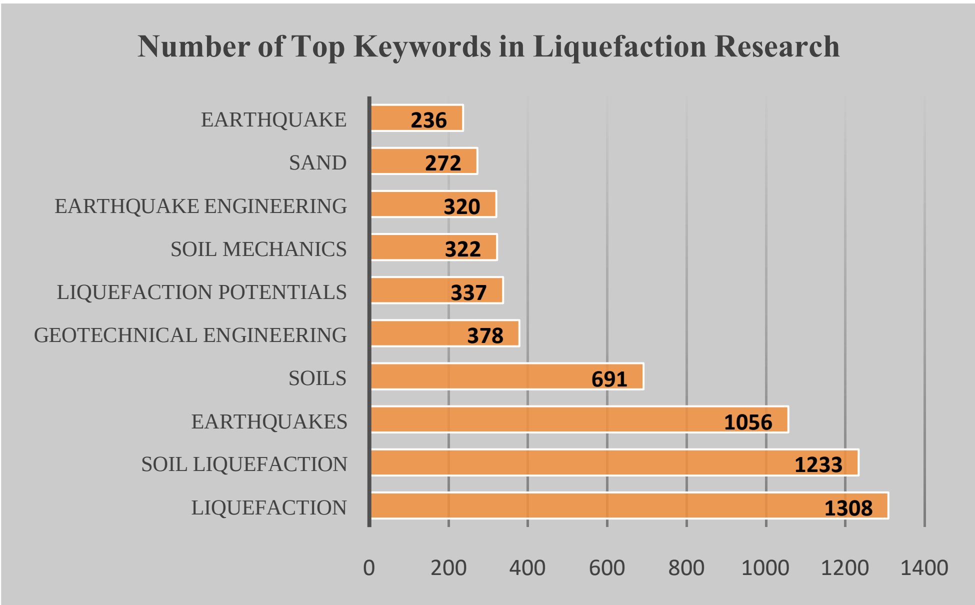

Figure 5. Top Keywords to search for Liquefaction

Some dominant subject areas related to liquefaction are listed in Table 1. The three most prominent subject areas were found in "Earth and Planetary Sciences" with 1,535 documents, in "Engineering" with 932 papers, in "Environmental Science," with 474 documents.

Table 1. Subject Area in studies related to Liquefaction

No	Subject Area	Number of Documents
1	Earth & Planetary Sciences	1,535
2	Engineering	932
3	Environmental Science	474
4	Agricultural & Biological Sciences	282
5	Computer Science	97
6	Materials Science	75
7	Energy	62
8	Physics and Astronomy	60
9	Social Sciences	51
10	Mathematics	43

3.2 Distribution of Publication across Countries and Institutions

The distribution of published papers among different countries can be seen in Figure 6. As shown in Figure 6, 461 papers originated from the US has, 395 followed from China, 302 from Japan, 195 from India, 127 from Italy, 125 from New Zealand, 100 from Turkey, 95 from Indonesia, 95 from Iran, and 94 from the United Kingdom.

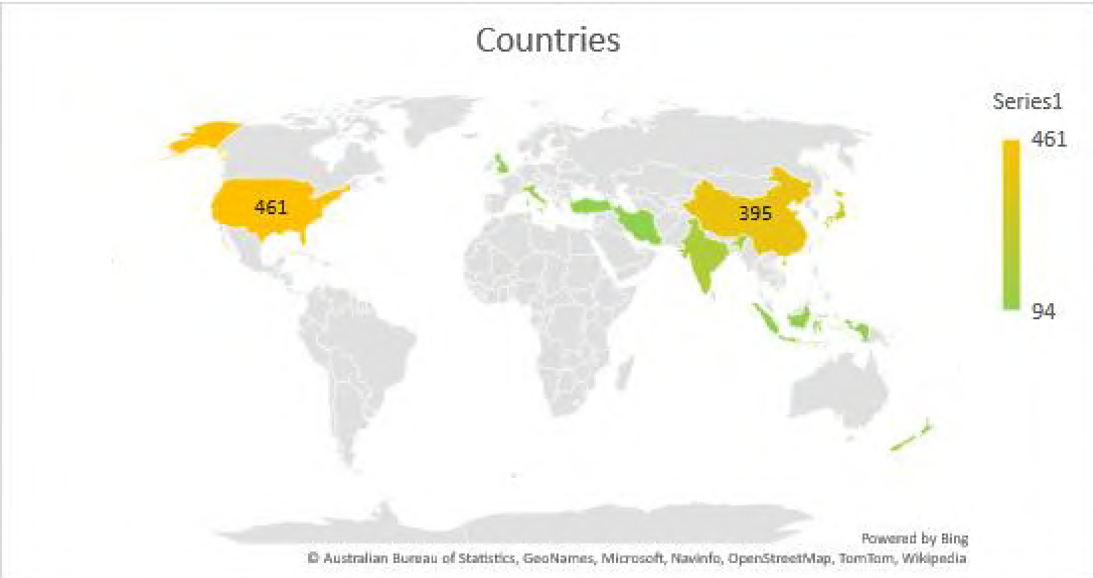

Figure 6. Number of documents across countries

Table 2 shows the classification of the number of documents related to liquefaction published by institutions. The University of Canterbury in New Zealand published 77, the China Earthquake Administration 60, the Ministry of Education China and the University of Tokyo 49 each, the University of California 44, the University of Auckland, the Virginia Polytechnic Institute, and State University 43 documents, Tongji University 42, the University of California at Davis 40, and the Brigham Young University 39.

Table 2. Documents by institutions

No	Institution	Number of Documents
1	University of Canterbury	77
2	China Earthquake Administration	60
3	Ministry of Education China	49
4	The University of Tokyo, Japan	49
5	University of California, Berkeley, USA	44
6	The University of Auckland	43
7	Virginia Polytechnic Institute and State University	43
8	Tongji University	42
9	University of California, Davis	40
10	Brigham Young University	39

3.3 Top Ranking of Authors in Researching Liquefaction

The list of research authors on liquefaction is shown in Figure 7. The most prolific authors for 2011 to 2021 were Owen, Kayen, Boulanger, Xiao, Cubrinovski, Yasuda, Van Ballegooy, Bhattacharya, Zhang, and Boulanger.

Figure 7. Top authors in researching liquefaction

The list of the top 10 citations on liquefaction research is indicated in Table 3 and Figure 8. Most of the articles cited were by Owen and Moretti (2011), with 240 based on the distribution. Kayen et al. (2012) had 212, Boulanger and Idriss (2016) had 173, Xiao et al. (2018) had 143, Cubrinovski et al. (2011) had 142, Yasuda et al. (2012) had 140, Van Ballegooy et al. (2014) had 136, Bhattacharya et al. (2011) had 130, Zhang J.M (2012) with 123, and Boulanger and Idriss (2012) had 107.

Table 3. Top citations on liquefaction documents

Author (s)	Journal	Number of Citations
Owen, G., Moretti, M. (2011)	Sedimentary Geology 235(3-4), 141-147	240
Kayen, R., Moss, R.E.S., Thompson, E.M., Tokimatsu, K. (2013)	J._ Geotechnical & Geoenvironmental Engineering 139(3), 407-419	212
Boulanger, R.W., Idriss, I.M. (2016)	J. Geotechnical and Geoenvironmental Engineering 142(2),04015065	173
Xiao, P., Liu, H. Liu, H., Xiao, Y., Stuedlein, A.W., Evans, T.M. (2018)	Soil Dynamics & Earthquake Engineering 107, 9-19	143
Cubrinovski, M., Bray, J.D., Taylor, M., Zupan, J. (2011)	Seismological Research Letters 82(6), 893-904	142
Yasuda, S., Harada, K., Ishikawa, K., Kanemaru, Y. (2012)	Soils & Foundations 52(5), 793-810	140
Van Ballegooy, S., Malan, P., Lacrosse, V., Cowan, H. (2014)	Earthquake Spectra 30(1), 31-55	136
Bhattacharya, S., Hyodo, M., Goda, K., Tazoh, T., Taylor, C.A. (2011)	Soil Dynamics and Earthquake Engineering 31(11), 1618-1628	130
Zhang, J.-M., Wang, G. (2012)	Acta Geotechnica 7(2), 69-113	123
Boulanger, R.W., Idriss, I.M. (2012)	J. Geotechnical and Geoenvironmental Engineering 138(10), 1185-1195	107

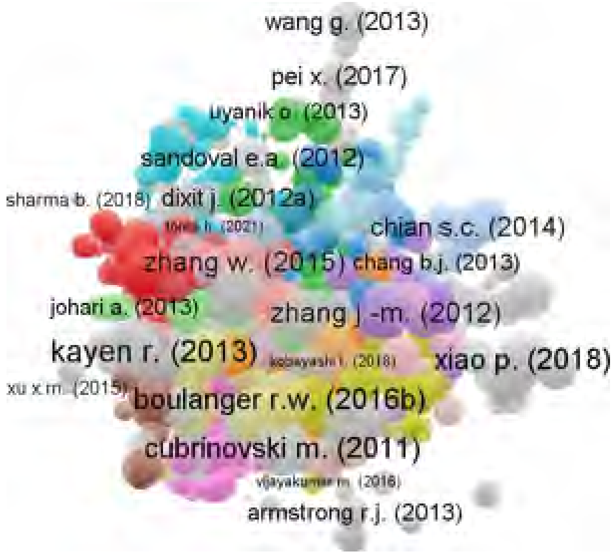

Figure 8. Top citations in researching liquefaction

3.4 Publication Patterns

Table 4 lists 12 journals and proceedings that contributed the most to liquefaction. At the top of the ranking, the journal Geotechnical Special Publication published the most documents on liquefaction (144 documents) and "Earthquake Geotechnical Engineering for Protection and Development of Environment and Constructions Proceedings of the 7th International Conference on Earthquake Geotechnical Engineering", and "Soil Dynamics and Earthquake Engineering" with 137 and 128 papers, respectively.

Table 4. Source title of documents

No	Source Title	Number of Documents
1	Geotechnical Special Publication	144
2	Earthquake Geotechnical Engineering for Protection and Development of Environment and Constructions Proceedings of The 7th International Conference on Earthquake Geotechnical Engineering 2019	137
3	Soil Dynamics and Earthquake Engineering	125
4	Journal of Geotechnical and Geoenvironmental Engineering	68
5	Lecture Notes in Civil Engineering	53
6	Engineering Geology	46
7	Bulletin of Earthquake Engineering	34
8	Soils and Foundations	34
9	Earthquake Spectra	31
10	Iop Conference Series Earth and Environmental Science	30
11	Yantu Gongcheng Xuebao Chinese Journal of Geotechnical Engineering	30
12	Natural Hazards	28

3.5 Visualization Maps of Liquefaction

This study used VOSViewer software and 3,489 liquefaction documents in the Scopus database. Figure 9 below is a visualization of liquefaction topics from 2011 to 2021. Scientists worldwide visualizations produce five colors: yellow, red, green, blue, and purple clusters. The first cluster (green) relates to the reliability and accuracy of the liquefaction documents. Followed by the second cluster (yellow) corresponds to liquefaction consistency. The third cluster (red) is regarding the map and city of liquefaction. The fourth cluster (blue) relates to the deformation of liquefaction. Moreover, the last cluster (purple) is for the country that experienced effects of liquefaction. Figure 10 indicates the central dominance of research in the interval of 2016-2018 from an overlay visualization.

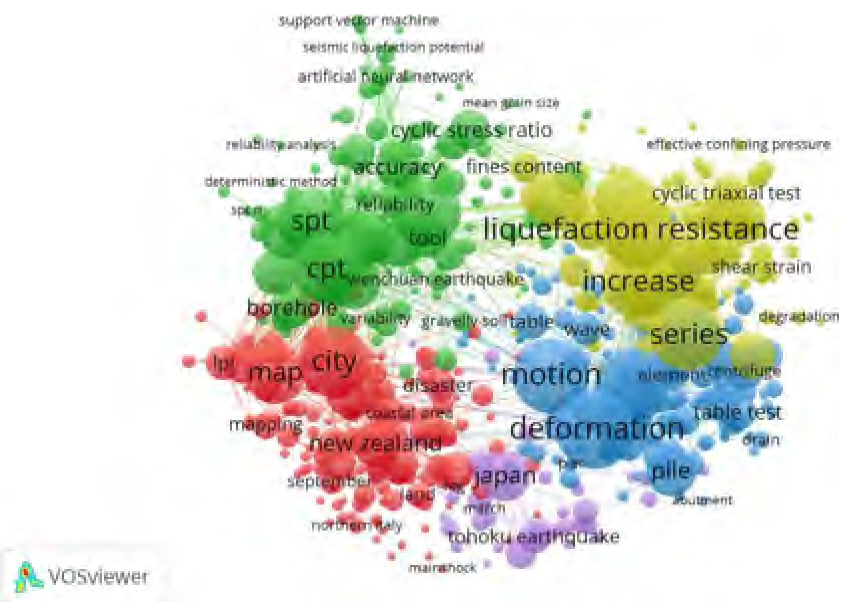

Figure 9. Network visualization (all years)

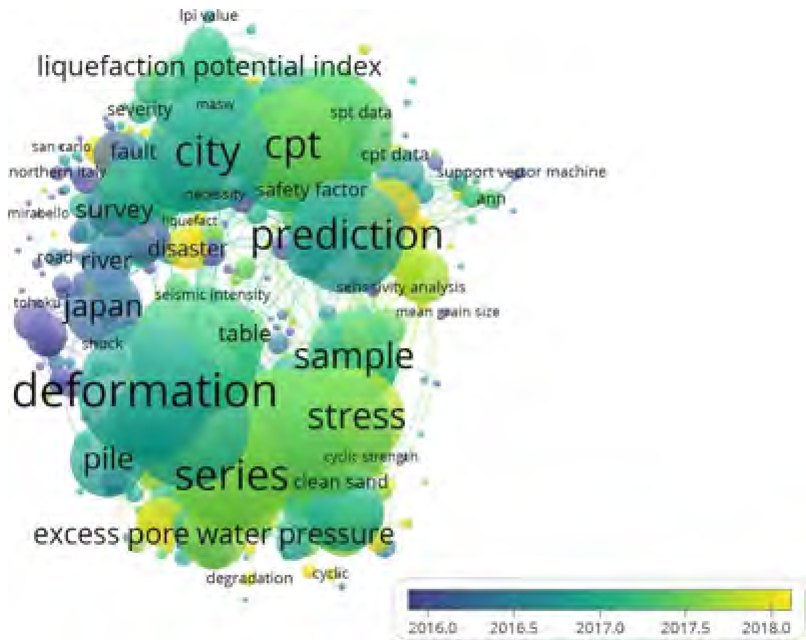

Figure 10. Overlay visualization (for 2016-2018)

Figure 11a shows the principal authors, co-authors, and the most influential authors of publications regarding Liquefaction. The visualization differentiates six main groups of writers, such as Cubrinovski et al., Boulanger R.W et al., Yuan X et al., Orense R.P et al., Kramer S.L et al., and Flora A et al. Moreover, in Figure 11b, a visualization of co-occurrence across all keywords is mapped, which indicates that "Liquefaction" is the most frequent keyword, followed by "liquefaction potential" and "liquefaction resistance".

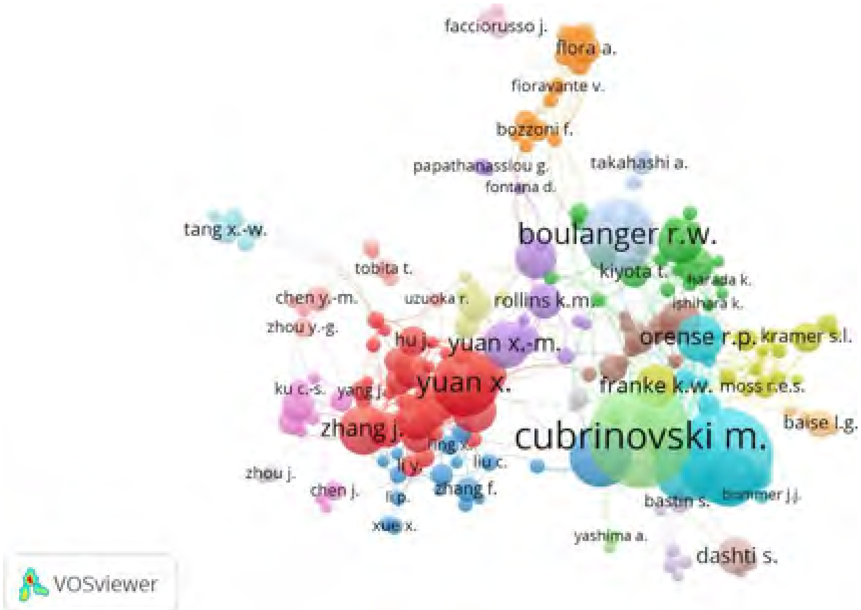

Figure 11 (a) "A network visualization of co-authorship",

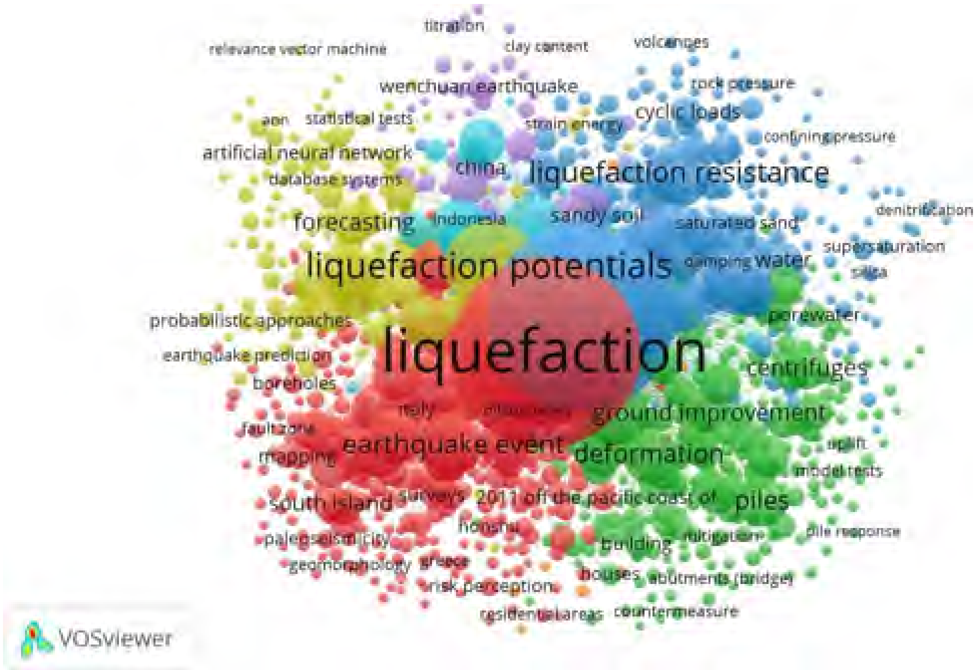

Figure 11 (b) "A network visualization of co-occurrence across all keywords"

Since ground liquefaction is a natural disaster that occurs in numerous parts of the world, researchers from across countries are involved in researching it. Therefore, it is necessary to indicate the countries of researchers involved in the topic of liquefaction research. Figure 12 depicts the visualization of co-authorship from different countries, and Figure 13 shows the visualization of co-citation from different authors (Figure 13a) and the visualization of citations from countries (Figure 13b).

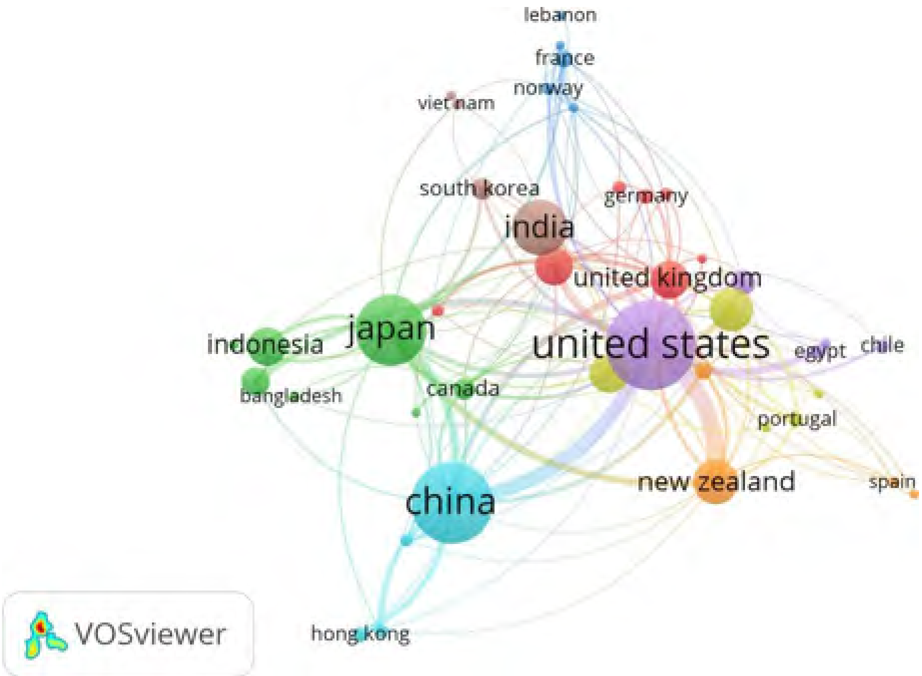

Figure 12. A network visualization of co-authorship across countries

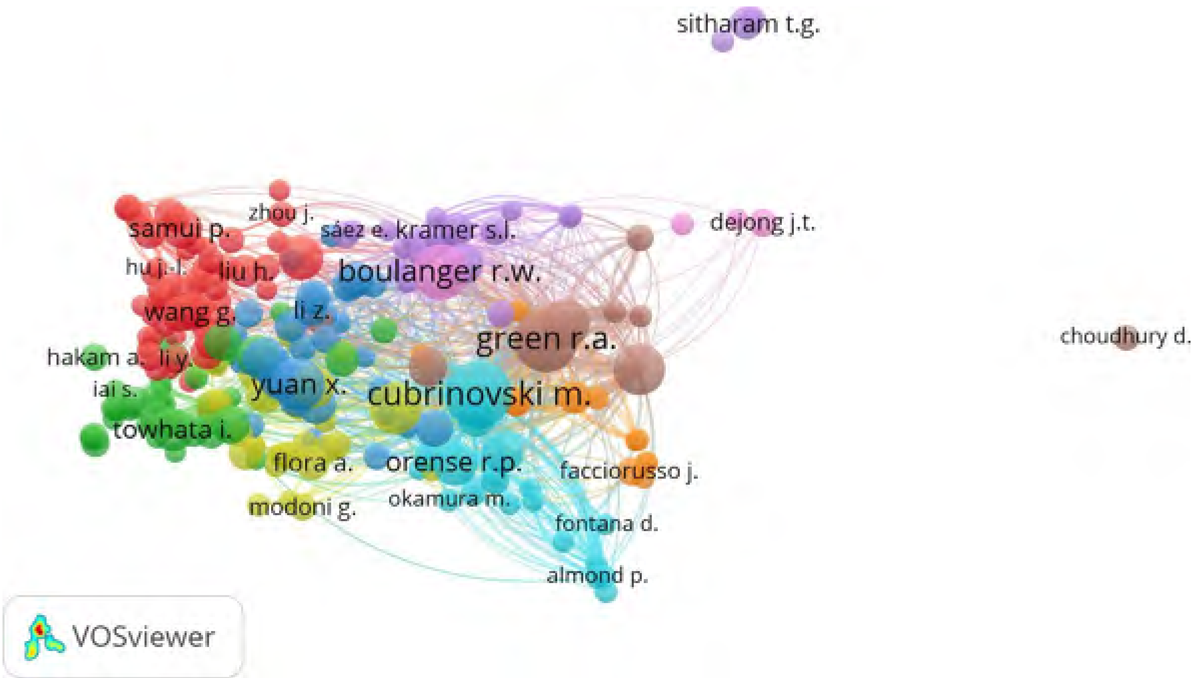

Figure 13 Visualization of co-citation from different authors

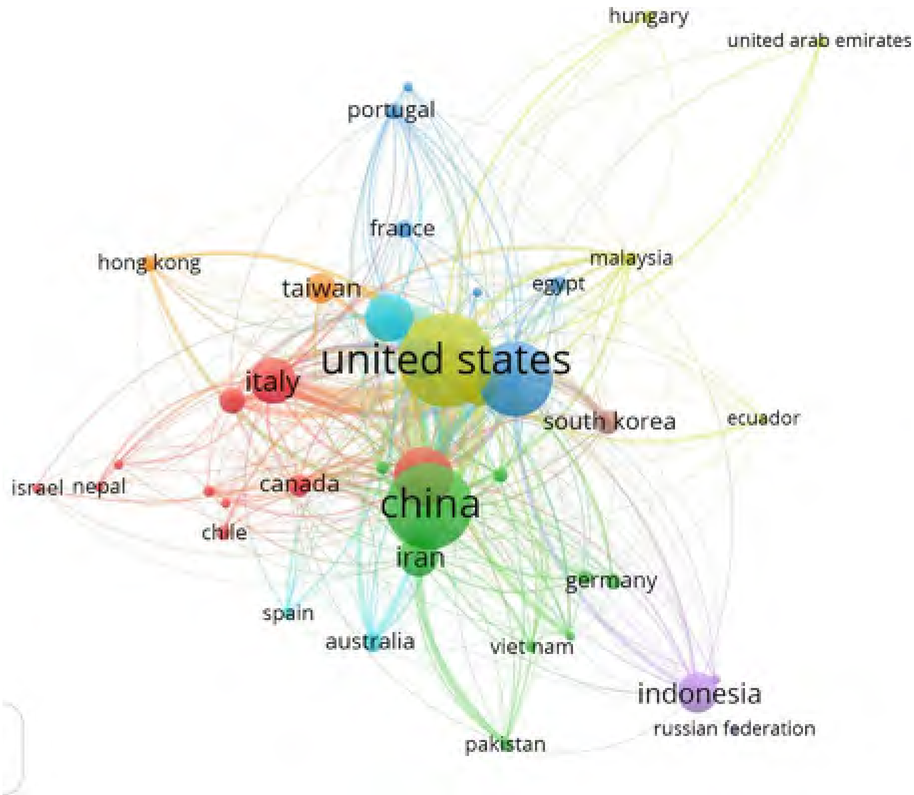

Figure 13. (b) Network visualization of citation across countries”

3.6 Indonesian Contribution to the Topic of Ground Liquefaction

Indonesia participated with 95 published documents on liquefaction in the last ten years (2011-2021). It can be seen in Figure 14 that there has been an enhancement in paper numbers in the previous four years, from 2017 to 2020.

Figure 14. Annual number of research documents on liquefaction in Indonesia

As international scientists delivered five clusters related to ground liquefaction research, Indonesian authors had three clusters (red, green, and blue) of similar work, as shown in Figure 15. The first cluster (green) related to the terminology of liquefaction. The second cluster (red) relates to the type of liquefaction and the potential of liquefaction. The last cluster (blue) refers to the effect of liquefaction.

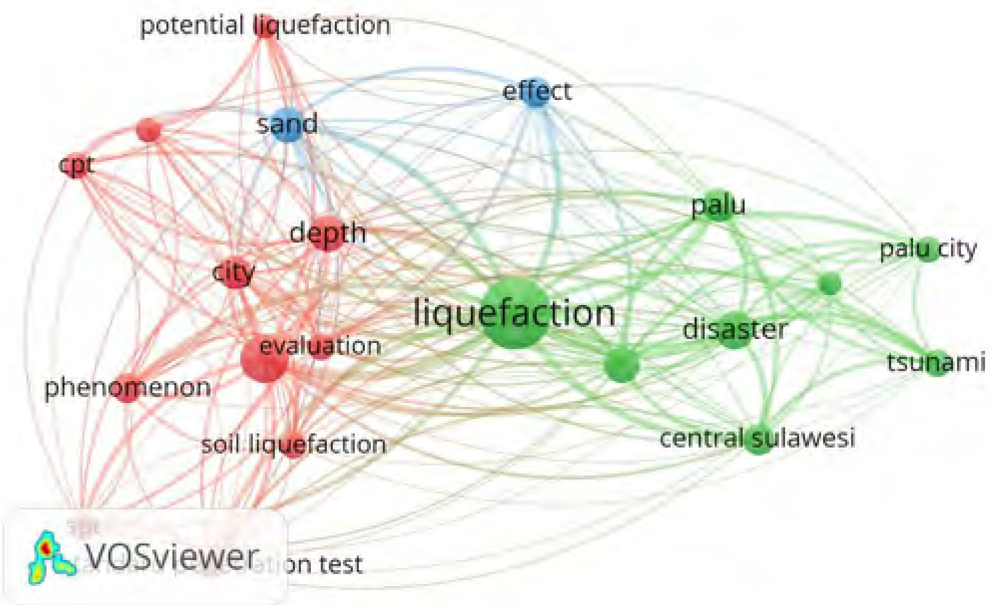

Figure 15. A network visualization of metadata (Indonesian documents)

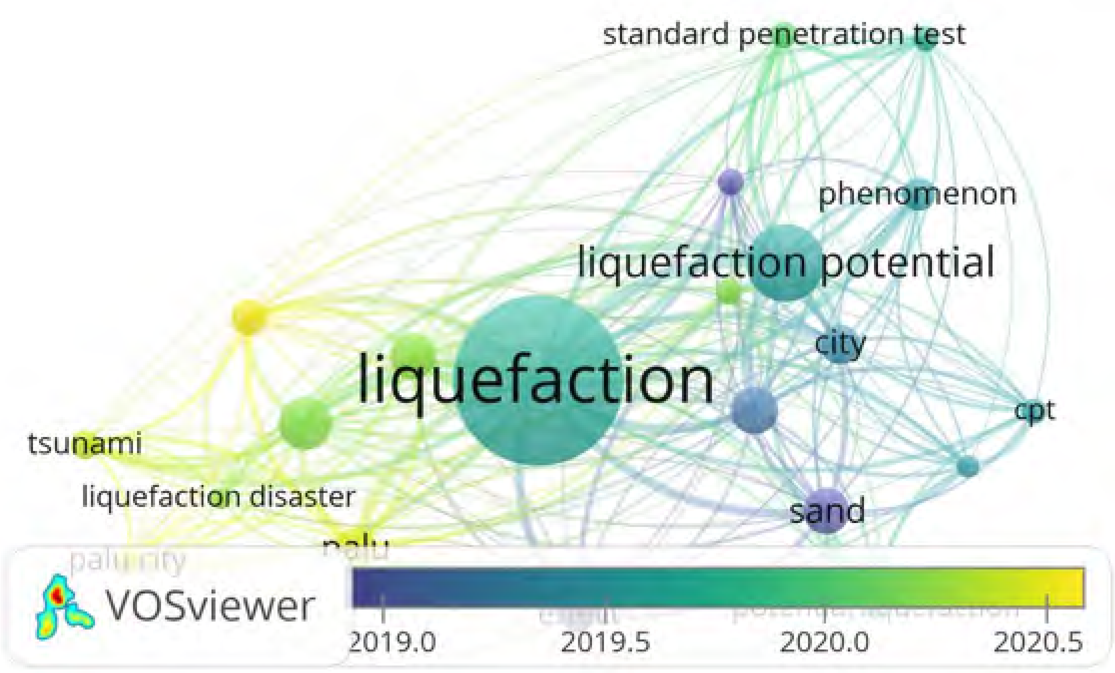

Figure 16. An overlay visualization 2019- 2020.5 (Indonesian documents)

The top 10 rankings of sources among Indonesian liquefaction researchers are presented in Table 5. First of those was “the IOP Conference Series Earth and Environmental Science” with 20 papers, followed by “the E3s Web of Conferences” with 11 papers. Then “IOP Conference Series Materials Science and Engineering” and “Journal of Physics Conference Series” with six papers, respectively. At the same time, other journals or proceedings published less than six documents.

Table 5. Document by source title (Indonesia data)

No	Source Title	Number of Documents
1	IOP Conf. Ser. Earth & Environmental Science	20
2	E3s Web of Conf.	11
3	IOP Conf. Ser. Materials Science and Engineering	6
4	Journal of Physics Conf. Series	6
5	AIP Conference Proceedings	5
6	International Journal of Geomate	5
7	Geoenvironmental Disasters	3
8	Journal of Engineering and Technological Sciences	3
9	16th Asian Regional Conference on Soil Mechanics and Geotechnical Engineering ARC 2019	2
10	Indonesian Journal on Geoscience	2

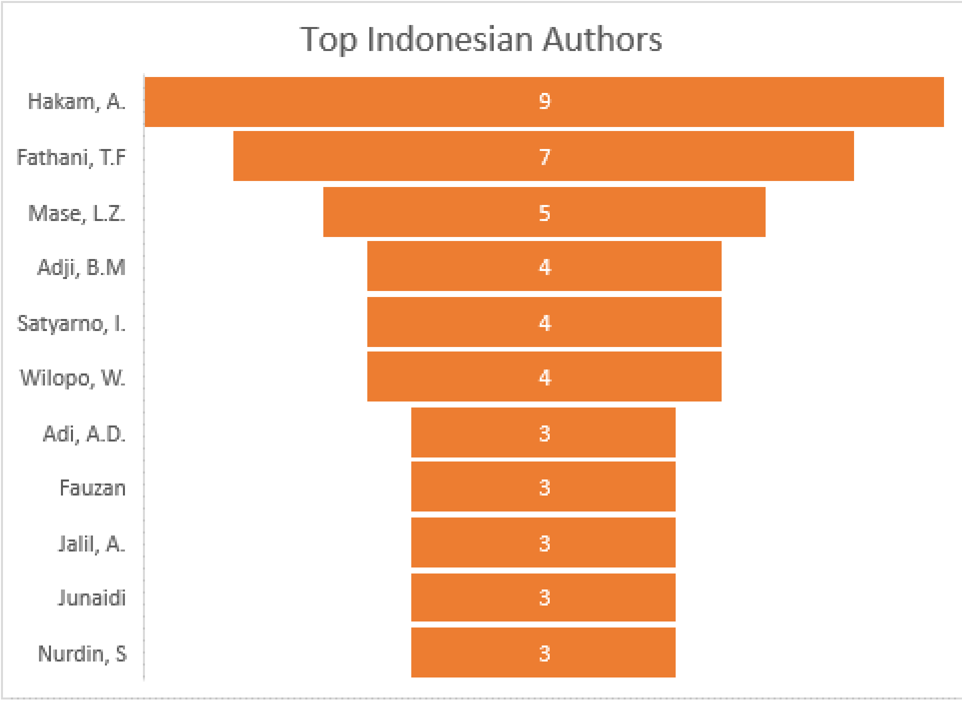

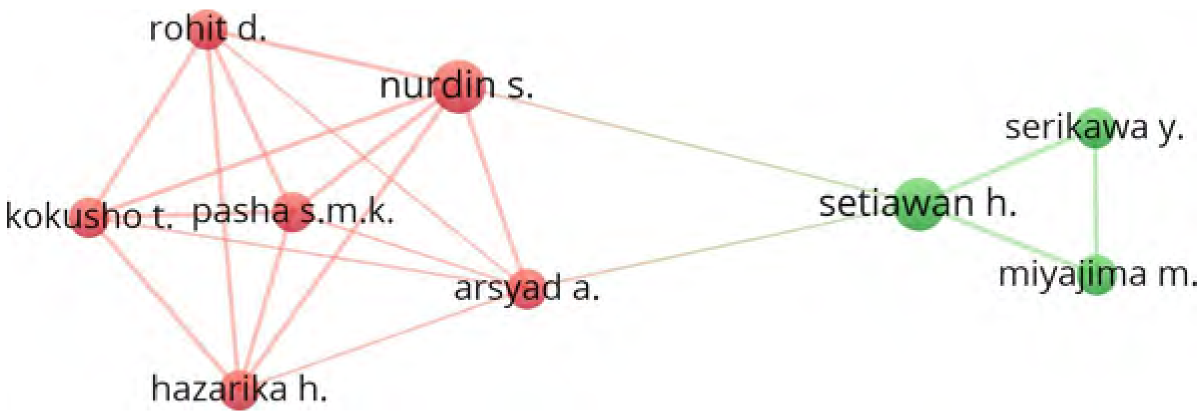

Figure 17. (a) Indonesia's leading authors on liquefaction. (b) A network visualization of Indonesian co-authorships

The visualizations of the top Indonesian authors and their colleagues who have contributed to research trends on liquefaction are presented in Figures 17a and 17b. Based on the graphs, it can be seen that Hakam, A. is the most voluminous author on this topic in Indonesia, followed by Fathani, T.F, and Mase L.Z.

Almost the same as the keywords related to research trends on liquefaction globally, in Indonesia, the keywords are voluminous by liquefaction, soil liquefaction, earthquake, and disasters (Figure 18).

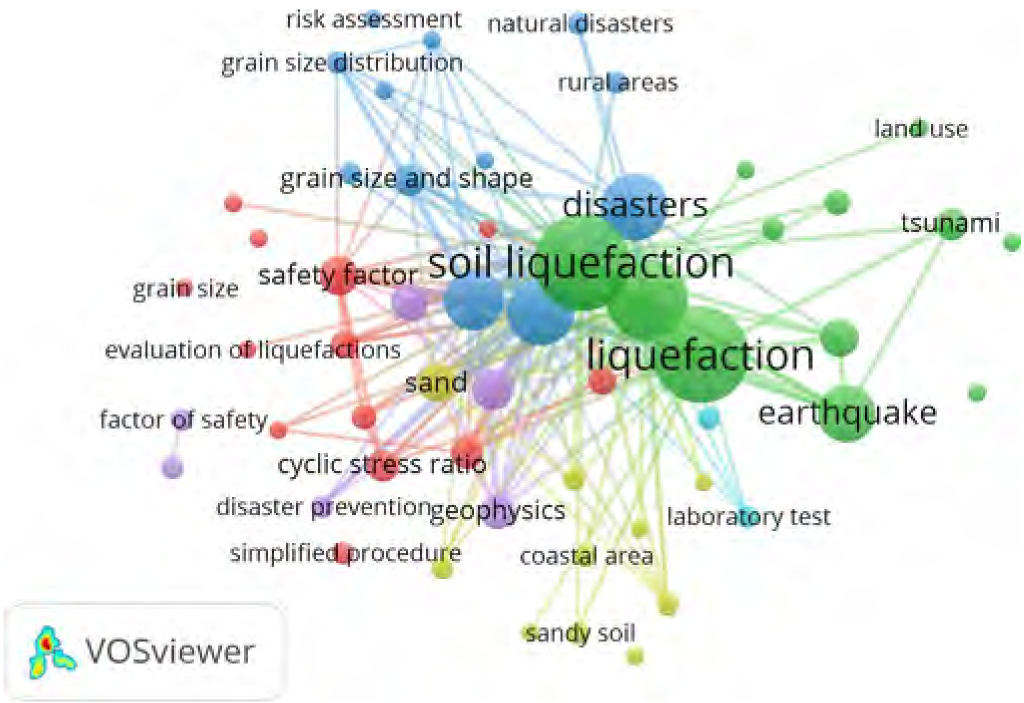

Figure 18. “A network visualization of co-occurrence among all keywords”

4. SUMMARY OF FINDINGS

As explained before, liquefaction decreases soil strength due to increased pore water pressure and a decrease in the adequate pressure of the soil layer due to dynamic repetitive loading. In the soil layer, dynamic periodic stresses are generated by seismic wave propagation of crustal motions. The phenomenon of liquefaction has attracted the attention of experts, especially in the field of engineering geology, after dramatic events resulting from the 1964 Japan and Alaska earthquakes. The number of papers related to ground liquefaction fluctuated year by year. Hundreds of documents on this crucial topic are being completed every year. This research trend has increased significantly in the last ten years. Based on this trend, it is expected that there will be a significant increase in the number of articles in the next five years.

Based on the distribution of papers among different countries, most of them originated in the United States, followed by China, Japan, India, Italy, New Zealand, Turkey, Indonesia, Iran, and the United Kingdom. The University of Canterbury topped the rankings with 77 documents, followed by the China Earthquake Administration with 60. The Ministry of Education of China and the University of Tokyo were ranked 4th and 5th with 49 documents each. The University of California published 44 documents, and he University of Auckland, the Virginia Polytechnic Institute, 43 documents. The Tongji University published 42 documents, the University of California at Davis published 40, and the Brigham Young University 39.

Based on the distribution, most of the cited articles were 240 by Owen G. (2011), 212 by Kayen R. (2012), 173 by Boulanger R.W. (2016), 143 by Xiao P. (2018), 142 by Cubrinovski M. (2011), 140 by Yasuda S. (2012), 135 by Van Ballegooy (2014), 130 by Bhattacharya S. (2011), 123 by Zhang J.M. (2012), and 107 by Boulanger R.W. (2012).

The top 10 rankings of document sources which contributed most to liquefaction research are presented in Table 5. First was the IOP Conference Series Earth and Environmental Science with 20 papers, followed by the E3s Web of Conferences with 11 papers. The IOP Conference Series Materials Science and Engineering and the Journal of Physics Conference Series published six papers, respectively. All other journals or proceedings published were less than six documents.

Scientists worldwide visualizations produced five distinct clusters on ground liquefaction. The first relates to the reliability and accuracy of the liquefaction. The second corresponds to liquefaction consistency. The third provides the map and city where such liquefaction occurred. The fourth relates to the type of deformation of liquefaction. Finally, the last cluster shows the countries that experienced such impact of ground liquefaction. Specifically, in the last ten years (2011-2021), Indonesia contributed and published 95 documents on this subject. From 2017 to 2020, there has been an increase in the number of papers. Hakam, A. is the most prolific author on this topic in Indonesia, followed by Fathani, T.F, and Mase L.Z.

CONCLUSIONS

During the period 2011 to 2021, some crucial points regarding research on liquefaction increased significantly throughout the years, dominated by articles in journals. Based on the number of documents published by countries, most papers were those by the United States. The institution that produced the more significant number of papers relating to liquefaction was the University of Canterbury in New Zealand.

The most contributing author on the subject of liquefaction for the present study period was Owen G.. The source that contributed most to liquefaction research for the study period was “the IOP Conference Series Earth and Environmental Science”. Visualization of research trends on liquefaction showed in five clusters: (1) Reliability and accuracy in reporting liquefaction; (2) Liquefaction consistency; (3) Map and city of liquefaction; (4) deformation due to liquefaction; and (5) The country that experienced liquefaction.

Indonesia contributed to documents related to liquefaction, which were published in the last ten years (2011-2021). There has been an enhancement in the number of papers in the previous four years, from 2017 to 2020. Hakam, A. is the most prolific author on this topic in Indonesia, followed by Fathani, T.F., and Mase L.Z. The above cited work can help researchers and readers identify trends related to liquefaction globally and provide an overview for future investigative work.

5. ACKNOWEDGEMENT

This study is part of the Fundamental Research (*Penelitian Dasar*) 2022 funded by DRTPM, DIKTI, the Ministry of Education, Culture, Research, and Technology in Indonesia, with the theme of bibliometric study in physics education.

REFERENCES

Anda, M., Purwanto, S., Suryani, E., Husnain, & Muchtar. (2021). Pristine soil property and mineralogy as the strategic rehabilitation basis in post-earthquake-induced liquefaction, tsunami and landslide in Palu, Indonesia. *Catena*, *203*,105345.

Bhattacharya, S., Hyodo, M., Goda, K., Tazoh, T., & Taylor, C. A. (2011). Liquefaction of soil in the Tokyo Bay area from the 2011 Tohoku (Japan) earthquake. *Soil Dynamics and Earthquake Engineering, 31*(11), 1618-1628.

Boulanger, R. W., & Idriss, I. M. (2016). CPT-based liquefaction triggering procedure. *Journal of Geotechnical and Geoenvironmental Engineering, 142*(2),04015.

Boulanger, R. W., & Idriss, I. M. (2012). Probabilistic standard penetration test-based liquefaction-triggering procedure. *Journal of Geotechnical and Geoenvironmental Engineering, 138*(10), 1185-1195

Cilia, M. G., Mooney, W. D., & Nugroho, C. (2021). Field insights and analysis of the 2018 Mw 7.5 Palu, Indonesia earthquake, tsunami and landslides. *Pure and Applied Geophysics, 178*(12), 4891-4920.

Cubrinovski, M., Bray, J. D., Taylor, M., Wotherspoon, L., & Zupan, J. (2011). Soil liquefaction effects in the central business district during the February 2011 Christchurch earthquake. *Seismological Research Letters, 82*(6), 893-904.

Hidayat, R., Arymurthy, A. M., & Dewantara, D. S. (2021). Disaster impact analysis uses land cover classification, case study: Petobo liquefaction. *2020 3rd International Conference on Computer and Informatics Engineering, IC2IE 2020, 9274573*, 432-436.

Ho, T.-C., Satake, K., Watada, S., Gusman, A. R., & Lu, C.-H. (2021). Tsunami Induced by the Strike-Slip Fault of the 2018 Palu Earthquake (Mw = 7.5), Sulawesi Island, Indonesia. *Earth and Space Science, 8*(6), e2020EA001400.

Kayen, R., Moss, R.E.S., Thompson, E. M., Tanaka, Y., & Tokimatsu, K. (2013). Shear-Wave velocity-based probabilistic and deterministic assessment of seismic soil liquefaction potential. *Journal of Geotechnical and Geoenvironmental Engineering, 139*(3), 407-419.

Kusumawardani, R., Chang, M., Upomo, T. C., Fansuri, M. H., & Prayitno, G. A. (2021). Understanding of Petobo liquefaction flowslide by 2018.09.28 Palu-Donggala Indonesia earthquake based on site reconnaissance. *Landslides, 18*(9), 3163-3182.

Lee, D. H., Ku, C. S., & Yuan, H. (2003). A study of the liquefaction risk potential at Yuanlin. *Taiwan Engineering Geology, 71*, 97-117.

Liou, C. P. (1976). *A numerical model for liquefaction in sand deposits*. University of Michigan, Department of Civil Engineering.

Mase, L. Z., (2013). *Analisis potensi Likuifaksi di Kali Opak Imogiri Daerah Istimewa Yogyakarta (Studi Eksperimental dan analisis empiris)"*, Tesis, Jurusan Teknik Sipil (Geoteknik) dan Lingkungan, Universitas Gadjah Mada.

Nurhasan, N., Prahani, B. K., Suprapto, N., Setiawan, B., Deta, U. A., & Al Ardha, M. A., (2022). Sports Research Trends in the Last 10 Years: Information to Librarians, Researchers, and Policy Makers. *TEM Journal, 11*(1), 289-296.

Owen, G. & Moretti, M. (2011). Identifying triggers for liquefaction-induced soft-sediment deformation in sands. *Sedimentary Geology, 235*(3-4), 141-147.

Pararas-Carayannis, G., (2020). Tsunami generation from major earthquakes on the outer-rise of oceanic lithosphere subduction zones: Case study earthquake and Tsunami of 29 September 2009 in the Samoan Islands Region. *Science of Tsunami Hazards, 39*(1), 2020, 33 -51.

Pararas-Carayannis, G., (2019). Earthquake of 21 February 2011 in New Zealand - Generation of glacial tsunami. *Science of Tsunami Hazards, 38*(3), 142-150. http://www.tsunamisociety.org/383GPC.pdf

Pararas-Carayannis, G., (2003). Near and far-field effects of tsunamis generated by the paroxysmal eruptions, explosions, caldera collapses and massive slope failures of the Krakatau Volcano in Indonesia on August 26-27, 1883 based on water wave records. *Science of Tsunami Hazards, 21*(4), 191-201.

Prahani, B. K., Nisa, K., Amiruddin, M. Z. B., Suprapto, N., Madlazim, & Mahtari, S. (2022). Analysis of the top 100 cited publications in earthquake research during 1991 to 2021. *Science of Tsunami Hazards, 41*(1), 77-94.

Seed, H. B., Idriss, I. M., Lee, K. L., & Makdisi, F. I. (1975). Dynamic analysis of the slide in the Lower San Fernando Dam during the earthquake of February 9, 1971. *Journal of the Geotechnical Engineering division, 101*(9), 889-911.

Seed, H. B. (1968). The fourth Terzaghi lecture: Landslides during earthquakes due to liquefaction. *Journal of the Soil Mechanics and Foundations division*, *94*(5), 1053-1122.

Setyabudi, A. P. (2013) *"Analisis probabilitas likuifaksi menggunakan metode liquefaction severity index untuk Kabupaten Bantul, Sleman, dan Kotamadya Yogyakarta*", Tugas Akhir, Jurusan Teknik Sipil (Geoteknik) dan Lingkungan, Universitas Gadjah Mada.

Sonmez, H. & Gokceoglu, C. (2005). A liquefaction severity index suggested for engineering practice, *Environmental Geology, 48*, 81-91.

Soekamto, R. A. B., Sumadirdja, H., Suptandar, T., Hardjoprawiro, S., & Sudana, D. (1973). *Peta Geologi Lembar Palu Skala 1:250.000, Sulawesi*. Pusat Penelitian dan Pengembangan Geologi, Bandung.

Suprapto, N., Kholiq, A., Prahani, B. K., & Deta, U. A. (2021a). Research on physics of photography: A bibliometric study (2000-2020). *Journal of Physics: Conference Series, 2110*(1),012017

Suprapto, N., Prahani, B. K., & Deta, U. A. (2021b). Research trend on ethnoscience through bibliometric analysis (2011-2020) and the contribution of Indonesia. *Library Philosophy and Practice*, 1-17.

Suprapto, N., Prahani, B. K., & Deta, U. A. (2021c). Top 100 cited publications in physics education in the last thirty years: A bibliometric analysis. *Library Philosophy and Practice*, 1-13.

Suprapto, N., Yanti, V. K., & Hariyono, E. (2022). Global research on tsunami education and tsunami mitigation: A bibliometric analysis. *Science of Tsunami Hazards, 41*(2), 130-148.

Tonkin & Taylor International Ltd. (2013). *Canterbury New Zealand earthquake sequence 2010- 2011*", Seminar on disaster preparedness in the Philippines.

UNDRR. (2019). *Global assessment report on disaster risk reduction.* United Nations Office for Disaster Risk Reduction (UNDRR), Geneva, Switzerland.

Van Ballegooy, S., Malan, P., Lacrosse, V., Crawford, S. A., & Cowan, H. (2014). Assessment of liquefaction-induced land damage for residential Christchurch. *Earthquake Spectra, 30*(1), 31-55.

Van Eck, N. J., & Waltman, L. (2020). *VOSviewer manual*. Retrieved from https://www.vosviewer.com/documentation/Manual_VOSviewer_1.6.16.pdf

Wijanarko, T. (2019). *Kerugian Gempa Sulawesi Tengah 2018 Mencapai Rp 18.48 Triliun*. Jakarta: Koran Tempo. Retrieved from: https://nasional.tempo.co/read/1201601/kerugian-gempa-sulawesi-tengah-2018-mencapai-rp-18-48-triliun

Xiao, P., Liu, H., Xiao, Y., Stuedlein, A. W., & Evans, T. M. (2018). Liquefaction resistance of bio-cemented calcareous sand. *Soil Dynamics and Earthquake Engineering, 107*, 9-19.

Yasuda, S., Harada, K., Ishikawa, K., & Kanemaru, Y. (2012). Characteristics of liquefaction in Tokyo Bay area by the 2011 Great East Japan Earthquake. *Soils and Foundations, 52*(5), 793-810.

Yogatama, B. A. (2012). *Analisis potensi likuifaksi di kawasan Kabupaten Bantul dan Kotamadya Yogyakarta*, Jurusan Teknik Sipil (Geoteknik) dan Lingkungan, Universitas Gadjah Mada.

Youd, T. L. & Perkins, D. M. (1978). Mapping liquefaction-induced ground failure potential". *Journal of the Geotechnical Engineering Division 104*(GT4), 433-446.

Yulianur, A., Saidi, T., Setiawan, B., Rusdi, M., & Affan, M. (2020). Microtremor datasets at liquefaction site of Petobo, Central Sulawesi-Indonesia. *Data in Brief, 30*,105554.

Zakhiyah, I., Suprapto, N., & Setyarsih, W. (2021). Prezi mind mapping media in physics learning: A bibliometric analysis. *Journal of Physics: Conference Series, 2110*(1),012015.

Zhang, J.-M. & Wang, G. (2012). Large post-liquefaction deformation of sand, part I: Physical mechanism, constitutive description and numerical algorithm. *Acta Geotechnica, 7*(2), 69-113.

Zhao, B. (2021). Landslides triggered by the 2018 Mw 7.5 Palu supershear earthquake in Indonesia. *Engineering Geology, 294*,106406.

ISSN 8755-6839

SCIENCE OF **TSUNAMI HAZARDS**

Journal of Tsunami Society International

Volume 41 Number 3 2022

HUNGA-TONGA-HUNGA-HA'PAI VOLCANIC ERUPTION/EXPLOSION AND TSUNAMIS OF 14-15 JANUARY 2022 – Overview and Analysis

George Pararas-Carayannis
Tsunami Society International

ABSTRACT

The explosive eruption/collapse of the submarine portion of the volcano Hunga-Tonga-Hunga-Ha'apai (HT-HH) on the Tonga Kermadec volcanic arc in the southwest Pacific on 15 January 2022 occurred at the end of many weeks of activity. It was a truly global event, as was the 1883 explosive eruption/collapse of the volcano of Krakatau in Indonesia and the 1490 BC explosion, caldera and flanc collapses of the Santorin volcano in the Aegean Sea, both generating destructive tsunamis. The eruption of HT-HH was a combination of a major submarine Surtsean (phreatomagmatic) and of a subsequent ultra-Plinian atmospheric explosion which generated a very damaging local tsunami by the crustal displacements of the volcano's caldera and flanc collapses, but also an atmospheric paroxysmal explosion similar to that of the Krakatau event. In recent years, the development of new instrumentation and of an expanded array of terrestrial and space instruments - including atmospheric pressure sensors, seismometers and a fleet of satellites monitoring the Earth across the entire spectrum of light – provided better global monitoring of the effects of this particular and unusual 2022 Hunga-Tonga volcanic event. Specifically detected were concentric atmospheric gravity waves, which also resulted in unusually-traveling ionospheric disturbances (CTIDs) – mapped on both of the earth's northern and southern hemispheres along conductive magnetic field lines, and which circled the earth three or four times many hours after the eruption/explosion. In addition to local destructive tsunami generation in the immediate area and elsewhere in the Paciific, the violent eruption created an impulsive Lamb wave propagation on the surface air pressure which, moving near the speed of sound at ~340 m., traveled faster than sea surface tsunami wave(s) and was observed globally - reaching Japan, Australia, Central and South America and elsewhere. Tsunami-like waves were observed or recorded, particularly along coastal areas of Central and South America. The present study provides an overview, an analysis and a brief comparison with past volcanic events and of their different tsunami generation mechanisms, as well as a brief description of the recorded atmospherically-generated waves and disturbances following the eruption/collapse of the HT-HH volcano.

1. INTRODUCTION

Hunga Tonga-Hunga Ha'apai (HT-HH) is a stratovolcano along the Tofua Volcanic Arc, a line of volcanoes fed by magma from the Pacific Plate's subduction beneath the Indo-Australian Plate. Its initial eruptive activity in December 2021, increased on 14 January 2022 and on 15 January 2022 the volcano exploded, creating atmospheric shock waves, sonic booms, tsunami waves and global sea level oscillations. Observed for many hours after the eruption were hurricane-speed winds and unusual electric currents in the ionosphere.

The final eruption of the HT-HH volcano (Tonga volcano) of 15 January 2022, was a combination of a major submarine Surtsean (phreatomagmatic) and of a subsequent ultra-Plinian atmospheric explosion which, not only generated a local and very damaging tsunami by the crustal displacements of its caldera and flanc collapses, but also an atmospheric paroxysmal explosion similar to that of 1883 Krakatau volcano in Indonesia (Pararas-Carayannis, 2004, 2006), and to the 1490 BC explosion, caldera and flanc collapses of the Santorin volcano in the Aegean Sea (Pararas-Carayannis, 2004; 2006; 2019).

The colossal explosion of the HT-HH volcano produced various types of atmospheric pressure waves that spread around the world. Repeated explosions of the event in the audible frequency range, were heard thousands of kilometers away.

Similar atmospheric air pressure perturbations can be also generated by large earthquakes involving significant vertical crustal displacements, as was the case with the 1964 Earthquake in Alaska, the 1975 Hilina Slump of the East Rift Zone of the Kilauea volcano in Hawaii, and elsewhere (Pararas-Carayannis G., 1967; 2018).

Tsunami or tsunami-like generation from volcanic sources may also result from a volcano's flank instabilities and subsequent gravitational collapses. Whether a strato-volcano has effusive or explosive eruptive activity is determined by the relative stability of its slopes. Thus, volcanoes with lavas of high andesitic composition and explosive type of eruptive activity tend to have steeper and more unstable flanks that often can fail massively. However, even shield stratovolcanoes - characterized by mainly effusive activity - can have significant flank failures and caldera collapses, although most are sub-aerial.

The following sections of the present study provide a brief description of the near and far-field effects of the tsunami generated by the 15 January 2022 Tonga volcanic eruption/explosion. Additionally included are a brief review of different mechanisms that can result in volcanic flank failures and the generation of tsunami or tsunami-like waves (Pararas-Carayannis, 1975, 2002; Toulkeridis EtAl. 2022). As further discussed, volcanic flank failures may result from isostatic load adjustments, extensive erosion, gaseous pressures, violent phreato-magmatic eruptions, magmastatic pressures, gravitational collapses of magmatic chambers, dike and cryptodome intrusions, as well as from the buildup of hydrothermal and supra-hydrostatic pore fluid pressures. Other sources of tsunami generation and of atmospheric disturbances may be caused by flank failures of coastal or oceanic volcanoes.

In addition to the volcanic sources, large magnitude earthquakes involving significant vertical crustal displacements can also generate atmospheric pressure waves. For example, the 1964 Alaskan earthquake generated such waves, which were recorded by distantly located microbarographs. Since the propagating speed of these atmospheric waves were faster than that of tsunami waves, the use of such microbarographs was proposed to serve as a precursory method of forecasting/warning about potential tsunami generation (Pararas-Carayannis. & Vitousek, 1967).

Furthermore, tsunami waves can be generated by a rapid, significant and progressive drop in atmospheric pressure which may be caused by a moving storm or hurricane, in which case the impact would be localized and directional, as was the case with the meteo-tsunami of 29 August 1916 at Santo Domingo, in the Dominican Republic – as documented in a report published by the Russian Academy of Sciences (Pararas-Carayannis, 2019). Finally, most of the mechanisms mentioned above have the potential of becoming sources of destructive tsunami generation.

What makes the present study of the Tonga volcanic eruption/explosion more interesting and relevant, is a better understanding of the far-field effects of the tsunami-like waves that were generated, based on the present technological ability to better measure the broad range of atmospheric waves generated by the force of the eruption, as well as by the instrumental detection of the atmospheric surface-guided Lamb wave perturbations that travelled at different propagation speeds - observed globally by ground-based and by space instrumentation. Also, it should be mentioned that historically less than 5% of volcanic eruptions/collapses have generated any significant tsunamis with far-reaching impacts, with the exception of that of 1490 BC of the Santorin volcano in the Aegean Sea, the 1883 A.D. Krakatau volcano in the Sunda Strait beteween Java and Sumatra in Indonesia, and a few other volcanoes in the Indian, Pacific and Atlantic oceans. Although rare, mainly local destructive tsunamis can also be generated by large scale sudden flanc failures of island statovolcanoes such those of Mauna Loa and Kilauea in 1868 and 1975, and of Cumbre Vieja on the island of La Palma in the Canary Islands (Pararas-Carayannis, 2002). However, greater source dimensions and longer wave periods are required to generate tsunamis that can have significant, far field effects.

The following sections of the present report present a brief description of the Tonga volcanic arc, ridge, adjacent trench and of the islands of Tonga, and an overview of the activity of the HT-HH volcano prior, during, and after the volcanic eruption/explosion of 15 January 2022, of the near-source and far-field tsunami generation, of the resulting atmospheric Lamb wave oscillations, of the ionospheric pertrubations, as well as of a cursory analysis and comparison of tsunami generation by other historical large volcanic eruptions, explosions and flanc collapses.

2. THE TONGA VOLCANIC ARC, RIDGE, AND TRENCH

The Kingdom of Tonga is a group of about 170 islands, of which about 45 are inhabited. The largest island of the group is Tongatapu, inhabited by about two-thirds of the country's population. It is a relatively flat coral island, where its capital Nuku‘alofa is located, as well as several towns and villages such as Mu‘a, Nukunuku, Holonga, Pea, and the country’s Fua‘amotu International Airport. The Tonga island chain sits on an underwater mountain range, the 3,000 km long Tonga-Kermadec Rid**ge**, which is the most seismically active subduction boundary on planet Earth, and has the highest density and number of undersea volcanoes. Figure 1 below show the bathymetry of the Tonga Trench and Forearc.

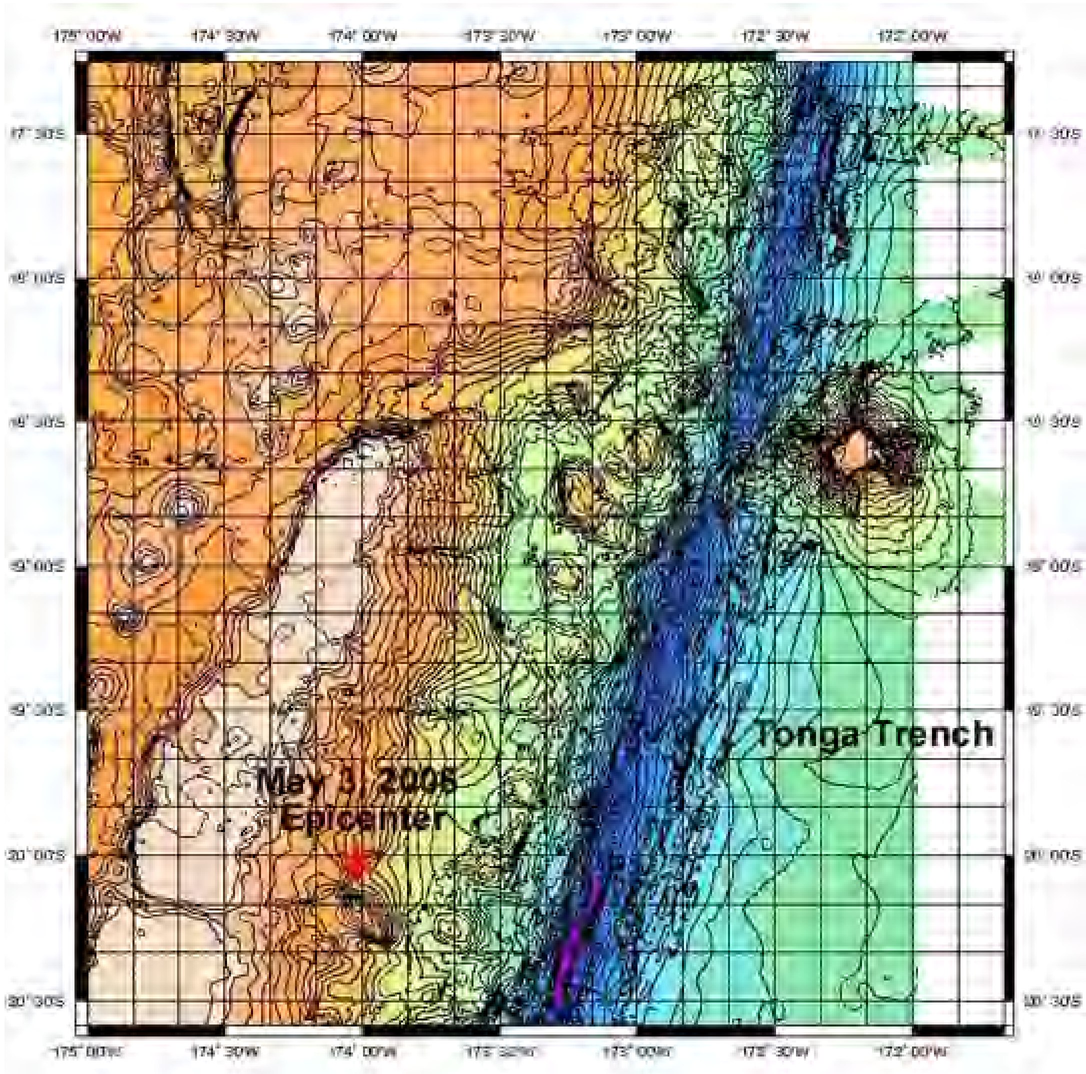

Figure 1. Bathymetry of the Tonga Trench and Forearc (after Pararas-Carayannis, 2006, modified map after Wright et al., 2000 - from http://dusk2.geo.orst.edu/tonga/fig9.gif)

The Tonga Ridge parallels the Tonga Trench, which is the deepest oceanic trench in the Southern hemisphere and the second deepest oceanic trench on Earth after the Mariana Trench, which is located east of Guam. The Horizon Deep South of the Tonga Trench is located about 220 km southeast of the main island Tongatapu and has a maximum depth of 10,800 m. To the west of the Tonga-Kermadec Ridge is the chain of underwater volcanoes, known as the Tonga Volcanic Arc (Colombier, EtAl. 2018; Dingwell, 2018). Within this arc are the island nation's volcanic islands of Hunga Tonga, Nomuka, Tofua, Kao, Late and Niuafo'ou. Tonga’s highest mountain is the island of Kao - a volcano which rises 1,033 m above sea level. Figure 2 is a relief map showing the territory of Tonga, north of the Tropic of Capricorn, the Tonga Ridge, the adjacent volcanic arc, the Tonga Trench, and the location of the Horizon Deep. Subduction of the oceanic Hikurangi Plateau impacts on the Kermadec arc (Tim EtAl, 2014).

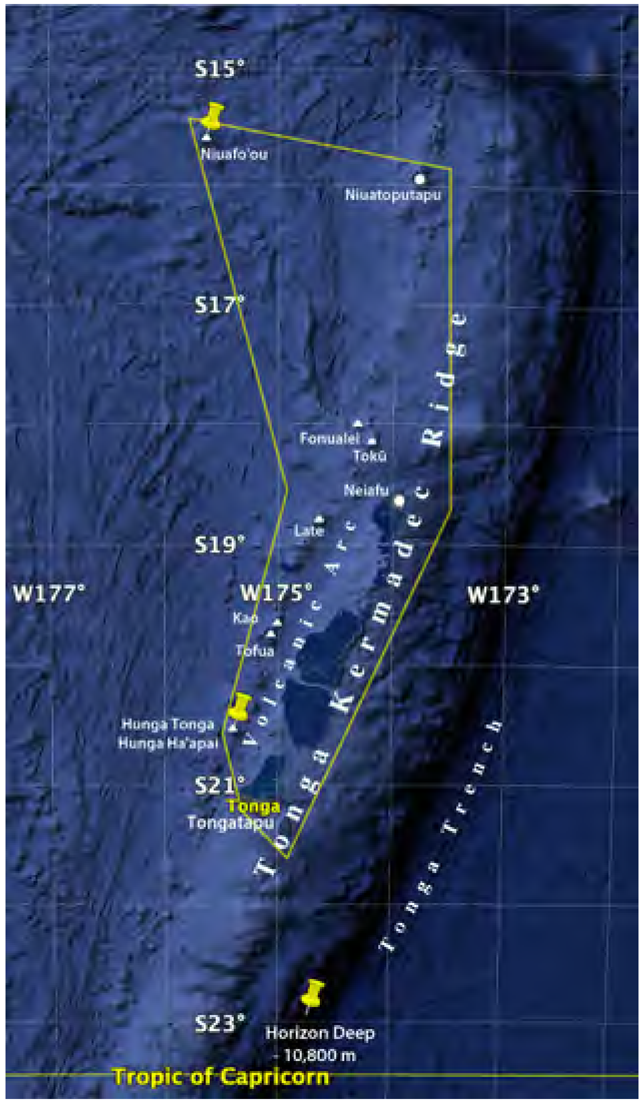

Figure 2. Relief map of the territory of Tonga, north of the Tropic of Capricorn, of the Tonga Ridge and the adjacent volcanic arc, of the Tonga Trench, and of the location of the Horizon Deep. (Source: Google Earth)

2A. Geodynamic Setting and Underwater Structure **of Hunga Tonga-Hunga Ha'apai Volcano**

Dacitic volcanism prevails along the Tonga-Kermadek volcanic arc where the HT-HH exists and was developed by subduction of slabs beneath the eastern Indonesia–Tonga region (Worthington EtAl. 1999; Hall & Spakman, 2002). The image below (Fig. 3) is a Planet Labs PBC/via REUTERS SkySat image which shows the upper, above-sea rim of the Hunga Tonga-Hunga Ha'apai (HT-HH) on January 15, 2022, two hours before the underwater volcano's hydro magmatic eruption/explosion at 5:10 p.m. on the same day (GoogleEarthTM, 2022).

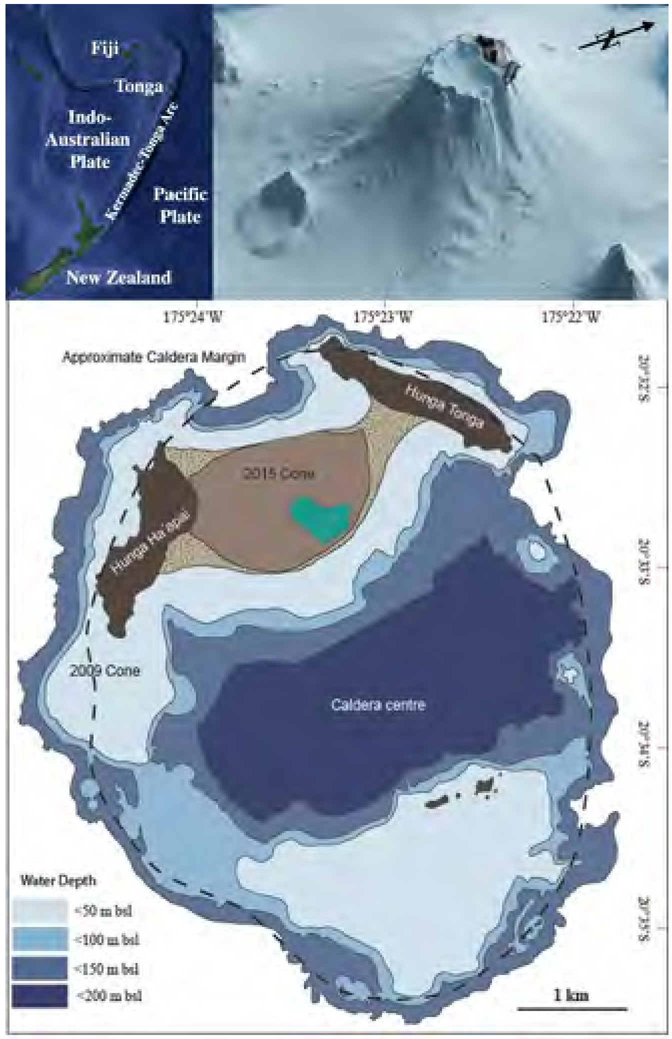

Figure 3. Upper left: Geodynamic setting of Tonga. Credit GoogleEarthTM (2022). Upper right: A rendering of the HT-HH volcano shows the part of the peak that is known as the two Tongan islands Hunga-Tonga and Hunga-Ha'apai. Credit Frederik Ruys; Below: Volcanic structure of Hunga Tonga-Hunga Ha'apai volcano based on elevation and a bathymetric map of the underwater portion of the volcano. Credit Shane Cronin / The Conversation, 2022. (After Toulkeridis EtAl., 2022).

This upper right portion of Figure 3 shows the geodynamic setting of the Tonga group of islands and the peak comprising of the two Tongan islands of Hunga-Tonga and Hunga-Ha'apai. The portion below the same image shows the above and below water volcanic structure of the entire HT-HH volcano - including both the above water elevation and its underwater bathymetry which appeared in a news report (Credit Shane Cronin /T Conversation, 2022), and also combined and reproduced in a paper published in the January 2022 issue of the journal Science of Tsunami Hazards (Toulkeridis EtAl. 2022).

3. THE HUNGA-TONGA-HAPA'I VOLCANO'S ERUPTION/EXPLOSION SEQUENCE

Figure 4 below are satellite NASA photos showing the eruption/explosion sequence before and following pre-existing smaller caldera's initial activity. All that remained locally after the paroxysmal expliosion were the two mentioned preexisting small islets of Hunga Tonga and Hunga Ha'apai, again separated by the sea.

Figure 4. Eruption/Explosion Sequence: Upper left: Hunga Tonga-Hunga Ha'apai prior to As eruption.(Credit GoogleEarthTM in2021). Upper right: Status of Eruption by January 7. 2022. (Credit: Planet Labs PBC/EYEPRESS/Shutterstock), Lower left: A Planet SkySat image shows Hunga Tonga-Hunga Ha'apai two hours before its eruption on January 15, 2022. (Credit:Planet Labs PBC/via REUTERS); Lower right: Remains of the island as seen on January 17, 2022. (Credit: Maxar Technologies Original Source: Copernicus/ESA/Sentinel Hub, PlanetLabs, Maxar (BBC))

3A. The Hunga-Tonga-Hunga-Ha'apai (HT-HH) Volcano's Prior Above-water Dimensions on the Northern Rim.

Monitoring and modeling the rapid evolution of the HT-HH volcanic island since its increasing activity in 2014-2015, begun in 2018 using high spatial resolution satellite observations (Garvin EtAl, 2018). But even earlier activity of the volcano was included in weekly reports of the Smithsonian Institution and of the U.S. Geological Survey (Global Volcanism Program 2009, 2014, 2015, 2021 a b and c., and 2022).

The HT-HH volcano is located about 65km (40 miles) north of the kingdom of Tonga's capital, Nuku'alofa, on the main island of Tongatapu. Before its latest eruptive activity which begun in November 2021, its maximum height from the bottom of the sea was about 1,800 meters, its width was about 20 km, and a portion of its height above sea level was 114 meters. Earlier volcanic activity in 2014 and 2015 had joined the Tonga volcano with the adjacent islands of Hunga Tonga and Hunga Ha'apai, both of which had been produced by older volcanic eruptions in the northern segment of the Tonga Kermadec volcanic arc (Fig. 5).

Following an earlier eruption of 20 December 2021, on 11 January 2022, the Tonga volcano was declared dormant. However, satellite photos taken by Planet Labs PBC from 17 November 2021 up to Friday, 14 January 2022 showed that a larger island had been created on the north side of the undersea volcano.

Figure 5. NASA satellite image of the uppermost, above water pre-existing part of the rim and secondary caldera of the HT-HH volcano of Hunga in December 2021.

The dimensions of the above water portion of the northern rim of the volcano that existed before the 15th January 2022 eruption/explosion were about 3.5 km in lenght and 1.7 km wide. On either side of this newly formed, above water section – and stil partly remaining – were the preexisting islets of Hunga Tonga and Hunga Ha'apai, which had been joined into a single landmass by an earlier eruption of the volcano in December 2014. Subsequently, and as shown in Figure 5, the above water middle portion of the volcano's upper land mass begun to grow in size due to the volcano's renewed activity of the above water smaller caldera, shown in the satellite photo above. By 14 January 2022, the volcano begun to erupt again with greater force, and a local partially destructive tsunami was generated. The source mechanism of this local preliminary tsunami is puzzling and needs to be further investigated. The question arises whether this initial and local tsunami was generated by uplift within a smaller caldera which may have been of the"Smith Caldera" type, similar to the one which followed the 2015 volcanic tsunami earthquake near Torishima in Japan (Fukao EtAl., 2018), or simply by a partial preliminary collapse of the rim of the HT-HH volcano. Whether such type of calderas exists along the

Tonga Kermadec volcanic arc is not known. However it is known that about 30 million years ago, massive ash and debris from nearby volcanoes had filled smaller calderas, which hardened into rock which resulted caldera-floor uplift of ~1.5 m when the volcanic tsunami earthquake of 2015 occurred on Torishima.

3B. Activity of the Hunga-Tonga-Hunga-Ha'apai (HT-HH) Volcano Prior to the Paroxysmal Eruption/Explosion of 15 January 2022

The HT-HH volcano was relatively inactive since January 2015, but reactivated on 20 December 2021, forming a large plume of ash visible from Tonga's capital city Nuku'alofa on the island of Tongatapu. The eruption continued until 2:00am on 21 December 2021 and included explosions, the sounds of which could be heard as far as 170 km away (Toulkeridis EtAl.. 2022; Fukao EtAl., 2022).

The volcanic activity reduced by 5 January 2022, but restarted strongly again on 13 January. On 14 January 2022, images of a strong eruption were captured by NOAA’s GOES-17 satellite, and on the same day the National Emergency Operations Centre was activated. This included the outer island Emergency Operations Centers in Ha'apai and Vava'u. At 4:40am local time a nationwide Tsunami warning was issued by the Tonga Meteorological Servicesa for all the islands of the Kingdom of Tonga. At 11:12am abnormal sea level fluctuationa were observed at Nuku'alofa’s waterfront. Tsunami waves up to 30 cm were initially recorded at the tidal gauge in Nuku'alofa. However waves of greater height arrived subsequnrly

Later in the afternoon of the same day, a Tonga Geological Services (TGS) team observed the eruption from a distance of 2 to 3 miles between 5:00pm and 6:30pm local time. (Fukao EtAl., 2022). The eruption continued until the next day, and probably resulted in the partial collapse of the HT-HH’s caldera, leaving most of the volcano submerged and leading to the separation of the Hunga Tonga inlet from the Hunga Ha'apai inlet (as captured by satellite imagery the next day at 3:25pm on 15 January 2022 – in Fig. 6. A plume of ash, steam and gas rose to altitude 18 to 20 km above sea level. The plume expanded radially up to a radius of 240 km from the volcano, passing over the Tongatapu, 'Eua, Ha'apai and Vava'u island groups. Ashfall was observed in Tongatapu and other islands.

3C. Paroxysmal Eruption/Explosion of the Hunga-Tonga-Hunga-Ha'apai (HT-HH) Volcano on 15 January 2022

About 24 hours later after this local tsunami on 15 January 2022, a series of hydromagmatic explosions of the underwater portion of the volcano toward the south-east, obliterated the newly formed middle portion of the joined islets of Hunga Ha’apai islet and of Hunga Tonga. The big blast and caldera collapse of the undersea volcano occurred at about 5:15 pm local time on Saturday 15 January 2022 and lasted less than 60 minutes.

Figure 6 . Images of the eruption of January 15, 2022. Credit Left: Digicel Tonga (After Toulkeridis Et. Al 2022).

This eruption was captured by the GOES-17 and Himawari-8 (JMA) satellites (Fig.7 & 8). The main eruption column rose to a 35 km altitude**.** The 2022 Hunga Tonga event was probably the largest volcanic eruption in the 21st century and the largest since the 15 June 1991 eruption of Mount Pinatubo in the Philippines' Luzon Volcanic Arc - which had been the second-largest volcanic eruption of the 20th century after the 1912 eruption of Novarupta in Alaska. The Hunga-Toga eruption ejected about 10 km^3 (2.4 cu mi) of material in the atmosphere about the same as that of the devastating eruption of Pinatubo (Philippines) in 1991.

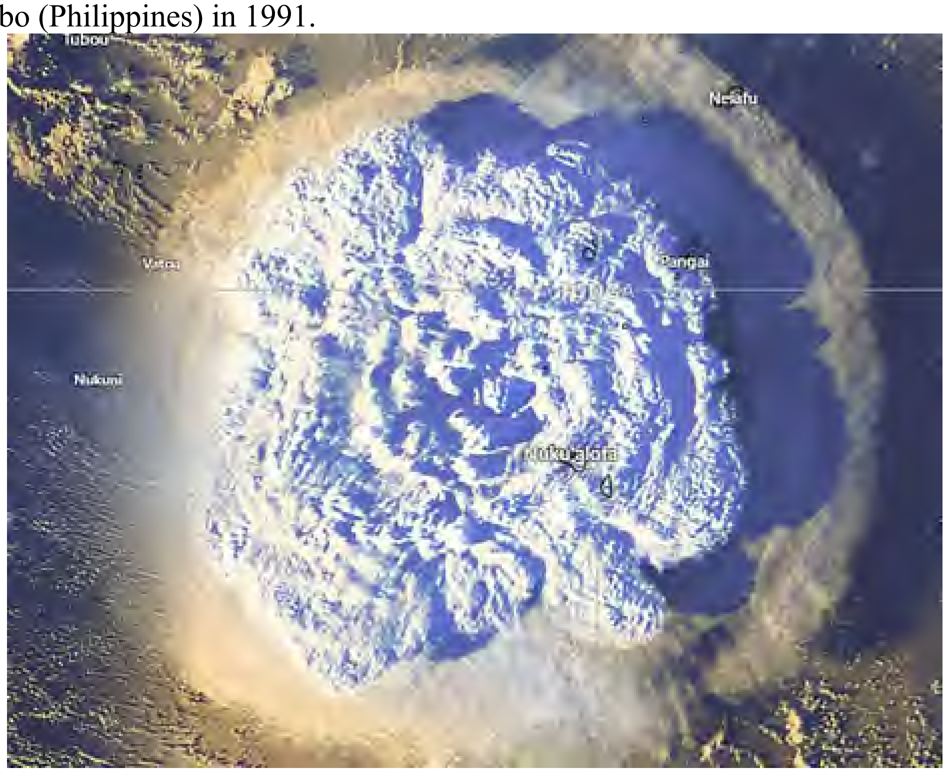

Figure 7. The enormous explosion as seen from the satellite. Credit US Geological Survey and Tonga Meteorological Services. Width of image is of about 600 km.

At 6.15pm of the same day and after the 5:19 and later in the same evening of 15 January 2022, the Tonga volcano continued to rain ash on the neighboring islands, and darkness covered the sky. The “volcanic mushroom plume” that was generated from the eruption, eventually reached the stratosphere and extended to cover Tonga’s roughly 170 islands, where more than 100,000 people lived. Attempts from Australia and New Zealand to assess from the air the damage to critical infrastructure such as roads, ports and power lines, were delayed because of the ash cloud which had covered the islands. According to a report of New Zealand’s meteorological service, by 3pm of 17 January the huge cloud of the volcanic ash spread to 160 miles (260km) in diameter and rose up to 19 miles (30km) high, and was seen drifting towards northern Australia at an altitude between 12-20km.

Also, the atmospheric pressure shockwaves generated from the violent eruption begun to be recorded as far away as Australia, New Zealand, United States, the United Kingdom and elsewhere. According to a bulletin of the Australian Bureau of Meteorology, the shockwave travelling faster than 1000 km/h – almost as fast as the speed of sound – resulted in a noticeable jump in the atmospheric pressure, reported earlier. Sonic booms from the eruption were heard across the Pacific, including Fiji, Vanuatu, and as far as Alaska.

Following the explosion of the HT-HH volcano, residents in Fiji and Vanuatu (more than 1600 Km away) reported that ground and buildings were shaking and that sonic booms were heard. Also, the United States Geological Survey (USGS) reported that an earthquake of magnitude 5.8 occured at 5:15 pm. Immediately that night tsunami warnings were isssued for the islands of Fiji and Samoa and massive evacuation of coastal areas begun (Fukao EtAl., 2018).

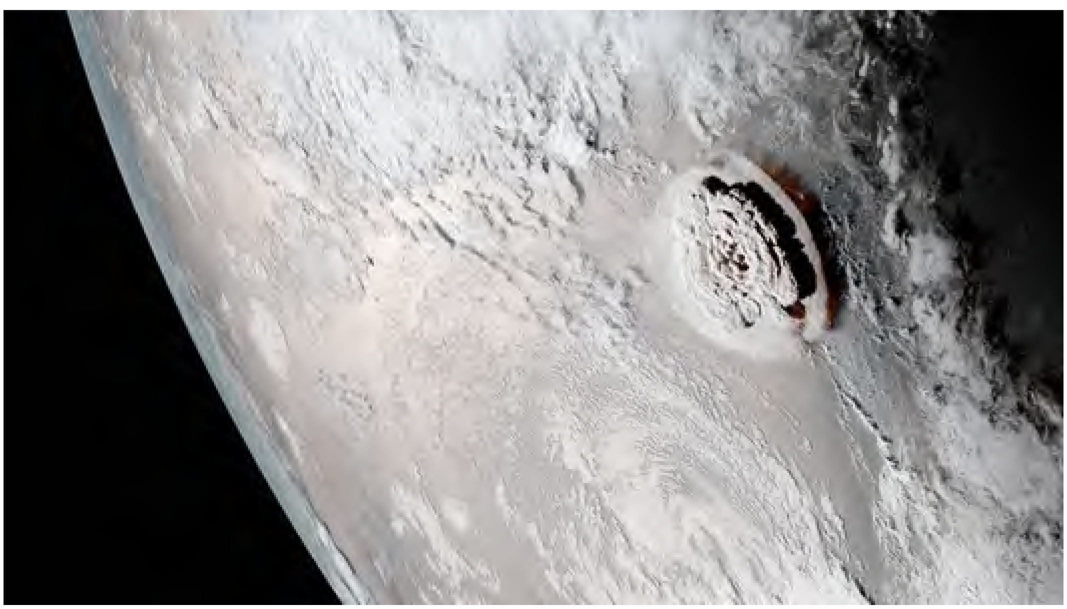

Figure 8. Global view of the eruption/explosion of the Hunga-Tonga volcano on the 15 January 2022, of the ash cloud formation and of the initial atmospheric pressure wave https://www.bbc.com/news/world-australia-60027360

Figure 8 is a global view of the eruption/explosion of the Hunga-Tonga volcano on the 15 January 2022, of the ash cloud formation, and of the initial expanding atmospheric pressure wave. The ultra-Plinian explosion and concurent crustal displacements of the volcano's caldera and flanc collapses, generated a very damaging near and far-field tsunami, but also an atmospheric paroxysmal explosion similar to that of 1883 Krakatau event, and a Pacific–wide tsunami, as well as far-reaching atmospheric Lamb wave perturbations and subsequent concentric wave-shape traveling ionosphere disturbances (TIDs oscillations) – the latter observed simultaneously in both the northern and southern hemispheres.

3D. Ash Cloud Formation and Atmospheric Pressure Waves from the Eruption/Explosion of the Hunga-Tonga-Hunga-Ha'apai (HT-HH) Volcano

The eruption/explosion of the HT-HH volcano had many similarities to the 1883 eruption of Krakatau (Krakatoa), which caused a devastating tsunami in the Indian Ocean, but also had a global impact. Krakatoa's violent eruption was reported to have been heard 4,800km away, and atmospheric pressure waves generated tsunami-like waves at great distances, although there was not sufficient technological monitoring back then. However, recent technological developments and satellite monitoring allowed good documentation in real time of the Tonga volcanic eruption/explosion, of the ash cloud formation, and as stated of the atmospheric pressure waves.

3E. Power of the Hunga-Tonga-Hunga-Ha'apai (HT-HH) Volcano's Blast Explosion - Generation of Acoustic Gravity Waves

As reported by early research of the 1883 explosion of Krakatau (Press & Harkrider, 1966) acoustic gravity waves can excite water gravity waves (tsunami) having the same phase velocity. The distant sea level disturbances that were observed following the explosion of Krakatoa were correlated with recently discovered atmospheric acoustic and gravity modes having the same phase velocity as long waves on the ocean. These atmospheric waves jumping over land barriers re-excited the sea waves with amplitudes exceeding the hydrostatic values. An explosion of 100 to 150 megatons would be required to duplicate the Krakatoa atmospheric pressure pulse.

Observation of acoustic gravity waves from the Tonga explosion and images collected by the Atmospheric Infrared Sounder (AIRS), mounted on NASA's Aqua satellite, in the hours after the eruption of the Hunga Tonga–Hunga Ha'apai volcano showed that the HT-HH blast explosion generated atmospheric gravity waves, which appeared as concentric circles, involving vertical oscillations of air molecules in an air column extending from the surface to the ionosphere (elevation of about 50 km),

To what extend the acoustic gravity waves from the blast explosion of HT-HH contributed to the tsunami wave heights observed locally or at great distances is rather difficult to quantify. According to NASA estimates, the power of the blast of the HT-HH volcano was equivalent between 4 to 18 megatons of TNT only. This amount of energy was released by the fourth paroxysmal explosion that blew away the northern two-thirds of Rakata island and almost instantaneously was followed by the collapse of the unsupported volcanic chambers which formed the huge underwater caldera (Pararas-Carayannis, 1989, 2003).

For comparison, scientists estimated that the power of the 1980 explosion of Mount St. Helens in the State of Washington in the USA was 24 megatons, and the power of the 1883 Krakatau (Krakatoa) volcano's explosion in the Sunda Strait of Indonesia (Sunda Strait, Indonesia) was equivalent to 200 megatons of TNT, about 13,000 times the nuclear yield of the bomb that devastated Hiroshima. Apparently there is a discrepancy in the estimate of Krakatau volcano's force of eruption which was assigned a volcanic explosivity index VEI=6, the same as that of the HT-HH event – which was also equivalent with the catastrophic 1991 eruption of Mount Pinatubo in the Philippines.

The coupling of the acoustic gravity waves from the Krakatau volcanic explosion with the sea surface apparently generated earlier tsunami waves having the same phase velocity which were recorded in Honolulu, San Francisco and Cardiff in Wales - much too early to have been propagated entirely through the oceans (Press & Harkrider, 1966; Latter, 1981, Pararas-Carayannis, 2003; Gabrielson, 2010; Chunchuzov EtAl, 2021).

3F. Lamb Wave Generation of Tsunami

The Hunga Tonga undersea volcanic eruption was one of the most powerful ever recorded. It generated audible sound detected more than 10,000 kilometers from the source, as well as infrasound and seismic recordings (Kubota EtAl, 2022; Matoza EtAl., 2022). An atmospheric lamb wave - characteristic of energetic atmospheric events - circled the earth four times and was very similar to the 1883 Krakatau eruption (Pararas-Carayannis, 2003).

Briefly, a Lamb wave in the atmosphere is a type of acoustic wave that is trapped at the earth's surface, propagating only in the horizontal direction in an isothermal windless atmosphere (Lamb, 1932/1947). However, in the real non-isothermal earth's atmosphere, earthquakes, volcanic eruptions, rapidly moving storms, falling meteorites, atomic bomb explosions and various other types of pressure pulses, generate enhanced Lamb-type of waves (Garrett 1969). The 15 January 2022 eruption/explosion of the Hunga volcano in Tonga, generated a wide range of such waves, which were detected globally by both ground and space instrumentation. Most important of these oscillations was a Lamb wave with frequency (≲0.01 hertz), which propagated for four (plus three antipodal) passages around Earth over a period of six days (Kubota EtAl, 2022; Lin EtAl, 2022; Matoza EtAl., 2022). The atmospheric wave contibuted to the generation of global tsunami waves arriving two hours earlier than expected Such was also the case with the 1883 volcanic eruption of Krakatau eruption/explosion and the tsunami-like waves observed in the Atlantic Ocean (Pararas-Carayannis, 2003). According to newspaper accounts and reports, the far field impact of the violent eruption of HT-HH and tsunami-like effects differed in many areas of Central and South America. For example the impact of tunami waves in Panama was not significant (El Siglo de Panamá , 2022), while in Peru the observed and recorded waves were substantial (El Universo, 2022).

4. MECHANISMS OF TSUNAMI GENERATION FROM THE HUNGA-TONGA-HAPA'I (HT-HH) VOLCANO'S ERUPTION/EXPLOSION

It has been well established that violent submarine volcanic eruptions can displace large volumes of water in a number of different ways, and have the potential to generate destructive tsunamis by different additional mechanisms. In general, such tsunami generation mechanisms may include: (1) displacement of large volumes of water and sudden sea surface oscillations; (2) flank failures and sub-marine landslides around the volcanic edifice; (3) flank caldera collapses into the empty magma chamber; (4) meteotsunamis triggered by atmospheric gravity waves following sub aerial volcanic blasts; and (5) meteotsunamis from rapidly moving storm fronts near a shore (Pararas-Carayannis, 2019).

Before discussing the specific mechanisms of near and far field tsunami generation from the 15 January 2022 eruption/explosion of the HT-HH volcano, there is a need to review the possible sequence of events that occur before, during and following similar such events. Generally, preceding a major eruption, there may be direct or channelized volcanic blast episodes, collapses of lava domes, as well as aerial and partial submarine volcanic edifice mass edifice flank failures. All such events may generate destructive local tsunamis. A subsequent violent eruption/explosion of a submarine volcano, associated with a major caldera collapse, can generate near and far field destructive tsunami waves. Furthermore such a violent eruption will also generate collateral, faster traveling atmospheric perturbations, other tsunami-like sea level oscillations, and Lamb waves. All these were generated by the blast of the HT-HH volcano.

In addition to the generation of tsunamis from flank failures of volcanic domes during an eruption, following massive explosive volcanic events associated with above or below water structural collapses - coupling with atmospheric waves in resonance - can and have caused very long period water waves at distant locations away from the point sources of origin (Pararas-Carayannis, 1967; 2003; Toulkeridis EtAl. 2022; Terry EtAl. 2022; Gusman & Roger, 2022).

The 14 January 2022 and the subsequent paroxysmal 15 January eruption of the HT-HH volcano indicate that a combination of the above listed mechanisms were responsible for the generation of both near and far-field destructive tsunamis, as well as for the faster-traveling atmospheric waves which, coupled with the sea surface, generated the earlier observed and recorded tsunami-like waves at distant shores.

Collapses of lava domes often precede major eruptions, which may vary in intensity from Strombolian to Plinian. Locally catastrophic, short-period tsunami-like waves can be generated directly by lateral, direct or channelized volcanic blast episodes, or in combination with collateral air pressure perturbations, nuee ardentes, pyroclastic flows, lahars, or cascading debris avalanches. Submarine volcanic caldera collapses can also generate locally destructive tsunami waves. Significant tsunamis may be also generated by fast moving storm fronts and nuclear explosions (Pararas-Carayannis **&** Adams, 1966).

5. TSUNAMI GENERATION BY THE ERUPTION/ EXPLOSION OF THE HUNGA TONGA HUNGA HA'PAI (HT-HH) VOLCANO

Near and far field tsunami and other volcano-induced sea level oscilations and effects generated by the 2022 HT-HH eruption were studied, simulated or reported by many researchers, and institutional sources globally (Toulkeridis Et.Al. 2022; Gusman & Roger, 2022; Kubota EtAl, 2022; NOAA, 2022; PTWC, 2022; Science.org 2022; Sekizawa and Kohyama, 2022; Terry EtAl, 2022; TelesurTV 2022).

5A. Near-field Tsunami Generation of the HT-HH Volcano on 14-15 January 2022.

Eruption activity of the HT-HH volcano intensified in January 2022. On Friday the 14th of the month, crustal displacements within the volcanic cone generated tsunami waves that were locally destructive, as shown arriving at the main island of Tongatapu (Fig. 9). Figure 9 below is another photo taken by Tonga's geologist Taaniela Kula, which shows a local tsunami which occurred before the big explosion of the HT-HH volcano of Saturday 15 January, causing damage and destruction to a small fishing fleet at the harbor of Nuku'alofa.

Figure 9. Tsunami arrival at Tonga's main island of Tongatapu.

At 5:10 pm local time on that same day, a massive eruption/explosion begun to generate an enormous amount of energy and an initial volcanic explosion occurred and an ash plume of up to 12.5 km was formed. This ash plume grew, eventually rising to 30 km in height and spreading over an area of 260 km. At the same time volcanic ash begun raining over the islands in the region. Images from weather satellites recorded the great eruption which begun in the afternoon of 15 January 2022. The eruption and submarine crustal displacement severed a 514-mile fibre-optic cable which connected Tonga to Fiji and to international networks and damaged telephone and Internet lines.

5B. Mechanism of the Near-field Tsunami Generation and Destruction from the Violent Eruption/Explosion of the HT-HH Volcano on 15 January 2022.

According to the Australian Bureau of Meteorology, at 5.30 pm on 15 January 2022, about twenty minutes after the violent eruption of the HT-HH volcano, an initial tsunami wave of 1.2 meters in height struck the main island of Tongatapu and the city of Nuku'alofa, Tonga's capital. This wave and subsequent waves caused extensive destruction to the harbor seawall, to buildings and to local infrastructure (Figures 10 & 11). On Mango island, where about 50 people lived, all homes were destroyed. On Fonoifua Island only two houses remained and a woman lost her life. On Nomuka Island two people were lost. At Fua'amotu international airport, the runway was inundated and was partly covered by volcanic ash and sediments. Other satellite images show that flooding came in several blocks inland. Satellite imagery analyzed by the UN showed similar scenes in Kolomotu'a, Tongatapu, and Fafaa village, Kolofo'ou. Some buildings remained standing, others collapsed, and the entire landscape was coated with volcanic ash.

Figure 10. Initial tsunami damage and destruction of the small fishing fleet at the wharf of the Nuku'alofa boat harbor on 14 January 2022 (Photo: Mary Lyn Fonua / Matangi Tonga

Figure 11. Another photo of the destruction by the local tsunami of 15 January 2022 at Marangi (Photo: Mary Lyn Fonua / Matangi Tonga).

5C. Issuance of Tsunami Warnings

Although only an estimated 5% of tsunamis have historically resulted from volcanic eruptions, based on the intensity of the HT-HH volcano's eruption, beginning at 8:15 pm the same day, tsunami warnings were issued across the Pacific, including New Zealand, Australia and the west coast of the USA. In Japan, about 230,000 people across eight prefectures were ordered to evacuate from coastal areas. This event caused great difficulty in the issuance of timely and accurate tsunami warnings for the following three reasons. First, some agencies initially concluded that the earthquake itself, with magnitude 5.8, was not large enough to generate a tsunami with significant amplitude around the Pacific Ocean. Second, when tsunamis did arrive (Figure 12), their early arrival made it very difficult to reliably predict tsunami arrival times for use in warnings. Third, once it became clear that significant tsunami amplitudes had been generated, it was very difficult to reliably predict their heights for use in warnings because there was not sufficient information at that time on the coupling effect of atmospheric pressure waves. Figure --- below is tsunami travel chart based on the usual gravity wave propagation and not one the faster traveling waves generated by the atmospheric pressure disturbance caused by the volcanic blast.

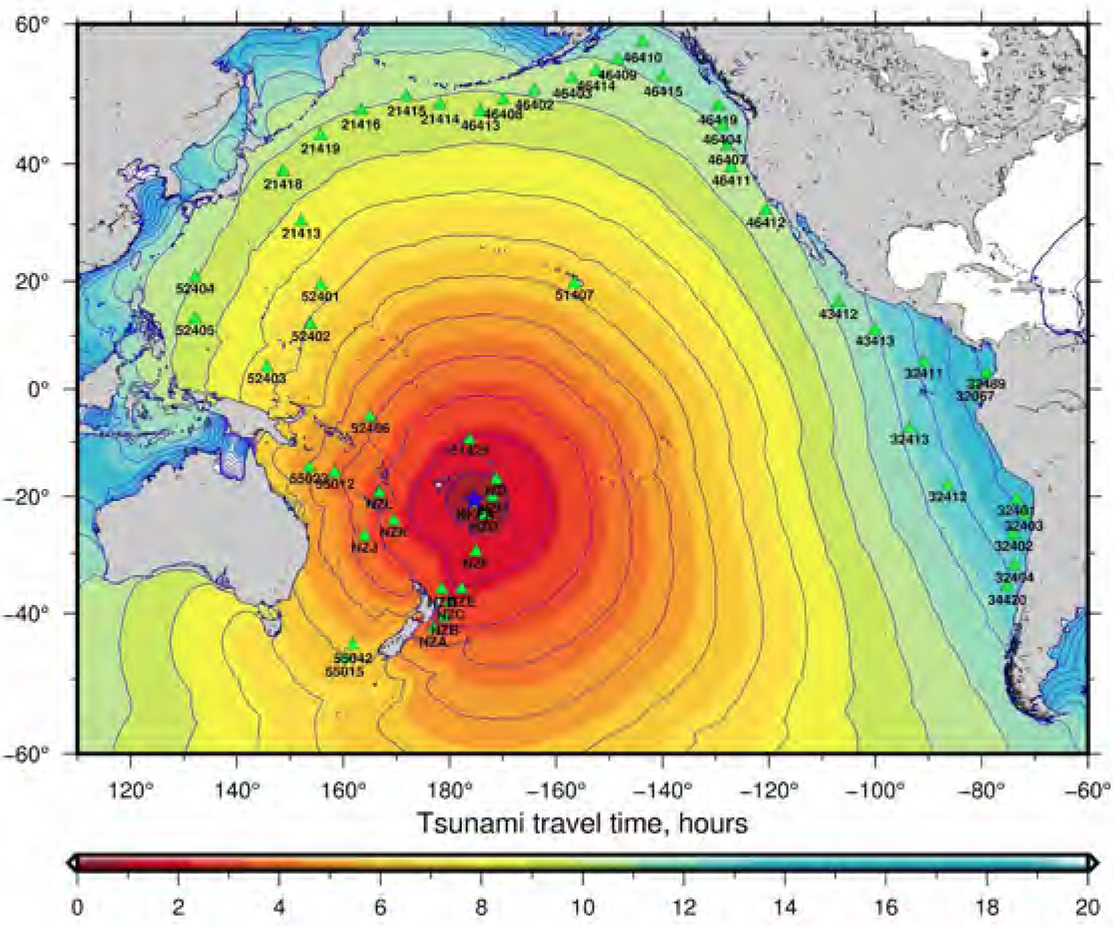

Figure 12. Tsunami travel time based on NOAA (NOAA, 2022a)

5D. Far-Field Tsunami Effects from the Violent Eruption/Explosion of the HT-HH Volcano.

The Hunga Tonga–Hunga Ha'apai volcanic eruption itself impacted widely and violently (BBC, 2022). Besides the near-field tsunami generation, large waves and strong currents resulting from the eruption/explosion of the Tonga volcano were recorded in many coastal areas on both sides of the Pacific Ocean. By the 16th of January, large waves and strong currents were recorded along Japan's North Pacific coast. Destructive waves of nearly 1.2 meters in height, arrived there in about 8 hours, about 2.5 hours earlier than the expected travel time of about 10.5 hours. In Sydney, Australia waves arrived in 2.75 hours - about 3 hours earlier than expected (Power, 2022).

There were also reports of damage from several islands of the South Pacific. A report from New Zealand stated that an undersea cable linking Tonga to Fiji was damaged. In the Lambayeque region of Peru unusually high waves were recorded, and 22 ports were closed. Along the west coast of the USA there was a report of flooding in Santa Cruz in California, and of damage to boats in the harbor.

Figure 13 below of a study in Japan (Watada. 2022), illustrates that coupling of the acoustic gravity waves with ocean gravity waves having similar phase velocities, and acting in resonance, were the cause of enhancing the height of the observed and recorded far-field tsunami waves

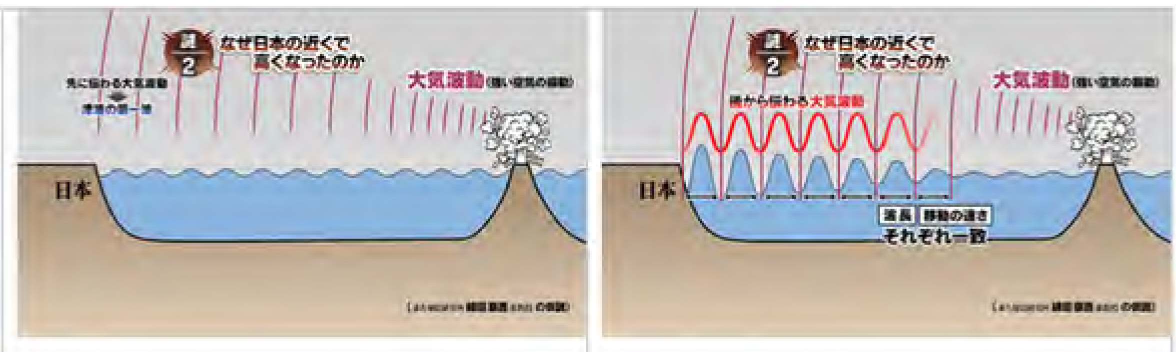

Figure 13. Left: Generation of the initial tsunami by the acoustic gravity wave close to the recording site. Right: Generation of later arriving tsunami by the coupling of the acoustic gravity waves with ocean gravity waves having similar phase velocities, causing resonance. (Source: Watada (2022).

Provided in the next sections of the present report are brief reviews of the above cited events of the eruptions/explosions of the Krakatau and Santorin volcanoes, and of the tsunami generations mechanism of major volcanic eruptions in the Eastern Caribbean regions, in the Pacific and the Indian oceans, and of a few other significant volcanic events elsewhere around the world.

The recordings of this water level oscillation and of the barometric pressure wave are shown in Figure 14 (provided by Dr. Greg Dudek of NOAA), which indicate that an acoustic wave arrived in Mayaguez just before the sea level oscillation - thus suggesting that this acoustic wave acted as a local source.

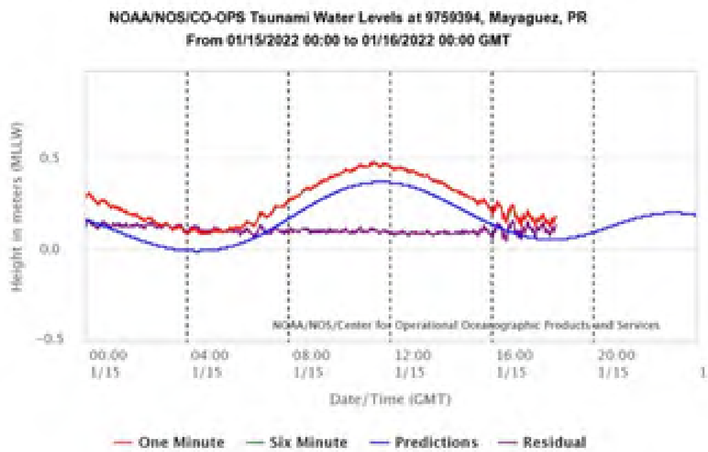

Figure 14. Tide gauge recording (top) and of a barograph (bottom) of the Tonga explosion at Mayaguez, Puerto Rico. The purple line in the top panel shows the record after removal of the tides. (Source: Dr Greg Dusek, NOAA).

6. COMPARISON OF THE 2022 OF THE HUNGA TONGA HUNGA HA'PAI (HT-HH) VOLCANIC ERUPTION/EXPLOSION AND ITS TSUNAMI GENERATION MECHANISMS WITH PAST AND RECENT MAJOR VOLCANIC EVENTS

As stated previously, the eruption of the HT-HH volcano on the 14 January 2022 resulted in the collapse of the caldera, leaving most of the volcano submerged. This earlier eruption and collapse was recorded as only minor disturbance on the tide gauge record at Nuku'alofa, in Tonga as shown on the right side of Figure 14, thus indicating that it was not the source of an early Pacific-wide tsunami. However, the major eruption/explosion of the volcano on the next day 15 January 2022 generated a major tsunami in the Pacific by the interaction and coupling of acoustic gravity waves with the sea surface. Additionally to such enhanced tsunami waves in the Pacific, small sea level oscillations were also recorded in Mayaguez, Puerto Rico in the Caribbean Sea. Such small sea level oscillation and a barometric pressure wave were observed following the Tonga volcanic explosion. The 15 January 2022 eruption/explosion/collapse of the submarine portion of the HT-HH volcano on the Tonga Kermadec volcanic arc in the southwest Pacific was a unique event but not unprecedented. Although tsunami generation from volcanic sources is not frequent, the historic record indicates that many such tsunamis were generated in the past, by volcanic events having similar as well as different source mechanism characteristics.

What makes the 15 January 2022 volcanic event more significant is the present improvement in the technical ability to better understand and measure collateral effects that such violent volcanic events have on a global scale, particularly on the atmosphere and the ionosphere. Thus, another pending paper will be provided in the near future by the present author, with a brief review and comparison of the recent Tonga eruption/explosion and of its tsunami generation mechanisms and collateral impacts, with other volcanically-generated tsunamis elsewhere around the world's oceans and seas. Specifically, will be reviewed are some of the destructive volcanically-generated tsunamis in the Pacific and in the Caribbean region, as well as tsunami generation mechanisms caused by different arc stresses, and tensional back-arc spreading, due to down-dip tectonic tensions (Seno & Yamanaka, 1998).

Other similar to the 2022 HT-HH volcanic eruption/explosion mechanism – and of a combination of related mechanisms – will be discussed in greater detail in the subsequent report. This report will include the 1883 eruption of the Krakatau volcano in Indonesia, the 1690 BC eruption/collapse of the Santorin volcano in the Aegean Sea, and tsunami-generating eruptions of volcanoes in the Caribbean Sea, the Indian Ocean in the Pacific Ocean and elsewhere around the world.

CONCLUSIONS

The final explosive eruption/collapse of the volcano Hunga-Tonga-Hunga-Ha'apai (HT-HH) on the Tonga Kermadec volcanic arc on 15 January 2022 was a truly global event, and almost as great as that of the 1883 explosive eruption of the Krakatau volcano in Indonesia both resembling the 1490 BC explosion, caldera and flanc collapses of the Santorin volcano in the Aegean Sea, the latter considered even much greater. These three events generated destructive volcanogenic tsunamis. The eruption of HT-HH was a combination of a major submarine Surtsean/ phreatomagmatic events and of a subsequent ultra-Plinian atmospheric explosion which generated a very damaging local tsunami. In addition to local destructive tsunami generation in the immediate area, the violent eruption created impulsive Lamb surface air pressure waves.

Recent development of instrumentation and of an expanded array of terrestrial and space instruments - including atmospheric pressure sensors, seismometers and a fleet of satellites monitoring the Earth across the entire spectrum of light – provided good global monitoring of the effects of this particular and unusual HT-HH volcanic event. The interaction of acoustic gravity waves caused by the explosion, interacting with the sea surface, generated tsunami waves, which arrived much earlier and were much larger than expected and were observed globally. Also, the eruption resulted in unusually traveling ionospheric disturbances (CTIDs) – detected and mapped on both of the earth's hemispheres.

REFERENCES

BBC (2022). Tonga eruption: How its impact spread so widely and violently. https://www.bbc.com/news/world-australia-60027360

Chunchuzov, I. P., S. N. Kulichkov, O. E. Popov, and V. G. Perepelkin. "Infrasound Generation by Meteorological Fronts and Its Propagation in the Atmosphere", Journal of the Atmospheric Sciences 78, 5 (2021): 1673-1686, https://doi.org/10.1175/JAS-D-20-0253.1… #JAtmosSci

Colombier, M., Scheu, B., Wadsworth, F. B., Cronin, S., Vasseur, J., Dobson, K. J., Hess, K-U., Tost M.,Yilmaz, TI, Cimarelli, C., Brenna, M., Ruthensteiner, B.and Dingwell, DB. 2018. Vesiculation and Quenching During Surtseyan Eruptions at Hunga Tonga-Hunga Ha'apai Volcano, Tonga. Journal of Geophysical Research: Solid Earth 123(5):3762-3779 May 201**DOI:**10.1029/2017JB015357

Dingwell, D. B. (2018). Vesiculation and Quenching During Surtseyan Eruptions at Hunga Tonga‐Hunga Ha'apai Volcano, Tonga. *Journal of Geophysical Research: Solid Earth*, *123*(5), 3762-3779.

El Siglo de Panamá (2022). Erupción de volcán en Tonga no ha generado amenaza en costas panameñas. http://elsiglo.com.pa/panama/erupcion-volcan-tonga-generadoamenaza-costas-panamenas/2419182

El Universo (2022). Perú registró oleajes anómalos e inundaciones leves tras erupción volcánica en Tonga. https://www.eluniverso.com/noticias/internacional/peruregistrooleajes-anomalos-e-inundaciones-leves-tras-erupcion-volcanica-en-tonga-nota

Fukao Y., Sandanbata O., Sugioka H., Shiobara H., Watada S., and Satake K., 2018. Mechanism of the 2015 volcanic tsunami earthquake near Torishima, Japan. Science Advances. April 2018, Vol. 4, Issue 4. DOI: 10.1126/sciadv.aao0219

Gabrielson, T.B., 2010. KRAKATOA AND THE ROYAL SOCIETY: THE KRAKATOA EXPLOSION OF 1883. Acoustics Today pp.14 -18 April 2010

Garrett, C.J.R., 1969. Atmospheric edge waves. Quartely Journal of Royal Meteorological Andersen, K. (2018). Monitoring and modeling the rapid evolution of earth's newest volcanic island: Hunga Tonga Hunga Ha'apai (Tonga) using high spatial resolution satellite observations. *Geophysical research letters*, *45*(8), 3445-3452.

Global Volcanism Program (2009). Report on Hunga Tonga-Hunga Ha´apai (Tonga). In: Sennert, S.K. (ed.), Weekly Volcanic Activity Report, 18 March-24 March 2009. Smithsonian Institution and US Geological Survey

Global Volcanism Program (2014). Report on Hunga Tonga-Hunga Ha´apai (Tonga). In: Sennert, S.K. (ed.), Weekly Volcanic Activity Report, 24 December-30 December 2014. Smithsonian Institution and US Geological Survey

Global Volcanism Program (2015). Report on Hunga Tonga-Hunga Ha´apai (Tonga). In: Sennert, S.K. (ed.), Weekly Volcanic Activity Report, 21 January-27 January 2015. Smithsonian Institution and US Geological Survey

Global Volcanism Program (2021a). Report on Hunga Tonga-Hunga Ha´apai (Tonga). In: Sennert, S.K. (ed.), Weekly Volcanic Activity Report, 15 December-21 December 2021. Smithsonian Institution and US Geological Survey

Global Volcanism Program (2021b). Report on Hunga Tonga-Hunga Ha´apai (Tonga). In: Sennert, S.K. (ed.), Weekly Volcanic Activity Report, 22 December-28 December 2021. Smithsonian Institution and US Geological Survey

Global Volcanism Program (2021c). Report on Hunga Tonga-Hunga Ha´apai (Tonga). In: Sennert, S.K. (ed.), Weekly Volcanic Activity Report, 29 December-4 January 2022. Smithsonian Institution and US Geological Survey

Global Volcanism Program (2022). Report on Hunga Tonga-Hunga Ha´apai (Tonga). In: Sennert, S.K. (ed.), Weekly Volcanic Activity Report, 12 January-18 January 2022. Smithsonian Institution and US Geological Survey

Gusman, A.R. & Roger, J. (2022). Hunga Tonga - Hunga Ha'apai volcano-induced sea level oscillations and tsunami simulations. GNS Science webpage, Accessed at https://doi.org/10.21420/DYKJ-RK41

Hall & Spakman, 2002. Hall, R. & Spakman, W. Subducted slabs beneath the eastern Indonesia-Tonga region: Insights from tomography. Earth Planet. Sci. Lett. 201, 321-336 DOI:10.1016/S0012-821X(02)00705-7

Heinrich, F., Roche, R., Mangeney, A., and Boudon, G. 1999b. Modeliser un raz de maree cree par un volcan, La Recherche, 318, 67

Hibiya, T., Kajiura, K. Origin of the*Abiki* phenomenon (a kind of seiche) in Nagasaki Bay. *Journal of the Oceanographical Society of Japan* **38,** 172–182 (1982). https://doi.org/10.1007/BF02110288

Gushchin R.A., Kopeikin V.M., Belikov I.B., Gubanova D.P., Karpov A.V. & TikhonovA.V. , 2022. Acoustic-Gravity Lamb Waves from the Eruption of the Hunga-Tonga-Hunga-Hapai Volcano, Its Energy Release and Impact on Aerosol Concentrations and Tsunami. *Pure and Applied Geophysics* volume 179, pages 1533–1548 (2022)

Gusman, A.R. & Roger, J. (2022). Hunga Tonga - Hunga Ha'apai volcano-induced sea level oscillations and tsunami simulations. GNS Science webpage, Accessed at https://doi.org/10.21420/DYKJ-RK41

Kubota T, Saito T, and Nishida K., 2022. Global fast-traveling tsunamis driven by atmospheric Lamb waves on the 2022 Tonga eruption. Science 12 May, Vol. 377. Issue 6601, pp. 91-94 , DOI: 10.1126/science.abo4364

La Crítica Panamá (2022). Sinaproc no hay amenaza de tsunami por erupción de volcán Tonga. https://www.critica.com.pa/nacional/sinaproc-no-hay-amenaza-de-tsunamipor-erupcion-de-volcan-tonga-620825

Lamb, H. 1932/1947. , *Hydrodynamics*, 6th ed. (Cambridge Univ. Press, Cambridge, 1932; Gostekhizdat, Moscow, 1947).

Lin, J. T., Rajesh, P. K., Lin, C. C., Chou, M. Y., Liu, J. Y., Yue, J., ... & Kung, M. M. (2022). Rapid Conjugate Appearance of the Giant Ionospheric Lamb Wave in the Northern Hemisphere After Hunga-Tonga Volcano Eruptions. Preprint February 2022 DOI: 10.1002/essoar.10510440.1

Lipman, P. W., Normark, W. R., Moore, J. G., Wilson, J. B., & Gutmacher, C. E. (1988). The giant submarine alika debris slide, Mauna Loa, Hawaii. *Journal of Geophysical Research: Solid Earth*, *93*(B5), 4279-4299.

Mangeney A., Heinrich F., Roche, R., Boudon, G., and J. L. Chemin. 2000. Modeling of debris avalanche and generated water waves. Application to real and potential events in Montserrat. Phys, Chem. Earth 25(9-11), 741-745.

Matoza EtAl., 2022. Atmospheric waves and global seismoacoustic observations of the January 2022 Hunga eruption, Tonga. *SCIENCE* 12 May 2022. Vol 377, Issue 660**1** pp. 95-100 DOI: 10.1126/science.abo706

NOAA (2022a). Hunga Tonga 2022 tsunami travel time. https://ngdc.noaa.gov/hazard/img/tsunami-timeline/

Nomikou, P., Druitt, T. H., Hübscher, C., Mather, T. A., Paulatto, M., Kalnins, L. M., ... & Parks, M. M. (2016). Post-eruptive flooding of Santorini caldera and implications for tsunami generation. *Nature communications*, *7*(1), 1-10.

Otsuka S., 2022, Research Letter 15 April 2022. Visualizing Lamb Waves From a Volcanic Eruption Using Meteorological Satellite Himawari-8. Open Access http://creativecommons.org/licenses/by/4.0/

Pararas-Carayannis G**.** & Vitousek M., 1966, On the Utilization of Atmospheric Data for the Evaluation of Potential Tsunamis. Res. Group Rec. No. 8, 4 pp. Honolulu: Hawaii Inst. Geophys.-Tsu., October 1966. **http://www.drgeorgepc.com/TsunamiEvaluationAtmospheric.pdf**

Pararas-Carayannis G. **&** Adams, W.M., 1966. Relative Susceptibility of the Hawaiian Islands to Waves Generated by Storms and Nuclear Explosions. (Report to the U.S. Atomic Energy Commission.). Oct.1966.

Pararas-Carayannis, G, 1967. A Study of the Source Mechanism of the Alaska Earthquake and Tsunami of March 27, 1964, Water Waves. In Contributions of the H.I.G. University of Hawaii for the Year 1967. Honolulu: s.n., 1967, pp. 237.cont. No. IR4

Pararas-Carayannis, G., 1975. Verification Study of a Bathystrophic Storm Surge Model. U.S. Army, Corps of Engineers Coastal Engineering Research Center, Washington, D.C., Technical Memorandum No. 50, May 1975. http://www.drgeorgepc.com/HurricaneBathystrophicSurgeModel.pdf

Pararas-Carayannis, G, (1983). Tsunami Effects from the Krakatau Eruption. Unpublishrd review of the Smithsonian Institution's book Krakatau 1883: The volcanic eruption and its effects: by Simkin, T., and Fiske, R.S., published in 1983 by the Smithsonian Institution Press: Washington, D.C., 464 p.

Pararas-Carayannis, G.: 1988, The tsunami generated from the eruption of the volcano of Santorin in the Bronze Age, *Sci. Tsunami Hazard* **6** (1), 23–30.

Pararas-Carayannis, 1989, 2003). Rakata

Pararas-Carayannis, G. (1992). The Tsunami Generated from the Eruption of the Volcano of Santorin in the Bronze Age.Natural Hazards 5:115-123, Kluwer Academic Publishers. Printed in the Netherlands

Pararas-Carayannis, G. (1999). The Tsunami Generated by the August 26, 1883 Explosion of the Krakatau Volcano, The Tsunami Page of Dr. George PC. http://drgeorgepc.com/Tsunami1883Krakatoa.html

Pararas-Carayannis, G. 2002. Evaluation of the threat of mega tsunami generation from postulated massive slope failures of island stratovolcanoes on La Palma, Canary Islands, and on the Island of Hawaii, Science of Tsunami Hazards, Vol. 20, 5, 251;277

Pararas-Carayannis, G., 2002a. Volcanically Generated Tsunamis, 2nd Symposium of the Tsunami Society, Honolulu, Hawaii, May 25-29, 2002.

Pararas-Carayannis, G. (2002b). Evaluation of the threat of mega tsunami generation from postulated massive slope failures of island stratovolcanoes on La Palma, Canary Islands, and on the island of Hawaii. *Science of Tsunami Hazards*, *20*(5), 251-277.

Pararas-Carayannis, G., (2003). Near and far-field effects of tsunamis generated by the paroxysmal eruptions, explosions, and massive slope failures of the Krakatau volcano in Indonesia on August 26-27,1883. Science of Tsunami Hazards, January 2003, 21 (4), 191-201. See also http://www.drgeorgepc.com/Tsunami1883Krakatau.html

Pararas-Carayannis, G. (2004). Volcanic tsunami generating source mechanisms in the Eastern Caribbean Region. *Science of Tsunami Hazards*, Vol *22*(2), 74-114.

Pararas-Carayannis G. 2004a, RISK ASSESSMENT OF TSUNAMI GENERATION FROM ACTIVE VOLCANIC SOURCES IN THE EASTERN CARIBBEAN REGION. NSF Caribbean Tsunami Workshop, Puerto Rico March 30-31.

Pararas-Carayannis, G. (2006). Risk Assessment of Tsunami Generation from Active Volcanic Sources in the Eastern Caribbean Region. Caribbean Tsunami Hazard, pp. 91-137. https://doi.org/10.1142/9789812774613_0005

Pararas-Carayannis, G. 2019. Meteotsunami of 29 August 1916 at Santo Domingo, Dominican Republic — Analysis of the destruction of the USS Memphis, Russian Academy of Sciences, Вычислительные технологии, Том 24, No 2, 2019, pp 16-36. https://resolver.caltech.edu/CaltechAUTHORS:20150928-113055558

Press F. & Harkrider D., 1966, Air-Sea Waves from the Explosion of Krakatoa. ***SCIENCE*** 9 Dec 1966 Vol 154, Issue 3754 pp. 1325-1327 DOI: 10.1126/science.154.3754.1325

Proudman J., 1929. The Effects on the Sea of Changes in Atmospheric Pressure. Geophysical Journal International: October 1929 https://doi.org/10.1111/j.1365-246X.1929.tb05408.x

PTWC (2022). Message: American Samoa Warn/Adv./Watch #1 Issued Sat Jan 15 05:52:38 UTC 2022. https://tsunami.gov/?p=PHEB/2022/01/15/22015050/1/WEZS40

Science.org (2022). Tonga shock wave created tsunamis in two different oceans https://www.science.org/content/article/tonga-shock-wave-created-tsunamis-two different oceans

Sekizawa S, and Kohyama T., 2022. Meteotsunami observed in Japan following the Hunga Tonga eruption in 2022 investigated using a one-dimensional shallow-water model, SOLA, 2022, Vol.18, pp.129-134. doi:10.2151/sola.2022-021

Seno T. and Yamanaka Y.,1998. Arc stresses determined by slabs: Implications for back-arc spreading, Earthquake Research Institute, University of Tokyo, Geopys. Res. Lett., 3227-3230 .

TelesurTV (2022). Perú cierra 80 puertos tras erupción de volcán en Tonga. https://www.telesurtv.net/news/peru-cierra-puertos-erupcion--volcan-tonga-20220117-0025.html

Terry, J.P., Goff, J., Winspear, N. *et al.* 2022. Tonga volcanic eruption and tsunami, January 2022: globally the most significant opportunity to observe an explosive and tsunamigenic submarine eruption since AD 1883 Krakatau. *Geosci. Lett.* **9,** 24 (2022). https://doi.org/10.1186/s40562-022-00232-z

The Conversation (2022). Why the volcanic eruption in Tonga was so violent, and what to expect next. https://theconversation.com/why-the-volcanic-eruption-in-tonga-was-soviolent-and-what-to-expect-next-175035

Timm C., Davy, B., Haase, K., Hoernle, K. A., Graham, I. J., De Ronde, C. E., ... & Gamble, J. A. (2014). Subduction of the oceanic Hikurangi Plateau and its impact on the Kermadec arc. *Nature Communications*, *5*(1), 1-9.

Toulkeridis T., Martinez N., Barrantes G., Rentería W., Barragan-Aroca G., Simón-Baile D., Palacios I., Salazar R., Salcedo-Hurtado E. , & Pararas-Carayannis G., 2022 IMPACT AND RESPONSE IN CENTRAL AND SOUTH AMERICA DUE TO THE TSUNAMI GENERATED BY THE SUBMARINE ERUPTION OF HUNGA TONGA-HUNGA HA'APAI VOLCANO. Science of Tsunami Hazards Vol 41. N 1 Y 2022. pp 1-38

Watada, S., 2022. (Earthquake Research Institute, University of Tokyo) (2022). Theory of tsunami generation. Reported by Koji Matsumoto, NHK. https://www.nhk.or.jp/kaisetsu-blog/100/459802.html

Worthington, T. J., Gregory, M. R., & Bondarenko, V. (1999). The Denham caldera on Raoul Volcano: dacitic volcanism in the Tonga–Kermadec arc. *Journal of Volcanology and Geothermal Research*, *90*(1-2), 29-48.

Woulff, G., McGetchin, T. R. (1976) Acoustic Noise from Volcanoes: Theory and Experiment. *Geophysical Journal International*, 45 (3). 601-616 doi:10.1111/j.1365-246x.1976.tb06913.x

Young R. S., 2004. Small scale edifice collapse and tsunami generation at eastern Caribbean volcanoes; a standard phase of the volcanic cycle. NSF Caribbean Tsunami Workshop, Puerto Rico March 30-31.

Zahibo, N. and Pelinovsky, E. 2001. Evaluation of tsunami risk in the Lesser Antilles, Natural Hazard and Earth Sciences, 3, 221&;231.

Zengaffinen, T., Løvholt, F., Pedersen, G. K., & Muhari, A. (2020). Modelling 2018 Anak Krakatoa Flank Collapse and Tsunami: effect of landslide failure mechanism and dynamics on tsunami generation. *Pure and Applied Geophysics*, *177*(6), 2493-2516.

ISSN 8755-6839

SCIENCE OF **TSUNAMI HAZARDS**

Journal of Tsunami Society International

Volume 41 Number 3 2022

GLACIAL LAKE TSUNAMI OF 13 OCTOBER 2000 ON "EL ALTAR" VOLCANO OF ECUADOR

Theofilos Toulkeridis[1]*, Izar Sínde-González[1] and Jheny Orbe[2]

[1]Universidad de las Fuerzas Armadas ESPE, Sangolquí, Ecuador
[2]Escuela Superior Politécnica del Chimborazo (ESPOCH), Riobamba, Ecuador
*Corresponding author: ttoulkeridis@espe.edu.ec

ABSTRACT

There are a number of unusual tsunamis, which occur within the continents rather than in the oceans, named inland tsunamis. One of these rare occasions occurred in the morning of the Friday the 13th October 2000 in a volcanic glacial lake of the horseshoe shaped extinct El Altar volcano in central Ecuador. A detailed mapping of available air photos and satellite images have been reviewed and evaluated in order to reconstruct the catastrophic event of 2000 and a previous one, evidencing that climate change and the associated subsequent reduction of the glacial caps have been responsible for the disassociation of a huge mass of rock(s), of which separation has resulted to an impact in the volcanic lake by an almost free fall of some 770 meters above lake level ground. This impact generated a tsunami wave capable to reach an altitude of 125 meters about the lake´s water level and leave to lower grounds killing some ten people and hundreds of animals with a mixture of a secondary lahar and debris avalanche. We tried to explain how the fall has occurred with some theoretical considerations, which resulted to imply that the rock hit at least once, probably twice the caldera wall prior lake impact. Such phenomena, even if rare, need to be better monitored in order to avoid settlements in potential areas in the reach of such devastating waves and subsequent avalanches, even more so, when due to climate change the accumulation of water in such lakes increases and the corresponding subglacial erosion and corresponding disassociation of lose rock material may set free more rocks with substantial volumes.

Keywords: *Inland tsunami, glacial lake, climate change, public preparedness, Ecuador*

1. INTRODUCTION

Tsunamis are usually known to be triggered by tectonic movements mostly along active continental margins (Pararas-Carayannis, 2006; 2012; Sulli et al., 2018; Zaniboni et al., 2014). The worldwide majority of tsunamis and their coastal impacts occur in the Pacific region, of which some prominent events caused enormous economic damage and or caused a relatively high death toll, like the tsunami of Sumatra in 2004, in Chile in 2010 and in Japan in 2011 (Fujii & Satake, 2007; Borrero & Greer, 2013; Nohara, 2011; Mori et al., 2011). A further way to generate tsunamis is attributed to volcanic activity which sometimes realize their subsequent marine or submarine mass movements due to flank or volcanic dome collapses, like those of occurred in Santorini in Late Bronze age, Unzen in 1792, Krakatau in 1883, Anak Krakatau in 2018, and of Hunga Tonga-Hunga Ha'apai in 2022 (Self & Rampino, 1981; Nomikou et al., 2016; Paris, 2015; Grilli et al., 2019; Sassa et al., 2016; Toulkeridis et al., 2022). Especially the dome collapse of Unzen volcano triggered a giant wave with a height of some 100 meters (Wang et al., 2019; Sassa et al., 2014).

Mass movements including iceberg collapses in oceanic environments have generated in the past often mega tsunamis also known as Iminamis with prominent examples such as Storegga in Norway, Big Island Hawaii, Teide in the Canaries, Roca Redonda in the Galapagos, Lituya Bay in Alaska, among many others (Bondevik et al., 1997; McMurtry et al., 2004; Paris et al., 2017; Cando et al., 2006; Kawamura et al., 2014; Völker et al., 2012; Greene & Ward, 2003; Harbitz et al., 2014; Mader & Gittings, 2002; Fritz et al., 2009; Ward & Day, 2010; Franco et al., 2020; Pararas-Carayannis, 1999; González-Vida et al., 2019). A fourth way to trigger tsunamis by natural processes occurred when space objects have impacted earth in an oceanic or sea environment like the famous impact in Yucatan, which accelerated mass extinction of most living species in the Cretaceous-Tertiary boundary, when the impact of an asteroid generated also a tsunami (Ward & Asphaug, 2000; Kharif & Pelinovsky, 2005; Hills & Mader, 1997; Matsui et al., 2002; Schulte et al., 2010; Kinsland et al., 2021; Kring, 2007; Glimsdal et al., 2007; Toulkeridis et al., 2021).

Nonetheless, besides the most known way to trigger tsunamis, by seismic activity, volcanic hazards, marine or submarine mass movements and impact of space objects in oceanic or sea environments, there is one more form of tsunami generation which occurs when a large amount of water displacement is caused by a sudden addition of material into a body of water like lakes. Therefore, when such tsunamis occur due to a sudden landslide or rock fall, they are named inland tsunamis (Hilbe & Anselmetti, 2015; Kremer et al., 2021). Some prominent examples are those occurred in the Mount St Helens volcano in 1980, when a wave with a height of some 260 was generated by a lateral blast and corresponding debris avalanche, or, the one generated in Genoa, Italy in 1963, when rocks hit a water reservoir generating a tsunami height of some 25 meters (Ward & Day, 2006; Gawel et al., 2018; Semenza & Ghirotti, 2000; Genevois & Ghirotti, 2005; Paronuzzi & Bolla, 2012).

Due to an analysis of historic data and eye witness reports, we are able to add one more rare case of an inland tsunami, which occurred in Ecuador, within a volcanic glacier lake at an altitude of 4180 meters above sea level. This tsunami occurred on a Friday the 13th of October 2000 and the resulting wave killed some ten persons and hundreds of animals of the livestock. The current research will reconstruct the event and explain how it occurred and explain the probability of how a repetition may be generated in close future times.

2. GEOLOGIC AND GEOMORPHOLOGIC SETTING

Ecuador is situated along the easternmost margin of the Pacific ocean, where several tectonic plates are responsible for the actual geodynamic setting (Lebras et al., 1987; Daly, 1989; Jaillard et al., 2009; Toulkeridis et al., 2019; Luna et al., 2017). There is the conjunction of the Pacific, Cocos and Nazca oceanic plates as well as the Galapagos microplate besides their interaction with the Caribbean and South American continental plates (Fig.1) (Lonsdale, 1988; Klein et al., 2005; Pennington, 1981; Gailler et al., 2007). Out of this constellation result seismic movements with the generation of strong earthquakes and severe tsunamis as recorded in past history (Mendoza & Dewey, 1984; Sennson & Beck, 1996; Graindorge et al., 2004; Pararas-Carayannis & Zoll, 2017; Toulkeridis et al., 2017; Yamanaka et al., 2017; Pulido et al., 2020; Yoshimoto et al., 2017). There are several studies about Ecuador´s past tsunami impacts and associated seismic hazards, paleo-tsunami deposits, economic damages, prevention and mitigation efforts as well as the vulnerabilities of the public and the infrastructure (Chunga and Toulkeridis, 2014; Toulkeridis, 2016; Matheus Medina et al., 2016; Mato and Toulkeridis, 2017; Toulkeridis et al., 2017; Rodríguez Espinosa et al., 2017; Chunga et al., 2017; Toulkeridis et al., 2018; Mato and Toulkeridis, 2018; Navas et al., 2018; Celorio-Saltos et al., 2018; Matheus-Medina et al., 2018; Chunga et al., 2019; Toulkeridis et al., 2019; Martinez and Toulkeridis, 2020; Edler et al., 2020; Suárez-Acosta et al., 2021; Del-Pino-de-la-Cruz et al., 2021; Toulkeridis et al., 2021; Ortiz-Hernández et al., 2022; Aviles-Campoverde et al., 2021). These studies also handled the impacts and corresponding responses of public and authorities have been studied of tsunamis regional and far-triggered origins such as those of Chile in 2010, Japan in 2011 and Tonga in 2022 on the continental shores of Ecuador as well as on their Galapagos Islands.

A high amount of volcanoes appear in Ecuador and the Galapagos Islands as a result of the subduction of the Nazca plate below the continent which gives rise on a variety of volcanoes aligned on NNE-SSW direction of four almost parallel lines forming different volcanic chains and the Galapagos hot spot, the latter responsible for the formation of the more than 3000 volcanoes in the Galapagos (Toulkeridis & Angermeyer, 2019). In the continental part, there are more than 250 volcanoes distributed in the Western Volcanic Cordillera (WC),

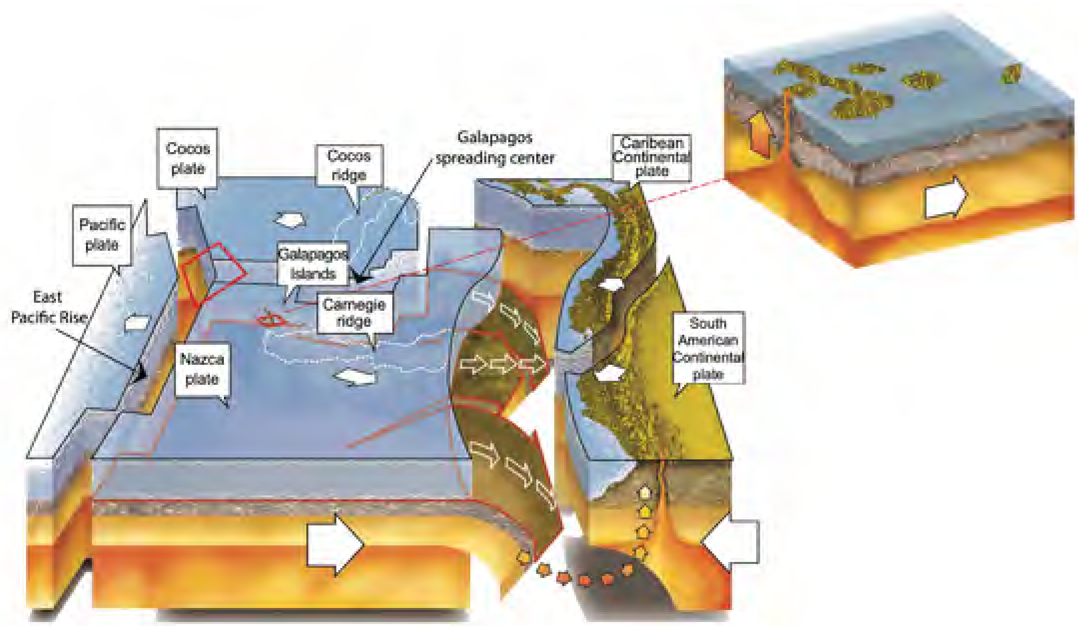

Fig. 1. The geodynamic situation of Ecuador and associated plates, micro-plates and volcanic ridges. The Guayaquil-Caracas Mega Fault is situated within the separation of the Caribbean and South American Continental Plates. The Galapagos microplate occurs in the triple junction between the three oceanic plates (red square).

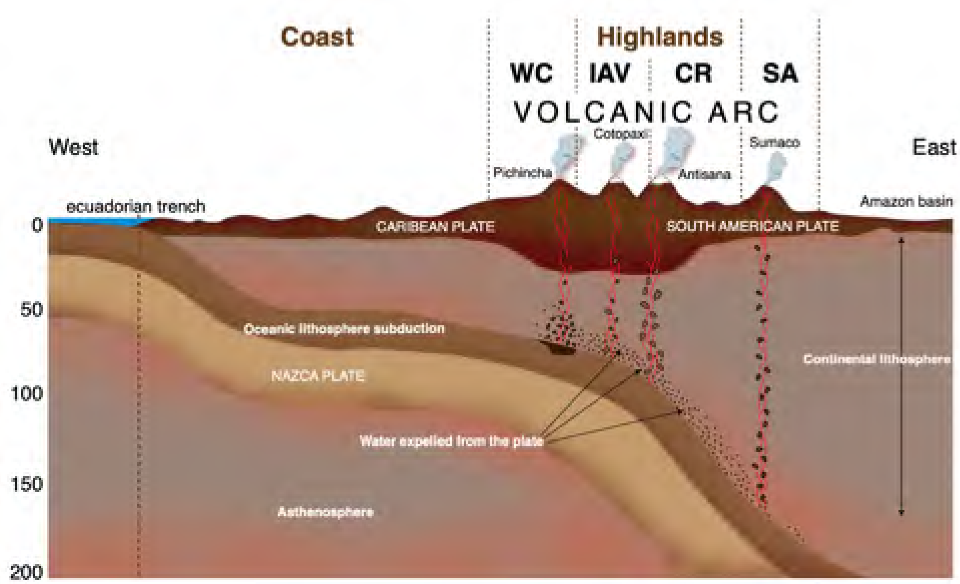

Fig. 2: Schematic profile from west to east within the subduction zone and the respective volcanic areas. WC = Western cordillera; IAV = Interandean valley; CR = Cordillera Real; SA = SubAndean region.

the Inter-Andean Volcanic Cordillera (IAV), the Eastern Volcanic Cordillera (CR), which is situated above the Cordillera Real and the easternmost Sub-Andean Volcanic Cordillera (SA) (Fig. 2). Of all these volcanoes, some 19 are considered to be active and occasionally very dangerous including a super volcano named Chalupas (Toulkeridis et al., 2007; Ridolfi et al., 2008; Padrón et al., 2008; 2012; Toulkeridis et al., 2015; Rodriguez et al., 2017; Toulkeridis and Zach, 2017; Melián et al., 2021).

The El Altar volcano, also known locally as Cápac Urcu (the mighty one or the lord of the volcanoes), being part of the Eastern Volcanic Cordillera is considered an extinct volcano since the middle Pleistocene. The maximum height of this volcano named El Obispo (The Bishop) reaches some 5,319 m.a.s.l., being one of seven prominent peaks, which are named El Canónico, Los Frailes, El Tabernáculo, La Monja Menor, La Monja Mayor, El Acólito (The Canon, The Friars, The Tabernacle, The Minor Nun, The Major Nun, The Acolyte). The horseshoe-shaped volcano is open to its west, as a result of a giant collapse (Fig. 3, 4). In its inner part, the caldera is composed of a gabbroic intrusion, which most likely represents a part of the magma chamber, besides andesitic and rhyolitic lavas and dikes, of which many are brecciated, especially in the upper part of the edifice.

3. THE CATASTROPHIC EVENT AND ITS POTENTIAL THEORETICAL RECONSTRUCTION

According to local witnesses, shortly before 6 a.m., in the morning of Friday the 13th of October 2000, a giant explosive sound was heard from the inner part of the volcano. Shortly after, a giant water wave overflow the fifty meters high wall from the western side of the glacial Lake Laguna Amarilla forming downstream a debris avalanche in the Valley of Collanes within the Río Blanco river, until it reached the confluence with the Río Tarau river. According to Civil Defense reports at the time, more than 400 families were affected, 10 people disappeared, 10 homes were destroyed, while 200 head of cattle were lost and some 600 hectares of crops were destroyed.

Based on topographic maps realized prior and after the year 2000, together with satellite images, and additional studies and observations in the field, it was determined that a piece of the inner wall of the volcano collapsed in the form of a rock from a height of 4955 meters above sea level (m.a.s.l.). This has been the initial tear-off edge and the whole lose part reached up to 5070 m.a.s.l., being its higher end some 230 meters below the peak in that part of the volcano. This loosening has occurred in the northern part of the peak called Monja Grande. The size of this rock wall was of about 115 meters high, about 90 meters wide and 35 meters thick in its widest part, so the maximum dimensions of the lost rock wall were then 115x90x35 meters. The rock, being an andesite breccia in this formation of the volcano, has had a density of 2.5–2.8 t/m^3, which means of having had a maximum weight of some 905,625 tons. This weight, although massive is just a tiny part compared with similar events, where in 1958, some 30,6 million cubic meter of rocks impacted the ocean in Lituya Bay Alaska, generating a tsunami wave height of some 524 meters (Mader & Gittings, 2002).

This piece of rock crashed at least once at a height of approximately 4640 meters above sea level, before hitting the lagoon. It is very likely that with this drop of about 315 meters, the rock broke, potentially splitting into two or more pieces of unknown proportions. From the initial tear edge to this crash it had a horizontal distance of maximum 260 meters. From that impact height of about 4640 meters, the rock(s) either fell into the lagoon or crashed again at a lower height but before the level of the lagoon before impacting in it. From this crash point to the edge of the lagoon we determined a horizontal distance of about 440 meters. The surface of the lake is approximately 4,182 meters above sea level. The maximum observable height of the subsequent tsunami wave has been of about 125 meters above the lagoon level, that is, more or less 4,310 meters above sea level, eroding the local moraine deposits.

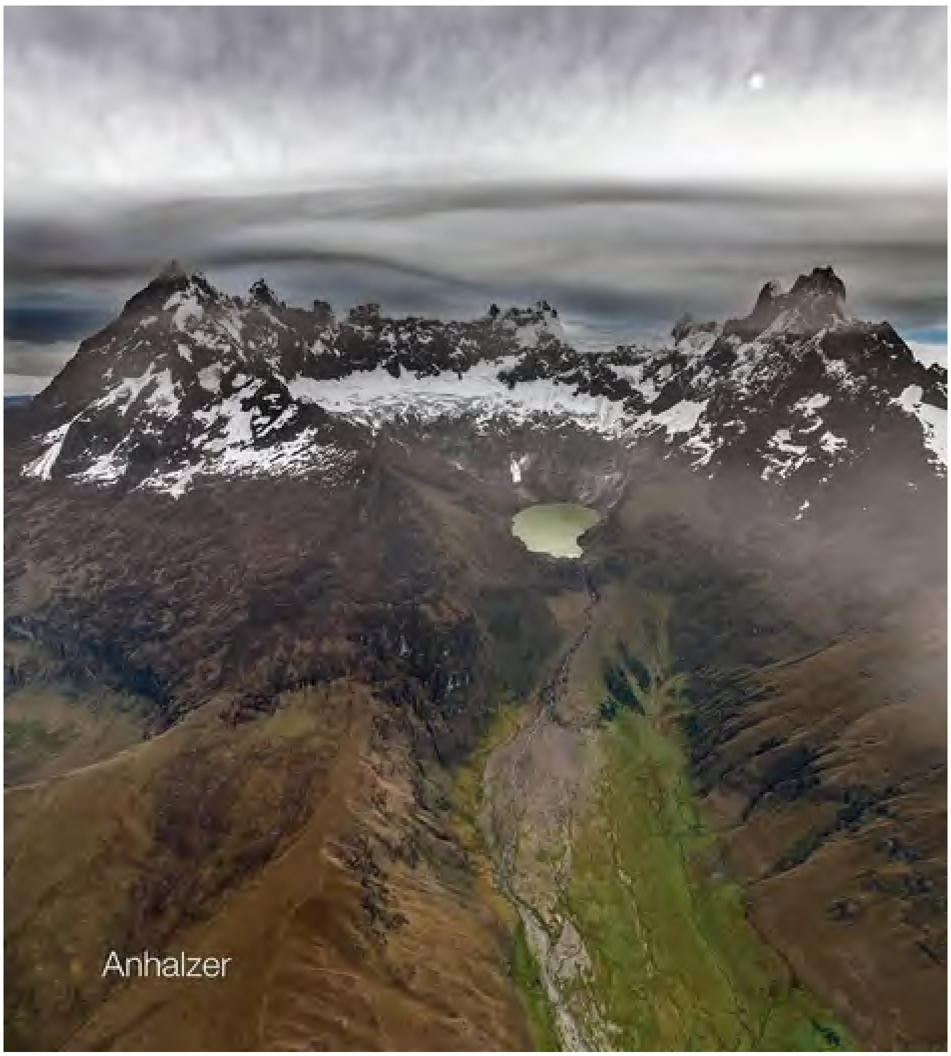

Figure 3. The horseshoe-shaped El Altar volcano, open towards west, with its glacial lake, the Laguna Amarilla. The Moja Grande peak is the second peak from right to left. Photo credit by Jorge Anhalzer.

When the giant wave overflow of the inland tsunami reached the Río Blanco river, the water got mixed and pushed the loose rocks of previous glacial deposits and other volcanic materials forming a debris avalanche. This avalanche reached the Río Tarau river, where a first damming of the waters occurred. Besides the deaths and the previously described destruction, an 800-meter section of the highway that connects Penipe with La Candelaria also disappeared, as well as the bridge that crosses the Blanco River where another damming of water, mud and rocks took place. Later, the muddy avalanche crossed the rivers Chambo and Pastaza reaching later the Amazonian basin on sites like Puyo and beyond. The rise of the debris material was also noted in the Hydroagoyan water plant further downstream, where even the timing of the arrival has been reported.

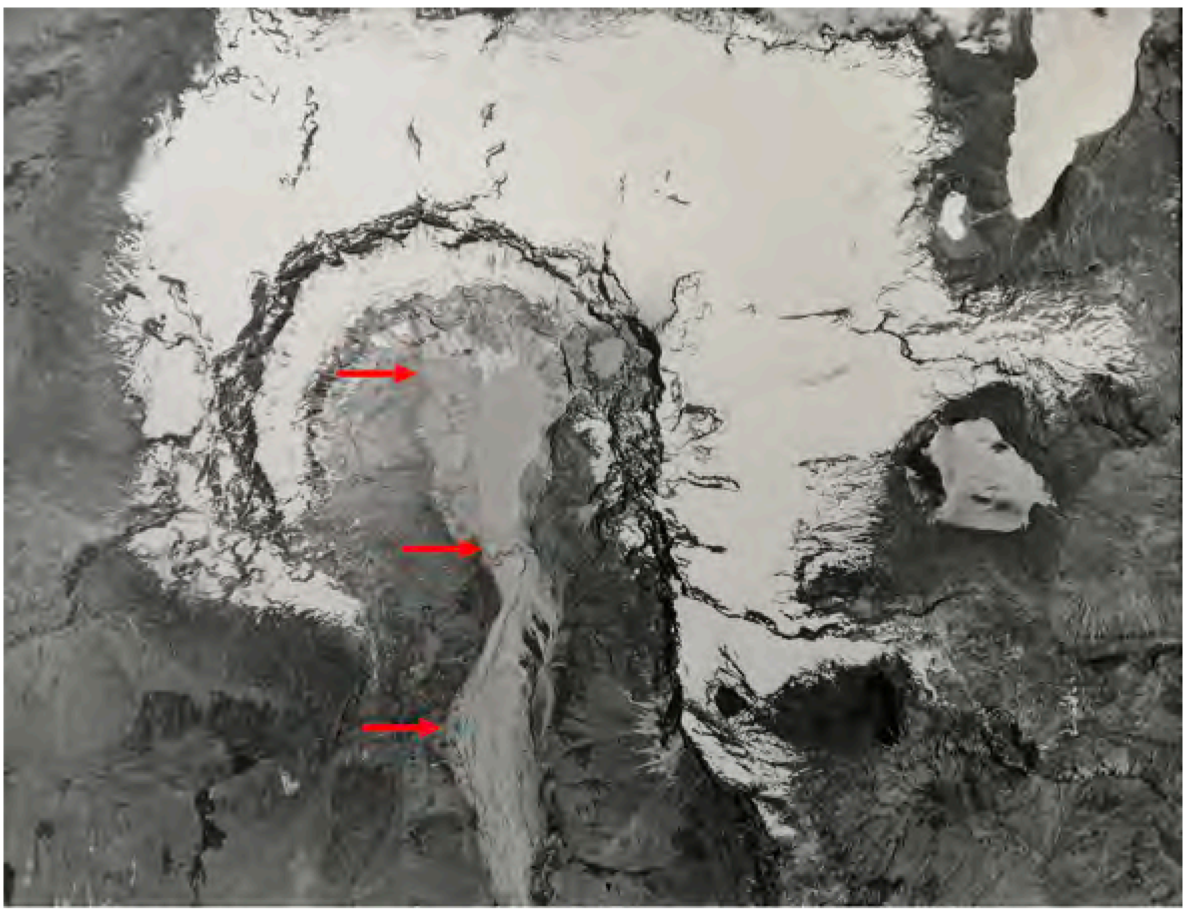

Figure 4. Two weeks after the event was taken this orthophoto from the Ecuadorian Military Geographical Institute (IGM), where we are able to evidence and proof the field observations, demonstrating the highest run-up at a 4,310 m.a.s.l. (upper arrow) at the northern inner caldera wall, the western lake barrier, being 50 meters higher than the lake water level (middle arrow) and the extension of the debris avalanche in the Valley of Collanes (lower arrow). North is on the left, while south is on the right of the black and white picture. Photo credit by IGM.

In order to reconstruct the fall and impact of the rock and its resulting giant tsunami wave within the lagoon, we used simple mathematical and physical considerations. In this sense we applied the known parameters, which are the rock size, its density and corresponding weight on the one hand, and on the other the known height of the wave. Hereby, the rock in free fall from a height of 773 meters is assumed, taking the surface of the lagoon as a reference system, if the initial velocity is zero, it will impact with an edge of the volcano's profile, located 315 meters below the point of detachment, with a maximum horizontal distance of 260 from the initial edge. All the aforementioned parameters were determined with a relative error of 2%. Therefore, the arrival time at the collision point is of about 8.0 ± 0.2 seconds (Equation 1), with a speed of approximately 78.6 ± 0.8 m/s (Equation 2).

$$t = \sqrt{\frac{2h}{g}} \qquad (1)$$

$$v_0 = \sqrt{2gh} \qquad (2)$$

Where:
t = elapsed time for the rock to reach the edge of the collision
h= height from the point of detachment of the rock to the point of collision with the edge
g = acceleration due to gravity
v_0 = speed of arrival of the rock at the collision point

Several trajectories of descent of the rock to the lagoon can be assumed, but in order to quantify some specific physical parameters of the phenomenon (time, speed, range, acceleration), two cases in which the rock is divided into two identical fragments, the collision is assumed elastic and the subsequent motion of the fragments is studied in two dimensions.

A) First Case

Figure 5 illustrates the situation prior and after the collision of the rock with the edge, while the velocities of the fragments generate equal angles with the horizontal.

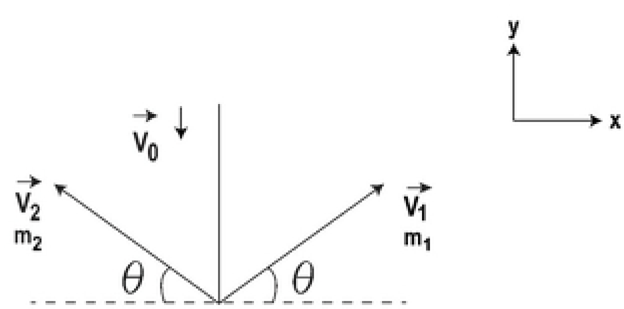

Figure 5: Collision of the rock with the edge, dividing it into two equal fragments with positive velocities on the y-axis.

The law of conservation of momentum is applied before and after the collision (Equation 3). The initial speed of the fragments is the same (Equation 4) and was calculated using Equation 5.

$$\vec{p}_0 = \vec{p}_f \qquad (3)$$

$$m_1 = m_2 = \frac{m}{2}$$

$$m\vec{v}_0 = \frac{m}{2}\vec{v}_1 + \frac{m}{2}\vec{v}_2$$

$$2\vec{v}_0 = \vec{v}_1 + \vec{v}_2$$

X direction:

$$0 = v_1 cos\theta - v_2 cos\theta$$

$$v_1 = v_2 \qquad (4)$$

Y direction:

$$-2v_{0y} = v_1 sen\theta + v_2 sen\theta$$

$$-2v_{0y} = 2v_1 sen\theta$$

$$v_1 = -\frac{v_{0y}}{sen\theta} = -\frac{v_0}{sen\theta} \qquad (5)$$

Where:
$\vec{p}_0$ = amount of movement before the collision
$\vec{p}_f$ = momentum after collision
m = rock mass
m_1 = mass of fragment 1
m_2 = mass of fragment 2
$\vec{v}_1$= speed of fragment 1
$\vec{v}_2$= speed of fragment 2
$\vec{v}_0$ = velocity vector of arrival of the rock at the collision point
θ = angle that the velocities of the fragments make with the horizontal

Figure 6 illustrates the case of fragment 1, thrown into the air with an angle θ and an initial speed $\vec{v}_1$, when it moves freely under the action of gravity only (air resistance is not considered). The acceleration of the rock fragment, acting downward, is 9.8 m/s^2. Motion is assumed to start when time equals zero (t=0) at the origin of a coordinate system, so $x_0=y_0=0$.

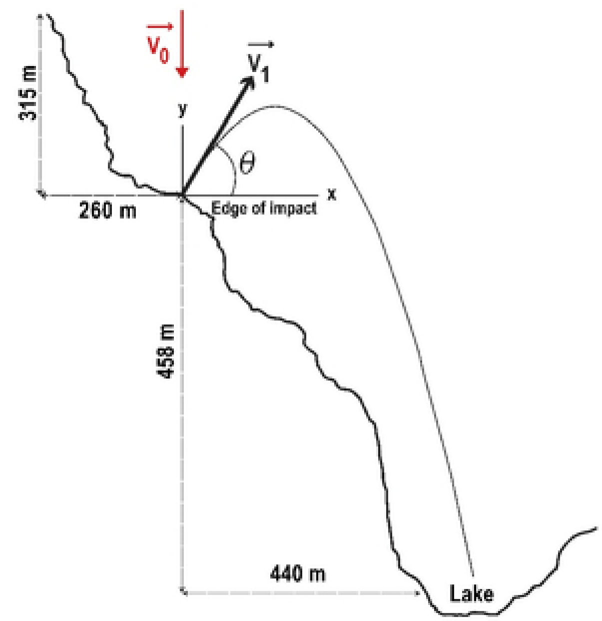

Figure 6. Trajectory of fragment 1 fired with an initial velocity $\vec{v}_1$ forming an angle θ (positive) with the edge plane.

The rock rise time to the maximum height was calculated with Equation (6). The maximum height that the rock reaches in the air was evaluated with Equation (7).

$$t_s = \frac{v_{0y}}{g} \qquad (6)$$

$$v_{0y} = v_0$$

$$h_{max} = h_i + v_0 t_s \quad (7)$$

Where:

t_s = rock rise time

v_{0y} = component of the velocity of the rock on the y-axis

h_{max} = maximum height that the rock reaches in the air

h_i = height from the shock point to the plane of the lagoon

The rock fall time from the maximum height to the lagoon surface is a parameter that was quantified with Equation (8). The time of flight is the total time of the rock in the air and was calculated with Equation (9).

$$t_c = \sqrt{\frac{2h_{max}}{g}} \quad (8)$$

$$t_v = t_s + t_c \quad (9)$$

Where:
$t_c =$ rock fall time from the maximum height to the lagoon plane
$t_v =$ time of flight

The horizontal distance that the rock travels from the point of impact to the point of arrival at the lagoon or at the ground (reach) was evaluated with Equation (10). The horizontal distance from the edge of the lagoon to the impact point of the rock was calculated with Equation (11).

$$x = v_{1x}\, t_v \quad (10)$$

$$v_{1x} = \frac{v_1}{\text{sen}\theta}\cos\theta$$

$$v_{1x} = v_1 \cot\theta$$

$$x_i = x - x_b \quad (11)$$

Where:
x_i = distance from the edge of the lagoon to the point of impact of the rock in the water
$x_b =$ horizontal distance from the point of rock collision to the edge of the lagoon
v_{1x} = component of the initial velocity on the x axis
x = reach.

The final speed with which the rock impacts the surface of the lagoon was calculated with Equation (12):

$$v_{1f} = \sqrt{v_{1xf}^2 + v_{1yf}^2} \quad (12)$$

$$v_{1xf} = v_{1x}$$

$$v_{1yf} = g\, t_v$$

Where:
v_{1f} = final velocity of the rock upon reaching the water
$v_{1yf=}$ final velocity in y-direction
v_{1xf} = final velocity in the x direction

Considering that the lagoon is 1,186 m long and 575 m wide, dimensions estimated with a relative uncertainty of 2%, it is observed that for launch angles in the range of 62 - 76 degrees. Hereby, the rock experiences a flying time of 22.9 ± 0.1 seconds, when it reaches a maximum height of 1088 ± 10 m and hits the surface of the lagoon at 57 ± 3 m from the right edge and 9.0 ± 0.5 m from the left edge, respectively, taking as reference system the one indicated in Figure 6. Therefore, the impact speed is of about 248 ± 2 m/s. For a launch angle of 68 degrees, the rock lands half the width of the pond. For angles less than 62 and greater than 76 degrees, the rock does not impact the lagoon.

B) Second Case

Figure 7 illustrates the situation prior and after the collision of the rock with the edge of the volcano profile. The velocities of the fragments form equal negative angles with the horizontal. Hereby, equations 3 and 4 are applicable to this case, while the initial velocity of the fragments was calculated using Equation 13.

Y direction:

$$-2v_{0y} = -v_1 sen\theta - v_2 sen\theta$$

$$2v_{0y} = 2v_1 sen\theta$$

$$v_1 = \frac{v_{0y}}{sen\theta} = \frac{v_0}{sen\theta} \quad (13)$$

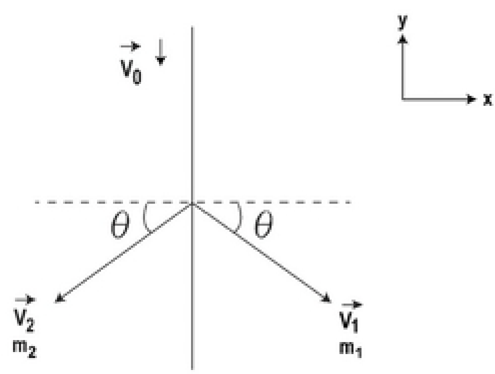

Figure 7: Collision of the rock with the edge, dividing it into two equal fragments with negative velocities on the y-axis.

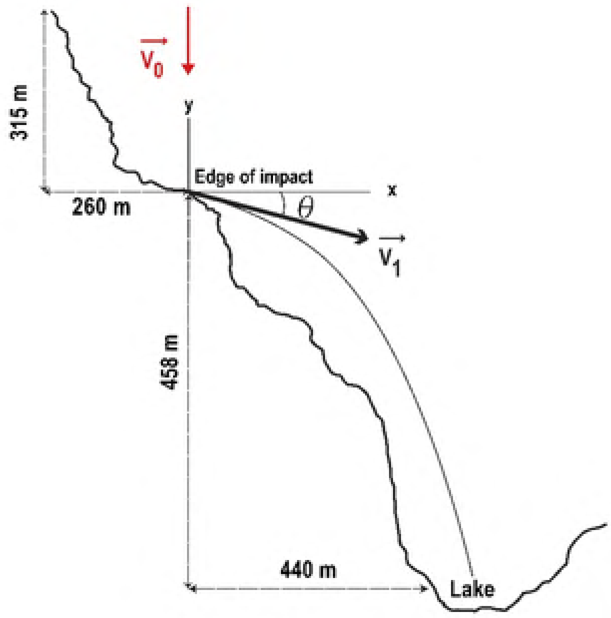

Figure 8. Trajectory of fragment 1 fired with an initial velocity $\vec{v}_1$ forming an angle θ (negative) with the edge plane.

Figure 8 presents the case of fragment 1, launched into the air with an angle θ (negative) and an initial speed $\vec{v}_1$. There is no rise time for the rock, while the initial velocity on the vertical axis is negative (in the same direction as gravity). The maximum height is the vertical distance between the point of impact and the surface of the lagoon (458 m). Equations 10 and 11 were used to calculate the reach and arrival point of the rock to the ground or the lagoon, respectively.

The final speed with which the rock hits the surface of the lagoon was calculated with Equation (14)

$$v_{1f} = \sqrt{v_{1xf}^2 + v_{1yf}^2} \quad (14)$$

$$v_{1xf} = v_{1x}$$

$$v_{1yf} = g\,t_v + v_{1y}$$

Where:

v_{1y} = component of the initial velocity on the y-axis

For launch angles in the range 37 - 59 degrees, the rock experiences a flying time of 9.7 ± 0.5 seconds, impacting the lagoon surface with 7 ± 0.4 m from the right edge and 9 ± 0.5 m from the left edge, respectively, considering the one indicated in Figure 8 as the reference system. Therefore, the impact speed is of about 202 ± 2 m/s. For a launch angle of 47 degrees, the rock falls about half the width of the lagoon. For angles less than 37 and greater than 59 degrees, the rock does not impact the lagoon.

In both cases presented, fragment 2 that starts with speed $\vec{v}_2$ will collide with the slope of the volcano until it reaches the lagoon.

The dimensions of the entire rock were estimated with an uncertainty of 2%, considering a height of 115 meters high, width of about 90 meters and a thickness of about 35 meters, so the volume was calculated as a cube, resulting in a value of 362250 ± 21735 m^3. According to Archimedes' principle, when the rock impacts, the surface of the lagoon will displace a volume of water equal to the volume of the rock, if a cylindrical column is considered, the water will reach a height given by equations 15 and 16.

$$V = \pi r^2 h \qquad (15)$$

$$h = \frac{V}{\pi r^2} \qquad (16)$$

Where:
r = radius of the water column
V = volume of displaced water
h = height of the water column

In this context, it is evident that the height of the water wave in the lagoon (as a function of the radius of the column) is independent of the trajectory during the descent and only depends on whether it arrived whole or in fragments. If the rock arrived as a whole, it would form a 125 ± 8 m column with a radius of 30.3 m. Taking this radius as a reference, if the rock was divided into two, three and four parts, each fragment would form a water column with a height of 62.7 ± 4 m, 41.8 ± 3 m and 31.3 ± 2 m, respectively.

4. CLIMATE CHANGE AS POTENTIAL TRIGGER?

Such catastrophic event based on al inland tsunami seems not to be the first occurring in this site. In 1953 impacted a similar event the less filled lake of El Altar, generating also an overflow and subsequently a debris avalanche in the Valley of Collanes. However, the impact has been of much less proportions as the lake has been in its beginning process of upfilling due to the initial stage of glacial reduction. In fact, explorers reported in the 18th century, that the glaciers occupied the entire interior of the caldera and also reached the upper slopes of the Valle de Collanes. That leads to the preliminary hypothesis, that lose rocks have been generated due to physical weathering in such subglacial environment, where due to glacial reduction based on the contemporaneous climate change such lose and or brecciated rock fragments followed gravity leading to a catastrophe such as those of Friday the 13th nightmare of the inland tsunami disaster at El Altar volcano in October 2000 (Toulkeridis et al., 2020).

Glacial retreat or reduction is a worldwide phenomenon which is interpreted as a direct result of global warming and climate change (Kaser et al., 2004; Byg & Salick, 2009; Roe EtAl, 2017; Bolch, 2007). The resulting landscape has often tremendous consequences for the aquatic system, the flora and fauna, the society as well as industry (Magnuson et al., 1997; Allison, 2017; Omambia & Gu, 2010). The reduction of glacial icecaps are contributing to a slow but steady worldwide sea level rise and sometimes often to sudden hazardous lake developments (Vilímek et al., 2005; Richardson & Reynolds, 2000; Emmer et al., 2014; Stuart-Smith et al., 2021).

In Ecuador, the accelerated reduction of glacial ice-covers on volcanoes and mountains is visible since the last century, while some of them disappeared completely. The remaining glaciers are limited to the peaks of Antisana, Cotopaxi, Chimborazo, Cayambe, Los Ilinizas (north and south), Carihuairazo and El Altar. In order to demonstrate and evidence the shrinkage of the El Altar volcano glacier, various images were downloaded from the Landsat satellites (Landsat 5, Landsat 7 and Landsat 8). In table 1, a summary is listed about the most fundamental characteristics of each image.

Table 1. Satellites Images of the studied area

Image date	Satellite	Cloud cover	Spatial resolution
1991/07/27	Landsat 5	29.00%	30 m.
1998/07/14	Landsat 5	9.00%	
2007/07/31	Landsat 7*	29.00 %	
2016/11/20	Landsat 8	19.81 %	

* In the case of the Landsat 7 image, a banding correction was applied

As a next step, in order to quantify the reduction in the size of the glacier over the years, the digitization of the glacier was conducted, with the support of a composition (SWIR, RED, GREEN), which corresponds to bands 5-3-2 for Landsat 5 and 7 satellites and bands 6-4-3 for Landsat 8 satellite. Hereby, we compared the shape of the glacier over several years with the corresponding compositions as illustrated in figure 9. Subsequently, to quantify the retreat of the glacier at different times, a polygon was digitized for each image, through which the surface of each of them could be calculated. This digitization and the surface of each glacier can be evidenced in figure 10.

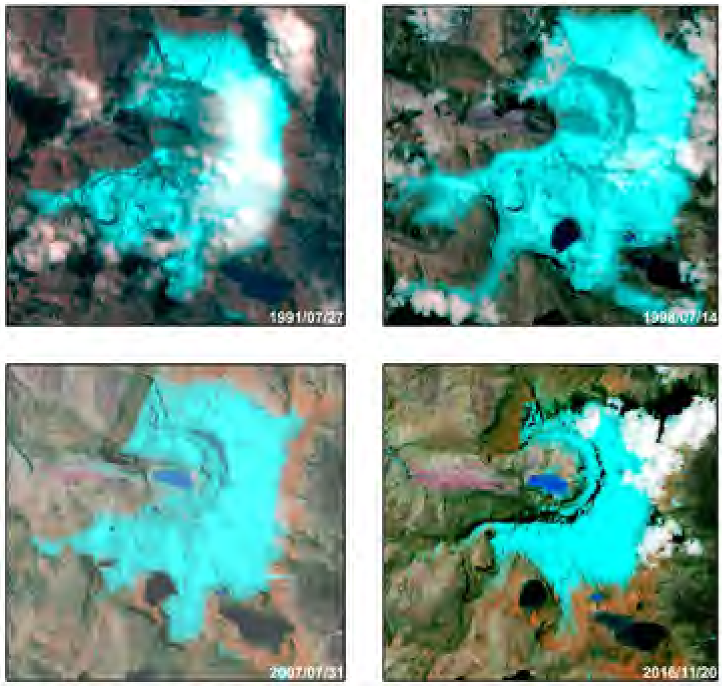

Figure 9. Composition (SWIR, RED, GREEN), of four different times in the Altar volcano.

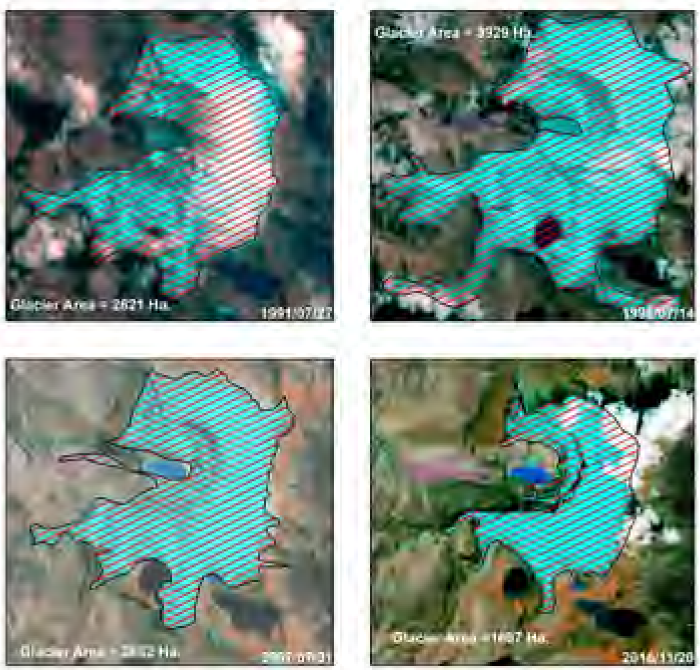

Figure 10. Quantification of El Altar´s glacial reduction between 1991 and 2016.

5. CONCLUSIONS

A combination of various circumstances has been responsible for the rare inland tsunami of the Friday the 13th of October 2000 in the extinct volcano El Altar, situated in the Eastern Volcanic Cordillera of the Ecuadorian Andes. These conditions included physical weathering in a subglacial environment, reduction of the glacial icecaps and the subsequent accumulation of meltwater in the lower parts of the volcano within an up-filling lake.

All these aforementioned circumstances are related to the evident climate change and thus will have even stronger repetitions in the near future due to an increase of extreme conditions as seen in other parts of the world.

Generally, the public preparedness in Ecuador does not coincide with the occurring natural events as catastrophic as they may have been, which leads to the conclusion, that a better awareness and education needs to be developed by the corresponding authorities.

6. REFERENCES

Allison, E. A. (2015). The spiritual significance of glaciers in an age of climate change. Wiley Interdisciplinary Reviews: Climate Change, 6(5), 493-508.

Aviles-Campoverde, D., Chunga, K., Ortiz-Hernández, E., Vivas-Espinoza, E., Toulkeridis, T., Morales-Delgado, A. and Delgado-Toala, D. (2021). Seismically induced soil liquefaction and geological conditions in the city of Jama due to the Mw7.8 Pedernales earthquake in 2016, NW Ecuador. Geosciences, 11, 20

Bolch, T. (2007). Climate change and glacier retreat in northern Tien Shan (Kazakhstan/Kyrgyzstan) using remote sensing data. Global and Planetary Change, 56(1-2), 1-12.

Bondevik, S., Svendsen, J. I., Johnsen, G., Mangerud, J. A. N., & Kaland, P. E. (1997). The Storegga tsunami along the Norwegian coast, its age and run up. Boreas, 26(1), 29-53.

Borrero, J. C., & Greer, S. D. (2013). Comparison of the 2010 Chile and 2011 Japan tsunamis in the far field. Pure and Applied Geophysics, 170(6), 1249-1274.

Byg, A., & Salick, J. (2009). Local perspectives on a global phenomenon—climate change in Eastern Tibetan villages. Global environmental change, 19(2), 156-166.

Cando, M., Arreaga, P., Toulkeridis, T., & De La Torre, G. (2006). Evidences for potential future sector collapse at Volcano Roca Redonda, northern Galápagos—Tectonics, simulation and consequences, paper presented at 4th Meeting, Cities on Volcanoes. Int. Assoc. of Volcanol. and Chem. of the Earth's Inter., Quito, Ecuador, 23-27.

Celorio-Saltos, J.C., García-Arias, J.M., Guerra-Luque, A.B., Barragan-Aroca, G. and Toulkeridis, T. (2018). Vulnerability analysis based on tsunami hazards in Crucita, central coastal of Ecuador. Science of Tsunami Hazards, 38(3): 225-263.

Chunga, K. and Toulkeridis, T. (2014). First evidence of paleo-tsunami deposits of a major historic event in Ecuador. Science of tsunami hazards, 33: 55-69.

Chunga, K., Mulas, M., Alvarez, A., Galarza, J. and Toulkeridis, T. (2019). Characterization of seismogenetic crustal faults in the Gulf of Guayaquil, Ecuador. Andean Geology, 46(1): 66-81.

Chunga, K., Toulkeridis, T., Vera-Grunauer, X., Gutierrez, M., Cahuana, N. And Alvarez, A. (2017). A review of earthquakes and tsunami records and characterization of capable faults on the northwestern coast of Ecuador. Science of tsunami hazards, 36: 100-127.

Daly, M. C. (1989). Correlations between Nazca/Farallon plate kinematics and forearc basin evolution in Ecuador. Tectonics, 8(4), 769-790.

Del-Pino-de-la-Cruz, C.E., Martinez-Molina, B.D., Haro-Baez, A.G., Toulkeridis, T. and Rentería, W. (2021). The proposed design of a smart parking area as a multiple use building for the eventual vertical evacuation in case of tsunami impacts in Salinas, Ecuador. Science of Tsunami Hazards, 40(3), 146-165.

Edler, D., Otto, K.H and Toulkeridis, T. (2020). Tsunami hazards in Ecuador – Regional differences in the knowledge of Ecuadorian high-school students. Science of Tsunami Hazards, 39(2), 86-112.

Emmer, A., Vilímek, V., Klimeš, J., & Cochachin, A. (2014). Glacier retreat, lakes development and associated natural hazards in Cordilera Blanca, Peru. In Landslides in cold regions in the context of climate change (pp. 231-252). Springer, Cham.

Franco, A., Moernaut, J., Schneider-Muntau, B., Strasser, M., & Gems, B. (2020). The 1958 Lituya Bay tsunami–pre-event bathymetry reconstruction and 3D numerical modelling utilising the computational fluid dynamics software Flow-3D. Natural Hazards and Earth System Sciences, 20(8), 2255-2279.

Fritz, H. M., Mohammed, F., & Yoo, J. (2009). Lituya Bay landslide impact generated mega-tsunami 50 th Anniversary. In Tsunami Science Four Years after the 2004 Indian Ocean Tsunami (pp. 153-175). Birkhäuser Basel.

Fujii, Y., & Satake, K. (2007). Tsunami source of the 2004 Sumatra–Andaman earthquake inferred from tide gauge and satellite data. Bulletin of the Seismological Society of America, 97(1A), S192-S207.

Gailler, A., Charvis, P., & Flueh, E. R. (2007). Segmentation of the Nazca and South American plates along the Ecuador subduction zone from wide angle seismic profiles. Earth and Planetary Science Letters, 260(3-4), 444-464.

Gawel, J. E., Crisafulli, C. M., & Miller, R. (2018). The New Spirit Lake: Changes to Hydrology, Nutrient Cycling, and Biological Productivity. In Ecological Responses at Mount St. Helens: Revisited 35 years after the 1980 Eruption (pp. 71-95). Springer, New York, NY.

Genevois, R., & Ghirotti, M. (2005). The 1963 vaiont landslide. Giornale di Geologia Applicata, 1(1), 41-52.

Glimsdal, S., Pedersen, G. K., Langtangen, H. P., Shuvalov, V., & Dypvik, H. (2007). Tsunami generation and propagation from the Mjølnir asteroid impact. Meteoritics & Planetary Science, 42(9), 1473-1493.

González-Vida, J. M., Macías, J., Castro, M. J., Sánchez-Linares, C., de la Asunción, M., Ortega-Acosta, S., & Arcas, D. (2019). The Lituya Bay landslide-generated mega-tsunami–numerical simulation and sensitivity analysis. Natural Hazards and Earth System Sciences, 19(2), 369-388.

Graindorge, D., Calahorrano, A., Charvis, P., Collot, J. Y., & Bethoux, N. (2004). Deep structures of the Ecuador convergent margin and the Carnegie Ridge, possible consequence on great earthquakes recurrence interval. Geophysical Research Letters, 31(4).

Greene, H. G., & Ward, S. N. (2003). Mass movement features along the central California margin and their modeled consequences for tsunami generation. In Submarine Mass Movements and Their Consequences (pp. 343-356). Springer, Dordrecht.

Grilli, S. T., Tappin, D. R., Carey, S., Watt, S. F., Ward, S. N., Grilli, A. R., ... & Muin, M. (2019). Modelling of the tsunami from the December 22, 2018 lateral collapse of Anak Krakatau volcano in the Sunda Straits, Indonesia. Scientific reports, 9(1), 1-13.

Harbitz, C. B., Løvholt, F., & Bungum, H. (2014). Submarine landslide tsunamis: how extreme and how likely?. Natural Hazards, 72(3), 1341-1374.

Hilbe, M., & Anselmetti, F. S. (2015). Mass movement-induced tsunami hazard on perialpine Lake Lucerne (Switzerland): scenarios and numerical experiments. Pure and Applied Geophysics, 172(2), 545-568.

Hills, J. G., & Mader, C. L. (1997). Tsunami produced by the impacts of small asteroids. Annals of the New York Academy of Sciences, 822(1), 381-394.

Jaillard, E., Lapierre, H., Ordonez, M., Alava, J. T., Amortegui, A., & Vanmelle, J. (2009). Accreted oceanic terranes in Ecuador: southern edge of the Caribbean Plate?. Geological Society, London, Special Publications, 328(1), 469-485.

Kaser, G., Hardy, D. R., Mölg, T., Bradley, R. S., & Hyera, T. M. (2004). Modern glacier retreat on Kilimanjaro as evidence of climate change: observations and facts. International Journal of Climatology: A Journal of the Royal Meteorological Society, 24(3), 329-339.

Kawamura, K., Laberg, J. S., & Kanamatsu, T. (2014). Potential tsunamigenic submarine landslides in active margins. Marine Geology, 356, 44-49.

Kharif, C., & Pelinovsky, E. (2005). Asteroid impact tsunamis. Comptes Rendus Physique, 6(3), 361-366.

Kinsland, G. L., Egedahl, K., Strong, M. A., & Ivy, R. (2021). Chicxulub impact tsunami megaripples in the subsurface of Louisiana: Imaged in petroleum industry seismic data. Earth and Planetary Science Letters, 570, 117063.

Klein, E. M., Smith, D. K., Williams, C. M., & Schouten, H. (2005). Counter-rotating microplates at the Galapagos triple junction. Nature, 433(7028), 855-858.

Kremer, K., Anselmetti, F. S., Evers, F. M., Goff, J., & Nigg, V. (2021). Freshwater (paleo) tsunamis–a review. Earth-science reviews, 212, 103447.

Kring, D. A. (2007). The Chicxulub impact event and its environmental consequences at the Cretaceous–Tertiary boundary. Palaeogeography, Palaeoclimatology, Palaeoecology, 255(1-2), 4-21.

Lebras, M., Megard, F., Dupuy, C., & Dostal, J. (1987). Geochemistry and tectonic setting of pre-collision Cretaceous and Paleogene volcanic rocks of Ecuador. Geological Society of America Bulletin, 99(4), 569-578.

Lonsdale, P. (1988). Structural pattern of the Galapagos microplate and evolution of the Galapagos triple junctions. Journal of Geophysical Research: Solid Earth, 93(B11), 13551-13574.

Luna, M. P., Staller, A., Toulkeridis, T., & Parra, H. (2017). Methodological approach for the estimation of a new velocity model for continental Ecuador. Open Geosciences, 9(1), 719-734.

Mader, C. L., & Gittings, M. L. (2002). Modeling the 1958 Lituya Bay mega-tsunami, II. Science of Tsunami Hazards, 20(5), 241-250.

Magnuson, J. J., Webster, K. E., Assel, R. A., Bowser, C. J., Dillon, P. J., Eaton, J. G., ... & Quinn, F. H. (1997). Potential effects of climate changes on aquatic systems: Laurentian Great Lakes and Precambrian Shield Region. Hydrological processes, 11(8), 825-871.

Martinez, N. and Toulkeridis, T. (2020). Tsunamis in Panama – History, preparation and future consequences. Science of Tsunami Hazards, 39(2), 53-68.

Matheus Medina, A.S., Cruz D´Howitt, M., Padilla Almeida, O., Toulkeridis, T. and Haro, A.G. (2016). Enhanced vertical evacuation applications with geomatic tools for tsunamis in Salinas, Ecuador. Science of Tsunami Hazards, 35, (3): 189-213

Matheus-Medina, A.S., Toulkeridis, T., Padilla-Almeida, O., Cruz-D´ Howitt, M. and Chunga, K. (2018). Evaluation of the tsunami vulnerability in the coastal Ecuadorian tourist centers of the peninsulas of Bahia de Caráquez and Salinas. Science of Tsunami Hazards, 38(3): 175-209.

Mato, F. and Toulkeridis, T. (2017). The missing Link in El Niño's phenomenon generation. Science of tsunami hazards, 36: 128-144.

Mato, F. and Toulkeridis, T. (2018). An unsupervised K-means based clustering method for geophysical post-earthquake diagnosis. 2017 IEEE Symposium Series on Computational Intelligence (SSCI). 1-8

Matsui, T., Imamura, F., Tajika, E., Nakano, Y., & Fujisawa, Y. (2002). Generation and propagation of a tsunami from the Cretaceous-Tertiary impact event. SPECIAL PAPERS-GEOLOGICAL SOCIETY OF AMERICA, 69-78.

McMurtry, G. M., Watts, P., Fryer, G. J., Smith, J. R., & Imamura, F. (2004). Giant landslides, mega-tsunamis, and paleo-sea level in the Hawaiian Islands. Marine Geology, 203(3-4), 219-233.

Melián, G.V., Toulkeridis, T., Pérez, N.M., Hernández Pérez, P.A., Somoza, L., Padrón, E., Amonte, C., Alonso, M., Asensio-Ramos, M. and Cordero, M. (2021). Geochemistry of water and gas emissions from Cuicocha and Quilotoa Volcanic Lakes, Ecuador. Frontiers in Earth Sciences, 1167

Mendoza, C., & Dewey, J. W. (1984). Seismicity associated with the great Colombia-Ecuador earthquakes of 1942, 1958, and 1979: Implications for barrier models of earthquake rupture. Bulletin of the seismological society of America, 74(2), 577-593.

Mori, N., Takahashi, T., Yasuda, T., & Yanagisawa, H. (2011). Survey of 2011 Tohoku earthquake tsunami inundation and run−up. Geophysical research letters, 38(7).

Navas, L., Caiza, P. and Toulkeridis, T. (2018). An evaluated comparison between the molecule and steel framing construction systems – Implications for the seismic vulnerable Ecuador. Malaysian Construct. Res. J. 26 (3), 87–109.

Nohara, M. (2011). Impact of the Great East Japan Earthquake and tsunami on health, medical care and public health systems in Iwate Prefecture, Japan, 2011. Western Pacific Surveillance and Response Journal: WPSAR, 2(4), 24.

Nomikou, P., Druitt, T. H., Hübscher, C., Mather, T. A., Paulatto, M., Kalnins, L. M., ... & Parks, M. M. (2016). Post-eruptive flooding of Santorini caldera and implications for tsunami generation. Nature communications, 7(1), 1-10.

Omambia, C. S., & Gu, Y. (2010). The cost of climate change in Tanzania: impacts and adaptations. Journal of American Science, 6(3), 182-196.

Ortiz-Hernández, E., Chunga, K. Pastor, J.L. and Toulkeridis, T. (2022). Assessing susceptibility to soil liquefaction, using the standard penetration test (SPT) – A case study from the city of Portoviejo, coastal Ecuador. Land, online

Ortiz-Hernández, E., Chunga, K. Toulkeridis, T. and Pastor, J.L. (2022). Soil liquefaction and other seismic-associated phenomena in the city of Chone during the 2016 earthquake of coastal Ecuador. Applied Science, online

Padrón, E., Hernández, P.A., Marrero, R., Melián, G, Toulkeridis, T., Pérez., N.M., Virgili, G. and Notsu, K. (2008). Diffuse CO2 emission rate from the lake-filled Cuicocha and Pululagua calderas, Ecuador. Journal of Volcanology and Geothermal Research (Special Volume on Continental Ecuador volcanoes), 176: 163-169.

Padrón, E., Hernández, P.A., Pérez, N.M., Toulkeridis, T., Melián, G., Barrancos, J., Virgili, G., Sumino H. and Notsu, K. (2012). Fumarole/plume and diffuse CO2 emission from Sierra Negra volcano, Galapagos archipelago. Bull. Of Volcanol., 74: 1509-1519.

Pararas-Carayannis, G. (1999). Analysis of mechanism of tsunami generation in Lituya Bay. Science of Tsunami Hazards, 17(3), 193-206.

Pararas-Carayannis, G. (2006). The potential of tsunami generation along the Makran Subduction Zone in the northern Arabian Sea: Case study: The earthquake and tsunami of November 28, 1945. Science of Tsunami Hazards, 24(5), 358-384.

Pararas-Carayannis, G. (2012). Potential of tsunami generation along the Colombia/Ecuador subduction margin and the Dolores-Guayaquil mega-thrust. Science of Tsunami Hazards, 31(3), 209-230

Pararas-Carayannis, G., & Zoll, P. (2017). Incipient evaluation of temporal El Nino and other climatic anomalies in triggering earthquakes and tsunamis-Case Study: The Earthquake and Tsunami of 16 th April 2016 in Ecuador. Science of Tsunami Hazards, 36(4), 262-291

Paris, R. (2015). Source mechanisms of volcanic tsunamis. Phil. Trans. R. Soc. A 373, 20140380.

Paris, R., Bravo, J. J. C., González, M. E. M., Kelfoun, K., & Nauret, F. (2017). Explosive eruption, flank collapse and megatsunami at Tenerife ca. 170 ka. Nature Communications, 8(1), 1-8.

Paronuzzi, P., & Bolla, A. (2012). The prehistoric Vajont rockslide: an updated geological model. Geomorphology, 169, 165-191.

Pennington, W. D. (1981). Subduction of the eastern Panama Basin and seismotectonics of northwestern South America. Journal of Geophysical Research: Solid Earth, 86(B11), 10753-10770.

Pulido, N., Yoshimoto, M., & Sarabia, A. M. (2020). Broadband wavelength slip model of the 1906 Ecuador-Colombia megathrust-earthquake based on seismic intensity and tsunami data. Tectonophysics, 774, 228226.

Richardson, S. D., & Reynolds, J. M. (2000). An overview of glacial hazards in the Himalayas. Quaternary International, 65, 31-47.

Ridolfi, F., Puerini, M., Renzulli, A., Menna, M. and Toulkeridis, T. (2008). The magmatic feeding system of El Reventador volcano (Sub-Andean zone, Ecuador) constrained by mineralogy, textures and geothermobarometry of the 2002 erupted products. Journal of Volcanology and Geothermal Research (Special Volume on Continental Ecuador volcanoes), 176: 94-106.

Rodríguez Espinosa, F., Toulkeridis, T., Salazar Martinez, R., Cueva Girón, J., Taipe Quispe, A., Bernaza Quiñonez, L., Padilla Almeida, O., Mato, F., Cruz D´Howitt, M., Parra, H., Sandoval, W. and Rentería, W. (2017). Economic evaluation of recovering a natural protection with concurrent relocation of the threatened public of tsunami hazards in central coastal Ecuador. Science of tsunami hazards, 36: 293-306.

Rodriguez, F., Toulkeridis, T., Padilla, O. and Mato, F. (2017). Economic risk assessment of Cotopaxi volcano Ecuador in case of a future lahar emplacement. Natural Hazards, 85, (1): 605-618.

Roe, G. H., Baker, M. B., & Herla, F. (2017). Centennial glacier retreat as categorical evidence of regional climate change. Nature Geoscience, 10(2), 95-99.

Sassa, K., Dang, K., He, B., Takara, K., Inoue, K., & Nagai, O. (2014). A new high-stress undrained ring-shear apparatus and its application to the 1792 Unzen–Mayuyama megaslide in Japan. Landslides, 11(5), 827-842.

Sassa, K., Dang, K., Yanagisawa, H., & He, B. (2016). A new landslide-induced tsunami simulation model and its application to the 1792 Unzen-Mayuyama landslide-and-tsunami disaster. Landslides, 13(6), 1405-1419.

Schulte, P., Alegret, L., Arenillas, I., Arz, J. A., Barton, P. J., Bown, P. R., ... & Willumsen, P. S. (2010). The Chicxulub asteroid impact and mass extinction at the Cretaceous-Paleogene boundary. Science, 327(5970), 1214-1218.

Self, S. & Rampino, M. R. (1981). The 1883 eruption of Krakatau. Nature 294, 699–704.

Semenza, E., & Ghirotti, M. (2000). History of the 1963 Vaiont slide: the importance of geological factors. Bulletin of Engineering Geology and the Environment, 59(2), 87-97.

Sennson, J. L., & Beck, S. L. (1996). Historical 1942 Ecuador and 1942 Peru subduction earthquakes and earthquake cycles along Colombia-Ecuador and Peru subduction segments. Pure and applied geophysics, 146(1), 67-101.

Stuart-Smith, R. F., Roe, G. H., Li, S., & Allen, M. R. (2021). Increased outburst flood hazard from Lake Palcacocha due to human-induced glacier retreat. Nature Geoscience, 14(2), 85-90.

Suárez-Acosta, P.E., Cañamar-Tipan, C.D., Ñato-Criollo, D.A., Vera-Zambrano, J.D., Galarza-Vega, K.L., Guevara-Álvarez, P.M., Fajardo-Cartuche, C.N., Herrera-Garcés, K. K., Ochoa-Campoverde, C.V., Torres-Orellana, J.S., Rentería, W., Chunga, K., Padilla, O., Sinde-González, I., Simón-Baile, D. and Toulkeridis, T. (2021). Evaluation of seismic and tsunami resistance of potential shelters for vertical evacuation in case of a tsunami impact in Bahia de Caráquez, central coast of Ecuador. Science of Tsunami Hazards, 40(1), 1-37.

Sulli, A., Zizzo, E., & Albano, L. (2018). Comparing methods for computation of run-up heights of landslide-generated tsunami in the Northern Sicily continental margin. Geo-Marine Letters, 38(5), 439-455.

Toulkeridis, T. (2013). Volcanes Activos Ecuador. Santa Rita, Quito, Ecuador: 152 pp

Toulkeridis, T. (2016). The Evaluation of unexpected results of a seismic hazard applied to a modern hydroelectric center in central Ecuador. Journal of Structural Engineering, 43, (4): 373-380.

Toulkeridis, T. and Angermeyer, H. (2019). Volcanoes of the Galapagos. 2nd Edition, Abad Offest, Guayaquil, Ecuador: 324pp

Toulkeridis, T. and Zach, I. (2017). Wind directions of volcanic ash-charged clouds in Ecuador – Implications for the public and flight safety. Geomatics, Natural Hazards and Risks, 8(2): 242-256.

Toulkeridis, T., Arroyo, C.R., Cruz D'Howitt, M., Debut, A., Vaca, A.V., Cumbal, L., Mato, F. and Aguilera, E. (2015). Evaluation of the initial stage of the reactivated Cotopaxi volcano - Analysis of the first ejected fine-grained material. Natural Hazards and Earth System Sciences, 3, (11): 6947-6976.

Toulkeridis, T., Barahona-Quelal, I.N., Pilco-Paguay, E.O., Cacuango-Casco, D.M., Guilcaso-Tipán, B.S. and Sailema-Hurtado, W.P. (2021). Evaluation of seismic and tsunami resistance of potential shelters for vertical evacuation in case of a tsunami impact in Manta and Salinas, central coast of Ecuador. Science of Tsunami Hazards, 40(4), 286-314.

Toulkeridis, T., Buchwaldt, R. and Addison, A. (2007). When Volcanoes Threaten, Scientists Warn. Geotimes, 52: 36-39.

Toulkeridis, T., Chunga, K., Rentería, W., Rodriguez, F., Mato, F., Nikolaou, S., Cruz D´Howitt, M., Besenzon, D., Ruiz, H., Parra, H. and Vera-Grunauer, X. (2017). The 7.8 Mw Earthquake and Tsunami of the 16th April 2016 in Ecuador - Seismic evaluation, geological field survey and economic implications. Science of tsunami hazards, 36: 197-242.

Toulkeridis, T., Echegaray-Aveiga, R.C. and Martinez-Maldonado, K.P. (2021) Shock metamorphism in volcanic rock due to the impact of the Miguir-Cajas meteorite in 1995 and its importance for Ecuador. Geojournal of Tourism and Geosites, 35(2), 315-321.

Toulkeridis, T., Martinez, N., Barrantes, G., Rentería, W., Barragan-Aroca, G., Simón-Baile, D., Palacios, I., Salazar, R., Salcedo-Hurtado, E.d.J. and Pararas-Carayannis, G. (2022). Impact and response in Central and South America due to the tsunami generated by the submarine eruption of Hunga Tonga-Hunga Ha'apai volcano. Science of Tsunami Hazards, 41(1), 1-38.

Toulkeridis, T., Mato, F., Toulkeridis-Estrella, K., Perez Salinas, J.C., Tapia, S. and Fuertes, W. (2018). Real-Time Radioactive Precursor of the April 16, 2016 Mw 7.8 Earthquake and Tsunami in Ecuador. Science of tsunami hazards, 37: 34-48.

Toulkeridis, T., Parra, H., Mato, F., Cruz D´Howitt, M., Sandoval, W., Padilla Almeida, O., Rentería, W., Rodríguez Espinosa, F., Salazar Martinez, R., Cueva Girón, J., Taipe Quispe, A. and Bernaza Quiñonez, L. (2017). Contrasting results of potential tsunami hazards in Muisne, central coast of Ecuador. Science of tsunami hazards, 36: 13-40

Toulkeridis, T., Porras, L., Tierra, A., Toulkeridis-Estrella, K., Cisneros, D., Luna, M., ... & Salazar, R. (2019). Two independent real-time precursors of the 7.8 Mw earthquake in Ecuador based on radioactive and geodetic processes—Powerful tools for an early warning system. Journal of Geodynamics, 126, 12-22.

Toulkeridis, T., Porras, L., Tierra, A., Toulkeridis-Estrella, K., Cisneros, D., Luna, M., Carrión, J.L., Herrera, M., Murillo, A., Perez-Salinas, J.C., Tapia, S., Fuertes, W. and Salazar, R. (2019). A potential early warning system for earthquakes based on two independent real-time precursors – the case of Ecuador´s 7.8 Mw in 2016. Proceedings of the International Conference on Natural Hazards and Infrastructure 2019, 2nd International Conference on Natural Hazards and Infrastructure, ICONHIC 2019; Chania; Greece; 23 June 2019 through 26 June 2019; Code 257429

Toulkeridis, T., Tamayo, E., Simón-Baile, D., Merizalde-Mora, M.J., Reyes –Yunga, D.F., Viera-Torres, M. and Heredia, M. (2020) Climate change according to Ecuadorian academics– Perceptions versus facts. La Granja, 31(1), 21-49

Vilímek, V., Zapata, M. L., Klimeš, J., Patzelt, Z., & Santillán, N. (2005). Influence of glacial retreat on natural hazards of the Palcacocha Lake area, Peru. Landslides, 2(2), 107-115.

Völker, D., Geersen, J., Behrmann, J. H., & Weinrebe, W. R. (2012). Submarine mass wasting off Southern Central Chile: distribution and possible mechanisms of slope failure at an active continental margin. In Submarine mass movements and their consequences (pp. 379-389). Springer, Dordrecht.

Wang, J., Ward, S. N., & Xiao, L. (2019). Tsunami Squares modeling of landslide generated impulsive waves and its application to the 1792 Unzen-Mayuyama mega-slide in Japan. Engineering Geology, 256, 121-137.

Ward, S. N., & Asphaug, E. (2000). Asteroid impact tsunami: a probabilistic hazard assessment. Icarus, 145(1), 64-78.

Ward, S. N., & Day, S. (2006). Particulate kinematic simulations of debris avalanches: interpretation of deposits and landslide seismic signals of Mount Saint Helens, 1980 May 18. Geophysical Journal International, 167(2), 991-1004.

Ward, S. N., & Day, S. (2010). The 1958 Lituya bay landslide and tsunami—A tsunami ball approach. Journal of Earthquake and Tsunami, 4(04), 285-319.

Yamanaka, Y., Tanioka, Y., & Shiina, T. (2017). A long source area of the 1906 Colombia–Ecuador earthquake estimated from observed tsunami waveforms. Earth, Planets and Space, 69(1), 1-11.

Yoshimoto, M., Kumagai, H., Acero, W., Ponce, G., Vásconez, F., Arrais, S., ... & Nakano, M. (2017). Depth−dependent rupture mode along the Ecuador−Colombia subduction zone. Geophysical Research Letters, 44(5), 2203-2210.

Zaniboni, F., Armigliato, A., Pagnoni, G., & Tinti, S. (2014). Continental margins as a source of tsunami hazard: The 1977 Gioia Tauro (Italy) landslide–tsunami investigated through numerical modeling. Marine Geology, 357, 210-217.

ISSN 8755-6839

SCIENCE OF **TSUNAMI HAZARDS**

Journal of Tsunami Society International

Volume 41 **Number 3** **2022**

WWW.TSUNAMISOCIETY.ORG

TSUNAMI SOCIETY INTERNATIONAL, 1325 South 33rd Avenue, Hollywood, Florida 33021, USA.

WWW.TSUNAMISOCIETY.ORG